801518

(1)

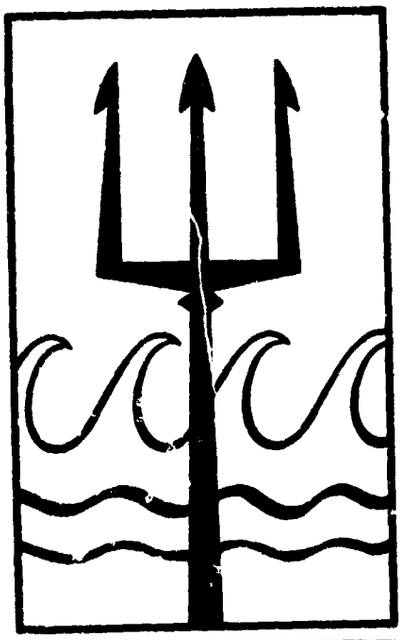

(6) U.S. NAVY SYMPOSIUM (3rd) ON MILITARY OCEANOGRAPHY.

THE PROCEEDINGS OF THE SYMPOSIUM.

VOLUME II.

11-13 MAY 1966.

U.S. NAVY ELECTRONICS LABORATORY
SAN DIEGO, CALIFORNIA
92152

(11) 1966

(12) 296 p.

WELCOME

From the Commanding Officer and Director
U.S. Navy Electronics Laboratory
San Diego, California

The Navy Electronics Laboratory is honored to host the Third Annual U.S. Navy Symposium on Military Oceanography.

Your direct interest and active participation in this Symposium keynotes the expanding importance of the oceans and combines to further our knowledge of this environment. The large number of excellent papers submitted is a measure of your interest. We regret that all the many high-quality submissions could not be selected for presentation during these three days.

It is a pleasure to have you as our guests. We hope the arrangements that have been made and the auditorium facilities extended for our use by Captain Fletcher Hale, USN, Commander, U.S. Naval Training Center, will all contribute to a successful Symposium.

W.R. Boehm
Captain, USN
Commanding Officer and Director

MESSAGE

From the Oceanographer of the Navy

When the first U. S. Navy Symposium on Military Oceanography was held in June 1964, with the U. S. Naval Oceanographic Office as host, it was thought of as an experiment, which, of course, it was. It was also an outstanding success, and the success was repeated last year when the Naval Ordnance Laboratory acted as host.

Now, with the convocation of this third Symposium with the U.S. Navy Electronics Laboratory as host, what was an experiment has become an institution.

Once again we are fortunate at the high caliber of the representatives who have enrolled from private industry, our educational and scientific institutions, and government agencies. Once again, too, we have reason to be pleased at the quality of papers that have been offered for presentation.

The Navy's problems, as a member of the United States defense team are, of course, as urgent as ever. The solution to many of these problems, particularly in the area of submarine and anti-submarine operations, depends upon our continued progress in oceanographic research and development, and our ability to apply our findings to the immediate needs of our Fleet Commanders. If the thoughtful papers that are to be presented to you and the free flow of ideas that I know will be generated in your open forum discussions lead to the solution of a single one of these problems, all of our efforts will have been worthwhile.

As sponsor of this Symposium I want to express my appreciation to the Navy Electronics Laboratory for acting as your host on this occasion. I am sure that the arrangements the Laboratory has made will contribute to the success of your deliberations.

Best wishes and good luck.

CDALE D. WATERS, JR.
Rear Admiral, USN
Oceanographer of the Navy

THE SECRETARY'S MESSAGE

It is gratifying that so many delegates from private industry and our great research and educational institutions have taken time from busy schedules to join our Navy representatives in this Third Annual Symposium on Military Oceanography.

Not all of you are primarily concerned, as the Navy must be, with the direct application of oceanography to the problems of national defense. To you who also have other interests let me say that anything anyone does in oceanography is important to the Navy, to some degree. There is not a single idea within the realm of oceanography that may not have its application to some naval aspect that can, in turn, contribute to our national defense.

As time goes on we must turn more and more to our oceanographers for direct help in naval problems: in the development of weapons systems, in long-range sound propagation, in the development of deep submergence vehicles, and in all the other facets of undersea technology that can help to ensure mastery of the seas.

On behalf of the Secretary of the Navy, I wish you every success in your important deliberations.

ROBERT W. MORSE
Assistant Secretary of the Navy
(Research and Development)

SPONSORS

Office of Chief of Naval Operations
Office of Naval Research
Office of Naval Material
Bureau of Naval Weapons
Bureau of Ships
Bureau of Yards and Docks
U. S. Naval Air Development Center
U. S. Naval Civil Engineering Laboratory
U. S. Naval Oceanographic Office
U. S. Naval Ordnance Laboratory
U. S. Naval Ordnance Test Station
U. S. Naval Research Laboratory
U. S. Naval Underwater Ordnance Station
U. S. Naval Underwater Sound Laboratory
U. S. Naval Weather Service
U. S. Navy Electronics Laboratory
U. S. Navy Mine Defense Laboratory
U. S. Naval Radiological Laboratory

STEERING COMMITTEE

Commander J. W. Davies, USN, NEL
Commander R. W. Haupt, USN, CNO (OP 09B5)
W. H. Hymes, CNO (OP 09B5)
Captain R. A. Zettel, USNR, CNO (OP 716)
Lieutenant (jg) J. J. Spigai, USNR, CNO (OP 716)
Dr. E. C. LaFond, NEL
B. K. Couper, BUSHIPS
M. H. Schefer, BUWEPS
B. G. Bingham, ONR
F. Knoop, BUDOCKS

COMMITTEE

Dr. E. C. LaFond, Program Chairman
C. M. Johnson, Publications
C. M. Hatcher, Public Affairs
Lieutenant W. C. Long, USN, Security
Commander J. W. Davies, USN, General Chairman

TABLE OF CONTENTS

OCEANOGRAPHIC FACTORS IN HARBOR DEVELOPMENT IN SOUTH VIETNAM

by

Joseph M. Caldwell and George M. Watts
U. S. Army Coastal Engineering Research Center

This paper will discuss the oceanographic factors which have a bearing on harbor development in South Vietnam. It is to be recognized basic data on these factors for Vietnam are minimal and considerable judgment must be exercised concerning certain decisions on port location and construction for this area.

GENERAL CONSIDERATIONS

The Vietnam Seacoast. First, let us consider a simplified version of the physiography of the seacoast. Figure 1 shows South Vietnam is some 700 miles in length (north to south) with a width varying from 30 miles in the north to 120 miles in the south. Much of the western border is characterized by a mountain ridge. Ranges of this mountainous formation extend easterly to the South China Sea. Where the ridges meet the sea they are picturesque and resemble parts of the California coast. The valleys and coastal plains between these headlands constitute rice lands and are the more populous areas of the country.

The only significant departure from this physiographic pattern is found in the Mekong River Delta area which occupies the southern one-fourth of the country. This area is flat and interlaced with numerous tidal streams. The Saigon River, located easterly of the Mekong, serves as the watercourse to the City of Saigon, situated some 80 miles upstream from the South China Sea.

Seaports. Until 1964, only two deep-draft harbors existed in the country. Saigon is a major port with controlling depths of 20 to 25 feet at low water leading up the Saigon River from Vung Tau on the South China Sea to the city wharves. Tide and fresh water induced currents in the river maintain these channel depths and no dredging has been done. The second port, Da Nang, is some 500 miles upcoast from Vung Tau. Da Nang has a partially protected deep-draft anchorage. The channel leading from the anchorage area to berthing has a controlling depth of about 20 feet. Unloading of the deep-draft vessels is by lighterage.

Along the 500 miles of coast between Vung Tau and Da Nang, the Vietnamese utilize a number of natural harbors to accommodate junks, used in local fishing, and small coastal shipping operations. The controlling depth into these smaller harbors is usually less than 6 feet at low water.

Another natural deep-draft harbor does exist along the 500-mile stretch from Vung Tau to Da Nang, this harbor being Cam Ranh Bay, located some 250 miles north of Vung Tau. The American forces are now developing this magnificent bay into a major port.

The Vietnamese economy has historically been agrarian. To provide for the movement of goods north and south, the French - during the colonial period - constructed a meter-gage railroad and a medium-sized highway along the coast. Though small by United States standards, these two routes were sufficient for the agrarian economy of the country. The railroad and highway pass through ridges and headlands along the coast and are vulnerable to destruction and/or attack by the Viet Cong forces. This is a factor in the use of these facilities, thus defense points such as airfields, troop bases, etc., have to be supplied either by air or water. For large, sustained operations, the heavy tonnages required are best supplied by water. It is this factor which has made the development of coastal harbors and port facilities a priority item in the area.

Other Considerations. One point should be recognized which complicates the Vietnam port development problem. Normally port development is a gradual process, carried out over decades or in some cases centuries. Thus most large ports are a result of gradual incremental development. The problems in Vietnam generally involve the creation of a port facility in a single step. Past experience on local physical factors which will influence the creation, operation, and maintenance of the port are therefore unknown. Important physical factors bearing on harbor design are military requirements and real estate problems. The harbor facility must be located to provide optimum support to military installations, yet be sited where real estate is available. Due to these and other constraints, harbors are in some cases necessarily sited in locations which have certain disadvantages.

OCEANOGRAPHIC FACTORS

Winds. The winds in the area are associated to a large extent with the monsoons. There are two monsoon seasons: the summer (or southwest) monsoons with dominant winds from the southwest quarter, and the winter (or northeast monsoons) with dominant winds from the northeast quarter. The southwest monsoons effect on the coast is most noticeable in the southern one-third of the coast; whereas the northeast monsoons affect the northerly two-thirds of the coast. The principal effects of these winds on harbor design are in wave generation. Winds seldom reach a sustained velocity of over 35 knots along the South Vietnamese coast and severe typhoons strike this coast only on very rare occasions.

Wave Action. A review of the coast of South Vietnam will show that the open water fetch is limited by Hainan Island 150 miles to the north; by the Philippines 700 miles to the east; Borneo 600 miles to the south;

and Malaya 300 miles to the southwest and west. These fetches are sufficient to permit sizable waves to be generated which impinge on the shores of South Vietnam. As could be expected, wave action reaching the various sectors of the coast is seasonal in character and related to the monsoon winds. Most segments of the coast experience five or six months of rather low wave action followed by several months of much rougher seas. Figure 2 shows the character of wave action with the season off the central east coast of Vietnam.

Tides. The tides are chiefly diurnal along the northern half of the coast. They are semi-diurnal along the southern half of the coast, though exhibiting a considerable inequality in the two low waters each day. The range of the tide varies considerably along the coast as shown in the following table:

Location	Average Diurnal Range (feet)
Vung Tau (Saigon River Entrance)	5.9
Saigon (City)	6.9
Phan Thiet	4.3
Cam Ranh Bay	3.8
Qui Nhon	3.6
Da Nang Bay	2.3
Hue River Inlet	1.6

Where the tide range is substantial, consideration can be given to providing what is called a high-tide channel. Meaning, of course, that channel depths (natural or dredged) are sufficient only at high tide to permit the vessel to enter the port. In effect, the high-tide channel is a compromise between dredging requirements and time-of-use of the channel. In some cases, particularly in times of rapid buildup of supply requirements, it may be the only practical solution to a supply problem. One of the supply ports on the coast of South Vietnam has operated for a year or more as a high-tide harbor, having a controlling channel depth of about 12 feet at low water and about 15½ feet at high water. A hopper dredge is now (May 1966) deepening this channel to a controlling depth of about 20 feet.

Inshore Hydrography. As indicated earlier, a part of the Vietnam coast is characterized by embayments, between headlands, which have wide sandy beaches. The beach material is transported to the coast by the streams flowing from the interior highlands. The beach and foreshore zone slope into the sea in various profiles, depending on the orientation of the shore and the rate of supply of sand to the beach area. With some exceptions, like the Saigon River mouth, Cam Ranh Bay entrance, Da Nang Bay, Quinhon Bay, etc., the shallow inshore contours are relatively unbroken along the entire length of coast. The entrances to the various rivers discharging to the coast are constricted by sand bars or shoals which usually have controlling depths of 6 feet or less at low water.

Two types of channels are to be considered in most cases: channels to accommodate LST or similar class vessels with loaded drafts of 16 to 18 feet; and channels to accommodate vessels with loaded drafts up to about 28 feet. Even a cursory scanning of the coastal hydrography shows the 24-foot contour is generally 1/2 to 2 miles offshore, therefore the initial dredging to establish channels of the required depth and cross-section is in many cases the problem of first magnitude which may require millions of cubic yards of dredging for a single harbor. Much of this dredging is in the open sea requiring the use of ocean-going hopper dredges, which themselves are a special vessel not in too plentiful supply.

Of the various oceanographic factors pertinent to harbor development in South Vietnam, this factor of relatively unfavorable shallow-water hydrography is probably the most dominant. It is true that in a number of places deep-water contours are relatively close to shore, however, these shore segments usually are rocky headlands with limited potential for development of a harbor complex.

Littoral Drift. The alongshore movement of sand (littoral drift) is a result of the wave action impinging on the shore. The rate of littoral material movement is related to the magnitude and/or characteristics of the waves, including their angle of approach to the shore. Drift rates are usually determined by measuring long-term accretion behind breakwaters or jetties, or by measurement of shoaling in a dredged channel. As far as known in all of South Vietnam there is not a breakwater or jetty extending into the littoral drift zone (generally considered to be the shoreface from the shoreline out to about the -18-foot contour). Nor has there (until the last few months) been a single channel maintained by dredging whereby the channel cut extended through the foreshore zone on the open coast. Thus there are no historic records in Vietnam on which to develop an estimate of the rate of littoral drift.

The U. S. Army Coastal Engineering Research Center (CERC) has, for a number of years, been perfecting a method for estimating littoral drift rates from known wave characteristics and measured littoral material movement. This method has a reasonable degree of usefulness where the wave climate is well defined, statistically, over a period of several years. Wave records for the Vietnam coast are limited and not of the quality to justify an intensive application of the CERC method. Preliminary evaluations have been made to compare the wave climate in Vietnam with wave climates around the coastline of the United States where drift rates are known. The drift rates on the New Jersey - Delaware - Maryland coast are about 1,000,000 cubic yards per year gross (north plus south) with a net drift of about 300,000 cubic yards per year to the south in most places. The gross rate on the Oregon - Washington coast is several million cubic yards per year with a net drift well over 1,000,000 cubic yards per year to the south. The wave climate in Vietnam is more comparable to the Middle Atlantic coast than to the Pacific northwest coast; therefore, a tentative conclusion follows that the drift rates

along the Vietnam coast should be of the same order as along the Middle Atlantic coast. The significance of this evaluation of the rate of littoral drift is to point out that any channel dredged through the surf zone will have to be protected by jetties, or frequent maintenance dredging is to be expected against a sizable but not overwhelming volume of littoral drift.

SUMMARY

The oceanographic factors which have influenced and are still influencing harbor development in South Vietnam have been described. These factors may not necessarily be controlling in establishing where a harbor will be located, as military needs and/or local economy may be overriding. However even when other factors dictate where a harbor shall be located, the oceanographic factors determine the magnitude of the work to be done in creating the harbor basin and entrance channel, and in thereafter maintaining these facilities to project dimensions.

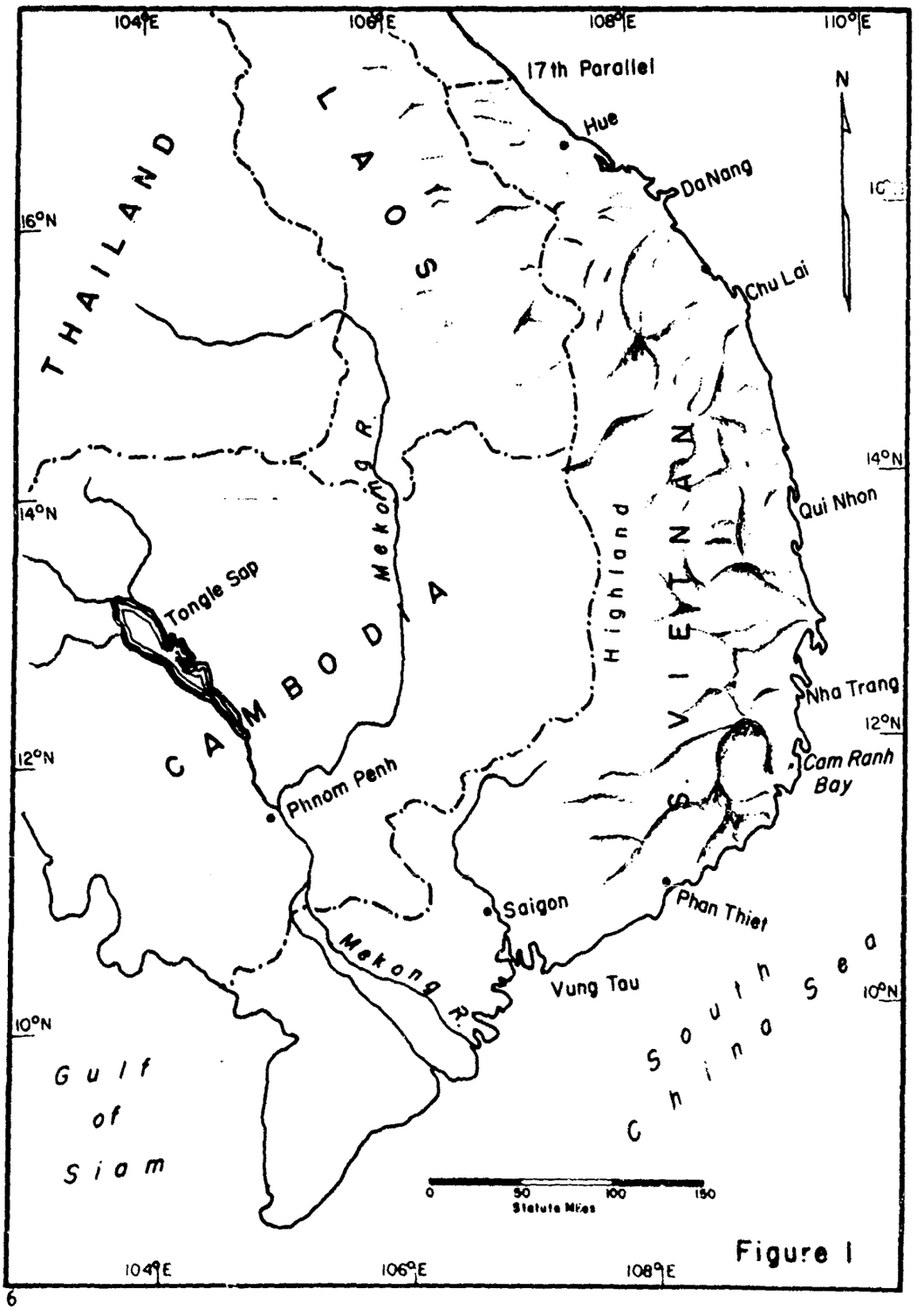
104°E
106°E
108°E
110°E
17th Parallel
N
Hue
DaNang
Chu Lai
16°N
THAILAND
LAOS
14°N
Qui Nhon
Mekong R.
Highland
VIETNAM
Tongle Sap
CAMBODIA
Nha Trang
12°N
Cam Ranh Bay
Phnom Penh
Saigon
Phan Thiet
Mekong R.
Vung Tau
South China Sea
10°N
Gulf of Siam
0
50
100
150
Statute Miles

Figure 1

PERCENTAGE OF TIME OF SEA AND SWELL OCCURRENCE AND DIRECTION

	NORTH		NORTHEAST		EAST		SOUTHEAST		SOUTH		TOTAL	
	SEA	SWELL	SEA	SWELL	SEA	SWELL	SEA	SWELL	SEA	SWELL	SEA	SWELL
WINTER MONSOONS												
Slight or moderate	14	8	32	16	6	2	0	0	0	0	-	-
Rough	8	17	9	21	0	2	0	0	0	0	17	40
Very rough or high	9	10	6	3	0	0	0	0	0	0	15	13
SPRING TRANSITION												
Slight or moderate	7	3	20	15	11	7	14	1	16	5	-	-
Rough	1	3	1	7	0	2	0	1	1	5	3	13
Very rough or high	0	1	0	1	0	0	0	0	0	0	0	2
SUMMER MONSOONS												
Slight or moderate	0	1	2	1	0	0	5	0	18	10	-	-
Rough	0	1	0	1	0	0	0	0	3	7	3	9
Very rough or high	0	0	0	0	0	0	0	0	2	1	0	2
AUTUMN TRANSITION												
Slight or moderate	17	12	25	12	6	1	4	0	4	1	-	-
Rough	3	2	4	14	0	1	0	0	1	1	8	17
Very rough or high	3	6	1	2	0	0	0	0	0	1	4	8
Percent of time rough or higher (based on entire year)											13%	26%

	SEA	SWELL
Slight or moderate	1-5 Ft	1-6 Ft
Rough	5-8 Ft	6-12 Ft
Very rough or high	over 8 Ft	over 12 Ft

FIGURE 2 TABULATION OF SEA AND SWELL STATISTICS SOUTH CHINA SEA OFF CENTRAL RYN

STATISTICAL STUDIES OF THE OCEAN ENVIRONMENT RELATING TO PREDICTION

Edward V. Welser
Ordnance Research Laboratory
The Pennsylvania State University

INTRODUCTION

As part of the task of development of conversion techniques for use with acoustic homing torpedoes, statistical studies of the environment of the North Atlantic Ocean were implemented at the Ordnance Research Laboratory. Some of the results of those studies were applied as assumed thermal gradients for ray and intensity computations. Other results of the studies may be incorporated into environmental extrapolation schemes as well as environmental prediction techniques. This paper deals primarily with those statistical studies of the ocean environment relating to prediction.

DATA AND AREA

The data used in the investigations described in this paper were obtained through the efforts of the Naval Oceanographic Office and the National Oceanographic Data Center and consisted of those bathythermograph observations commonly referred to as the USNUSL Deck. The geographical area investigated was 20 through 60 degrees north latitude and 30 through 85 degrees west longitude inclusive.

HISTORICAL DATA SUMMARIZATION

The first phase of the statistical studies of the ocean environment dealt with oceanographic statistical summaries of historical bathythermograph data for the North Atlantic area. The statistical parameters studied were the frequency of occurrence, means, standard deviations and maximum and minimum observed values of the oceanographic variables, layer depth, temperature at various depths and thermal and sound velocity gradients of various depth intervals. Frequency distributions were computed on a seasonal basis while the means, standard deviations and maximum and minimum observed values of the oceanographic variables were computed for each month as well as on a seasonal basis.

The various parameters were computed for each one degree grid point centered at each latitude and longitude intersection in the North Atlantic area where one or more observations were available.

Table 1 presents the winter season temperature frequency distribution for the Key West, Florida area (24 degrees north latitude and 80 degrees

TABLE 1

PORTION OF THE WINTER SEASON TEMPERATURE FREQUENCY DISTRIBUTION FOR THE KEY WEST, FLORIDA AREA

TEMPERATURE (°F)	DEPTH IN FEET									
	0	30	50	100	150	250	330	490	655	820
65.0				2	3	30	38			
65.5					2	18	38			
66.0	2	3	4	2	3	23	40			
66.5	2	2		1	3	16	33	1		
67.0	2	1	2	6	2	41	47	2		
67.5			1	4	2	35	27			
68.0		2	2	2	10	44	35	2		
68.5	3	4	5	4	17	56	31			
69.0	8	4	3	6	28	67	44			
69.5	2	2	3	14	20	68	34			
70.0	8	10	13	28	46	81	39			
70.5	5	4	7	20	38	50	20			
71.0	8	16	22	51	81	79	28			
71.5	12	12	26	33	64	42	22			
72.0	31	43	47	65	87	65	26			
72.5	36	32	34	65	81	55	15			
73.0	56	71	75	96	76	50	20			
73.5	55	43	44	53	58	31	9			
74.0	74	91	95	98	98	35	9			
74.5	65	60	66	70	67	28	7			
75.0	116	119	111	104	94	24	4			
75.5	65	63	58	72	46	14	9			
76.0	128	116	125	98	63	23	4			
76.5	78	88	87	60	38	9	5			
77.0	109	108	98	62	33	14	8			
77.5	49	40	40	44	16	7	6			
78.0	72	75	65	40	30	8	7			
78.5	56	53	44	24	14	10	1			
79.0	60	59	54	36	29	12				
79.5	31	29	30	27	19	11	3			
80.0	54	47	49	38	27	10				
80.5	46	53	48	34	20	4				
81.0	31	25	18	15	11	2				
81.5	13	5	7	3	1	1				
Total Obs	1296	1296	1296	1286	1233	1154	987	15	5	3
Mean Temp	76.2	76.1	75.8	74.9	73.8	70.4	66.0	62.1	54.4	53.0
St Dev	2.8	2.8	2.8	3.1	3.1	4.2	5.3	6.4	2.8	1.2
Max Temp	86.1	86.0	86.0	86.0	84.2	82.1	79.5	73.3	57.0	54.0
Min Temp	65.9	65.8	65.8	54.3	64.2	50.0	48.7	50.0	50.3	51.7

west longitude). Temperature in degrees Fahrenheit for each half degree temperature over the observed temperature range is listed down the left side. The depth in feet is listed across the top. The value 116, located to the right of the 75.0 temperature, represents the number of times a temperature in the temperature range of 74.8 through 75.2 degrees Fahrenheit was observed at zero depth. The total number of observations, mean temperature, standard deviation, maximum and minimum observed temperatures for each depth for the winter season are listed across the bottom.

Table 2 displays the winter season sound velocity gradient frequency distribution for the Key West, Florida area. Sound velocity gradient in feet per second per 100 feet depth over the observed sound velocity range is listed down the left side. Depth intervals in feet are listed across the top. For example, the third column to the right of -25 contains the number 45 which represents the number of times a sound velocity gradient, computed using Wilson's equation, which fell in the range of -22.6 through -27.5 feet per second per 100 feet was obtained for the 100 through 150 foot depth interval. The total number of observations, means, standard deviations and also maximum and minimum computed sound velocities for each depth interval for the winter season are listed across the bottom.

Similar listings for thermal gradient and layer depth frequency distributions were computed but examples will not be presented at this time.

A tabular summary of the monthly mean temperature, standard deviation of the temperature, maximum and minimum observed temperatures and number of observations for various depths were prepared for publication for each latitude and longitude intersection for the North Atlantic area. Table 3 contains an example of the temperature summary printout. Each group is headed by its location in latitude and longitude. Depth in feet is listed down the left side. Each group consists of five columns containing the number of observations, mean temperature, standard deviation of temperature and maximum and minimum observed temperature for each depth listed. The locations are ordered by ascending longitude within ascending latitude. Missing locations indicate that there were no observations available for that particular latitude and longitude intersection.

Table 3 also illustrates the January temperature gradient and sound velocity gradient summaries for the Key West, Florida area. The temperature gradient summary, right, has depth interval in feet, number of observations, mean temperature gradient in degrees Fahrenheit per 100 feet, temperature gradient standard deviation and maximum and minimum observed temperature gradients listed from left to right at the top. The location, in this case the Key West area, heads each group. The sound velocity gradient summary, lower, has the same general format as the temperature gradient summary.

TABLE 2

PORTION OF THE WINTER SEASON SOUND VELOCITY GRADIENT
FREQUENCY DISTRIBUTION FOR THE KEY WEST, FLORIDA AREA

VELOCITY GRAD (FT/SEC/100')	DEPTH INTERVAL IN FEET						
	0-30	30-50	50-100	100-150	150-250	250-300	330-490
						1	
-150							
-145			1			1	
-140							
-135							
-130							
-125							
-120		1					
-115						1	
-110							
-105					1	1	
-100							
- 95						5	
- 90						3	
- 85					1	4	
- 80		1			1	6	
- 75		1		1	1	10	
- 70			1		2	15	
- 65		1	1		5	20	
- 60			2		8	16	1
- 55		4			12	36	
- 50	1	5	1		15	30	1
- 45	1	5	4	4	21	63	
- 40		8	9	8	25	71	1
- 35	4	13	15	22	34	101	
- 30	2	22	24	31	66	117	1
- 25	7	28	61	45	148	134	2
- 20	7	28	66	83	209	128	2
- 15	26	39	97	152	238	116	4
- 10	56	59	125	206	225	66	2
- 5	126	111	217	231	140	39	1
0	993	912	649	436	2	1	
5	71	53	12	11			
10	1	5	1	1			
15				1		1	
20	1			1			
Total Obs	1296	1296	1286	1233	1154	987	15
Mean Gradient	- 1.1	- 3.7	- 6.8	- 8.6	- 14.7	- 26.6	-19.0
Standard Dev	5.4	10.8	11.1	9.9	12.4	18.7	15.6
Max Negative	-49.9	-122.3	-144.4	-72.0	-102.5	-151.8	-53.9
Max Positive	22.5	11.5	8.1	18.9	3.6	74.7	2.0

TABLE 3

JANUARY OCEANOGRAPHIC SUMMARIES FOR THE KEY WEST, FLORIDA AREA

TEMPERATURE SUMMARY						TEMPERATURE GRADIENT SUMMARY					
DEPTH	OBS	MEAN	ST DEV	MAX	MIN	DEPTH	OBS	MEAN	ST DEV	MAX	MIN
0'	334	75.40	2.94	86.1	65.9	0-30'	334	- .44	1.01	1.7	- 8.7
30'	334	75.27	2.96	86.0	65.8	30-50'	334	- .80	2.03	1.5	-26.0
50'	334	75.11	3.00	86.0	65.8	50-100'	329	- 1.15	2.09	1.4	-26.0
100'	329	74.60	3.16	86.0	54.3	100-150'	309	- 1.14	1.27	.6	- 8.8
150'	309	74.04	3.06	84.2	65.0	150-250'	282	- 3.19	2.54	.3	-13.6
250'	282	70.81	4.03	82.7	61.5	250-330'	246	- 6.46	3.07	.0	-17.0
330'	246	65.63	4.94	78.2	53.5	330-490'	5	- 5.50	2.41	-3.1	- 9.4
490'	5	56.20	4.31	60.9	50.0	490-655'	3	- 2.44	0.67	-1.8	- 3.2
655'	3	52.67	2.06	54.1	50.3	655-820'	1	0.00	0.00	-1.2	- 1.2
820'	1	51.70	0.00	51.7	51.7						

SOUND VELOCITY GRADIENT SUMMARY

DEPTH	OBS	MEAN	ST DEV	MAX	MIN
0-30'	334	- .32	4.51	8.5	- 37.8
30-50'	334	- 1.92	9.37	8.6	-122.3
50-100'	329	- 3.58	10.45	8.1	-144.4
100-150'	309	- 3.51	5.73	4.2	- 36.3
150-250'	282	-13.42	12.33	3.0	- 63.7
250-330'	246	-30.94	16.38	1.6	- 88.7
330-490'	5	-29.62	14.91	-16.0	- 53.9
490-655'	3	-13.42	3.86	- 9.5	- 17.2
655-820'	1	0.00	0.00	- 5.7	- 5.7

TEMPERATURE (^{o}F)

TEMPERATURE GRAD (^{o}F/100 FT)

SOUND VEL GRAD (FT/SEC/100 FT)

The above-mentioned historical data summarizations are being used by the Ordnance Research Laboratory in detection range prediction techniques in order to determine pre-firing weapon settings for specified torpedoes.

BATHYTHERMOGRAPH CLASSIFICATION

Bathythermograph data can also be summarized by defining classes of traces and then assigning each individual bathythermograph observation to the class in which it falls. The second phase of the statistical study of the North Atlantic area relating to prediction employed a classification scheme.

The Naval Research Establishment (NRE Report 60/3, 1960) devised a routine for the machine classification of bathythermograph profile types based on thermal gradients. A slightly modified version of that routine, which contained twelve profile types (See Figure 1) was computer programmed and bathythermograph data for the North Atlantic area were analyzed. Table 4 presents the monthly per cent of occurrence for each class for the entire North Atlantic area as well as the annual summary for each classification type and the number of observations which did not fit any of the twelve profile types (UNCL). Note that only about 0.02 per cent of the observations did not fit one of the twelve classes. In general, type 7 (the quasi-isothermal case) is a winter phenomenon occurring in 51 per cent of the January observations. It occurred less than 1 per cent of the time in each of the summer months of July, August and September. Type 11 also occurred primarily in the winter. Type 7 and/or type 11 occurred in approximately 75 per cent of the January observations. Types 5 and 6 are mostly summer phenomena and account for 44 per cent of the July observations. Types 3 and 12 tend to be more prevalent in the late summer and early fall and account for 57 per cent of the October observations.

Monthly sums for each class for each latitude and longitude intersection in the area were part of the classification analysis; however, a poor areal distribution of observations prohibited conclusions about the areal distribution of class types for a given month. The results were encouraging enough to warrant analyses of the data on a seasonal basis. A cursory look at the winter season distribution of the per cent of occurrence of types 7 and 11, which were analyzed without regard to area variation or sample size, revealed a relatively constant percentage for each type in the mid-latitudes except for the Gulf Stream area. The investigation of the areal distribution of classification types is continuing.

The NRE classification scheme allows a relatively large variation of temperature gradients within each classification type. Figure 2 illustrates the extreme cases of type 1. For computation of ray diagrams and intensity losses calculated for a particular torpedo, the extremes

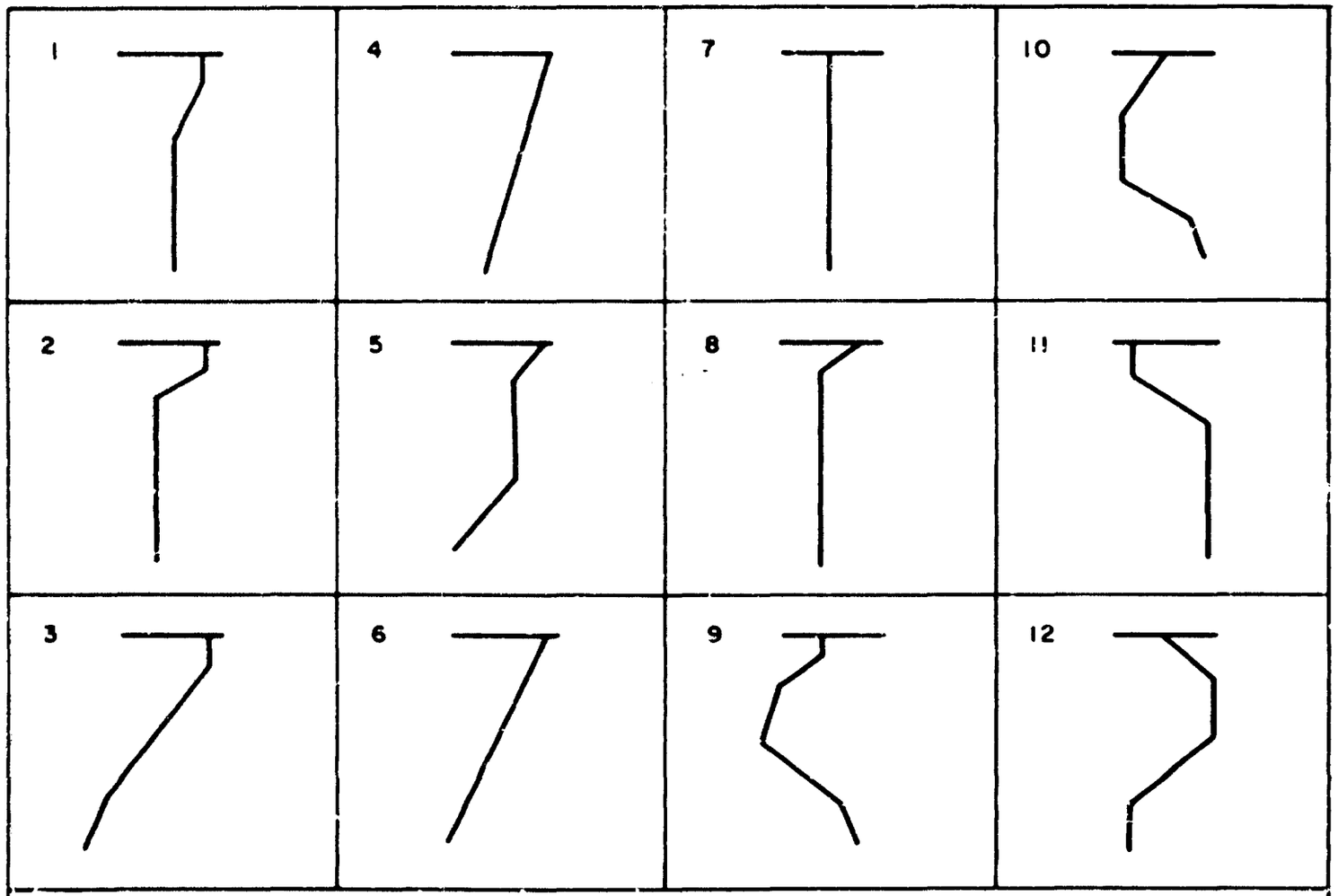

Figure 1. Simplified NRE Thermal Profile Types

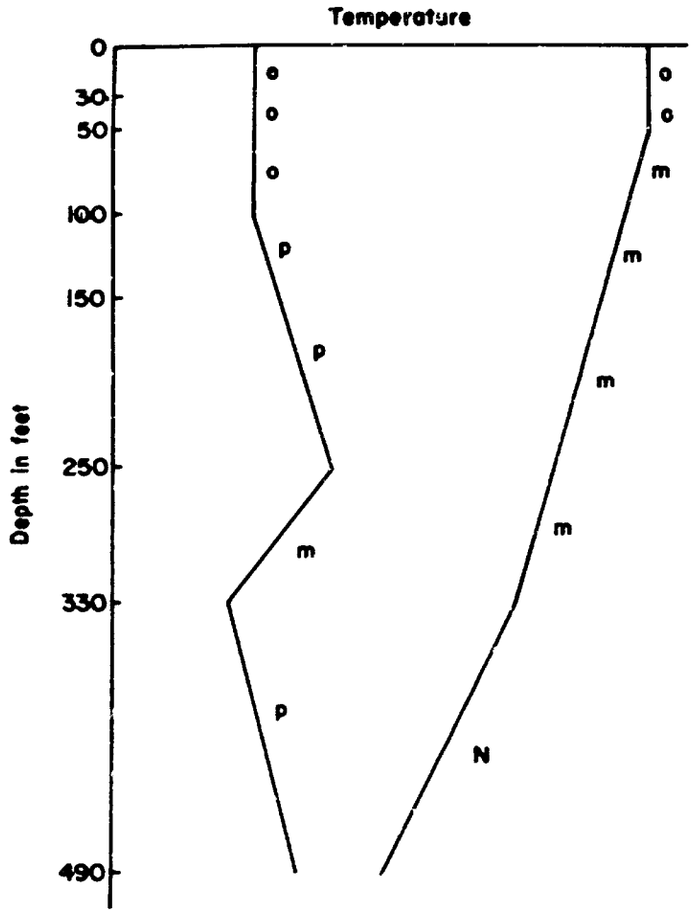

Sign and Intensity of the Temperature Gradient per 100 Feet Depth

Description	Symbol	Temperature Gradient (°F)
Strong Positive	P	>1
Weak Positive	p	1 to 0.3
Zero	O	0.3 to -1
Weak Negative	n	-1 to -2
Moderate Negative	m	-2 to -4
Strong Negative	N	< -4

Figure 2. Extreme Cases of Bathythermograph Classification Type I.

TABLE 4

PER CENT OF OCCURRENCE OF BATHYTHERMOGRAPH TYPES FOR THE NORTH ATLANTIC AREA

	CLASSIFICATION TYPE													
MONTH	1	2	3	4	5	6	7	8	9	10	11	12	UNCL	OBS
JAN	8.38	.60	4.35	2.02	.74	1.09	51.08	2.71	2.21	.72	23.59	2.49	1	5977
FEB	9.05	.44	4.06	1.77	1.24	3.38	49.29	3.61	1.33	.70	22.74	2.36	2	6310
MAR	9.10	.34	4.07	3.29	1.56	3.29	43.93	6.72	1.55	1.09	21.80	3.20	5	7055
APR	15.40	1.76	3.42	6.28	3.98	3.01	29.33	7.70	3.13	2.93	17.27	4.75	3	8569
MAY	18.57	3.58	7.85	9.06	11.02	9.49	8.32	3.57	4.92	8.36	5.81	9.42	2	9462
JUNE	13.92	6.26	16.14	5.34	12.48	17.11	2.04	.71	5.53	8.49	.76	11.22	1	13283
JULY	4.35	7.28	18.30	2.01	20.43	23.82	.55	.24	2.78	9.12	.63	10.48	1	10397
AUG	3.01	8.74	28.43	.84	12.82	19.74	.25	.05	3.29	6.95	.12	15.76	1	10347
SEPT	4.13	8.80	36.56	1.41	8.06	11.58	.39	.13	6.56	4.28	.36	17.71	1	9734
OCT	11.29	4.87	38.52	2.06	3.57	2.71	3.68	.26	9.54	1.54	2.57	18.91	0	7345
NOV	16.63	1.94	24.00	2.24	1.57	1.08	17.11	.97	12.63	.90	7.90	13.01	1	6872
DEC	13.33	.53	15.00	2.38	1.26	.36	35.00	1.90	7.45	.79	16.26	5.70	1	6038
ANNUAL	10.47	4.39	17.52	3.40	7.85	9.74	16.30	2.17	5.01	4.66	8.22	10.24	19	101409

are acoustically dissimilar. For that reason ORL is in the process of defining sub-classes of the thermal gradient classification scheme.

The object of the investigation of the areal distribution of the per cent of occurrence of a classification type is to try to predict the type of temperature profile that is to be expected given latitude, longitude and the season and then provide the proper torpedo settings for that acoustical structure.

MULTIPLE REGRESSION WITH PARSIMONY

Multiple regression analysis was also investigated as to its feasibility to be used to determine the thermal structure of the medium given certain meteorological and oceanographic data.

Table 5 presents the thirty variables used in the original analysis. As part of the regression analysis, simple correlations (See Table 6) were computed for all combinations of pairs of the thirty variables as well as the mean and standard deviation for each variable. Simple correlations permit conclusions as to a linear relationship between two variables, but do not indicate which variable causes the variation of the other. Indeed, simple correlations may indicate a relationship between two variables because of autocorrelation with a third variable. For example, Table 6 indicates that the temperature at zero feet depth is highly correlated with the 30 foot depth temperature while the 30 foot depth temperature is highly correlated with the 50 foot depth temperature; however, partial correlations reveal that the relationship between the 30 and 50 foot depth temperatures may have been induced because both have a "real" correlation with the zero foot depth temperature. Recognizing this limitation, one may still subjectively draw useful conclusions from the linear relationship between two variables.

Multiple regression with parsimony analysis was used to study how well different variables may be predicted from known values of other variables as well as to objectively eliminate those variables from the regression equation which do not contribute significantly to the explained variance of the regression. In other words, the least square technique was used to fit the data while parsimony objectively eliminated those variables which were poorly related to the variable being predicted. Only bathythermograph observations that were complete to a depth of 820 feet were used in the investigation.

Table 7 is an example of the multiple regression with parsimony printout. The 50 foot depth temperature is the dependent variable. Listed are the regression coefficients, partial correlation coefficients, number of variables eliminated, variable having the smallest partial correlation coefficient (candidate for elimination), the F-ratio which is the ratio of the variance of the eliminated variables and candidate variable to the unexplained variance with none eliminated, multiple correlation coefficient and the intercept of the regression equation.

TABLE 5

VARIABLES USED IN THE INITIAL MULTIPLE REGRESSION
WITH PARSIMONY ANALYSIS

1	WATER TEMPERATURE AT 0' DEPTH
2	WATER TEMPERATURE AT 30' DEPTH
3	WATER TEMPERATURE AT 50' DEPTH
4	WATER TEMPERATURE AT 100' DEPTH
5	WATER TEMPERATURE AT 150' DEPTH
6	WATER TEMPERATURE AT 250' DEPTH
7	WATER TEMPERATURE AT 330' DEPTH
8	WATER TEMPERATURE AT 490' DEPTH
9	WATER TEMPERATURE AT 655' DEPTH
10	WATER TEMPERATURE AT 820' DEPTH
11	LAYER DEPTH
12	WIND SPEED
13	BUCKET TEMPERATURE
14	WET-BULB TEMPERATURE
15	DRY-BULB TEMPERATURE
16	WEATHER
17	SEA STATE
18	CLOUD COVER
19	LATITUDE
20	LONGITUDE
21	MONTH
22	0-30' TEMPERATURE GRADIENT
23	30-50' TEMPERATURE GRADIENT
24	50-100' TEMPERATURE GRADIENT
25	100-150' TEMPERATURE GRADIENT
26	150-250' TEMPERATURE GRADIENT
27	250-330' TEMPERATURE GRADIENT
28	330-490' TEMPERATURE GRADIENT
29	490-655' TEMPERATURE GRADIENT
30	655-820' TEMPERATURE GRADIENT

TABLE 6

PORTION OF THE WINTER SEASON SYMMETRIC CORRELATION MATRIX
FOR THE NORTH ATLANTIC AREA 879 CASES

Variable	0'	30'	50'	100'	150'	250'	330'	490'	655'	820'
30' Temperature	0.998									
50' Temperature	0.999	0.998								
100' Temperature	0.997	0.996	0.998							
150' Temperature	0.989	0.988	0.990	0.995						
250' Temperature	0.968	0.966	0.968	0.975	0.988					
330' Temperature	0.935	0.934	0.936	0.944	0.960	0.981				
490' Temperature	0.856	0.855	0.857	0.863	0.880	0.897	0.925			
655' Temperature	0.783	0.782	0.783	0.789	0.809	0.825	0.851	0.932		
820' Temperature	0.703	0.703	0.703	0.711	0.732	0.745	0.764	0.838	0.942	
Layer Depth	-0.332	-0.332	-0.335	-0.330	-0.310	-0.271	-0.195	-0.016	-0.112	0.112
Wind Speed	-0.071	-0.066	-0.066	-0.066	-0.069	-0.079	-0.088	-0.072	-0.067	-0.051
Bucket Temperature	0.975	0.974	0.975	0.977	0.972	0.955	0.923	0.848	0.778	0.703
Wet Bulb Temperature	0.781	0.780	0.781	0.783	0.783	0.780	0.765	0.688	0.632	0.579
Dry Bulb Temperature	0.849	0.847	0.848	0.852	0.854	0.851	0.832	0.751	0.692	0.634
Weather	-0.081	-0.080	-0.077	-0.080	-0.083	-0.096	-0.106	-0.095	-0.088	-0.086
Sea State	-0.086	-0.081	-0.084	-0.080	-0.076	-0.074	-0.087	-0.097	-0.106	-0.069
Cloud Cover	-0.109	-0.109	-0.107	-0.108	-0.114	-0.119	-0.116	-0.036	-0.014	-0.003
Latitude	-0.811	-0.809	-0.810	-0.812	-0.814	-0.813	-0.799	-0.715	-0.575	-0.461
Longitude	0.119	0.119	0.118	0.111	0.101	0.087	0.076	0.119	0.080	-0.006
Month	0.192	0.191	0.187	0.184	0.178	0.165	0.182	0.301	0.235	0.172
0-30' Temp Grad	-0.064	-0.003	-0.053	-0.052	-0.051	-0.052	-0.048	-0.041	-0.039	-0.030
30-50' Temp Grad	-0.023	-0.071	-0.008	-0.006	-0.003	-0.007	-0.004	-0.006	-0.017	-0.019
50-100' Temp Grad	-0.137	-0.135	-0.134	-0.074	-0.025	0.015	0.037	0.016	0.024	0.060
100-150' Temp Grad	-0.158	-0.158	-0.157	-0.128	-0.028	0.045	0.085	0.098	0.136	0.152
150-250' Temp Grad	-0.364	-0.364	-0.367	-0.354	-0.311	-0.158	-0.101	-0.101	-0.095	-0.096
250-330' Temp Grad	-0.368	-0.366	-0.366	-0.362	-0.346	-0.308	-0.117	-0.055	-0.051	-0.065
330-490' Temp Grad	-0.455	-0.454	-0.455	-0.462	-0.465	-0.478	-0.463	-0.093	-0.056	-0.048
Mean	70.345	70.342	70.299	70.208	70.051	69.748	69.320	67.224	65.076	65.353
Standard Deviation	5.318	5.308	5.294	5.261	5.220	5.024	4.813	4.284	3.968	3.986

TABLE 7

MULTIPLE REGRESSION WITH PARSIMONY

WINTER SEASON - 50' TEMPERATURE IS DEPENDENT

INDEPENDENT VARIABLE	REGRESSION COEFFICIENT	STANDARD DEVIATION FOR COEFFICIENT	PARTIAL CORRELATION
0' DEPTH TEMPERATURE	0.97352	0.00615	0.9831
WIND SPEED	0.00170	0.00048	0.1200
BUCKET TEMPERATURE	0.02693	0.00641	0.1413
WET-BULB TEMPERATURE	0.00612	0.00357	0.0581
DRY-BULB TEMPERATURE	-0.01564	0.00447	-0.1179
WEATHER	0.00124	0.00062	0.0677
SEA STATE	0.00008	0.00072	0.0040
CLOUD COVER	0.00040	0.00031	0.0440
LATITUDE	-0.00977	0.00326	-0.1011
LONGITUDE	-0.00069	0.00062	-0.0373
MONTH	-0.00380	0.00096	-0.1333

NUMBER OF VARIABLES ELIMINATED - 0

CANDIDATE FOR NEXT ELIMINATION - SEA STATE

F-RATIO OF VARIANCE OF AGGREGATE ELIMINATED AND CANDIDATE VARIABLES TO UNEXPLAINED VARIANCE WITH NONE ELIMINATED - 0.0137

FRACTION OF EXPLAINED VARIANCE - 0.998

MULTIPLE CORRELATION COEFFICIENT - 0.9992

INTERCEPT (B(o)) - 0.9238

Note that the eleven independent variables explain 0.998 of the variance; the multiple correlation coefficient, which is a measure of how well the regression equation fits the data, is 0.9992 and that sea state has the smallest partial correlation coefficient 0.0040. Table 8 presents the regression analysis with sea state removed from the analysis. Note that even though sea state was removed, the variance of the 50 foot depth temperature explained by the remaining ten variables as well as the multiple correlation coefficient remained the same. Longitude was the next variable to be eliminated. The procedure was repeated until only one independent variable remained.

Table 9 illustrates the terminal regression analysis for the 50 foot depth temperature. Only the temperature at the zero foot depth remained, but it alone explained the same amount of the variance of the 50 foot depth temperature as all eleven variables had (.998) and the fit of the regression remained the same (.9992).

Thus, regression analysis with parsimony revealed that in the winter the temperature at the 50 foot depth could be predicted by using the equation:

$$T_{50} = 0.328 + 0.995\ T_o \qquad \text{(Winter)}$$

A similar analysis for the summer season resulted in the following equation:

$$T_{50} = -0.632 + 1.003\ T_o \qquad \text{(Summer)}$$

A cursory investigation of the explained variances of the summer and winter season analyses indicated that temperatures to a depth of 100 feet and 250 feet respectively may be adequately described by one or more of the independent variables: bucket temperature, zero depth bathythermograph temperature, latitude or month of the year.

Additional investigations are being carried out utilizing the technique of multiple regression with parsimony. Other independent variables are being introduced into the regression analysis and the analysis will be extended to areas of adequate observations on a monthly basis. It is hoped that given latitude, longitude, month or season, and a limited number of surface or sub-surface variables, the acoustical structure may be adequately predicted.

TABLE 8

MULTIPLE REGRESSION WITH PARSIMONY

WINTER SEASON - 50' TEMPERATURE IS DEPENDENT

INDEPENDENT VARIABLE	REGRESSION COEFFICIENT	STANDARD DEVIATION FOR COEFFICIENT	PARTIAL CORRELATION
0' DEPTH TEMPERATURE	0.97344	0.00611	0.9833
WIND SPEED	0.00171	0.00047	0.1227
BUCKET TEMPERATURE	0.02697	0.00640	0.1417
WET-BULB TEMPERATURE	0.00611	0.00357	0.0580
DRY-BULB TEMPERATURE	-0.01563	0.00447	-0.1178
WEATHER	0.00124	0.00062	0.0677
CLOUD COVER	0.00040	0.00031	0.0445
LATITUDE	-0.00980	0.00325	-0.1019
LONGITUDE	-0.00069	0.00062	-0.0378
MONTH	-0.00381	0.00095	-0.1342

NUMBER OF VARIABLES ELIMINATED - 1

IDENTITY - SEA STATE

CANDIDATE FOR NEXT ELIMINATION - LONGITUDE

F-RATIO OF VARIANCE OF AGGREGATE ELIMINATED AND CANDIDATE VARIABLES TO UNEXPLAINED VARIANCE WITH NONE ELIMINATED - 0.6267

FRACTION OF EXPLAINED VARIANCE - 0.998

MULTIPLE CORRELATION COEFFICIENT - 0.9992

INTERCEPT (B(o)) - 0.9296

TABLE 9

MULTIPLE REGRESSION WITH PARSIMONY

WINTER SEASON - 50' TEMPERATURE IS DEPENDENT

INDEPENDENT VARIABLE	REGRESSION COEFFICIENT	STANDARD DEVIATION FOR COEFFICIENT	PARTIAL CORRELATION
0' DEPTH TEMPERATURE	0.99468	0.00135	0.9992

NUMBER OF VARIABLES ELIMINATED - 10

IDENTITY - SEA STATE
LONGITUDE
CLOUD COVER
WET-BULB TEMPERATURE
DRY-BULB TEMPERATURE
LATITUDE
WEATHER
BUCKET TEMPERATURE
WIND SPEED
MONTH

CANDIDATE FOR NEXT ELIMINATION - 0' DEPTH TEMPERATURE

F-RATIO OF VARIANCE OF AGGREGATE ELIMINATED AND CANDIDATE VARIABLES TO UNEXPLAINED VARIANCE WITH NONE ELIMINATED - 52204.4340

FRACTION OF EXPLAINED VARIANCE - 0.998

MULTIPLE CORRELATION COEFFICIENT - 0.9992

INTERCEPT (B(o)) - 0.3281

VALUE OF THE DETERMINANT - 0.000099

AVERAGE ABSOLUTE DEVIATION FROM ORIGINAL ELEMENTS OF INVERSE INVERSE MATRIX ELEMENTS - 0.000005528

SUMMARY

As part of the task of development of conversion techniques for use with acoustic homing torpedoes, statistical studies of the North Atlantic Ocean environment related to prediction were implemented. The investigation of the environment was initiated for each one degree of latitude and longitude in three ways: (1) historical data summarization, (2) bathythermograph profile classification and (3) multiple regression with parsimony analysis.

As part of the historical summarization, frequency distributions of temperature, temperature gradient, sound velocity gradient and layer depth were tabulated on a seasonal basis. Means, standard deviations and maximum and minimum observed values were computed for temperature, temperature gradient and sound velocity gradient for each month.

The classification of bathythermograph observations by months for the entire North Atlantic area revealed that most observations fell into one of the NRE classes. Types 7 and 11 account for 75 per cent of the winter cases, types 5 and 6 account for 44 per cent of the July cases, while types 3 and 12 account for 57 per cent of the October cases.

The areal distribution of bathythermograph observations was poor; however, a cursory examination of the winter season summarization of profile types by one degree squares showed a relatively even distribution of the per cent of occurrence of types 7 and 11 in the mid-latitudes. The initial multiple regression analysis of the North Atlantic area bathythermograph data which were complete to 820 feet revealed that summer and winter season temperatures to a depth of 100 feet and 250 feet respectively may be predicted from such independent variables as the bucket temperature, zero depth temperature, latitude or month.

DEPTH AND STRENGTH OF THE SEASONAL THERMOCLINE IN SHALLOW WATER OFF SOUTHERN CALIFORNIA

By

J. L. Cairns
U. S. Navy Electronics Laboratory
San Diego, California 92152

INTRODUCTION

Vertical thermal structure data recorded continuously over a two month period at the U. S. Navy Electronics Laboratory Oceanographic Research Tower indicate that periodic oscillations occur in the strength of the seasonal thermocline. In view of the effects that thermocline strength and depth oscillations have on underwater sound transmission, an increased knowledge of these phenomena is of vital importance to Naval operations.

This study has shown that relative changes in thermal gradient strength may be inferred from its state of vertical motion, which, in turn, is related principally to the tides, and the local wind velocity. The most pronounced variations in both thermocline depth and strength occur as a result of tidal forces. It has been found that based on the phase of the tide it is possible to draw some conclusions as to the strength, and state of motion of the thermal gradient layer.

DATA

Collection

Data for this study were acquired utilizing a vertical array of temperature sensors at the NEL Tower, located one mile off Mission Beach, California, in sixty feet of water. The lowest of these sensors was located two feet above the sea floor, with nine others located at intervals of six feet thereafter, the uppermost being 56 feet from the sea floor. These thermistor bead sensors were potted in polyeurathane to increase their thermal response time to 20 minutes. Data were collected by scanning the array from bottom to top once every ten minutes, the scan cycle being controlled by a precision clock. The absolute accuracy of the system in the range of interest was $\pm 0.06^{\circ}C$, with a relative accuracy of measurements between adjacent sensors of $\pm 0.03^{\circ}C$. Results of each scan were recorded to the nearest hundredth degree Celsius on a digital printer system. The present study is based on data acquired with this system from 28 April 1965, to 25 June 1965.

Description

A typical example of the data from one scan of the array is shown in figure 1. Bathythermograph records taken throughout past years indicate that the strong seasonal thermocline exhibited by this figure becomes established along the Southern California coast by about the end of March, and remains strong until late fall. It has been shown (Cairns, LaFond; 1965) that the thermal gradient layer undergoes vertical oscillations of as much as 50 feet in this area, and that except for short period internal waves, these are predominantly of diurnal and semi-diurnal periods. The object of the present study was to determine what effects, if any, these oscillations and other factors have on the strength of the vertical temperature gradient in the thermocline.

Analysis

To examine in detail the strength and extent of thermal gradients present in the water column, temperature values were computed for depths between those of the temperature sensors as shown in figure 2. In this figure points have been smoothly interpolated between the measured values of figure 1 by computing the second derivative of each measured point using a five point difference equation. The second derivatives were then linearly interpolated in the intervals between points to compute intermediate temperature values. The resulting set of points are spaced at depth intervals of 1.5 feet throughout the water column. The thermal gradient in °C/ft in each of these small intervals was computed.

Through the above method it was possible to examine the vertical distribution of gradient strength as well as temperature for each scan of the array. The gradient distribution information was then plotted as a function of time by contouring areas of equal gradient strength, resulting in a contoured record that clearly illustrates the behavior of the thermal gradient as a function of time.

GRADIENT STRENGTH, GENERAL

During the period of observation, thermal gradient strength changes of 0.2° to 0.3°C/ft were often seen to occur within several hours, and at no time was the strength constant for more than a few hours at a time. However, the temperature near the center of the steep section of the gradient, remained approximately constant. Typical sections of the contoured thermal gradient record averaged hourly are shown in figures 3, 4, and 5 which each include six semi-diurnal cycles and which were chosen to exhibit its behavior during spring tide (fig. 3), neap tide (fig. 4), and a period after spring tide (fig. 5). With few minor exceptions, the 14°C isotherm, shown

in these figures, was centrally located in the steep section of the thermal gradient during the entire record, a fact which adds considerable support to work done in the past on thermocline motion based on isotherm follower data (LaFond, 1961). This temperature stability is best shown in figure 3 where the gradient appears to diffuse on several occasions, only to strengthen a short time later at the same temperature.

Another feature noted is that only one strong thermal gradient was present in the water column during the experiment. As shown in the figures, transient gradients did appear frequently, however these never persisted for more than a few hours and, compared to the main thermocline, were always weak. These formed below the main thermocline nearly as often as above it. Inversion gradients, on the other hand, were found to occur only above the principal gradient. Only four relatively strong inversions ($\frac{dT}{dz} < -0.1°C/ft.$) were observed, two of which are shown as very dark shaded areas on May 17, in figure 5. None of these lasted for more than two hours. The feature most clearly brought out by the contoured record, however, is the tendency of the gradient strength to oscillate with the tides.

THEORY

There is good reason to expect that the thermocline should be weaker at the ascending and descending phases of the tide than at the tidal highs and lows, and also that it should remain stronger during neap tide than during spring tide. The mechanism responsible for this is turbulent mixing due to shear. Turbulent mixing of the thermocline occurs when there are strong opposing currents above and below the gradient - a situation which occurs near the coast twice during each semi-diurnal tidal cycle as shown in figure 6. Single frequency sinusoidal internal and surface tides have been used in this figure for ease of interpretation. In keeping with existing information in this area (Cairns, LaFond; 1965) the internal tide is shown lagged behind the surface tide by four hours, and is five times as great as the surface tide in amplitude.

At point A in figure 6, just past the high of the internal tide, the relative current above and below the thermocline is zero, and a strong undisturbed gradient is to be expected. At point B, however, the relative current velocity is maximum causing the gradient to weaken. At point C the relative current is again zero and the gradient should be strong. When point D is reached, the shear is high with an expected weaker gradient. It should be pointed out that the minimum currents occur at the tidal highs and lows along the coastal boundary only, since in the open sea the maximum horizontal particle velocities occur at the extremes of the tide rather than midway between the highs and lows.

In the present case, where the internal tidal oscillation is given as

$$z = A \sin (\omega t + \gamma)$$

the variations in gradient strength resulting from shear turbulence may be written as

$$\frac{\partial}{\partial t} \left\{ \frac{\partial T}{\partial z} \right\} \propto A \sin (2\omega t + \gamma)$$

or, upon integration

$$\frac{\partial T}{\partial z} \propto - \frac{A}{2\omega} \cos (2\omega t + \gamma)$$

where

$\frac{\partial T}{\partial z}$ is the thermal gradient
ω is the internal tidal frequency
A is the internal tidal amplitude
γ is the initial phase angle, and
t is the time.

With the high amplitude spring tides the relative current velocity above and below the thermocline is high, causing increased disturbance of the gradient and diminishing its strength. The disturbance during neap tide, however, is decreased and generally stronger gradients are to be expected.

THE SEMI-DIURNAL GRADIENT CYCLE

Throughout most of the data record the strength of the thermal gradient was found to vary in a definite pattern as the thermocline moved through its semi-diurnal depth cycle. In this pattern, the thermocline was strongest during the low of the internal tidal cycle. As it ascended from low tide, the gradient strength decreased sharply, as seen in figures 3, 4, and 5. Approaching the high of the internal tide the thermocline strengthened, reaching relatively high values at the tides crest. Subsequent descent was then accompanied by a decrease in strength, and later an increase as the low of the tide approached.

Although internal tidal cycles are often distorted as a result of wind transport effects, in the record under study 78 of these cycles were found to be well defined. This represents over 90% of the entire record length. As an indication of the regularity with which the previously described strength variation pattern occurred,

in 82% of the 78 tidal cycles the gradient was found to be weaker on the ascending tide than both the preceding low tide gradient and the subsequent high tide gradient. And in 68% of the tidal cycles the gradient was weaker on the descending tide than both the preceding high and the following low tide gradients. In other words, these two categories include only cases where the gradient strength passed through a minimum during the ascending and descending tide respectively.

The strength of the maximum gradient in the thermocline was averaged over one hour intervals at high tide and low tide and at one hour intervals midway between successive highs and lows. Table 1 lists these values at the various phases of the internal tidal cycle further

TABLE 1

Phase of Internal Tide	Gradient Strength (°C/ft) Spring Tide	Neap Tide
High	.22± .01	.28± .08
Descending	.20± .05	.26± .08
Low	.24± .06	.33± .11
Ascending	.18± .02	.25± .06

averaged over four day periods two days before and after peak spring tides and over the same periods during neap tides. This table illustrates the changes in gradient strength just described. Although the standard deviations listed with these values are large, it must be remembered that these represent deviations in the gradient strength due to all causes, and do not necessarily represent deviations in this cyclic pattern of variations.

THE BI-WEEKLY GRADIENT CYCLE

A change in the behavior of the thermal gradient has been found to occur in the interval from spring to neap tide. The surface tides in the tower area are the ordinary mixed type with the semi-diurnal components dominating; thus, spring tides, those with the greatest range, and neap tides, those with the least range, reoccur at intervals of 14.3 days (Sverdrup, et al; 1942). The gradient record shows that the oscillations of the internal tide during spring and neap periods were much the same as those of the surface tide; growing in amplitude with spring tide (fig. 3), and decreasing at neap tide (fig. 4). A shift in the strength and character of the thermocline was discernible with this change in amplitude.

As shown in figure 4, during neap tide the gradient remained relatively strong and coherent through the tidal depth oscillations. With the onset of higher spring tides, however, it weakened, showing a greater tendency to break up and diffuse, (fig. 3). This variation is also evident in the average of the maximum gradient in the thermocline taken from the values in table 1 where the average during spring tides was 0.21± .05°C/ft as compared to that during neap tides which was 0.28± .09°C/ft, indicating that on the average the gradient was about 25% stronger during neap tide than during spring tide.

SUMMARY AND CONCLUSIONS

Several important aspects of the seasonal thermocline have been concluded from this study. Among these are:

(1) The strength of the thermocline is highly variable, however many of these variations occur in an orderly, and to some extent predictable manner. Those changes which occur regularly are: (A) that the gradient is relatively stronger during neap tide than during spring tide, and (B) that the gradient is stronger during the highs and lows of the internal tide than during the ascending and descending phases of the tide.

(2) Throughout the 14 day cycle of spring and neap tides the tidal oscillations at the internal boundary behave much the same as those of the surface tide; growing in amplitude with spring tides, and decreasing with neap tides.

Thus, the phase of the tide provides an indication of the relative strength and oscillation amplitude of the thermal gradient layer.

REFERENCES

Cairns, J. L., E. C. LaFond, 1965, Prediction of Summer Thermocline Depth off Mission Beach, Proceedings, Second U. S. Navy Symposium on Military Oceanography, Vol. 1:113-132.

LaFond, E. C., 1961, The Isotherm Follower, J. Mar. Res., 19, 1:33-39.

Sverdrup, H. U., M. W. Johnson, R. H. Fleming, 1942, The Oceans, 14:545-565.

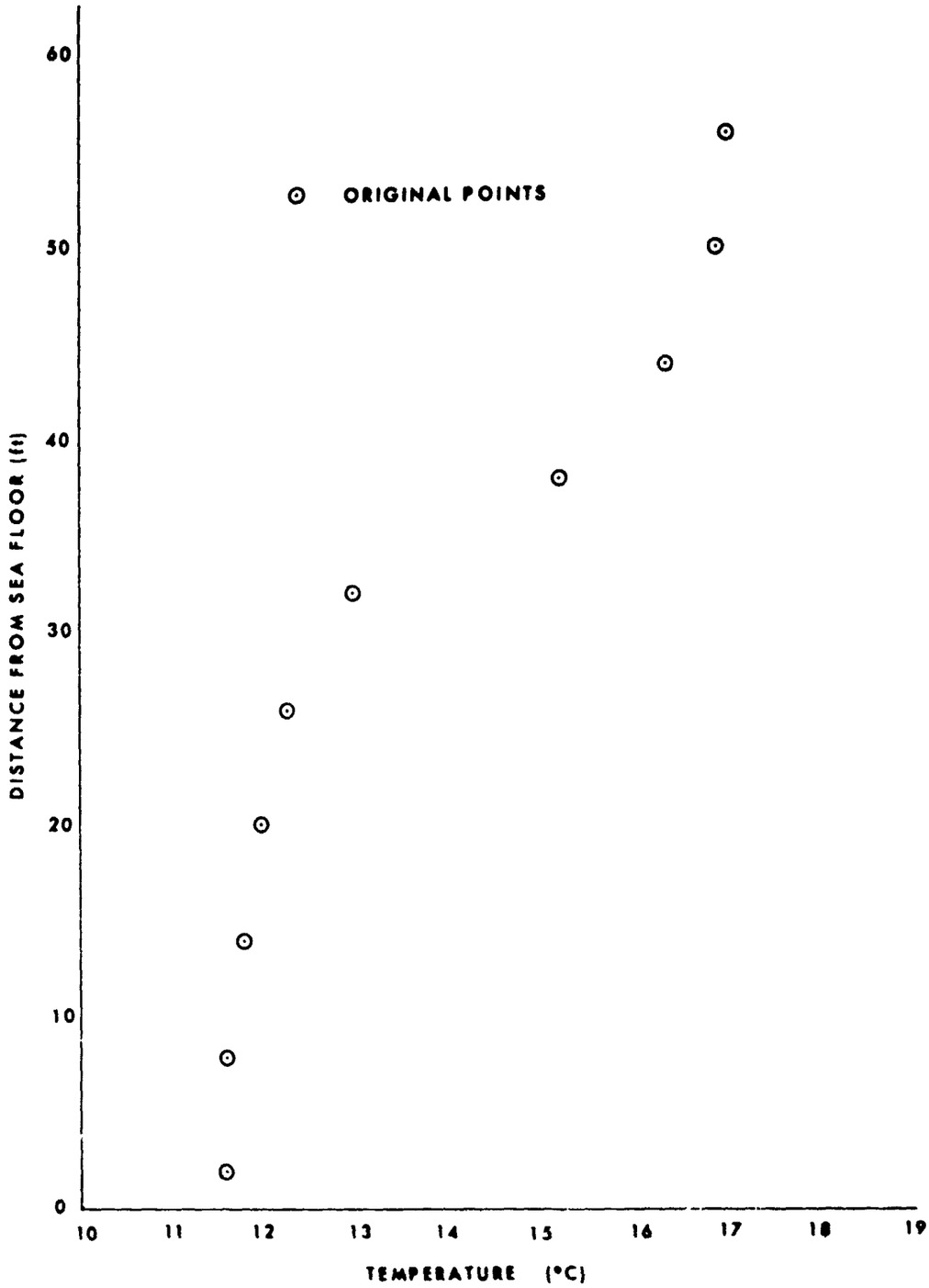

Figure 1 Temperature measurements from one scan of the array.

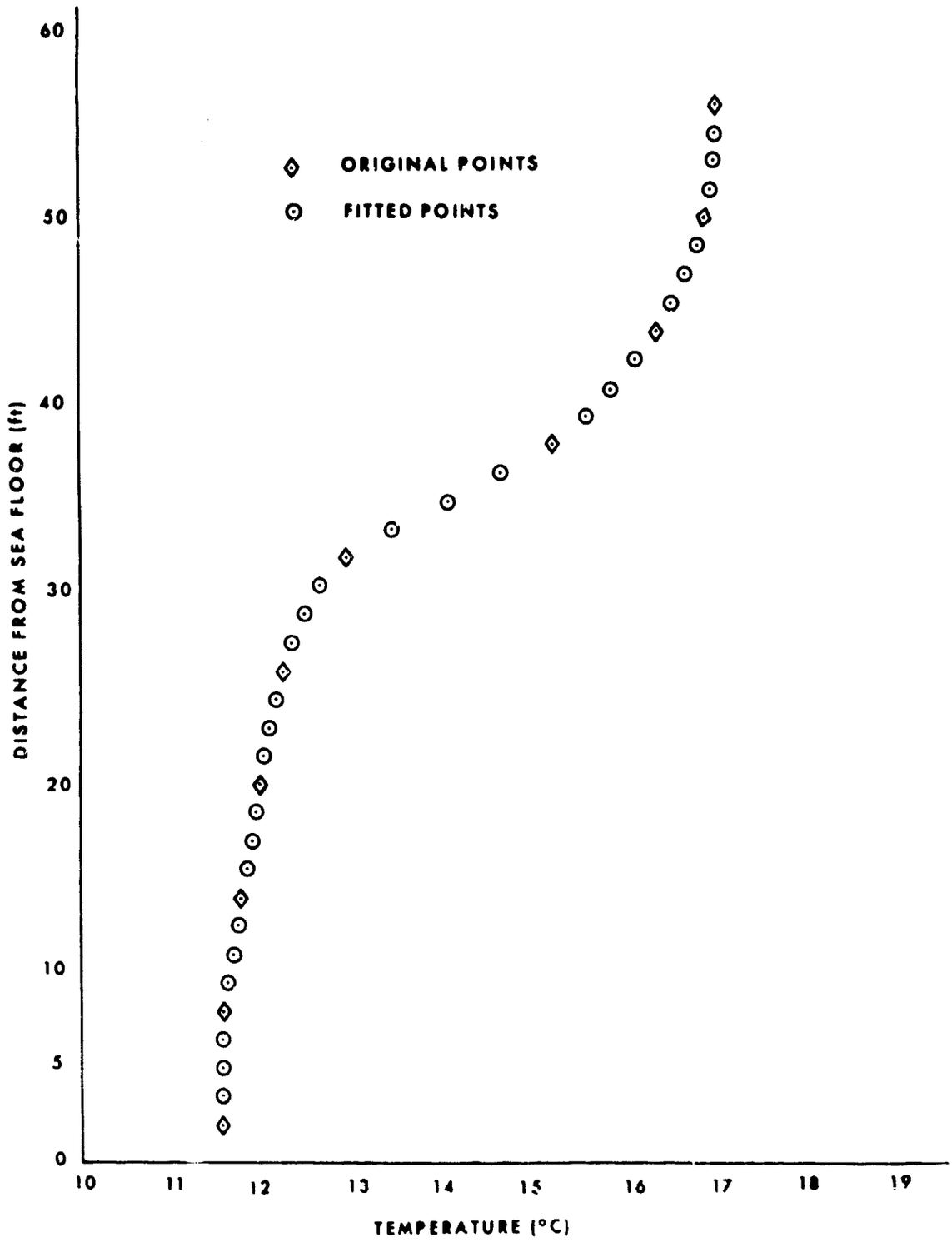

Figure 2 Temperature measurements from one scan of the array with fitted intermediate temperature points.

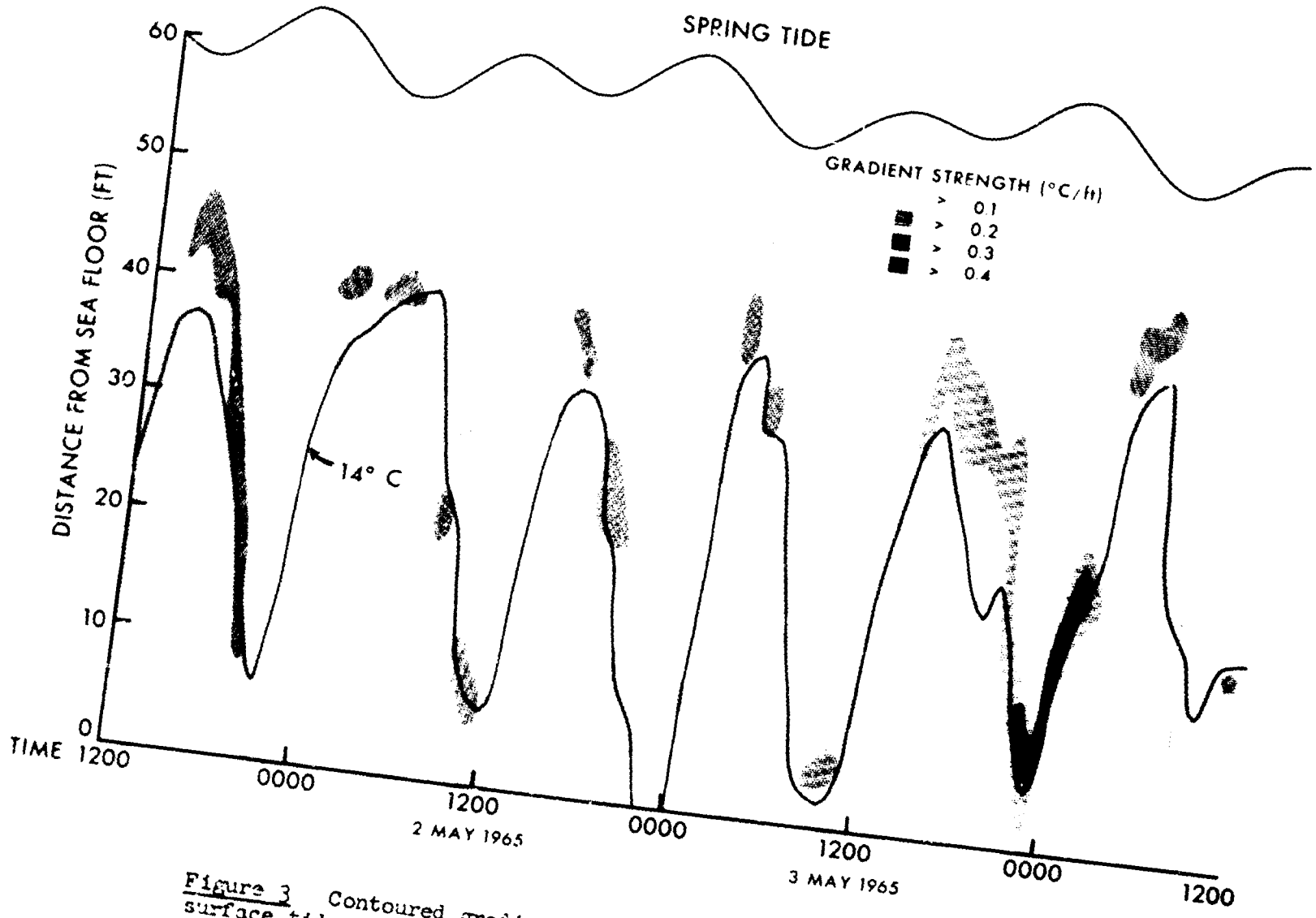

Figure 3 Contoured gradients during spring surface tides showing surface tide at top of figure.

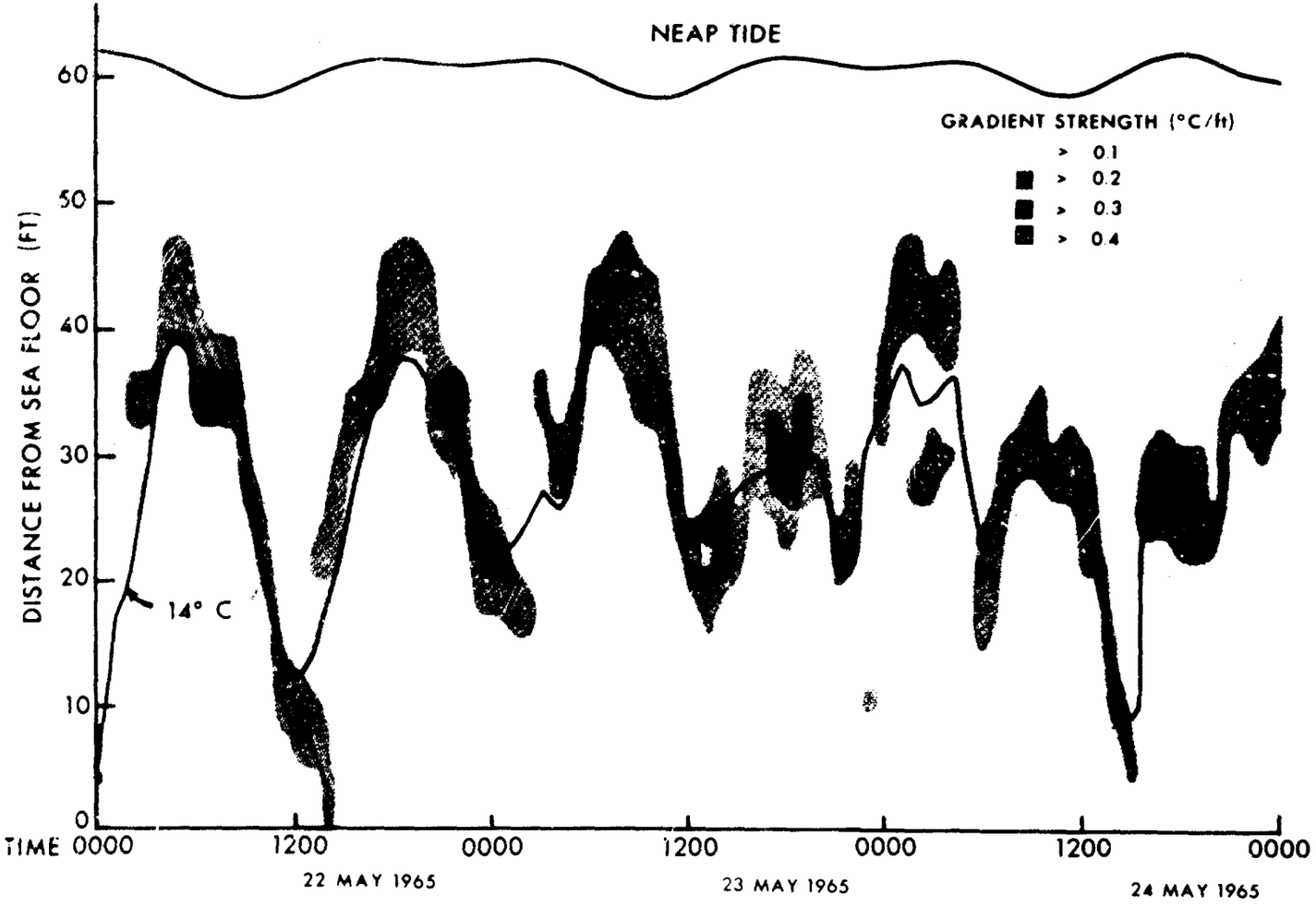

Figure 4 Contoured gradients during neap surface tides showing surface tide at top of figure.

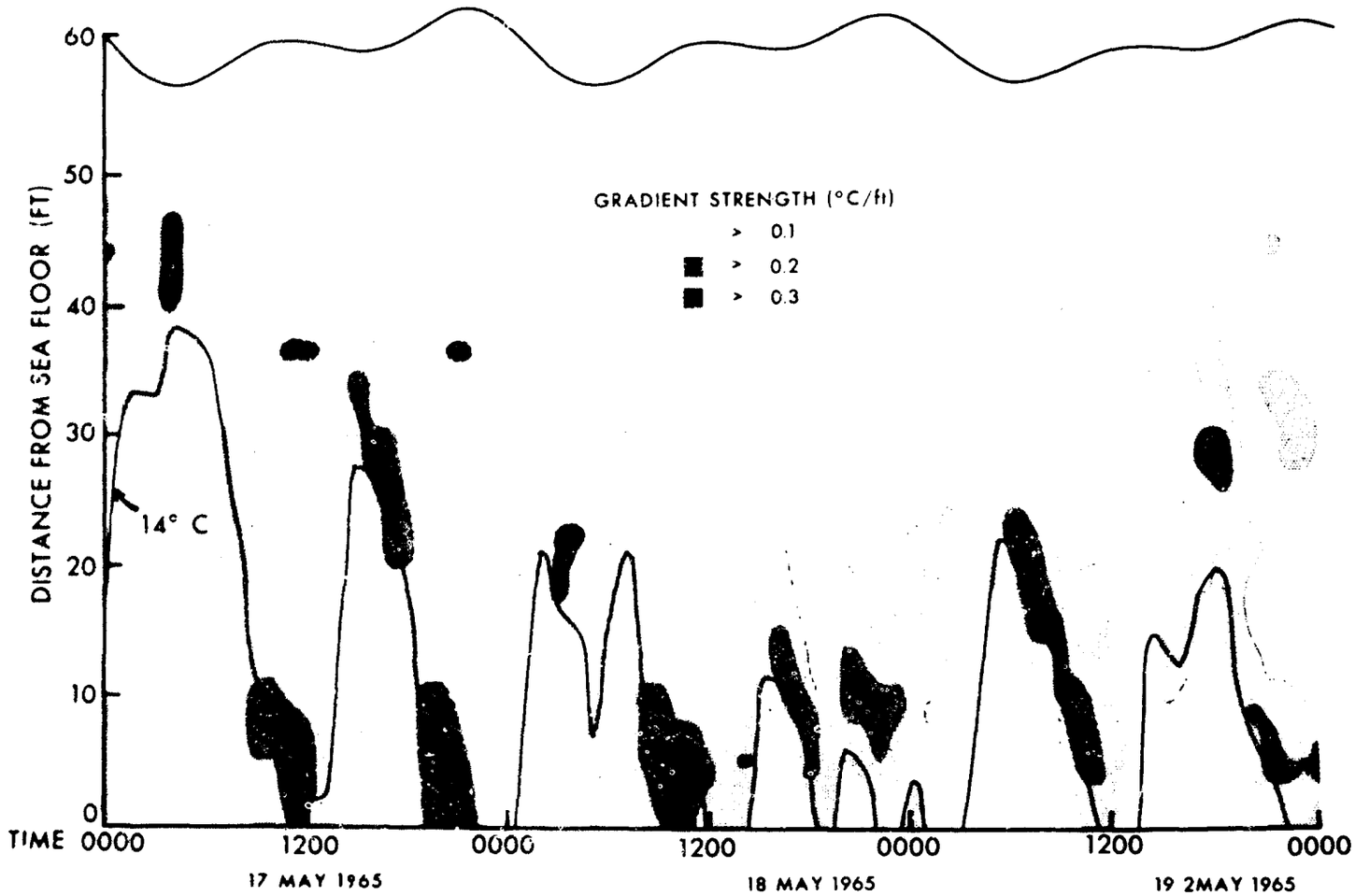

Figure 5 Contoured gradients during interval between spring and neap surface tides showing surface tide at top of figure.

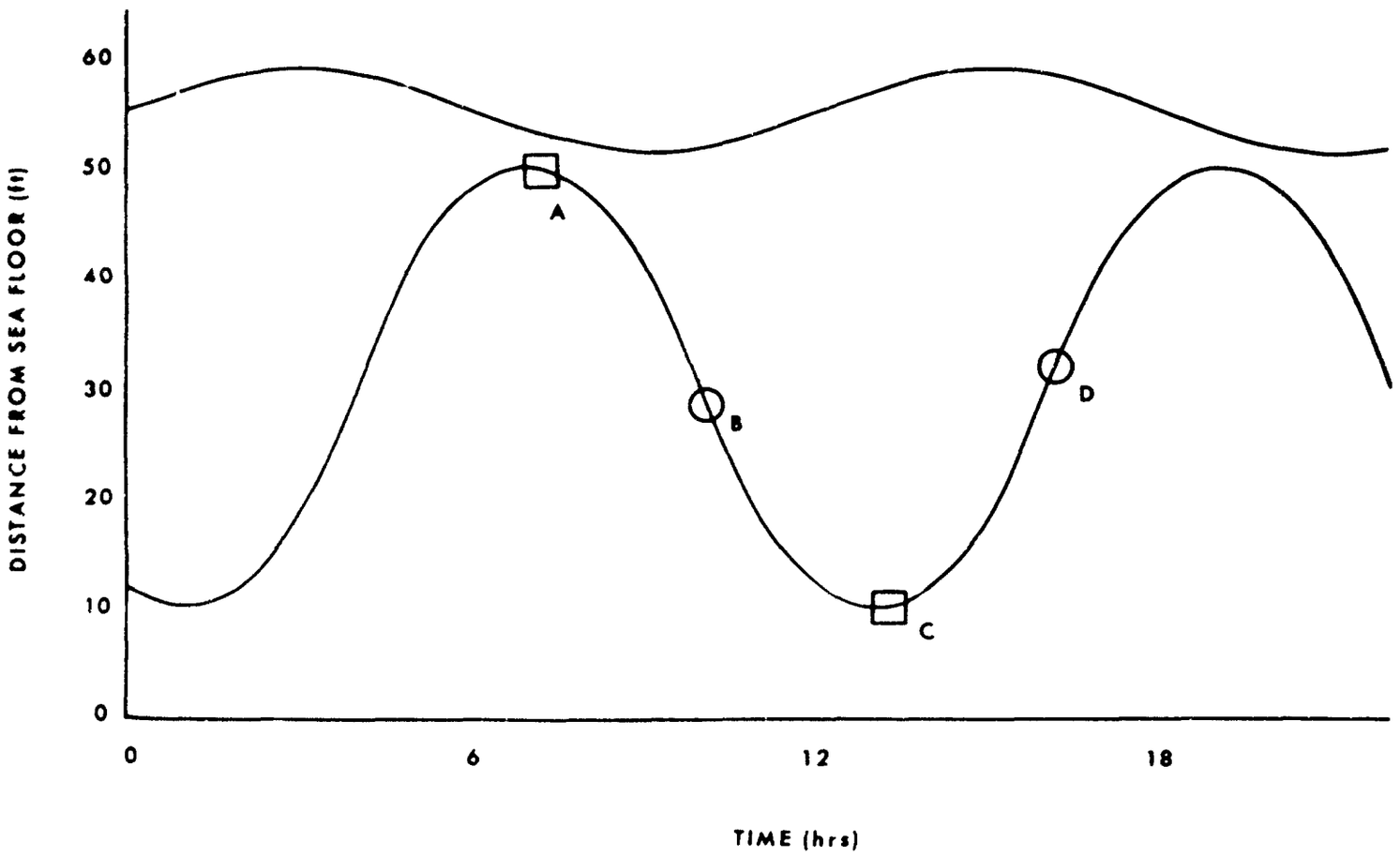

Figure 6 Idealized model showing average relative motion of surface and internal tides.

SHORT-PERIOD CHANGES AND ANOMALIES OF TEMPERATURE IN THE OCEANS AND THEIR EFFECTS ON SOUND PROPAGATION

W. E. Hubert, Captain, USN
and
T. Laevastu
Fleet Numerical Weather Facility
Monterey, California

ABSTRACT

It is demonstrated that the surface layers of the sea respond relatively rapidly to atmospheric driving forces. The changes over a period of two days frequently are of the same magnitude as the total annual climatological range of a given position. The causative relations between the changes in the sea and the atmospheric driving forces are analyzed and typical values and ranges are listed. The effects of short-term fluctuations on sound propagation are pointed out.

SYNOPTIC SEA SURFACE TEMPERATURE CHANGES

Oceanographic research has mainly considered the ocean in a climatological (hydroclime) manner in recent years. This has left an impression that the ocean is sluggish and reacts slowly to the driving forces (mainly of atmospheric origin). There are, however, a number of earlier studies describing synoptic changes in the oceans which, in some locations and conditions, have larger magnitude in a few days than the total annual range at the same location (e.g. Rodewald, 1964).

The synoptic oceanographic analyses made at U. S. Fleet Numerical Weather Facility (FNWF), Monterey show that pronounced synoptic changes in the surface layers of the oceans are quite common. Some of these changes are illustrated on Figure 1 which shows a sea surface temperature (SST) plot at five locations from 20 April to 9 June 1965. The data were taken from FNWF twice-daily synoptic SST analyses (Wolff, Carstensen, Laevastu, 1965); the positions were selected from relatively dense synoptic data areas (Figure 2). As can be seen from Figure 1, the SST changes can be of the order of half the annual range quite frequently. In some areas and conditions they can even exceed the total annual range.

Studies conducted at FNWF indicated that the average period of the SST changes is shorter (a few days) in higher latitudes, in the areas of passing cyclones, and somewhat longer at lower latitudes in the areas of semi-permanent anticyclones. The magnitudes of the changes are usually largest near the stronger gradients of SST (current boundaries) and

smallest in areas of small horizontal SST gradients. Exceptions from this rule do occur, however.

CAUSES OF THE SYNOPTIC CHANGES IN THE SURFACE LAYERS

Explanations for the synoptic changes in the properties of the surface layers in offshore waters can, in most cases, be found in the atmospheric driving forces. The advective changes by surface currents are most easily demonstrated. The two main components of the surface currents are the gradient (thermo-haline) flow and the wind current. It should be noted that Ekman's theory is not directly applicable to wind currents; the direction of this component is, in fact, approximately parallel to the surface isobars.

Some relatively pronounced SST changes in the beginning of June 1965 are indicated with letters on Figure 1. Figures 3 to 5 give portions of FNWF surface analyses, on which the positions of the temperature curves on Figure 1 as well as the corresponding letters are shown. A visual examination of these figures establishes the predominantly advective cause of the indicated SST changes. Another set of figures (6 to 13) illustrates profound changes of SST over three days in the NW Atlantic, the causes of which are apparent from the corresponding surface pressure and surface current analyses. Figures 6 and 10 give the SST distribution at 12Z 28 December 1965 and at 12Z 31 December 1965, respectively. The change of sea surface temperature is quite clear in these charts as well as in the local sea surface temperature anomaly (SD) charts (Figures 7 and 11) for the same dates. (The derivation of SD anomalies is described in the next chapter.) The boundary between the Labrador Current and Gulf Stream is between the positive and negative anomalies, along the 'zero' line (intentionally omitted from these charts). Special attention is invited to the "eddy" and "break" in positive anomaly SSE of the Grand Banks on 12Z 28 December 1965 and the re-establishment of normal conditions in this area three days later. The surface pressure analysis on 06Z 28 December 1965 (Figure 8) gives the reason for the abovementioned large "eddy" and the "break" in the Gulf Stream. The southward bend of surface streamlines on 12Z 28 December 1965 (Figure 9) indicates the effect of the northwesterly wind current component on the Gulf Stream at this location. The corresponding quasi-normal conditions on 31 December are shown on Figures 12 and 13.

Some typical sea surface and subsurface temperature changes, caused by heat exchange, advection and convergence/divergence are shown in Tables 1 to 3. As can be concluded from these tables, SST changes of 1.5°F in 24 hours can occur under certain conditions. The subsurface temperature changes can be of the same order of magnitude. Figure 14 gives results of similar calculations for defined surface meteorological conditions. It can be seen that SST changes of 5°F and more can occur at middle and high latitudes during summer season.

A generalized scheme for the causes of SST and mixed layer depth (MLD) changes is shown on Figures 15 and 16. A thoughtful examination of these figures shows that most of the driving forces change in the same rhythm as weather conditions at the surface but some are even faster (e.g. tides). Furthermore several of the causative forces are independent of each other and several of them can operate in opposite directions. Thus the changes in the surface layers of the sea (e.g. SST, MLD and other properties) normally change at least as rapidly as does the surface weather. Consequently, oceanographic analyses and forecasts should be carried out with the same frequency as weather analyses/forecasts, and in conjunction with each other (as is done at FNWF).

TYPES OF SEA SURFACE TEMPERATURE ANOMALIES AND THEIR BEHAVIOR

Although in practice (i.e. naval and fisheries application of synoptic oceanography) we are concerned with the actual values of the elements (properties) of the environment, we are also concerned with their anomalies.

By definition, three types of SST anomalies might be considered. According to common usage, an anomaly is the deviation in a given region or location over a specified time (e.g. given day, week, month, season) from the normal (i.e. long-period average) value for the same region or location and time. Thus anomalies can be computed as the difference between the daily SST analysis and some long-period average. These are not anomalies in the usual oceanographic sense, which by definition are differences between temperatures actually observed and those that would have existed at given points had the water all been of a given arbitrary temperature (e.g. specific volume anomaly, thermosteric anomaly).

An example of the first type of anomaly chart is given on Figure 17, which gives the average SST anomaly for the period 16 to 20 February 1965 from the long-term mean. The long-term mean of SST for the Pacific Ocean was taken from work by the Bureau of Commercial Fisheries (Stanford Biological Laboratory) and the mean SST for the Atlantic is from work by Mrs.M. Robinson (Scripps Institution of Oceanography). A similar fifteen-day anomaly chart (1 to 15 February) is given in Figure 18. The positive areas are shaded on these charts. These types of anomalies will be considered in detail in another study in progress at FNWF. Three observations in respect to these anomalies are pointed out here. First, these anomalies are relatively large in horizontal extent; secondly, some of them can be persistent over longer periods while some appear and disappear relatively rapidly; and finally, some of these anomalies migrate with the average surface current. A fifteen-day period seems to be the optimum for computation of the large-scale, more persistent anomalies.

The anomalies more extensively considered in this report are of a third type (following meteorological usage of the term), i.e. deviations of SST values at given places from the smoothed latitudinal values of SST during the same period of time. The computation of these anomalies can be done numerically by scale and pattern separation. For mapping of the two different scales on a daily basis, an iterative procedure was developed at Meteorology International, Monterey and FNWF which permits a scale separation by heat diffusion analogue equations (Holl, 1963). The method consists of repeated application of a smoothing operator which reduces first the amplitudes of the shortest wave lengths and gradually affects longer and longer wave lengths.

This technique has proved to be an objective method for quantitative separation of individual features from the large-scale pattern. Removal of small-scale disturbances from the initial analysis leaves the large-scale pattern; finally, removing the purely zonal portion of the large-scale pattern yields the large-scale anomalies.

A set of large and small-scale anomalies, derived by the scale and pattern separation from the SST distribution on 00Z 13 January 1966 (Figure 19) is shown on Figures 20 and 22. The relative patterns on the large-scale SST anomalies (SL) are similar to the global annual average anomalies according to Dietrich and Kalle (1957) (see Figure 21). The large-scale SST anomalies (SL) (Figure 20) can be classified, by cause, into two major groups. These are identified with the sign of these anomalies.

The four major negative (low) anomalies indicate southward advection of colder water and coastal upwelling. Two of them (Labrador and Oyashio anomalies) are mainly caused by cold advection, whereas the other two (Californian and Moroccan) are connected with upwelling along the coast and cooling by evaporation. The positive (high) anomaly areas are caused by northward transport of warm water and excessive local heating. The Alaskan, Kuroshio, Gulf Stream and Norwegian Sea anomalies are mainly due to advection. The Central American, the Mediterranean, and Central Pacific anomalies are partly due to local heating and partly due to advection.

The average SI patterns change but slowly from season to season. However in detail the patterns fluctuate considerably around a mean value in the same rhythm as the surface weather changes over the corresponding areas. This can best be demonstrated with time series movies of twelve-hourly SL analyses.

The small-scale (local) anomalies (Figure 22) can be classified into two groups. Into the group of local anomalies can be included those small-scale features which are caused by local upwellings (e.g. off California), heat exchange and mixing. The second group of advective anomalies consists of those caused by advection (currents) and meanders

along current boundaries and eddies (e.g. Labrador-Gulf Stream area). There appears to be a third group of smaller centers appearing and disappearing relatively rapidly on the periphery of the chart. These are not true anomalies, but mostly due to "data noise" in low data density areas.

The advective anomalies at major current boundaries (e.g. Labrador-Gulf Stream) are persistent, but show changes according to prevailing local winds. This has already been noticed by Chase (1959), who found that advection was an important factor in changing SST at Frying Pan Shoals. In general, warming occurred ahead of cold fronts (when southwesterly winds are prevalent) and cooling occurred after the frontal passage (when northerly winds prevail).

It can be noted that advective changes crossing a major current boundary can have opposite trends. This has been pointed out earlier by Templeman (1964) who indicated that waters close together, but with differing origins and temperatures, may exhibit different temperature trends.

The SD patterns also permit the delineation of major current boundaries. This can be observed from Figure 22 where the 'zero' line between positive and negative anomalies has been omitted, making the boundary clearly distinguishable in e.g. Gulf Stream/Labrador current area.

An experimental attempt to numericaliy delineate current and surface water types using synoptic SST anomalies is illustrated on Figure 23, which depicts the second derivative of the SST distribution (see Renard and Clarke, 1965).

There are a number of direct uses of synoptic SST anomaly charts. The use of the SST anomalies in fisheries has been demonstrated during the past half century. A typical recent description of the great negative anomalies in North European waters in the winter 1962/63, and their influence on fisheries, has been given by Eggvin (1963).

The SST anomalies have proven to be useful in subjective analysis of upwelling intensities, surface eddies (especially warmer eddies in colder environment), in delineation of major current convergences and their fluctuations and in the estimation of subsurface thermal structure.

Further use of SST anomalies can be and has been made in the study of cause-effect relations of sea-air interaction and in extended weather forecasts over ocean areas. They have proven useful for some local weather forecasting, e.g. for forecasting of stratus over coastal areas in Central California. There have been a number of other special uses of these anomalies in various naval problems as well as indirect inputs of these anomalies into other synoptic oceanographic analyses/forecasts at FNWF.

EFFECTS OF SHORT-TERM FLUCTUATIONS OF TEMPERATURE ON SOUND PROPAGATION

Several conventional sonar range computation formulas utilize the environmental data in a relatively simplified form; the main input parameters are SST, MLD and average gradient below the MLD. Obviously, short-period changes of these parameters with magnitudes of half their annual range could affect the sonar ranges considerably. Consequently, the highest accuracy in analyses/predictions is required during the season when the thermocline is relatively shallow and the below-layer gradient most pronounced.

The presence of "heat transients" makes hull-mounted sonars less effective. These transients can seldom be measured by conventional BT from a large, moving ship. Therefore probabilities of occurrence of these transients and their magnitudes are the most common product sent to the operating forces.

During the winter season, when the thermocline is deep, lesser accuracy is acceptable. Nevertheless any small inclination caused by advective processes which can change rapidly with time must also be recognized during this season.

Attempts are in progress at FNWF to compute the propagation loss profiles at 25 foot depth intervals. The propagation loss pattern is strongly dependent upon the thermal structure. As is well known, the range to convergence zone is also a function of surface temperature.

In certain defined areas and conditions small changes of SST are critical in determining channel propagation, especially where the main sound channel is close to the surface and the "lock" small.

The thermal fronts (water type boundaries) as well as internal waves have considerable influence on sound propagation. Their detailed investigation is in progress at NEL (LaFond, personal communication). The effects on sound propagation of the small-scale fluctuations and irregularities found in sound speed profiles below the thermocline (Piip, 1964) have yet to be investigated.

Table 1

Typical sea surface temperature changes, caused by heat exchange. (Assuming that the temperature change is limited to surface mixed layer above thermocline)

Q_n g cal cm^2 24h^{-1}	Temperature change ^{o}F	
	MLD 50 feet	MLD 100 feet
100	0.12	0.06
300	0.35	0.17
600	0.70	0.35

Table 2

Typical sea surface temperature changes caused by advection.

Current transport naut. miles 24h^{-1}	Sea surface temperature gradient ^{o}F/100 naut. miles	Sea surface temperature change ^{o}F 24 hours
24	6	1.44
	1.5	0.36
6	6	0.36
	1.5	0.09

Table 3

Typical temperature changes on subsurface levels, caused by divergence/convergence.

Temperature gradient ^{o}F/100 feet	Divergence/Convergence in feet	Temperature change ^{o}F
6	24	1.44
	8	0.48
2	24	0.48
	8	0.16

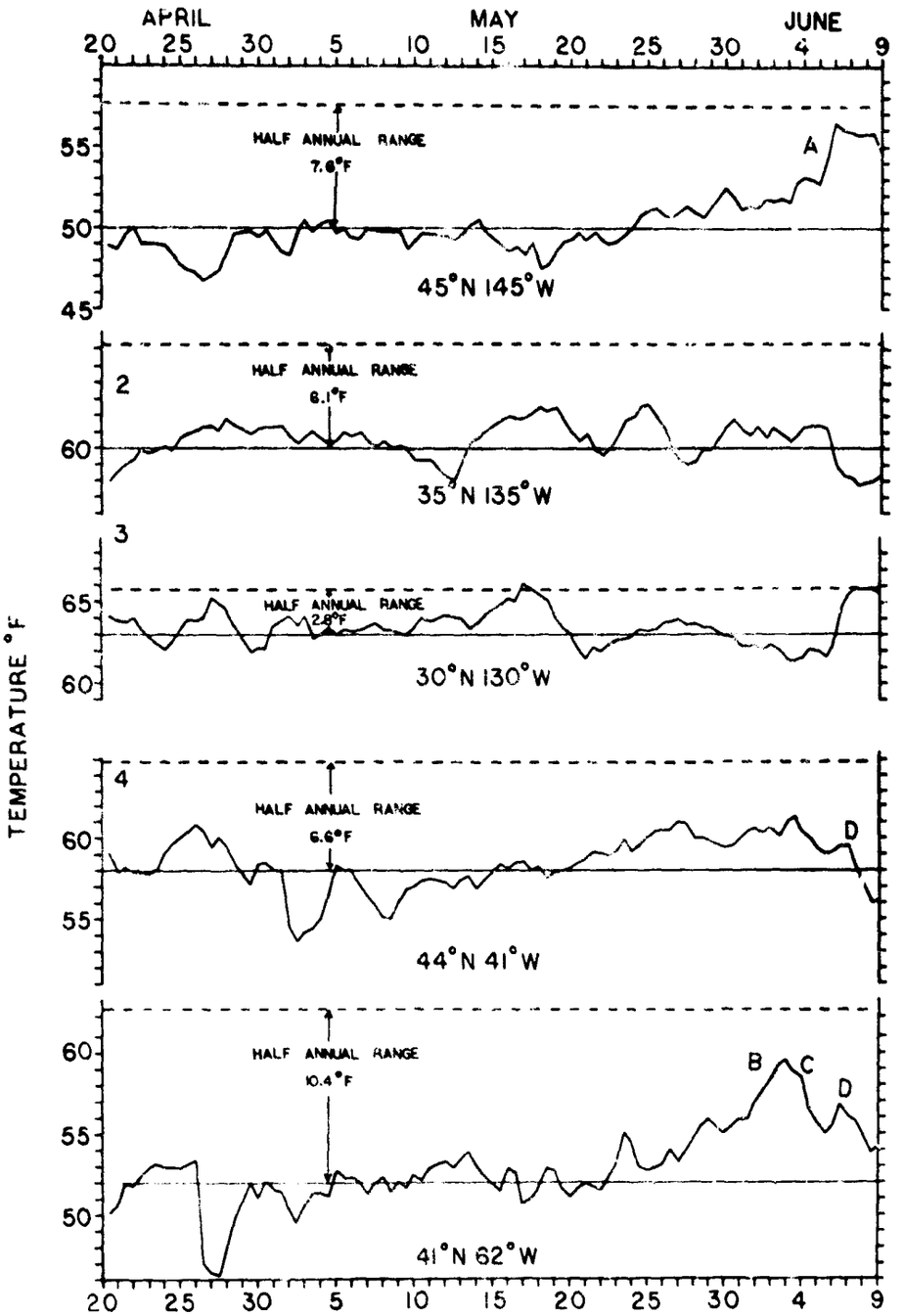

FIGURE 1 SEA SURFACE TEMPERATURE CHANGES AT FIVE LOCATIONS FROM 20 APRIL TO 9 JUNE 1965 (Positions of five locations, see figure 3)

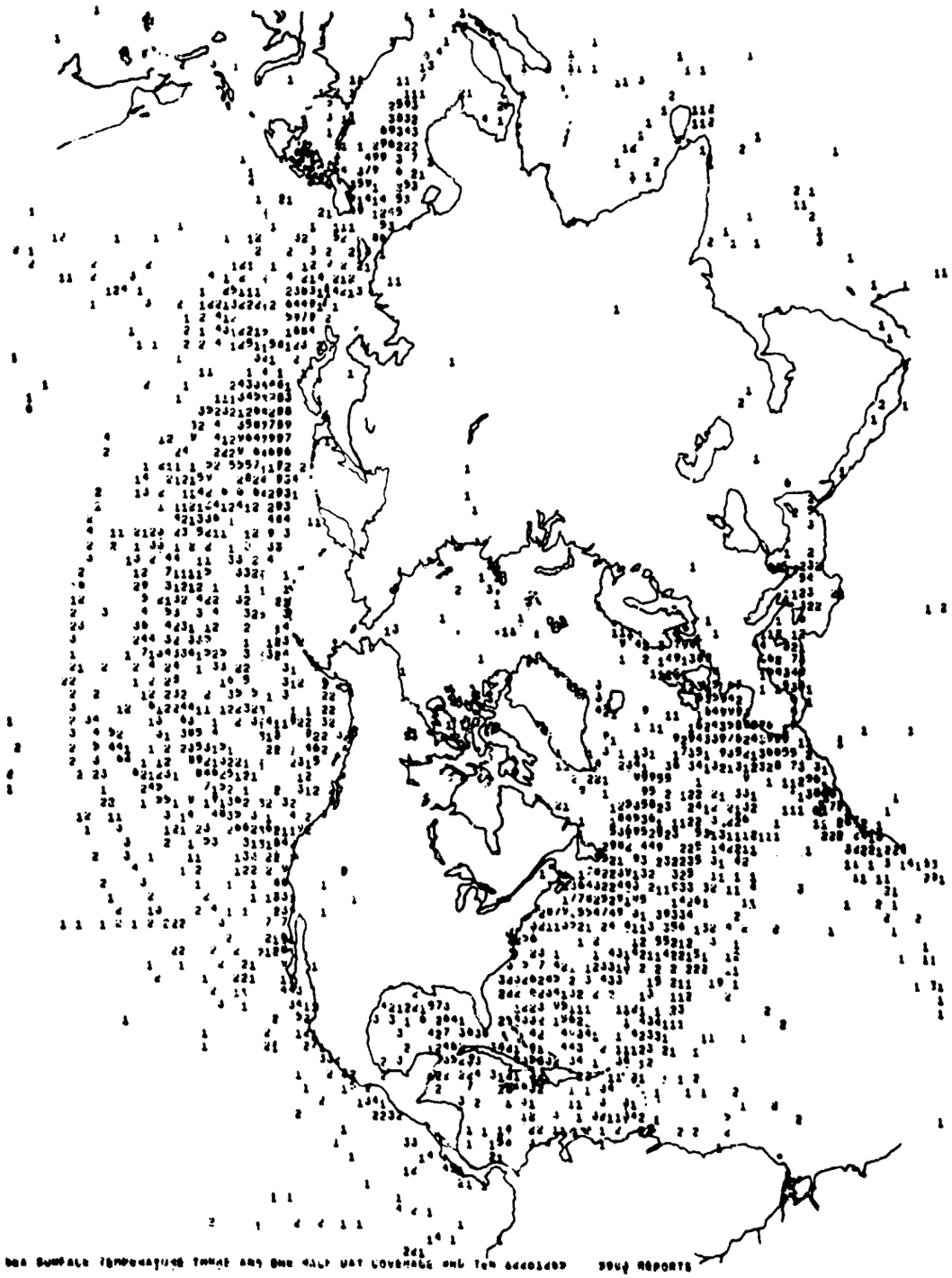

Figure 2 Density of synoptic sea surface temperature reports in SST analyses on 12Z 28 December 1965.

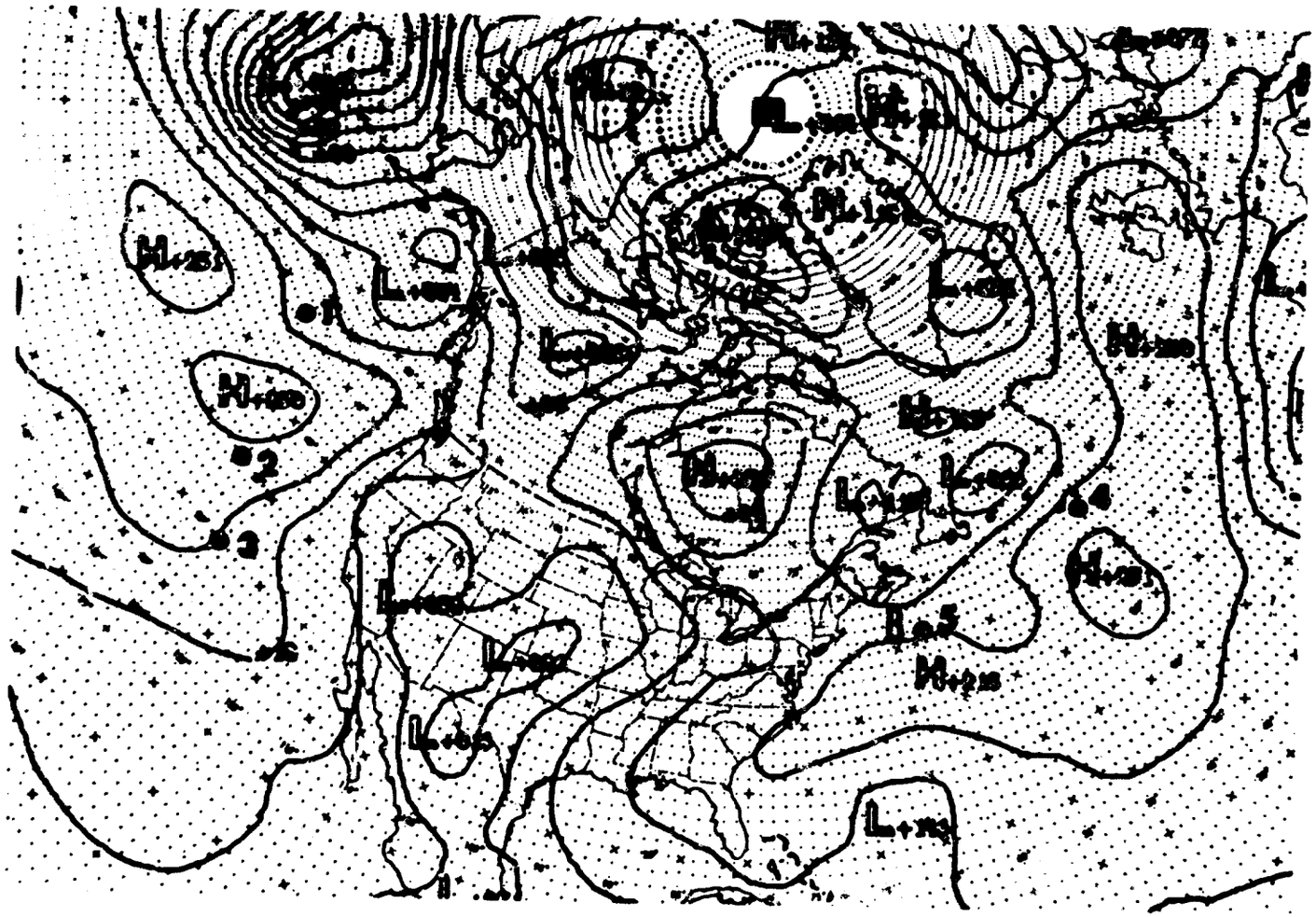

Figure 3 A portion of FNWF numerical hemispheric surface pressure analysis on 00Z 02 June 1965.

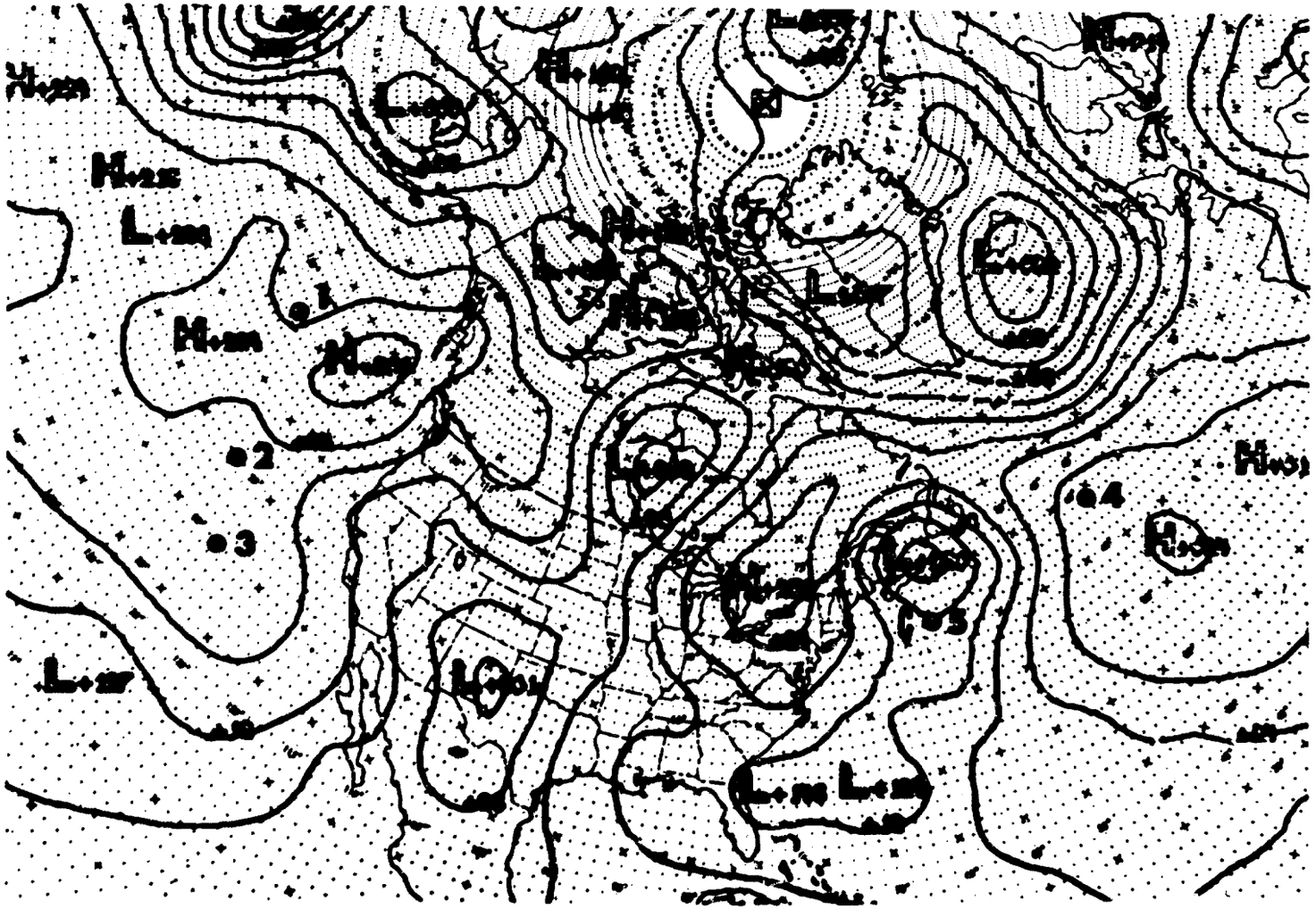

Figure 4 A portion of FNWF numerical hemispheric surface pressure analysis on 12Z 04 June 1965.

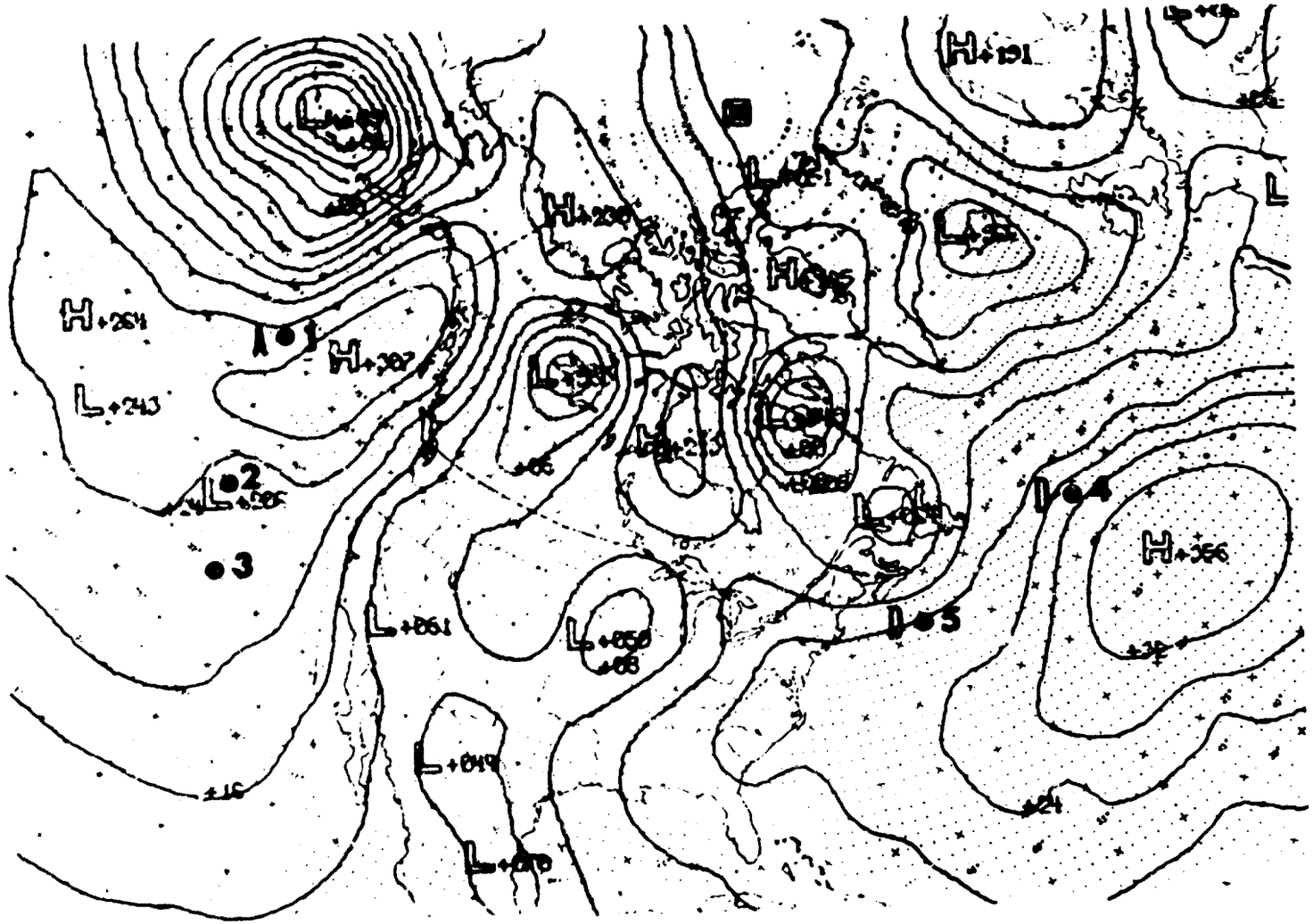

Figure 5 A portion of FNWF numerical hemispheric surface pressure analysis on 00Z 06 June 1965.

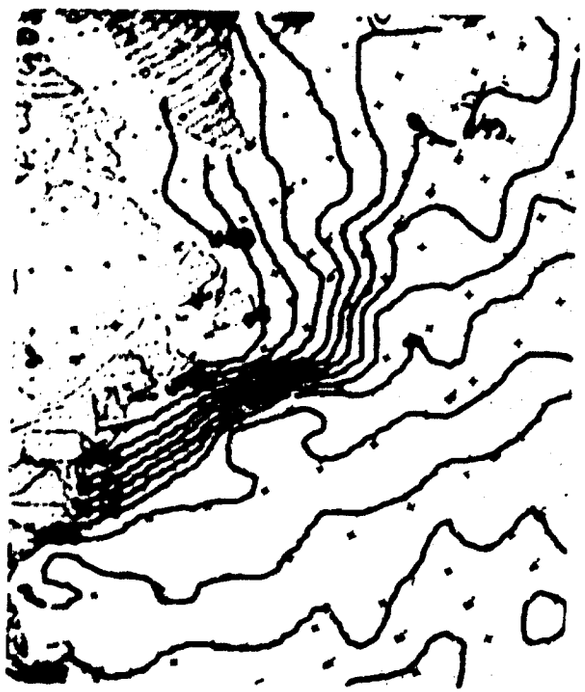

FIG. 6

Figure 6 Sea surface temperature analysis in NW Atlantic, 12Z 28 December 1965.

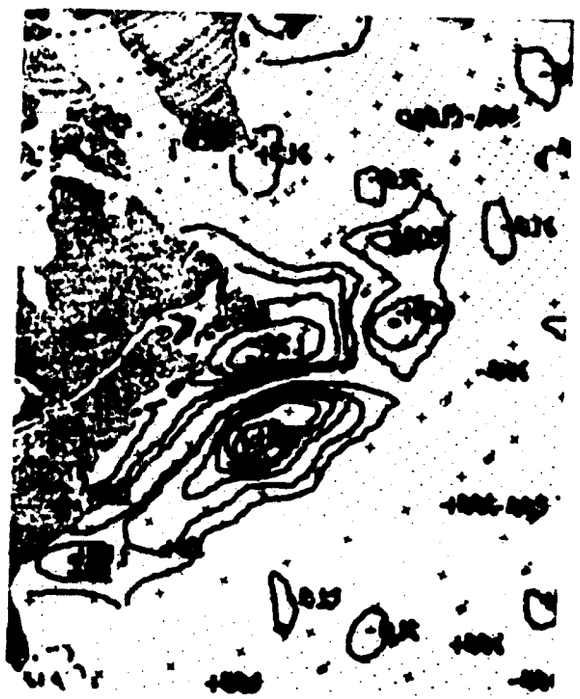

FIG. 7

Figure 7 Small-scale (SD) sea surface temperature anomalies in NW Atlantic, 12Z 28 December 1965.

FIG. 8

Figure 8 Surface pressure analysis over NW Atlantic, 06Z 28 December 1965.

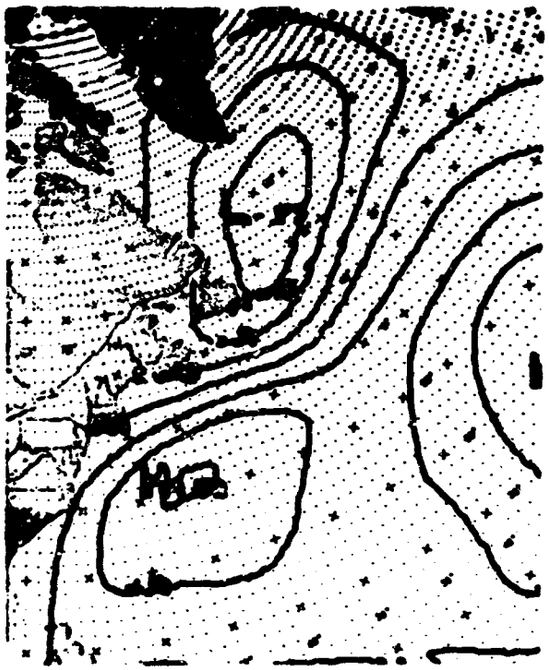

FIG 9

Figure 9 Sea surface current stream function in NW Atlantic, 12Z 28 December 1965.

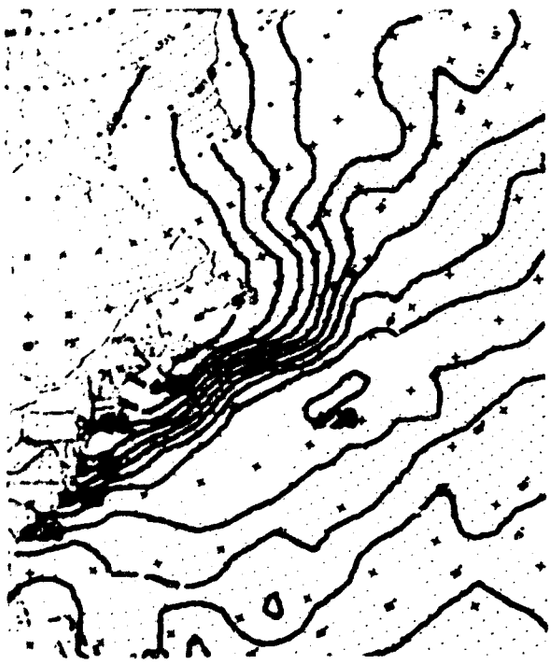

FIG. 10

Figure 10 Sea surface temperature analysis in NW Atlantic, 12Z 31 December 1965.

FIG. 11

Figure 11 Small-scale (SD) sea surface temperature anomalies in NW Atlantic, 12Z 31 December 1965.

FIG. 12

Figure 12 Surface pressure analysis over NW Atlantic, 06Z 31 December 1965.

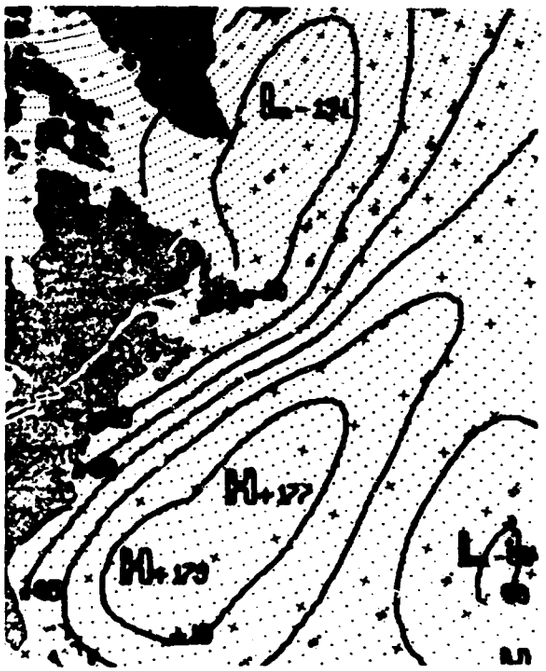

FIG. 13

Figure 13 Sea surface current stream function in NW Atlantic, 12Z 31 December 1965.

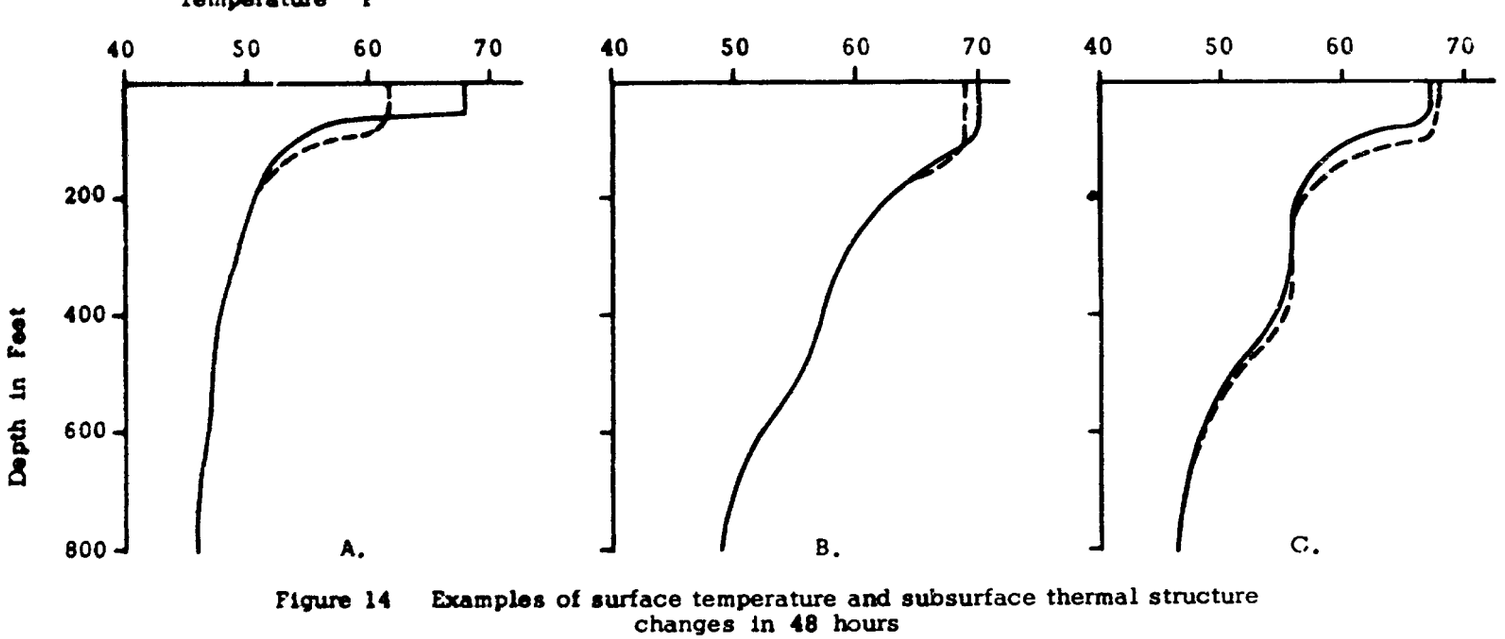

Figure 14 Examples of surface temperature and subsurface thermal structure changes in 48 hours

A. <u>In cold sector of a cyclone</u>

Sea surface temperature change:

1. Heat loss (ca 800 g cal cm^{-2} $24h^{-1}$)	$-1.6^{\circ}F$
2. Advection (grad $4^{\circ}F$/100 naut. miles, current 18 naut. miles/day)	$-1.4^{\circ}F$
3. Mixing (thermal from 50 to 75 feet, Temp 68°; 58°	$-3.3^{\circ}F$
Total	$-6.3^{\circ}F$

B. <u>In NE part of an anticyclone</u>

Sea surface temperature change:

1. Heat loss (ca 150 g cal cm^{-2} $24h^{-1}$)	$-0.2^{\circ}F$
2. Advection (grad $3^{\circ}F$/100 naut. miles, current 12 naut. miles)	$-0.7^{\circ}F$
3. Mixing (mainly combined with divergence)	$-0.2^{\circ}F$
Total	$-1.1^{\circ}F$

C. <u>Convergence/divergence</u>

(Some heating and warm advection. Change dependent on gradient within depth and convergence/divergence.)

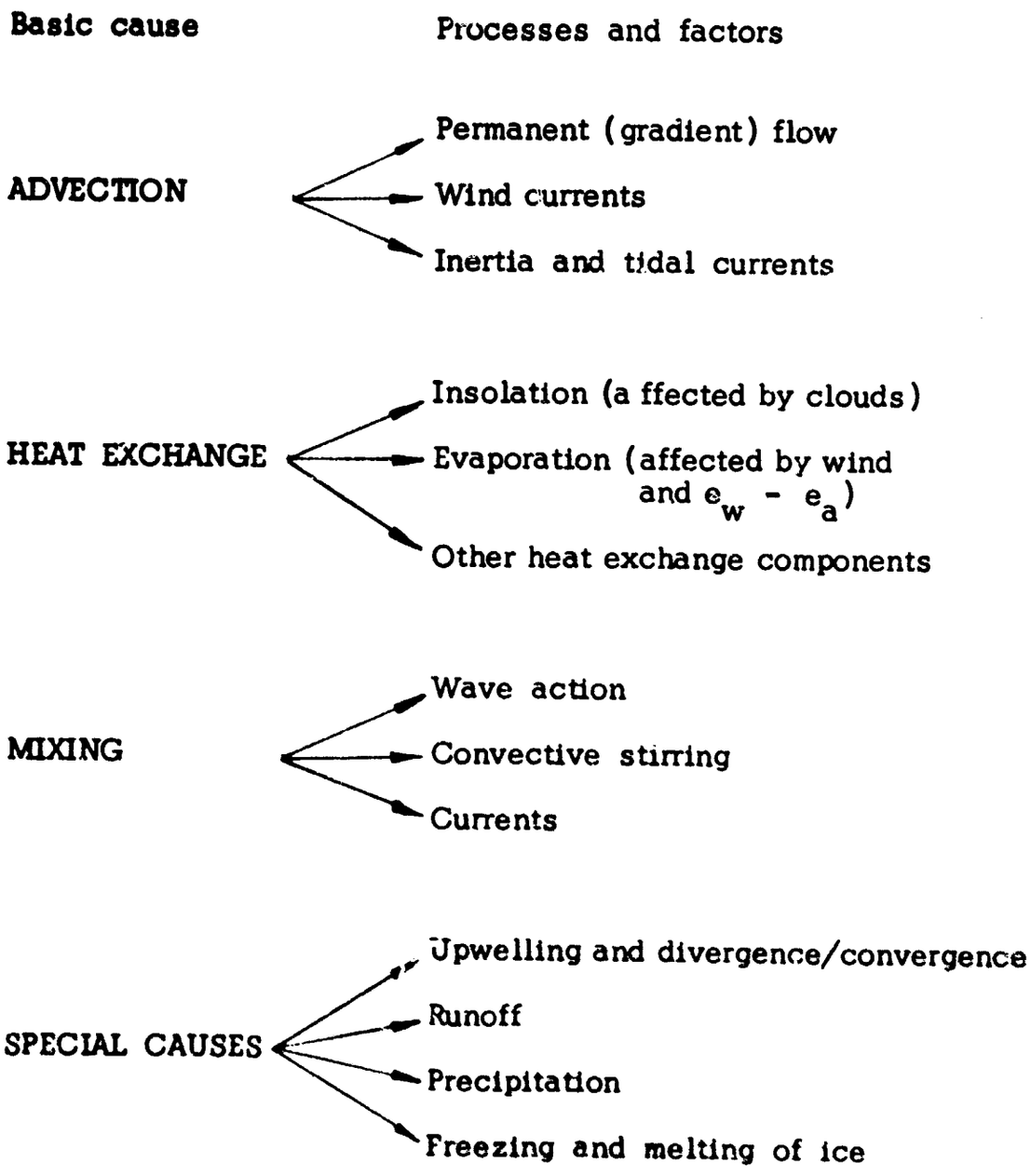

Figure 15 Major causes of sea surface temperature changes.

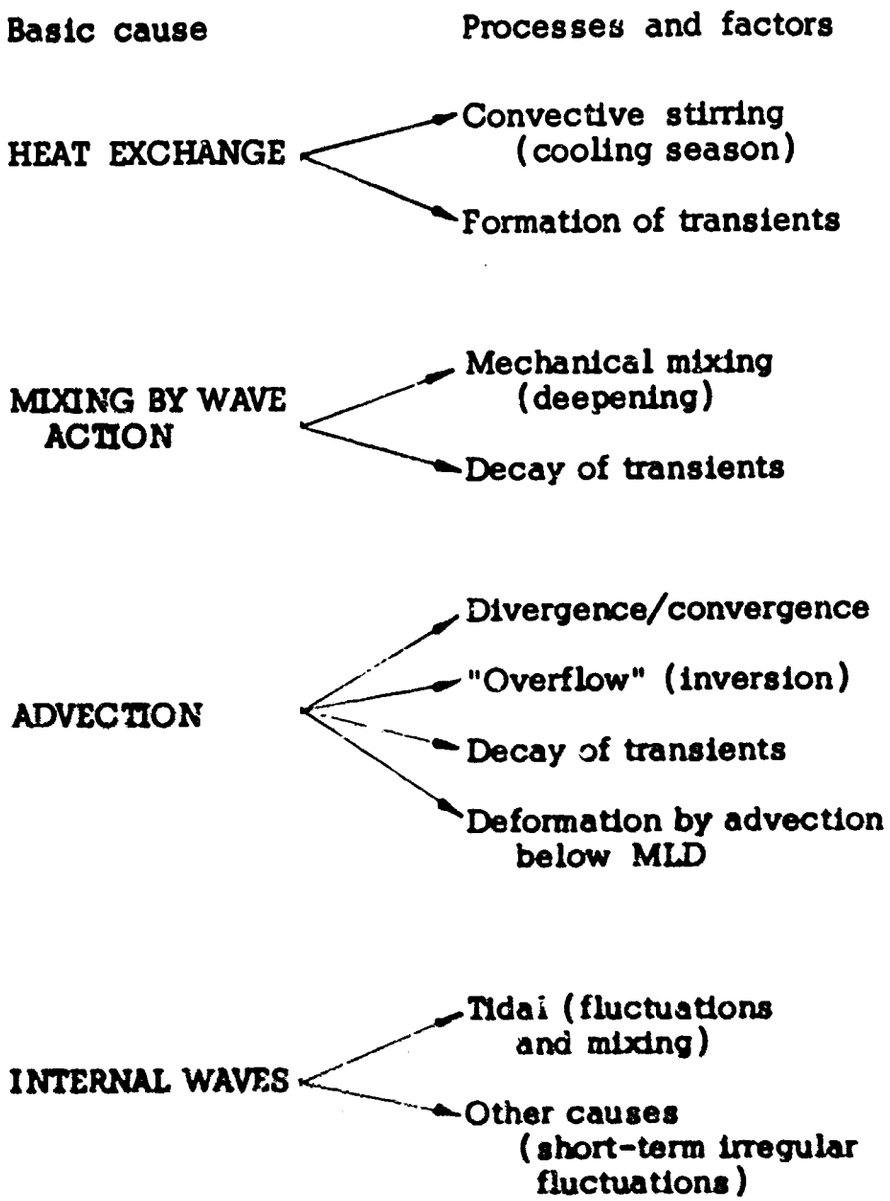

Figure 16 Major causes of potential mixed layer depth changes.

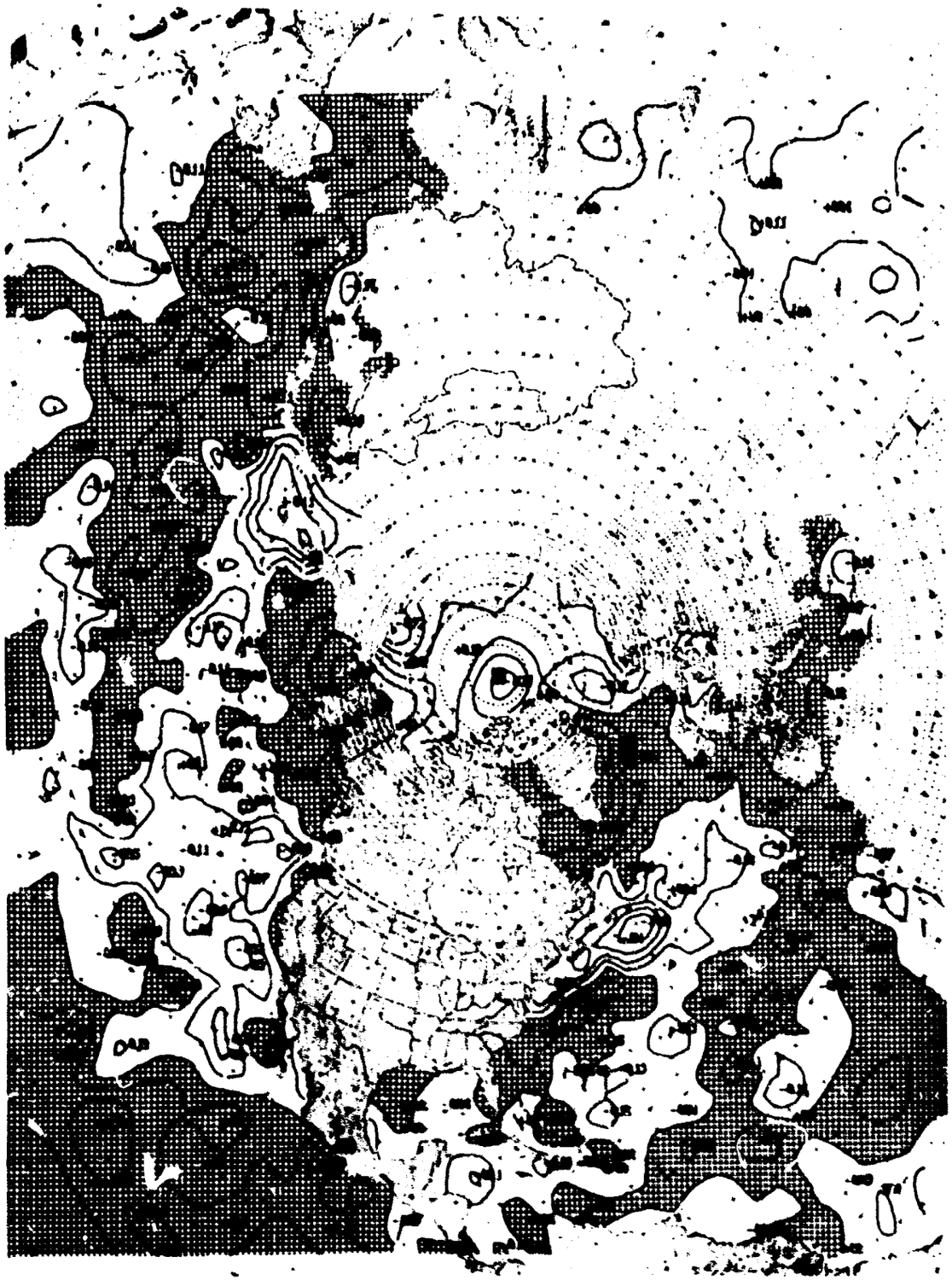

FIGURE 17 5-DAY SEA SURFACE TEMPERATURE ANOMALIES FROM LONG-TERM MEAN, 16 TO 20 FEBRUARY 1964.

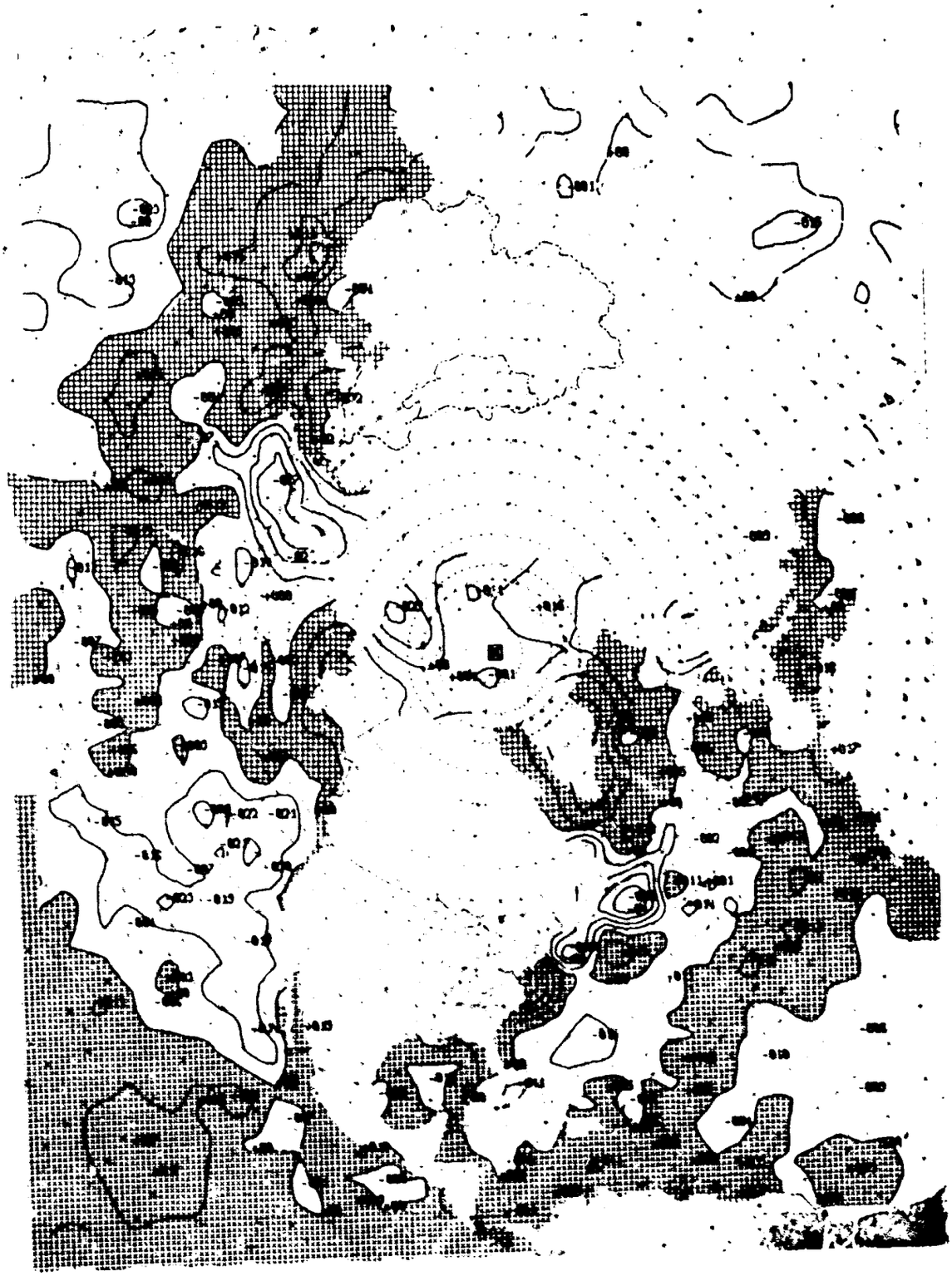

FIGURE 14 15-DAY AVERAGE SEA SURFACE TEMPERATURE ANOMALY FROM LONG-PERIOD MEAN (FROM 1 TO 15 FEBRUARY 1966).

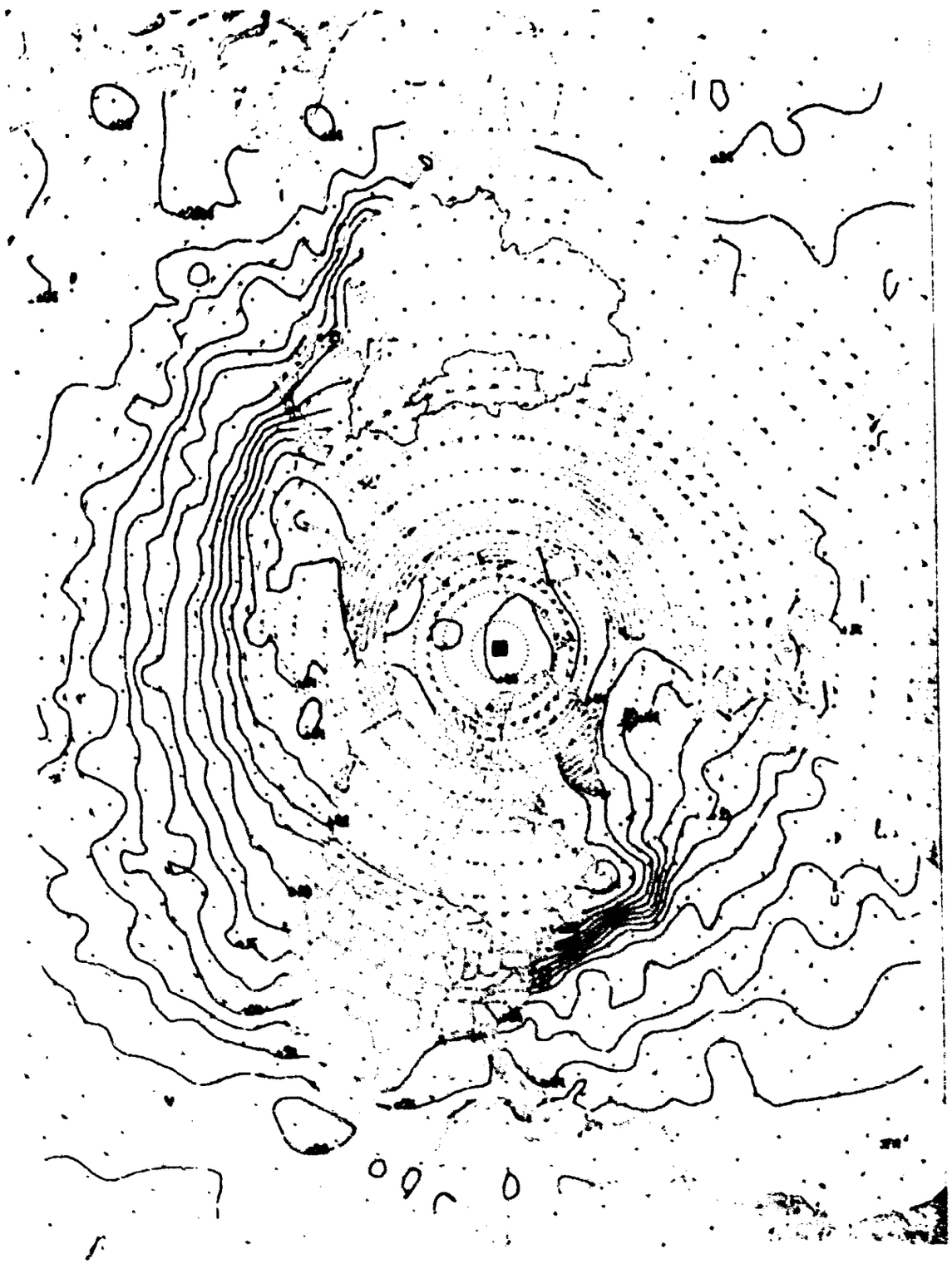

FIGURE 19 HEMISPHERIC SEA SURFACE TEMPERATURE ANALYSIS, DEC 12 JANUARY 1966.

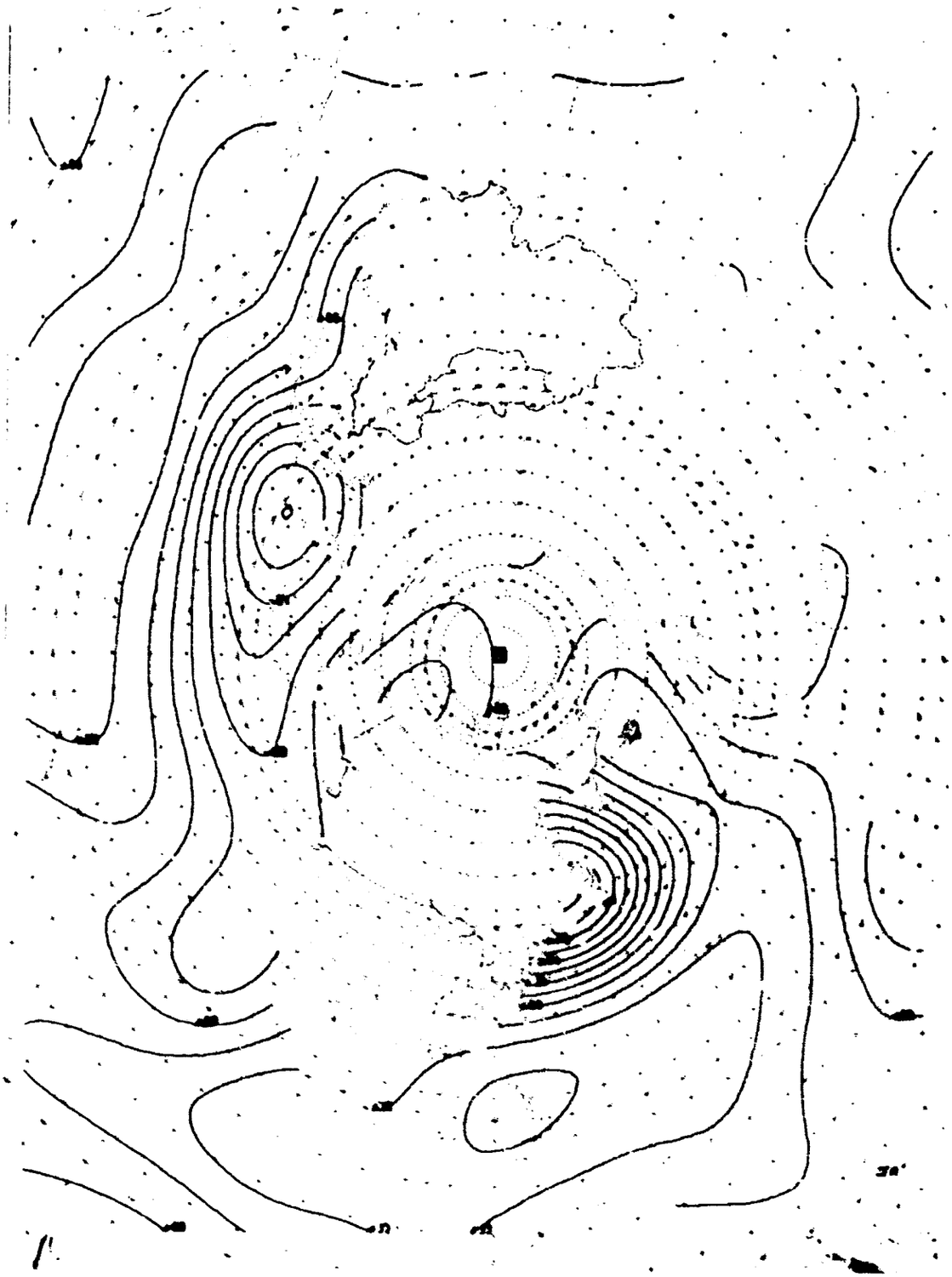

FIGURE 20 HEMISPHERIC LARGE-SCALE (SLP) SEA SURFACE TEMPERATURE ANOMALIES, 00Z 13 JANUARY 1964

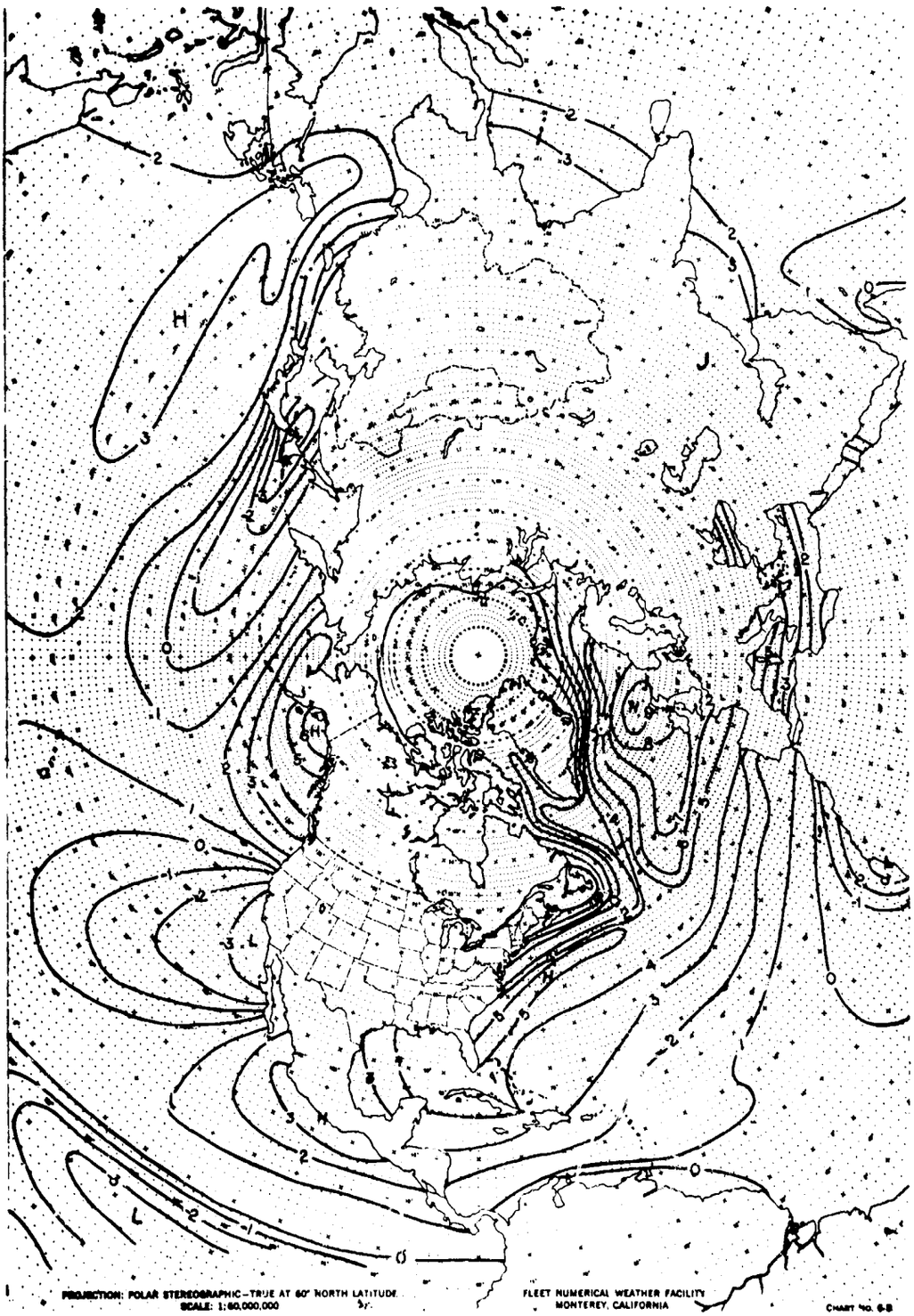

Figure 21 Average anomaly of sea surface temperature, after Dietrich.

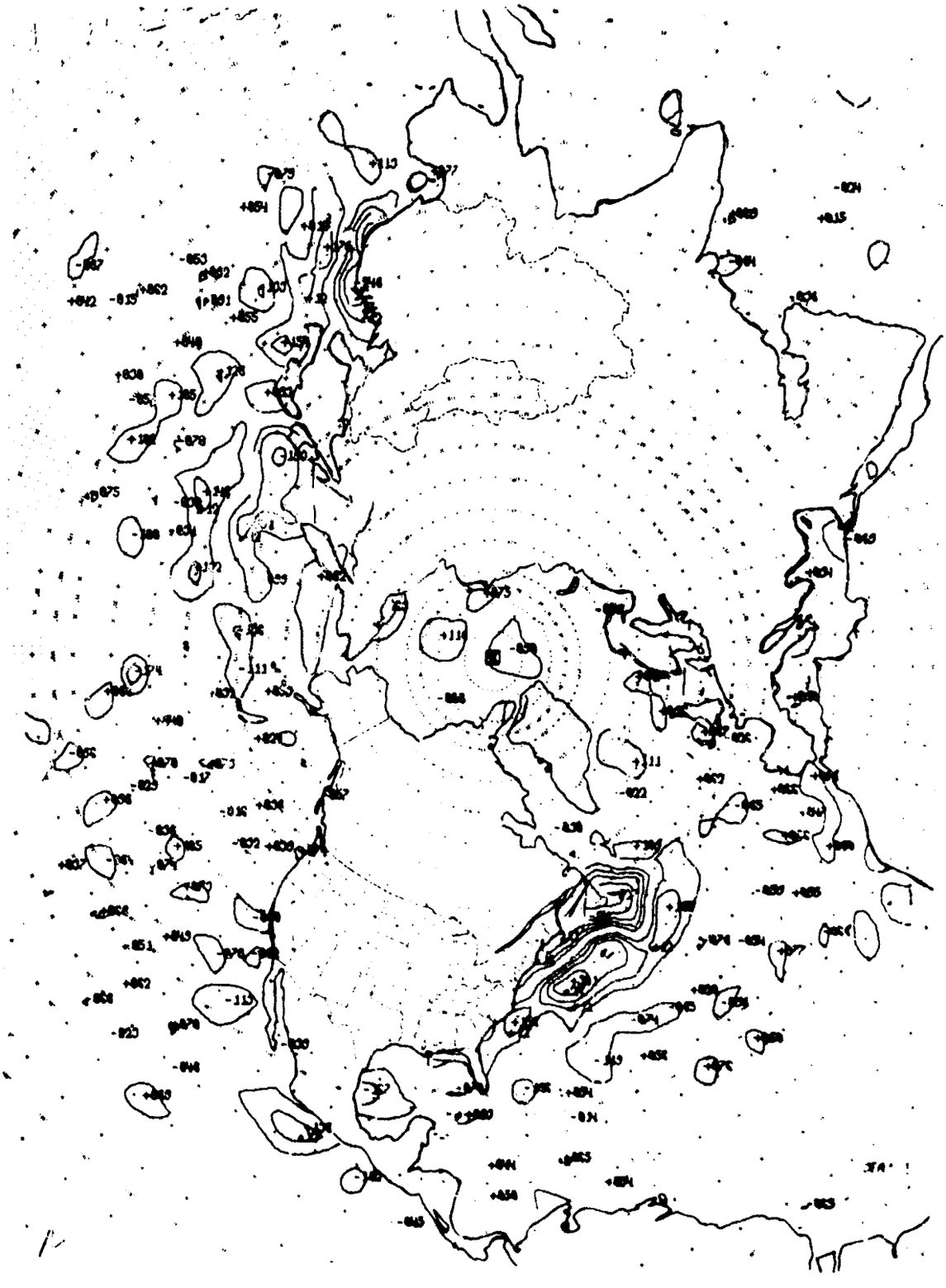

FIGURE 22 SMALL-SCALE (SD) SEA SURFACE TEMPERATURE ANOMALIES, 00Z 13 JANUARY 1966.

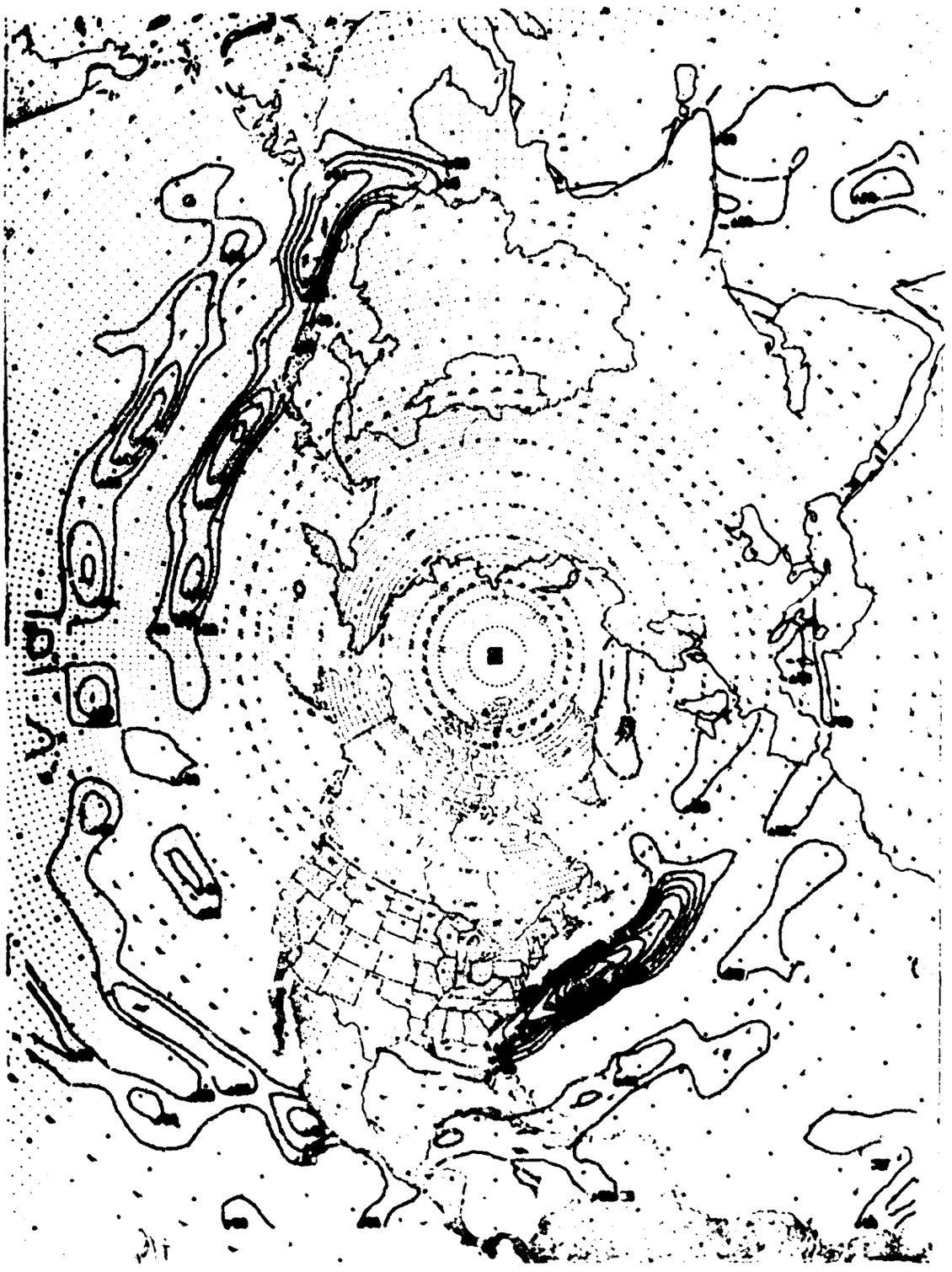

FIGURE 23 NUMERICAL COMPUTATION OF SURFACE CURRENT AND WATER TYPE BOUNDARIES AND AXES OF WARM CURRENTS, 12Z 13 JANUARY 1966.

REFERENCES

Chase, J. 1959 — Wind-induced changes in the water column along the East Coast of the United States. J. Geophys. Res. 64(8): 1013-1022.

Dietrich, G. and K. Kalle 1957 — Allgemeine Meereskunde, Gebr. Borntraeger, Berlin - Nikolasse, 492 pp.

Eggvin, J. 1963 — Tilstanden i havet under den unormale vinter 1963; Fisken og Havet 1 (1963) 9-16.

Holl, M. M. 1963 — Scale-and-pattern spectra and decompositions. Meteorology International, Monterey, Techn. Memo 3.

LaFond, E. C. — Personal Communication.

Piip, A. T. 1964 — Fine structure and stability of the sound channel in the ocean. J. Acoust. Soc. Am. 36(10): 1948-1953.

Robinson, M. — Monthly mean temperature charts from surface to 400 feet (in preparation).

Rodewald, M. 1964 — Beiträge zur Klimaschwankung im Meere. 13, Die Asymmetrie im zeitlichen Verlauf der Wassertemperatur-Anomalien in Puerto Chicama (Peru), Dtsch. Hydrogr. Zeitschr. 17 (3): 105-114.

Templeman, W. 1964 — Anomalies of sea temperature at Station 27 off Cape Spear and of air temperature at Torbay-St. John's. Paper pres. ICNAF Environmental Symp., Rome, January 1964 (ms.).

U.S. Bureau of Commercial Fisheries, Stanford Biological Laboratory. Long-term monthly mean sea surface temperature charts for Pacific Ocean (in preparation).

Wolff, P. M., L. P. Carstensen and T. Laevastu 1965 — Analysis and forecasting of sea surface temperature. FNWF Techn. Note 8.

ACOUSTIC EFFECTS OF INTERNAL WAVES IN THE OCEAN

by

H. Francis Eden
Arthur D. Little, Inc.
and
Michael Mohr
Massachusetts Institute of Technology

INTRODUCTION

Internal waves are one of the many phenomena which cause variations in the structure of the water column below the sea surface. They are similar to surface waves in that small elements of water travel in elliptical orbits with no appreciable net movements, and the energy travels at the group velocity. The maximum amplitude of the internal wave disturbance occurs at or near the pycnocline, which in the ocean corresponds to the thermocline, with only small amplitude variations occuring at the ocean surface. Internal waves differ from turbulence in that the elements of water in a turbulent eddy undergo translation, and the energy is transported as kinetic energy of the elements at a speed set by the speed of the turbulent flow.

A wide spectrum of internal waves occur in the oceans ranging from short period stability oscillations with periods of 1 to 2 minutes and amplitudes of centimeters to long period waves with periods of days or weeks, wavelengths of tens of miles and amplitudes of hundreds of feet. The temporal and spatial occurrence of internal waves is uncertain but diurnal and semi-diurnal tidal period waves are common along the continental shelves and may have amplitudes of tens of feet and short period (1 minute to 1 hour) waves occur frequently close to the coast. Figure 1 (taken from Defant, 1961) illustrates the circulation in an internal wave at the interface of two fluids of different densities. This is a fairly good approximation to the ocean where the thermocline separates two almost homogeneous layers. The occurrence and possible effects of such waves are of interest from the point of view of naval operations (Morey, Mohr and Birkett, 1966). In this paper we will outline possible effects on underwater sound propagation.

QUALITATIVE DESCRIPTION OF ACOUSTIC EFFECTS

Temperature gradients in the ocean are the primary cause of refraction of sound waves and so motion of the thermocline, because of internal waves, will cause corresponding effects in acoustic propagation in that region.

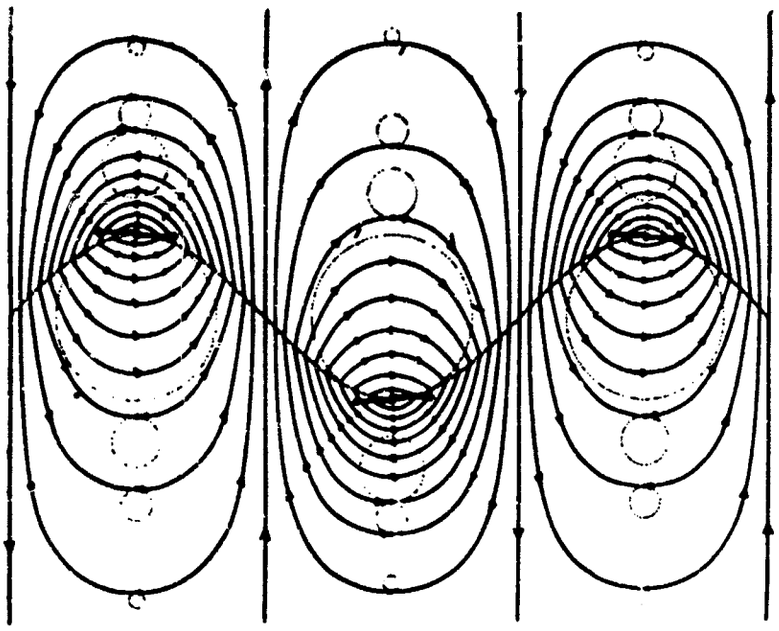

Figure 1 Streamlines and Orbits in a Progressive Internal Wave Travelling from Left to Right at the Boundary of Two Fluids (After Defant)

In discussing possible acoustic effects of internal waves it seems desirable from a practical point of view to compare possible or known effects of internal waves with the effects of the random inhomogeneities in the ocean which to some extent always occur. We can distinguish random inhomogeneities into acoustically weak and acoustically strong. In a similar manner to internal waves, the turbulence in the oceans causes the temperature, density and sound velocity in the medium to vary spatially and temporally but in a random fashion. Thus we can write that $C_0/C = 1 + \nu(x.t)$ when ν is the fluctuating part of the acoustic index of refraction C_0/C and is much less than unity.

The time fluctuations of the index of refraction are very slow compared to the passage time of sound waves. Therefore, from the point of view of propagating sound waves the medium has a stationary spatial structure. This microstructure changes slowly in the course of time due to advection of the temperature patches causing correspondingly slow changes in the amplitude and phase of the transmitted sound. Turbulent fluctuations of temperature are acoustically weak inhomogeneities. The upper and lower boundaries of the ocean, air bubbles, marine organisms or even submarines are acoustically strong inhomogeneities, and have major effects on sonar operation. Figure 2 tabulates some possible acoustic effects in the ocean and their orders of magnitude.

The fluctuations in acoustic signals due to ocean turbulence must be expected to occur always and at a point may be ±6 db of the unscattered signal intensity which would have occurred (see e.g., Liebermann. 1951; Skudrzyk, 1963). The strong acoustic effects such as air bubble screens or surface image interference do not always occur but can cause variations in signal intensity of tens of db. Fluctuations in the sound scattered by the deep scattering layer may be of the order of 10 db. It is against this background that we should consider the acoustic effects of internal waves.

There have been several theoretical attempts (e.g., Barakos, 1965) at predicting the effects of internal waves on acoustic transmission but there exists very little experimental evidence of acoustic effects which can be correlated with the presence of well defined internal waves. The main published analysis of the possible effect of internal waves is the paper by Lee (1961). This paper deals with a specific case and will be discussed later, following a qualitative discussion of the general problem. We can distinguish at least four different cases in this discussion depending on the ratio of the ocean distance scale R (perhaps the sonar range for direct path detection) to λ the wavelength of the internal wave. The cases are:

1. $R/\lambda << 1$ Long waves in open ocean. The thermocline appears flat but depth of TC and hence sonar range changes over periods of hours. "Non-noisy effect."

2. $R/\lambda < 1$ No periodicity apparent to sonar signal, but slope of TC noticeable.

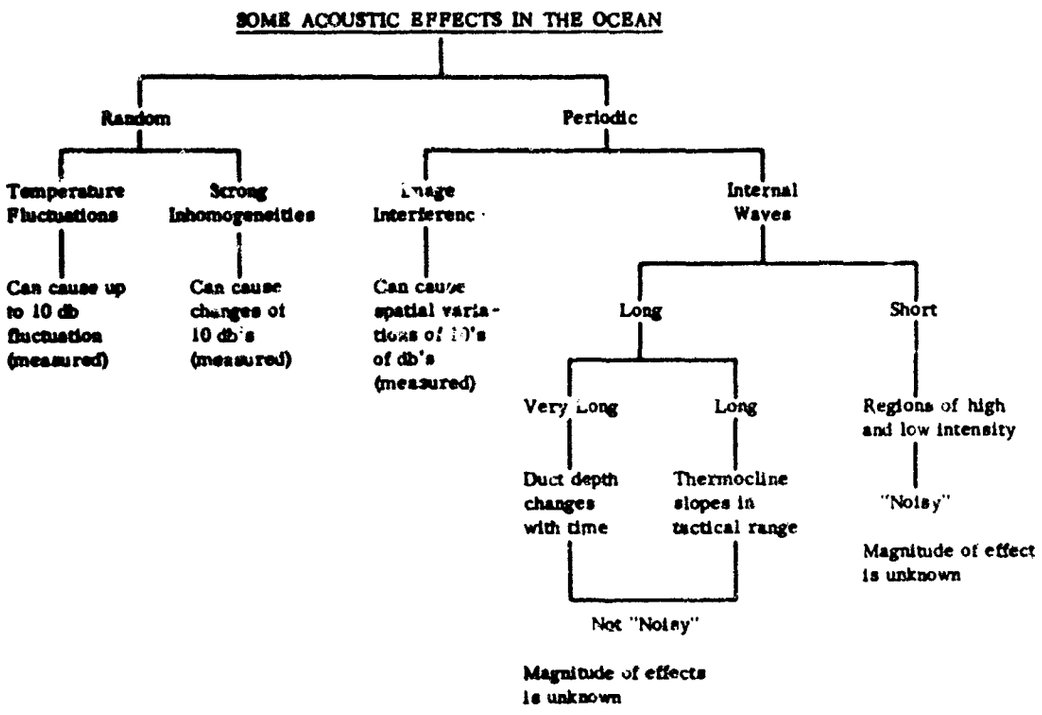

Figure 2 Some Acoustic Effects in the Ocean

3. $R/\lambda \sim 1$ Short range effect of short waves found in shallow water. (Subject of Lee's analysis.)

4. $R/\lambda >> 1$ Short waves over continental shief. No data available, but "noisy" effect anticipated.

Little further can be said about case (1). Obviously there will be a change in sonar performance in the surface duct over a period of hours resulting perhaps in considerable changes in probability of detection for a submarine hovering near the surface. However, it seems fairly likely that the slow rise and fall of the thermocline would be obvious to a submarine commander who wished to remain below the surface duct and the sub would have sufficient time to take action.

In case (2) the wavelength of the internal wave becomes comparable with a tactical range for sonar operation, i.e., a distance of several kilometers. In this case the internal wave results in a gentle rise (fall) of the thermocline and a consequent narrowing (deepening) of the surface duct over the entire operational range. Here we can see qualitatively some effects on sonar performance in various modes; e.g.,

a. Surface duct transmission: The signal is always in a region strongly influenced by the internal wave.
b. Direct path transmission through the thermocline: For small angles if incidence this will be similar to (a).
c. V.D.S: Direct path transmission below the thermocline is probably effected if the angle of incidence is low.
d. Bottom bounce: Probably little effect due to steep incidence.
e. Convergent zone: Same as (d).

It appears that internal waves may be significant in cases a,b,c.

Figure 3 is a simple illustration of the effects of the first example of surface duct transmission. It shows three cases. In case (a), there is no internal wave and the thermocline remains at Z_d over the tactical range. We can define R_a^* as the maximum range for direct path detection in the surface duct. We assume a velocity profile as shown to the right of (a), i.e., the velocity increases slighely with depth to the thermocline and then falls off with increasing depth. The predicted shadow zone is shaded.

In (b) a long internal wave has raised the thermocline in the direction of signal propagation so that at a horizontal distance equal to $0.5\ R_a^*$ the surface duct has narrowed to $0.5\ Z_d$. Obviously the shadow zone advances towards the source and $R_b^* < R_a^*$ so that the possibility of direct path detection is less.

In case (c) the thermocline is taken down by the wave and R_c^* is increased over R_a^*. It is possible to write analytic expressions for $R_{a,b,c}^*$

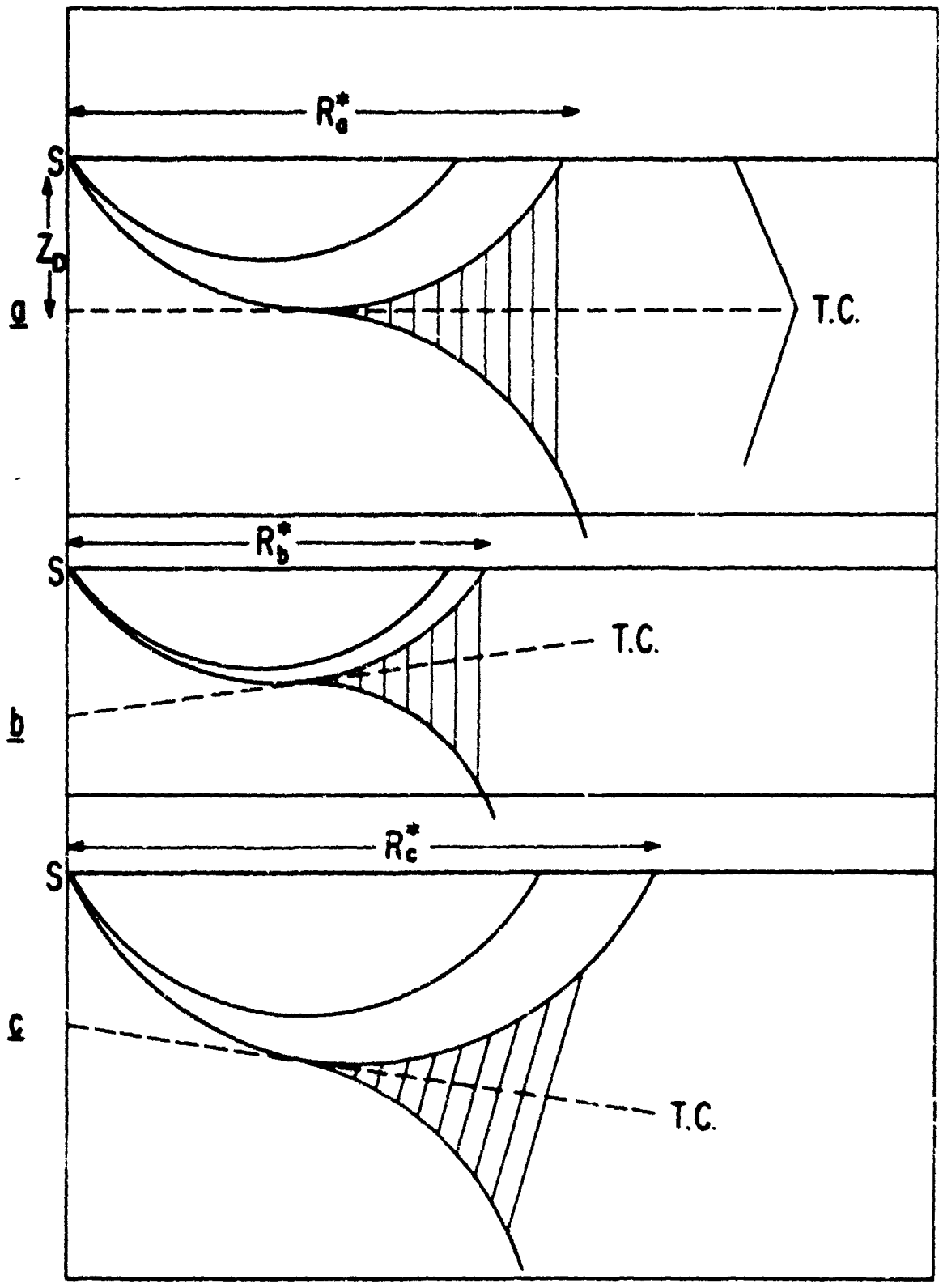

Figure 3 The Effect of a Sloping Thermocline on Direct Path Transmission in the Duct

in terms of the velocity profile and assuming a linear rise with distance of the thermocline. Figure 4 shows corresponding situations for v.d s. transmission in direct path. This is virtually the mirror image of duct transmission.

In case (3) many cycles of an internal wave occur within the acoustic range of interest. This indeed is the case which has been treated by Lee. Using ray tracing he found that the internal wave caused areas of focussing and defocussing of the sound. We must point out here that interference effects due to phase changes cannot be determined by such a treatment. Only effects due to refraction (the lens-like quality of the wave) are determined.

Lee considered linear velocity profiles and a three layer ocean of depth 60 feet such that

$$0 < z < z_1(x) \qquad \frac{dc}{dz} = 0 \text{ sec}^{-1}$$

$$z_1(x) < z < z_2(x) \qquad \frac{dc}{dz} = -4.8 \text{ sec}^{-1}$$

$$z_2(x) < z < 60 \qquad \frac{dc}{dz} = -0.6 \text{ sec}^{-1}$$

In the absence of the internal wave the thermocline lay between $z = 30$ and $z = 40$. The internal wave raised or lowered the surfaces of the thermocline some 10 feet with a wavelength of 300 feet. These values corresponded to experimental data on internal waves off San Diego.

Lee found that the presence of the internal wave could cause acoustic contrasts of 22 db over distance of several internal wavelengths, wherein contrasts of 5 db occur in the absence of the wave.

The fourth case where $R/\lambda << 1$ has never been considered. The internal waves might be expected to cause fluctuations similar to the random thermal patches but in a spatially periodic manner. The nature of the periodicity would depend on the coherence of the internal wave and the direction of signal propagation relative to the direction of wave motion.

COMPUTER STUDIES

These effects are suitable for further investigation by computer models. However, difficulties will arise in these studies. For example, in Figure 3 we have assumed that raising the thermocline has little effect on the velocity gradient in the duct. This assumption is not necessarily valid. The more general case where dc/dz, the velocity gradient, and z_d, the depth of the duct, are both functions of the horizontal range R, leads to complicated problems in determining ray paths from geometrical acoustics. Indeed the problem of horizontal velocity gradients in the ocean is a major one in underwater acoustics. Two kinds of computer studies can be performed using ray tracing or normal mode calculations.

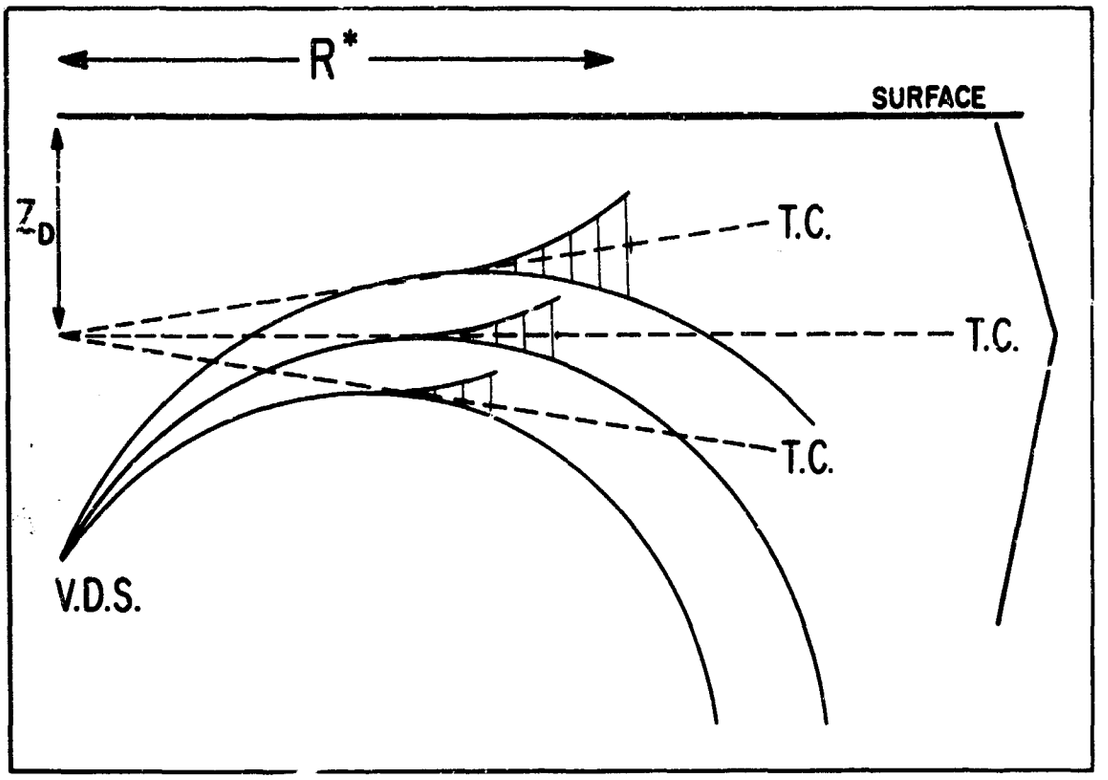

Figure 4 The Effect of a Sloping Thermocline on V.D.S. Transmission below the Duct

Ray tracing calculations determine ray directions and wave fronts. Variations in intensity are caused by a combination of losses and geometrical spreading. Ray tracing determines the geometrical spreading. Energy conservation requires that the integral of intensity F over the whole wave front accounts for all the energy except that lost by absorption. This requirement is met if the local rate of change of intensity $-\frac{1}{F}\frac{dF}{dS}$ due to spreading with distance S along a ray is proportional to the product of the two principal curvatures R_1 and R_2 of the wave front, i.e.,

$$-\frac{1}{F}\frac{dF}{dS} = \frac{1}{R_1} + \frac{1}{R_2}$$

Generally, in ray calculations it is postulated that the ocean properties are independent of azimuth and vary only with z. Thus changes in R_2 are regarded as being due to spherical spreading, i.e.,

$$\frac{1}{R_2} = \frac{\cos \Theta}{x}$$

where x is the horizontal range and Θ is the initial depression, and

$$-\frac{1}{F}\frac{dF}{dS} = \frac{1}{R_w} + \frac{\cos \Theta}{x}$$

$\frac{1}{R_w}$ is then computed step by step along the ray for the appropriate values of $\frac{dc}{dz}(z)$ where $\frac{dc}{dz}$ is variation in sound velocity with depth. In the event of horizontal velocity changes both curvatures will change along the ray and must both be computed in an iterative fashion.

In normal mode calculations it is difficult to describe in simple physical terms the effect of horizontal velocity changes on the mode structure of the duct. In the simpler case of the thermocline rising or falling without $\frac{dv}{dz}$ changing it is apparent that the varying duct will have a different mode structure as the range increases. In the case of $R/\lambda > 1$ the lower boundary of the duct is corrugated which will effect the leakage of energy out of the duct.

Further computer studies of the possible acoustic effects of internal waves would lead to interesting results and also to improved numerical simulation programs.

ACKNOWLEDGEMENTS

This paper is based on studies which were performed for and supported by the U.S. Navy Bureau of Ships.

REFERENCES

Barakos, P.A., 1965: On the Theory of Acoustic Wave Scattering and Refraction by Internal Waves, U.S. Navy Underwater Sound Laboratory Report No. 649.

Defant, A., 1961: Internal Waves, Physical Oceanography, Vol. 2, Pergamon Press.

Lee, O.S., 1961: Effect of an Internal Wave on Sound in the Ocean, J. Acoust. Soc. Am., 33, No. 5, 677.

Liebermann, L.J., 1951: The Effect of Temperature Inhomogeneities in the Ocean on the Propagation of Sound, J. Acoust. Soc. Am., 23, No. 9, 563.

Morey, C., Mohr, M., and Birkett, J., 1966: Internal Waves: Their Influence upon Naval Operations, Arthur D. Little, Inc., Report to the Navy Bureau of Ships, No. 4090266

Skudrzyk, E.J., 1963: Thermal Microstructure in the Sea and its Contribution to Sound Level Fluctuations, "Underwater Acoustics", ed. V.M. Albers, Plenum Press, New York.

QUASI-PERMANENT FEATURES OF THE CIRCULATION IN THE WESTERN NORTH ATLANTIC

D. Jean Keen
U.S. Naval Oceanographic Office

INTRODUCTION

Fifteen years ago Fuglister (1951) called attention to the fact that, in the western North Atlantic, charts of average temperature and salinity distributions and charts of average currents do not indicate certain features of the circulation that appear to be semi-permanent in nature. The collective of such averaged charts is commonly termed the "climatology" of the region thus described. The obscured features to which Fuglister had specific reference were multiple currents in the Gulf Stream System and it was these which aroused the greater interest at the time. His remarks about the inadequacies of climatological treatments, namely, the averaging processes used, are almost as pertinent now as they were in 1951.

What was once an interesting problem, today has become an important one as well. Thermal structure forecasts are being issued routinely to the Fleet. Their sole purpose is to help the planners and tacticians who must decide how best to deploy forces, place sensors, route convoys, space screens, station barriers -- all decisions which are, in part, contingent on preoperational knowledge of sonar and weapon performances. The link between such performance and thermal structure forecasts needs no elaboration. The forecasts rely heavily on the climatology of temperature at various levels as a tool. If the climatology in the forecast area is inadequate; particularly, if by masking real features it provides deceptive information, the forecasts are degraded and their value diminished.

The Naval Oceanographic Office has a particular interest in the western North Atlantic. It is our laboratory for developing improved techniques to forecast thermal structure. The area is dominated by the Gulf Stream System. Its dynamics are unknown. Stommel (1965) has neatly summarized the many theories advanced to explain why the Stream behaves as it does; but none of these are proven. Very short range forecasts can be made by computing short-term advection and the surface interactions collectively known as the heat budget and on the basis of persistence. Long range forecasts can be made with a modest degree of success using a combination of long-term anomalies, heat budget estimates, and recent trends. The middle period is the most difficult to forecast. It is at this time that the thermal structure begins to respond to the forces acting on the System as a whole. It is at this time that the inadequacies of the climatology are most evident, for in place of the unknown forces, we must extrapolate back from climatology.

Since there is no reason to think that dynamic solutions will be achieved in the very near future, we might profitably devote more time and thought right now to improving the climatology. If quasi-permanent features exist, it must show them. The first step is to try to identify those features which should be shown.

DISCUSSION OF THE FEATURES

Since the Gulf Stream System is a system in motion, the identification process resolves, more realistically, into the positioning of zones in which features that can be characterized by such specifics as direction, amplitude, wave length, width, etc. are most often found.

The data used were thirty-six monthly mean sea surface temperature analyses, a 3-year set. Each analysis is based on some nine to ten thousand synoptic ship reports, averaged by one-degree squares. The sample is certainly not optimum. The data contain spurious errors. The time period for averaging may be poorly chosen if the form of a meander persists less than 30 days or in multiples of other than 30 days. There is evidence that large features do maintain their form for long periods of time, however. Both Operation Cabot (Fuglister and Worthington, 1951) and Gulf Stream '60 (Fuglister, 1963) showed this to be true, so that on the basis of present knowledge, 30 days does not seem an unreasonable averaging period. The choice of one-degree squares is more suspect, since we have evidence that in some parts of the area, 20-minute averages better represent real conditions. Figure 1 is an example of one such analysis. Though much smoother than a synoptic analysis the pattern is still quite complex.

Figure 2 is a portion of the same analysis simplified by deleting several of the isotherms. The circled numbers correspond to the general positions of the feature-zones tentatively identified as quasi-permanent. First is the main counterflow along the southern edge of the stream. No limits for its most westerly surface manifestation could be defined. The southerly movement to the east of Bermuda is found in 75% of the analyses. Features 3, 4, and 5 are feeders off the primary northward flow. Of these, 3 is least distinct; its existence is probably dependent on the magnitude of the counterflow. Features 4 and 5 however, are evidenced in 90% of the sample. In the northwall of the Gulf Stream proper between Hatteras and the Grand Banks, the position of feature 6, where the isotherms indicate flow toward the coast, shows little variability. If one is partial to Warren's (1962) hypothesis of topographic influence on the course of the Stream, it is interesting to note that the position of this zone approximates that of Hudson Canyon. Features 9, 7, and 8 display greatest variability, in that order, but features 10 and 11 are more distinctly evidenced. In general, the features compare favorably with features indicated in Elizabeth Schroeder's (1952) analysis of temperatures at 200 meters.

Figure 3 is a seasonal grouping of the features of the northwall. The points indicate the most seaward excursion of a meander, except in zone 5, where the most shoreward position is marked. With so small a sample, no monthly or month-to-month relationship should be expected, nor was any found. The fact that no relationships were apparent, however, does not in any way preclude the possibility of persistence past 30 days; it only supports an inherent assumption that the analyses were independently prepared.

Figure 4 summarizes the seasonal groupings. The shaded areas were common to at least three seasons; the area within the solid line to two, and the dotted lines are the limits of overall spread.

Variability was greatest in summer, as might be expected. Best definition, however, obtained in the fall. There was a marked tendency for secondary features in spring and summer between 8 and 9. From Hatteras to the Grand Banks, mean wave length of the features was 195 nautical miles, but the seasonal means ranged from 120 to 250 nautical miles. The overall range was 90 to 300 miles. The migration, that is, the degree of shifting, along the axes of orientation (in a generally north-south direction) was greatest in summer, least in fall. Normal to the axis in the mean direction of flow, the zones were broadest in winter, summer being a close second, and narrowest in the fall. Numbers are being purposely avoided, since the superficial nature of this examination dictates a need for considerable restraint.

A fictitious analysis drawn to these generalities would look something like Figure 5. It fits neither a synoptic analysis nor the 30-day mean chart very well. It bears even less resemblance to the long term climatological analysis. What it does do is point up areas in which the space, and possibly, time scales used in the climatological treatments bear reexamination.

The climatological distribution of sea surface temperatures in November is shown in Figure 6, taken from Mazeika (1965). The climatological averages also reflect better definition in the late fall and early winter. This chart is the only one of the twelve monthly means that indicate the two northward extensions from the Antilles Current, which are quite well defined in the 30-day analyses.

To see how the fictitious analysis compares with synoptic data look at Figure 7, which shows the fictitious northwall and four paths of the 17°C isotherm as tracked last month with the airborne radiation thermometer (ART). We have good checks on these data with the R/V EXPLORER. Note that the envelope fits the synoptic data reasonably well, especially with respect to features 6, 7, and 8. Note also the persistence in the form of the meanders outlined here. Note also, however, that the manufactured analysis does not do a very good job of describing the actual form of the features.

SUMMARY

To summarize briefly, there are quasi-permanent features in the circulation of the western North Atlantic which are not adequately described by the climatology of that area. Until we better understand the dynamics of the Gulf Stream System, however, forecasting for this area will continue to place heavy reliance on its climatology. Therefore, the climatology must be refined to the time and space scales of the features that must be shown. Zones within which some of these features are most likely to occur have been tentatively identified from thirty-day mean sea surface temperature analyses. Other quasi-permanent features have been discussed elsewhere, primarily in reports by Fuglister (1951, 1963). The general agreement between features apparent from the 30-day means and those which have received more careful study and are supported by data at depth, indicates that further investigation of the features based on surface observations is tenable.

FUTURE PLAN

We plan to continue systematic ART flights during the next year, both along the northwall of the Stream and in the southern part of the area, to obtain better definition of the spatial and temporal variability of features in the surface circulation. Airborne expendable bathythermographs (BT's) will also be used, albeit sparingly, so that total reliance need not be placed on surface temperatures alone. One approach to climatological refinement has already been attempted. This is essentially a spatial separation into "water mass domains". Although of itself, this approach improves the forecasts only marginally, it is an encouraging sign. Coupled with a better description of quasi-permanent features within the domains, the climatology should substantially improve both the middle and long range forecasts.

PRINCIPAL REFERENCES

Fuglister, F.C., 1951. Multiple currents in the Gulf Stream System. Tellus, 3 (4), 230 - 233.

Fuglister, F.C., 1963. Gulf Stream '60. Progress in Oceanography, V. 1, 265 - 383. Pergamon Press.

Fuglister, F.C., and Worthington, L.V., 1951. Some results of a multiple ship survey of the Gulf Stream. Tellus, 3 (1), 1 - 14.

Mazeika, P.A., 1965. Prediction of the 400-foot temperature in the North Atlantic. U. S. Naval Oceanographic Office, Technical Report No. 147.

Schroeder, E.H., 1952. Serial Atlas of The Marine Environment, Folio 2: North Atlantic temperatures at a depth of 200 meters. American Geographical Society.

Stommel, H., 1965. The Gulf Stream. Second Edition, University of California Press.

Warren, B.A., 1963. Topographic influences on the path of the Gulf Stream. Tellus, 15 (2), 167 - 183.

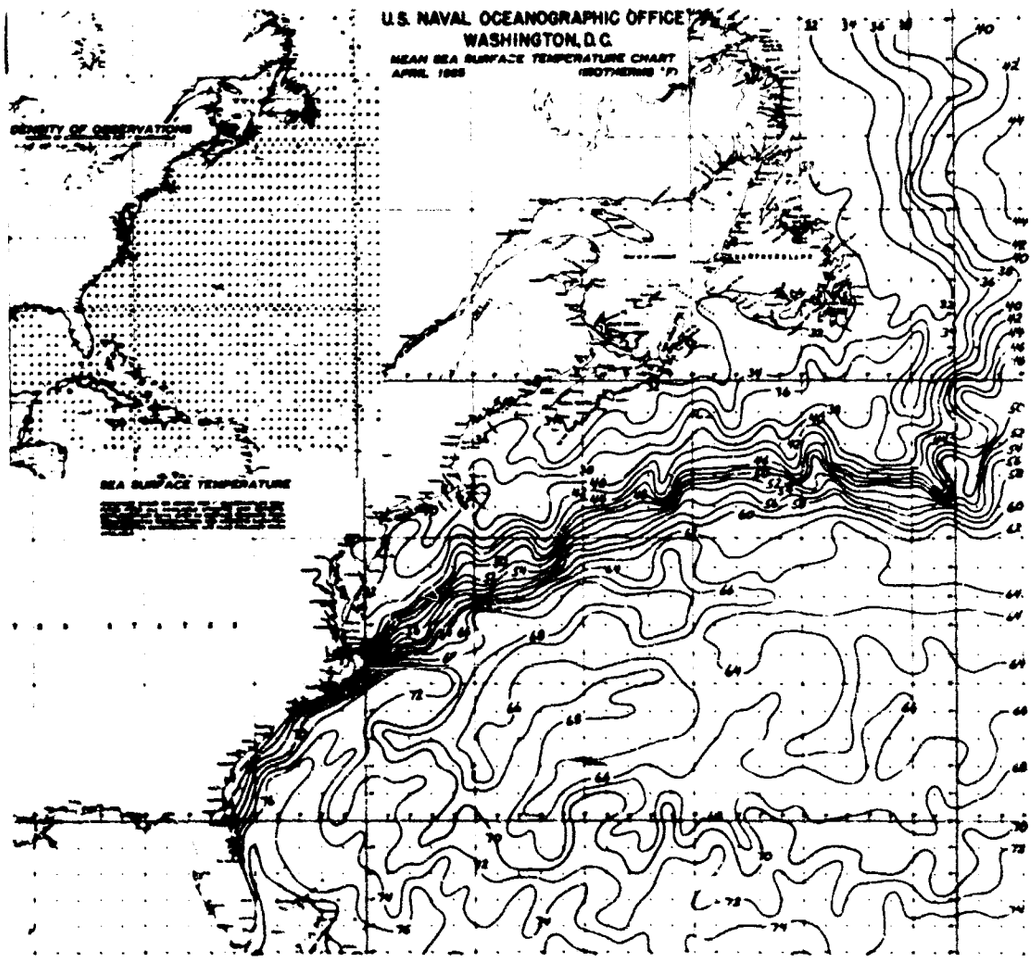

Figure 1. Examnle, monthly mean sea surface temperature analysis

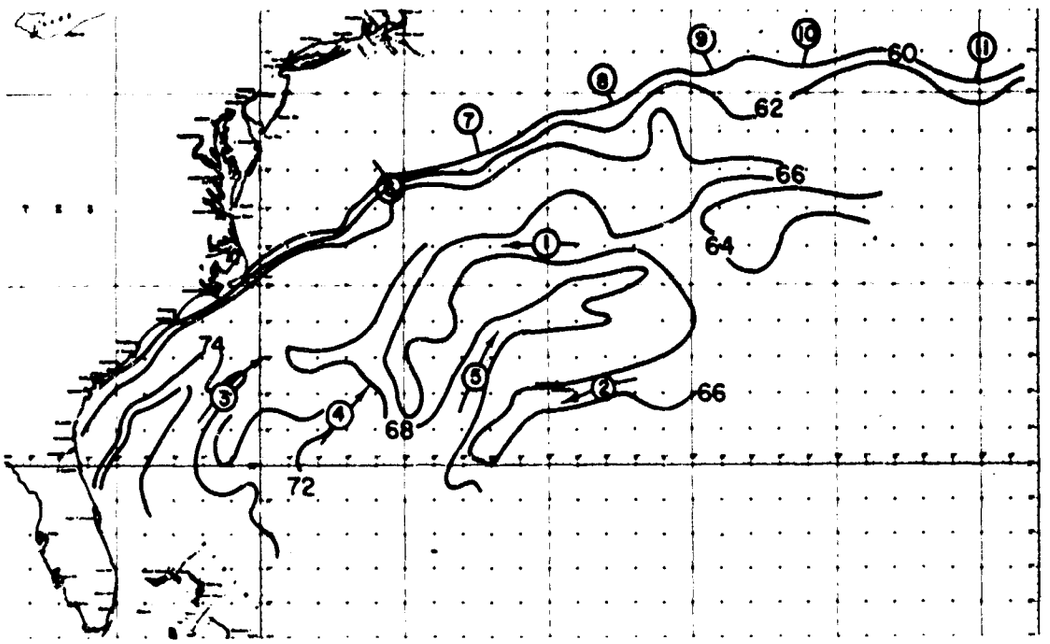

Figure 2. Quasi-permanent features

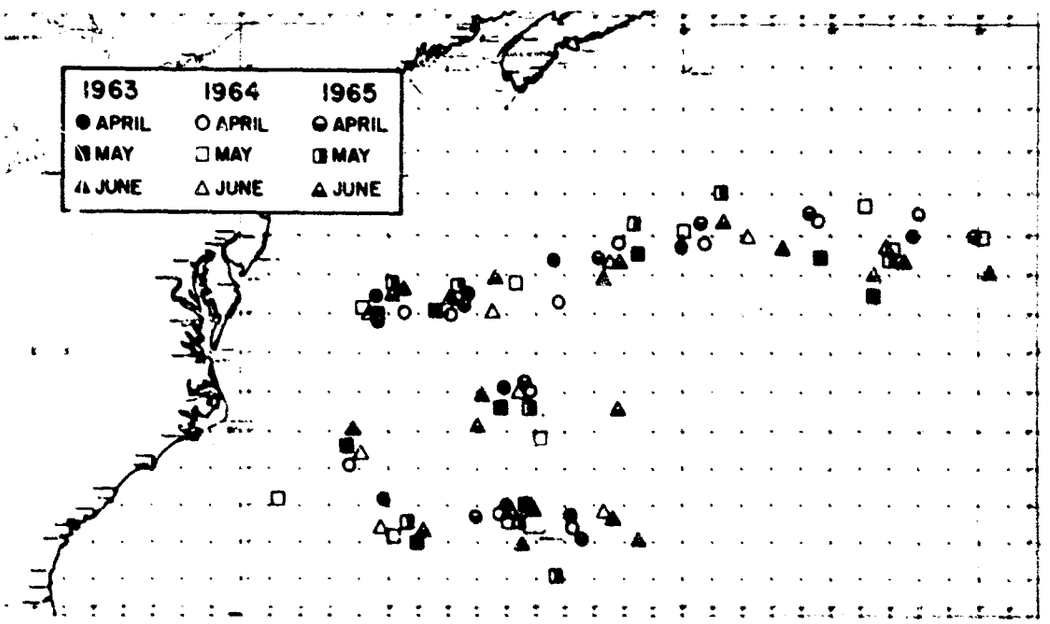

Figure 3. Seasonal plot, quasi-permanent features

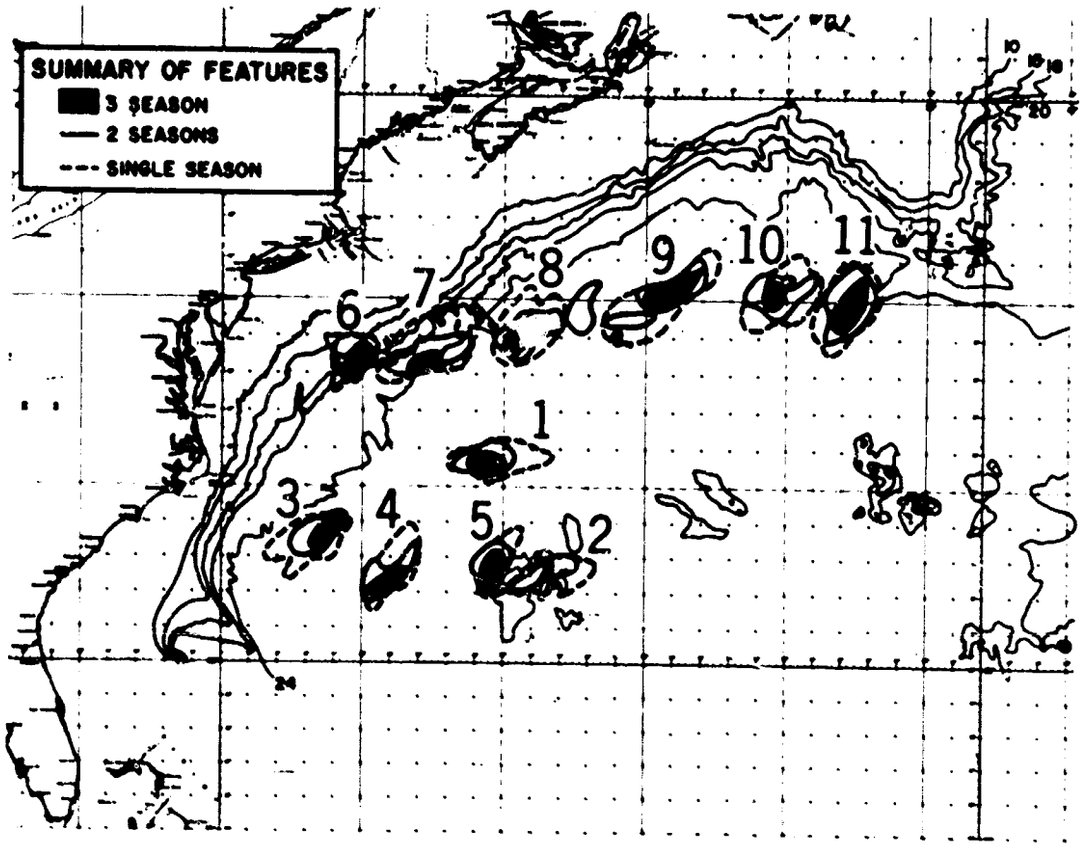

Figure 4. Summary of quasi-permanent features

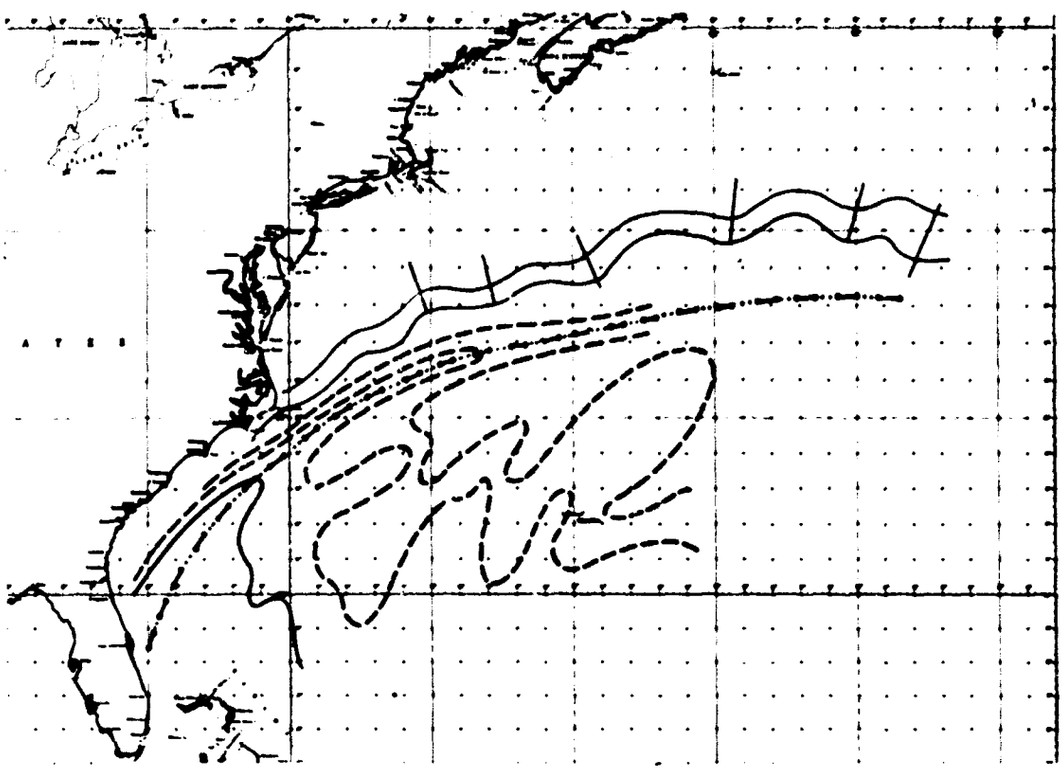

Figure 5. Fictitious analysis of surface temperature

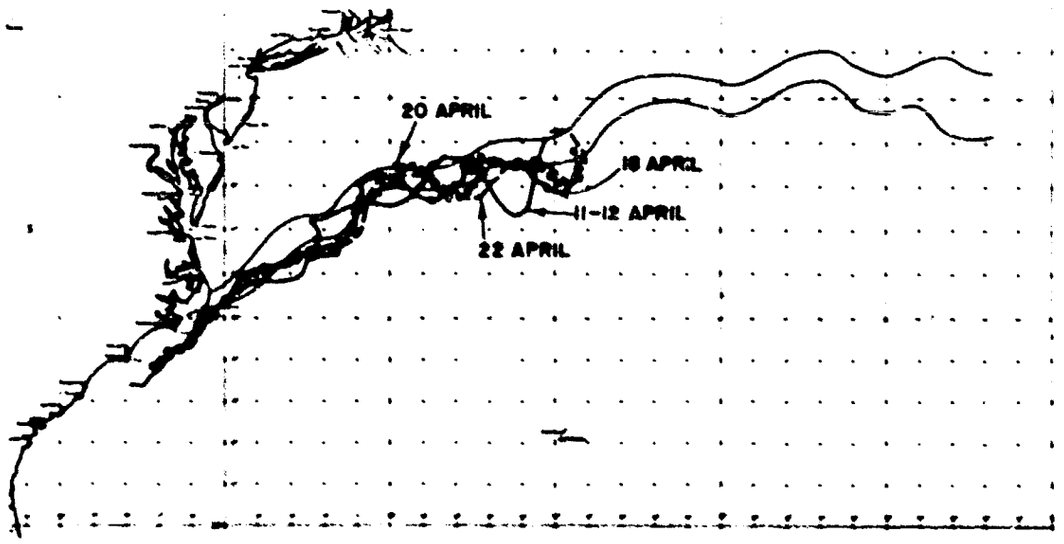

Figure 6. Comparison of synoptic data to reconstructed field

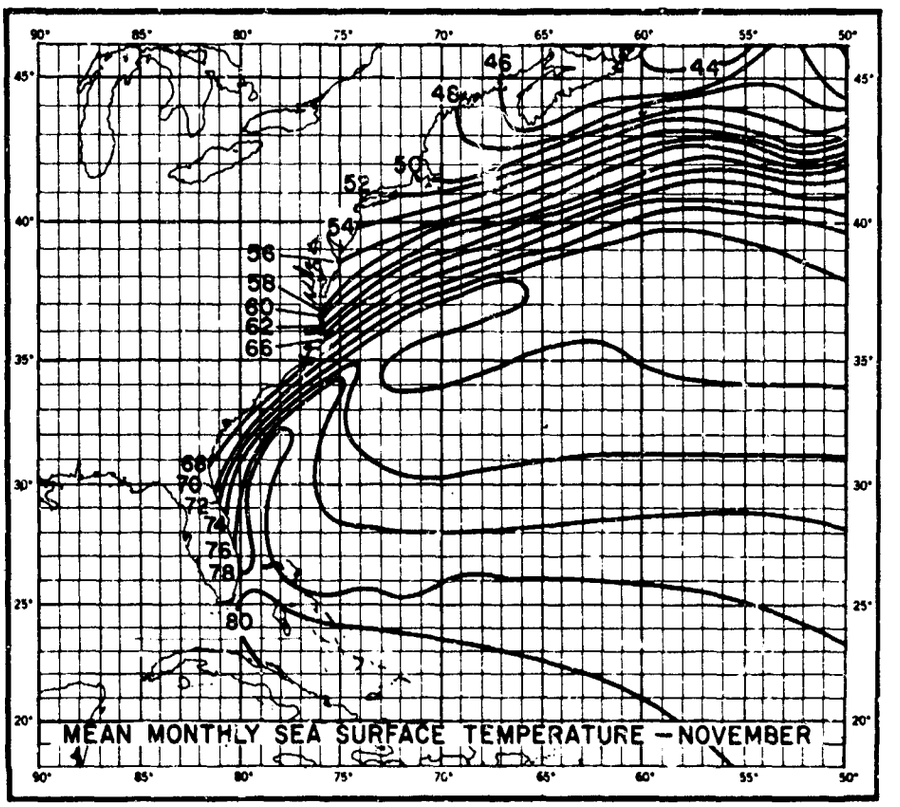

Figure 7. Example, climatological surface temperature chart

SAFETY CERTIFICATION OF DEEP RESEARCH VEHICLES

CDR. L. L. JACKSON, JR., USN

Headquarters, Naval Material Command
Main Navy Building, Washington, D. C.

ABSTRACT

The hazards of the deep ocean environment in which deep research vehicles operate are such that it is necessary to determine that the design and construction of the vehicles, the competence of the operators, and the conditions of use provide every reasonable assurance that personnel embarked for scientific research be safe. CSS HUNLEY is used as an example of an advanced type of submersible which, while ultimately successful in her mission, was indisputably unsafe. The Navy expects to establish procedures whereby the safety of any submersible vehicles regularly embarking Navy military or civilian personnel may be determined.

BACKGROUND

Undersea exploration and exploitation carried to the extent seen today must be considered a new experience for mankind. Modern navies of the world have designed, built and operated military submarines in great numbers since the beginning of this century, but it is only during this decade that the world has seen the design, construction and use of such a wide variety of submersibles for non-combatant purposes. Figure 1 lists many which are contracted for, or under construction, or operational in this country today. Many others are operating in other countries of the world. These submersibles are expensive vehicles, but far more valuable are the scientists, engineers, or other personnel who venture underwater in them.

To illustrate the hazards of submarining which tend to justify a certification process, one may consider the example of the first militarily successful submarine in America.

CSS HUNLEY VERSUS USS HOUSATONIC
(Reference 1)

This submarine was the second type built by Captain J. R. McClintock, Confederate Army, Mr. Horace L. Hunley (a successful sugar broker), and Mr. Dexter Watson. LT J. A. Alexander, an engineer officer, provided engineering assistance. Although the semi-submersible torpedo boats, the Davids, had had some success, notably against USS NEW IRONSIDES, it was the HUNLEY which was expected to break the Union blockade.

(Figure 2)

HUNLEY was designed, constructed, and ran first sea trials at Mobile, Alabama, in 1862. The builders were Thomas Parks and Thomas B. Lyons of Mobile. It was constructed by modifying a 25-foot long, 4-foot diameter ship's boiler, split in halves for fitting. Two small conning towers lined with glass ports and fitted with bolted covers were installed fore and aft. Inside was an eight-man crankshaft driving a single, shrouded, three-bladed propeller to provide a maximum speed of four knots. The shaft operators sat on the starboard side facing athwartships to turn the shaft. The conning officer manned the forward conning tower operating the bow planes, rudder, and bow ballast tank pump and flood cock, while a petty officer could man the rear conning tower and

NONCOMBATANT SUBMERSIBLES APRIL 1966

OPERATIONAL

U.S. NAVY	TRIESTE II	
	MORAY TV-IA	
	DEEP JEEP	
	SEA LAB II	
	ALVIN I	
U.S. PRIVATE INDUSTRY	ALUMINAUT	Reynolds Aluminum
	CUBMARINE PC3 A&B	Perry Cubmarine Co
	STAR I	General Dynamics
	ASHERAH	General Dynamics
	DEEP STAR 4000	Westinghouse
	BENTHOS V	Lean Siegler Inc

UNDER CONTRACT OR CONSTRUCTION

U.S. NAVY	USS DOLPHIN (AG SS 555)	
	NR-I	
	DSRV	
	TRIESTE III	
U.S. PRIVATE INDUSTRY	STAR II	General Dynamics
	STAR III	General Dynamics
	DEEP QUEST	Lockheed
	DOWB	General Motors
	CUBMARINE PC3C	Perry Cubmarine Co
	DEEP STAR 2000	Westinghouse

Figure 1

Figure 2

stern ballast tank when not assisting with main propulsion. Air for two hours submergence came through the hatches or through a 4-foot section of 1-1/2 inch piping which led to a vented iron box on the 12-inch wide deck topside. Candles were used for lighting and to warn of low oxygen levels. Normal reserve buoyancy was provided by water ballast tanks in the superstructure fore and aft. These were fitted with flood valves and were emptied by hand-driven pumps Emergency recovery was to be accomplished by means of detachable solid iron castings held to the keel by T-bolts which could be manually unscrewed to drop the weights, if needed. Manually operated bow planes and a rudder were provided for depth and course control. However, the submarine was longitudinally unstable. It was about 40 feet long, 4 feet wide, and 5 or 6 feet in depth. Freeboard was measured in inches. A magnetic compass and seaman's eye were the navigation aids.

Armament consisted of a copper torpedo carrying 90 lbs. of black powder ignited by a mechanically actuated chemical exploder. The 20-foot spar was strapped topside to the bow so that once a hull penetrator on the torpedo had been driven into the side of a target, the submarine could back away from the target, detonate the warhead from a 100-foot distance, and proceed back to port.

Although trials in Mobile Bay had been quite successful, a series of misfortunes befell HUNLEY after, following loss of Mobile, she was shipped by flatcar to Charleston. There, under command of Lt. John Payne, CSN, she was swamped and sunk in the wake of a passing steamer with the loss of all hands except LT Payne. According to another report, she capsized on a subsequent trial and only LT Payne and three of the crew escaped. (Reference 2) LT Payne refused to take her out again, but Mr. Hunley recruited a crew of volunteers from among those in Mobile who built her and continued operations. On a practice dive, October 15, 1863, Mr. Hunley and all hands were lost when the submarine buried her nose, at an angle of 35 degrees, in the bottom of the river, nine fathoms deep. She was recovered nine days later, but General Beauregard had had enough and ordered her docked for good.

However, the constant pleas of LT George E. Dixon, Twenty-First Alabama Regiment, and the engineer, LT J. A. Alexander, combined with the increasing difficulties of running the Union blockade, persuaded the General to allow another attempt. LT Dixon and LT Alexander carefully selected a crew from among the many available volunteers and trained them assiduously in the first Submarine School, Mount Pleasant, S C.

Finally, at about 1930, the night of February 17, 1864, having been ordered by General Beauregard to stay on the surface, LT Dixon got underway to attack the 1,240-ton wooden corvette, USS HOUSATONIC (23 guns) anchored off Beach Inlet, a few miles south of the entrance to Charleston Harbor. HOUSATONIC saw HUNLEY coming, slipped anchor, backed down and fired small arms attempting to evade or sink HUNLEY. Nevertheless, about 2100, LT Dixon succeeded in attacking and detonating the spar torpedo to the port side forward, but the explosion sank both HOUSATONIC and HUNLEY. (Reference 3)

Both HUNLEY and HOUSATONIC are still there, distinguished respectively by being the first submarine to sink a warship and the first man-of-war sunk by a submarine. The next ship sunk by an American submarine was the 8,663-ton Japanese ship ATSUTUSAN MARU sunk December 16, 1941, by USS SWORDFISH (SS193) under the command of LCDR Chester C. Smith, USN. (Reference 4)

HUNLEY'S HAZARDS

The loss of at least 26 valiant submariners in CSS HUNLEY may be analyzed from three points of view. The first is material adequacy to assure safety. Although the technology developed in submarine design and construction by David Bushnell, Robert Fulton, Wilhelm Bauer, L. D. Phillips, and the Frenchmen, Burgeoise and Brun, were probably available to the designers and constructors of HUNLEY, it appears that in the interest of making an early breakthrough in naval warfare, the Confederates did not study thoroughly enough, nor test carefully enough the basic concept, the design plans, the construction details, nor the feasibility of those features essential to safe operations. It is now clear that the conceptual errors in design contributing to HUNLEY's almost untolerable safety record were lack of longitudinal stability, too low a freeboard when running on the surface, unreliable surfacing system, unduly complex emergency deballasting, exceptionally hazardous ordnance, and absence of means for individual escape. The exigencies of war in this case, however, prevented a carefully studied development of this system; one which could have applied the accumulated experience of ship and ordnance designers and engineers to analyze critically each aspect of the design and construction in the interests of system safety.

Another point of view would examine the qualifications of the operators. Enthusiasm, bravery, daring, and eagerness to man the submarine

is not enough. CAPT McClintock reports no difficulty obtaining crews for HUNLEY, except for the wiser and probably sadder LT Payne who survived two disastrous sinkings of HUNLEY. However, only a few operators of HUNLEY had much opportunity to become proficient in the technical skills required of submarines, and under the circumstances, probably received only a cursory consideration of their physical qualifications for the assignment. Yet, detailed knowledge of each aspect of such a hazardous vehicle on the part of at least the principal operators may have prevented some loss of life. Ignorance of means to counter the effects of waves sloshing over the surfaced submarine may have caused the first sinking. A lack of command direction by the commanding officer, Mr. Hunley, could have caused the third disaster. The fourth and final disaster must be attributed to the valor, courage and determination of the commanding officer, who surely realized fully well the danger of his mission, yet carried on Even his maritime enemy, Admiral David Porter, expressed admiration for this "most sublime patriotism." Reference (3)

The third point of view would question the judgment of the operational commander, GEN P. G. T. Beauregard, C.S.A., Commander of the defenses at Charleston. That he should yield to the persuasion of a junior officer in allowing the HUNLEY to take again to the sea after three major disasters suggests a rather desperate frame of mind. His order not to dive the HUNLEY indicates the General knew the submarine was extremely difficult to handle underwater. However, the record of HUNLEY must surely have proven beyond doubt that she was in truth a "Peripatetic Coffin" for any who sailed her. Nevertheless, he authorized LT Dixon to recommission HUNLEY, and even turned his back as LT Dixon practiced submerged operations in Charleston harbor.

SAFETY CERTIFICATION POLICY

There appears to be an obligation to assure, to the extent possible, that naval military and civilian personnel going undersea in non-combatant submersibles will not be unduly hazarded. With the lessons learned from CSS HUNLEY and the other 160 odd submarines which have suffered disasters since 1851 from causes other than the result of action in war, the U. S. Navy is well learned in the dangers of submarine operations. Mr. R. D. Terry of North American Aviation, Inc. has studied 160 major submarine accidents for the years 1851 to 1960. The listing shown in Figure 3 is derived from his study. Adding USS THRESHER in

STATISTICAL TABULATION OF SUBMARINE ACCIDENTS 1851-1963

CAUSE	NUMBER	PERCENT
COLLISIONS	61	36.9
VALVES OR HATCHES OPEN	27	16.3
FUEL EXPLOSION OR FIRE	19	11.5
BATTERY GAS EXPLOSION	16	9.7
OTHER OPERATIONAL CAUSES	15	9.1
GROUNDING, TOWING, OR MOORED	10	6.1
STRUCTURAL FAILURE	3	1.8
CAUSE UNKNOWN	14	8.6
TOTAL	165	100.0

Figure 3

POLICY DIRECTIVE FOR CERTIFICATION

- DEFINE TYPES OF SUBMERSIBLES AND PERSONNEL
- ASSIGN RESPONSIBILITIES
- CITE REQUIRED ACTION
- SPECIFY APPLICABILITY
- IMPLEMENTATION DATE

Figure 4

the Cause Unknown line changes the statistical distribution very little, but does serve to emphasize the concern for submarine safety that is prevalent.

The discussions to date of a certification procedure have led to the opinion that a policy directive should be promulgated which would, as summarized in Figure 4:

a. Define the types of submersibles and personnel. For this purpose, a manned non-combatant submersible is defined as any ship, vessel, capsule or craft capable of operating with or without propulsion, on and under the surface of the water with the operator(s) and/or passengers embarked in a dry habitat, and which by its design is incapable of defensive or offensive action in combat. Operators are defined as those personnel who physically control the operating parameters of the non-combatant submersible; e.g., depth, course, speed, pitch, roll, etc. Passengers are defined as any other personnel embarked who are not involved in control of the vehicle itself.

b. Assign responsibilities. The Chief of Naval Operations would be responsible for determining that the operator(s) of a manned, non-combatant submersible carrying naval personnel is (are) technically and physically competent to operate the submersible in a safe manner. Also, it would be his responsibility to determine that the planned operations for the manned, non-combatant submersible would not hazard the naval personnel embarked; e.g., by reason of the mission assigned, the area of operations, natural environmental conditions existing or predicted therein, and the possibility of mutual interference with shipping, surface or submerged. It would be the responsibility of the Chief of Naval Material to determine whether any manned, non-combatant submersible carrying naval personnel is materially adequate. This responsibility would extend to specification of the operational limits within which material adequacy may be assured, and where warranted, a time period or other conditions under which a certification of material adequacy may be considered valid.

Provision would be allowed for delegating these responsibilities to subordinate echelons.

c. Cite the required action. The Chief of Naval Operations would develop and promulgate the criteria by which the competence of operator(s) of manned, non-combatant submersibles would be evaluated; and develop plans for the operational control of those vehicles to insure their

safety in the environment in which they may be employed. The Chief of Naval Material would develop and promulgate the procedures and criteria by which adequacy of a manned, non-combatant submersible would be evaluated.

The commanding officer or officer in charge of any naval command, office, or activity, planning to operate regularly a manned, non-combatant submersible in which naval military or civilian personnel might be embarked would obtain from the responsible authorities prior to using the submersible, certification that:

The operator(s) is (are) competent;

The submersible is, within specified constraints, materially adequate; and

The planned operation is not unduly hazardous by reason of the conditions existing or predicted in the environment. This responsible officer would be permitted to request a waiver, for cause.

d. Specify applicability. Such a directive would apply to any manned, non-combatant submersible built by the Navy, built by private industry and used by the Navy under contract, and/or built by private industry and subsequently purchased by the Navy. It would not be construed as prohibiting naval personnel with proper authority from embarking in a non-certified submersible on an occasional or one-time basis for specified purposes of indoctrination, evaluation or research. It could not be construed as infringing upon existing statutory authority and responsibility of the United States Coast Guard in the area of safety of vessels operating on the high seas. The requirements delineated in such a directive would be in addition to those requirements promulgated by the United States Coast Guard.

e. Implementation date. If issued, the directive would permit six months after the date of issue for implementation.

IMPLEMENTATION

In the event there is promulgated such a directive as described above, both the Chief of Naval Operations and the Chief of Naval Material would cause to be prepared implementing directives. Any estimate of

the details of such directives would be highly speculative at this time. However, in view of the years of experience in submarine design, construction, maintenance and repair accumulated in the offices of the Ships Systems Command, and the desirability of delegating the responsibility and authority for determining the material adequacy of these submersibles to one officer, it appears reasonable to expect that Commander, Naval Ship Systems Command will act for the Chief of Naval Material in this area.

CONCLUSIONS

In the interest of insuring that the Navy military and civilian personnel venturing underseas in exploration or exploitation of inner space are as safe in such endeavors as the Navy can reasonably assure, responsible authorities will determine that the operators are fully qualified, the operations are adequately controlled, and that the submersibles are materially adequate.

REFERENCES

(1) Infernal Machines - The Story of Confederate Submarine and Mine Warfare. Milton F. Perry, Louisiana State University Press, Copyright 1965.

(2) Submarine Boats - G. W. Hovgaard, Lieutenant in the Danish Navy, E.&F.N. SPON, London and New York, 1887.

(3) The Naval History of the Civil War - Admiral David Porter, USN.

(4) United States Submarine Operations in World War II - Theodore Roscoe, United States Naval Institute, 1949.

NEMO - NAVAL EDREOBENTHIC

MANNED OBSERVATORY

SUMMARY

A preliminary analysis of future Navy undersea research and development requirements has shown the need for a new type of manned submersible, which will provide unlimited visibility at nominal depths for long periods of operation. The NEMO concept includes the following operational characteristics: bottom tethered, transparent acrylic observatory under a one-atmosphere environment with positive buoyancy.

This observatory can be conveniently transported from one operational site to another. Operational usage includes a wide span of missions such as observation and supervision of underwater construction projects at various depths and the training of aquatic animals.

Scale models embodying the NEMO design concept have been fabricated of acrylic. One has been tested to destruction which occurred after 10-1/2 hours at 1,000 psi. Two models are currently undergoing pressure cycling tests.

It is planned to continue the testing of the acrylic material and models to determine the material characteristics as related to the NEMO structure. The results will serve as the basis for the design and fabrication of an intermediate size sphere of 66 inch diameter. Scaling factors will be analyzed and applied in the design of the full scale NEMO.

Current analyses of the life support requirements and winch design will be completed. Communication, anchor design and implantation problems will be investigated.

INTRODUCTION

An entirely new type of semi-mobile undersea laboratory, which would place human observers at the source of oceanographic information, is under design definition and experimental study at the U. S. Naval Missile Center (NMC). There are many ways to gather data about and in the ocean environment ranging from well-established, remote sampling techniques, to new methods involving the use of sophisticated submersibles and bottom facilities. Traditionally, during the initial phase of exploring a new frontier such as the ocean's depth, emphasis is on speed and mobility to

permit a cursory look at gross features. This is followed by a change in requirements toward long stay times as localities of interest are found for experimentation and collection of information.

In a sea bottom mounted habitat, the free diving observer has direct access to his environment for stay times less than approximately eight hours. Most of the new submersibles permit observation over a limited range at substantial depths in a comfortable one-atmosphere environment for relatively short periods of time. The observer's field of view is limited to that provided by pressure-proof portholes and periscopes. Scuba trained divers have demonstrated the feasibility of prolonged working in the ocean environment to depths of the order of hundreds of feet. A need is developing for a compromise vehicle or facility possessing the one-atmosphere environment and depth capability of submersibles, exceeding the scuba diver's stay time, and providing unrestricted opportunity for observation. The vehicle will act as a stable submerged viewing platform that could be used for detailed ocean study at one site for long periods and would permit correlation of data collected directly by visual, acoustical, and other means. Requirements for such a vehicle or facility include:

a. Panoramic Visibility: The human eye and a trained mind can study the sea environment more ably by direct observation than by photographs or television cameras. The eye is a better sensor than color film and detects information otherwise lost in black and white images of the ocean environment. Panoramic vision, in all directions, is a primary requirement.

b. Long Duration: For some studies, one place must be examined long enough to determine significant changes that might be associated with time of day, lunar phase or season of the year.

c. Portability: While long stay time at one site may be necessary for some missions, to be most useful the vehicle should be transportable from one site to another without serious operational problems.

d. Self-Contained: The observatory should be designed to accomplish its mission unaffected by surface weather conditions, hence it must be independent of a surface tender during observations.

e. Depth: The vehicle should be capable of moving vertically throughout its moderate depth capability.

f. Positive Buoyancy: For safety, the vehicle should be positively buoyant at all times.

g. One-Atmosphere Internal Pressure: Sea level atmosphere conditions will provide greatest utility to the greatest number of investigators without regard to physical condition, age, or training as a diver.

A need for such an underwater observatory is foreseen in connection with the Naval aquatic animal training program currently being pursued at NMC.

APPROACH

To meet these requirements, an underwater observatory concept known as NEMO (Naval Edreobenthic Manned Observatory) was generated at NMC. Edreobenthic is a coined adjective form of edreobenthos and means obligatorily sedentary on the bottom of the sea. NEMO is a positively buoyant manned observatory-laboratory giving scientists and engineers the capability of studying the marine environment and conducting experiments by means of direct visual observation over extended times on station. The observatory is essentially an undersea, bottom-tethered rigid balloon located over one site in the ocean. The buoyant element is a transparent pressure hull for the two man crew who can station the observatory, like an elevator, at any vertical point by winching the tether line connected to a bottom anchor. This observatory with its own life support system is independent of surface weather conditions or surface support. The anchor can be implanted and handled separately by any ship which can also transport the NEMO vehicle. Additionally, once the anchor is implanted, NEMO could be returned to the same location for repeated observations by leaving a marker buoy secured to the anchor.

In the NEMO, long duration, panoramic visibility and facilities for communication by acoustic and other means will permit the correlation of observations and events to an extent that cannot be obtained in any other manner. Long mission durations on station can be obtained with conventional power supplies. Since no power is used for horizontal propulsion, the stored power in excess of vertical positioning and azimuth control requirements is available for life support. The sea level atmosphere inside the observatory permits all scientists and engineers to enjoy free diver visibility without the delays and discomforts of a decompression schedule.

Even with depth capability limited to 1,000 feet, which is in excess of most of the continental shelf where much of the marine life of interest exists, the oceanographic science of marine biology could be adequately studied from NEMO. NEMO can be used for passive visual observation of such phenomena as the deep scattering layer or marine life in general and active experiments may also be conducted. For example, selected marine life could be attracted into the area to study interactions of different creatures in their natural habitat. Chemical and biological analyses may be performed at the site by sampling the sea water over a long period of time.

At NMC, NEMO is initially intended to assist in performance of training and experimentation with marine mammals such as porpoises and sea lions in the open sea at depths below scuba diver capability. The Naval

Civil Engineering Laboratory (NCEL) has requested the use of NEMO as an underwater observation and supervision platform for their concrete construction experiments in shallow water off Port Hueneme, California this year. Undersea research concerning weapons development and real time evaluation of weapons in test can use NEMO to collect environmental and performance data of new undersea weapons. Information about the undersea environment useful in weapon concepts and design can be visually and directly evaluated by observation from NEMO. This information could be used to generate weapon refinements and to define targets in terms of weapon sensors.

DESIGN

The design concept (Figure 1) for NEMO consists of a two man, transparent spherical pressure hull made of acrylic. (The sphere is the most efficient shape for underwater structures as shown by its low weight-to-displacement ratio.) Below this buoyant pressure hull is a flooded service module which includes batteries, an undersea winch, and the framework or undercarriage to contain the hardware and support the NEMO capsule when resting on the deck. Placement of the service module below the buoyant hull will lower the center of gravity and help trim and balance NEMO in the water. The winch can position the observatory at any height between the ocean surface and the bottom by reeling or unreeling the anchored non-spinning tether rope. Inside the 10 foot diameter acrylic pressure hull (Figure 2), crew members are seated back-to-back so that each person has nearly 2π steridians of visual field. This permits full exploitation of visual observation as the primary information collection method. Possible optical distortion induced by the curved shell is not more than 1/4 diopter and can be corrected by either eye glasses or a plastic lens placed against the wall. Between the two back-to-back seats is a central structure containing most of the life support equipment including blowers, scrubbers and gas supplies. Life support equipment is rated at 10 days for two crew members to ocean depths of 1,000 feet. In case of emergency, the buoyant pressure hull can be floated to the surface by either free-wheeling the winch, cutting the mooring rope (both gas and pyrotechnic operated), or detaching the service module (explosive bolts) from the hull.

The transparent spherical pressure hull of the NEMO vehicle was first suggested in 1956 by Professor August Piccard. He envisioned an all-acrylic hull for use to depths of 6,600 feet using 12 identical spherical pentagons bonded together (1).* In 1963, Dr. J. D. Stachiw constructed and tested two hollow 10 inch thick acrylic shells formed in this way (2). These tests indicated that the modular spherical dodecahedron shells were as strong as monolithic spherical shells of the same size. Stachiw also showed that the critical pressure of a hollow sphere assembled from spherical pentagons does not depend upon the tensile strength of the bond between individual spherical pentagons.

*References are listed at end of paper

Acrylic is an economical thermoplastic material with favorable fabrication properties. It has been used successfully as window material for depths to 35,800 feet. However, the hull size required for long mission times renders impractical casting of an acrylic shell from large monolithic pieces such as hemispheres. Available commercial sheet sizes and fabrication techniques are practical for the above modular construction approach. For a 10 foot diameter hull, the pentagons will require blanks approximately 80 inches diameter and four inches thick. This is approximately the maximum sheet size of four inch thick acrylic available on a custom basis.

To solve the practical problem of hull penetrations for electrical and hydraulic feedthroughs and a personnel hatch, a minimum circular area of the shell was replaced by two metal zones located within two diametrically opposite polar pentagons. A circular hatch was centered in a metal zone at the top while feedthroughs and fittings were installed in the other metal zone of identical size at the bottom of the hull.

The original design concept included the use of these metal zones as attachment points for external and internal loads. Preloaded vertical tie-rods were secured between the top and bottom zones. The object was to transfer the hoisting load to the bottom of the shell and the load due to weight of internal items and tether force to the top of the shell. The tie-rods would also retain the zones against the hull. Alternate methods for transfering loads without overloading the acrylic hull are available and under consideration.

a. Materials

For the transparent pressure hull material, commercial grade acrylic, type G, was selected because of its proven performance in aircraft applications, high strength-to-weight ratio, reasonable cost and toughness in compression. Compressive strength of acrylic is dependent on temperature, loading duration, loading rate, and number of previous loadings. The least understood property of acrylic is its creep phenomena, particularly with different loading conditions. The effects of creep on the NEMO hull must be experimentally evaluated.

The choice of material for the metal end plates was among several candidates. Titanium is corrosion-resistant and attractive in strength-to-weight ratio but expensive in the size and shape required for the present application, and aluminum while inexpensive, is less resistant to wear, stress-corrosion and scratches. Brass and bronze are suitable but a possible source of galvanic corrosion when used in contact with other metals. For protection against sea water at reasonable cost and ease of fabrication, the choice of material was 316 stainless steel with a yield strength of about 30,000 psi.

b. Structural Problems

Of the metals considered, stainless steel has a modulus of elasticity which is highest with respect to that of acrylic. This approximately 100-to-1 mismatch in modulus could lead to excessive strain in the acrylic at the steel-to-acrylic interface unless the steel section is properly designed and matched in stiffness to that of the acrylic shell.

If the deformation in the acrylic caused by the metal or by other stress raising effects in the design or material leads to sufficient shape deviation from an ideal sphere, failure of the shell in buckling may occur before reaching predicted critical loads. Consequently, the calculated collapse strength of the NEMO hull must be verified experimentally.

Because of the uncertainties noted above, the NEMO shell, planned for operation at 1,000 feet, will be designed for 3,000 foot pressure. The average stress for pure compression at 3,000 feet will be:

$$\sigma_{ave} = \frac{PR_o^2}{2hR}$$

$$= 10{,}320 \text{ pounds/square inch}$$

where σ_{ave} = average compressive stress in the shell

P = External pressure: 1,330 psi (3,000 feet)

R_o = Outside radius: 60 inches

R = Average radius: 58 inches

h = Nominal thickness: 4 inches

However, since failure may occur in elastic or plastic instability, rather than compression, the critical pressure must also be computed. The critical pressure for nearly perfect spheres (departure from sphericity over a critical length being less than 2-1/2 percent of shell thickness) is calculated as follows (reference 4):

$$P_c = \frac{0.8\ E\ (h/R_o)^2}{(1 - u^2)^{\frac{1}{2}}}$$

where P_c = Critical pressure for elastic buckling, psi

E = Modulus of elasticity

u = Poisson's ratio

In the derivation of this equation for the critical pressure of the sphere it has been assumed that the material of the sphere follows Hooke's law faithfully from zero stress to fracture. There are very few materials that behave in such a manner other than glass, and so the equation must be modified to apply to materials that do not follow Hooke's law. Engesser (5) and others (6) have developed expressions that account for the deviation of materials from Hooke's law while predicting the buckling of structural members.

To calculate the critical pressure due to elastic or plastic instability of a sphere the Engesser solution must be used. This solution for the buckling of structures fabricated from materials that do not have linear stress-strain properties consists of substituting the tangent modulus of elasticity for the modulus of elasticity. There is little experimental data available on the validity of Engesser solution as applied to the buckling of tubes and spheres besides the experiments performed by Stachiw (7) on aluminum and acrylic circumferentially stiffened sandwich shells subjected to external hydrostatic pressure. These experiments have shown that the substitution of tangential modulus of elasticity E_t for modulus of elasticity E in the general instability equation for circumferentially stiffened shells (7) provides good correlation between calculated values for critical pressure of such shells, and the pressure at which the collapse actually takes place. The difficulty lies in obtaining stress vs. tangent modulus of elasticity curves for materials like acrylic under biaxial compression. If such curves are unavailable, stress vs. tangent modulus of elasticity of materials under uniaxial compression may be used without the introduction of considerable error.

Further refinement to the critical pressure equation can be introduced by substituting u_s for u, where u_s is Poisson's ratio of the hull material at a given stress level. In the elastic strain region, Poisson's ratio changes very little with the increasing stress level, but in the plastic strain region this ratio increases considerably over the value that it has in the elastic strain region. The difficulty in applying this correction lies in the scarcity of published data on the change of u_s with the change in stress level and thus, it is usually disregarded. The failure to use u_s instead of u places some of the calculated critical pressure values in error, but since the error makes the calculated values smaller, it is accepted as a safe and conservation practice.

An average value for E_t of 350,000 psi for acrylic under 10,000 psi compressive stress was obtained from a review of supplier's values and various unpublished experimental data. Using this value and 0.35 for u in the above equation, a theoretical critical pressure of 1,300 psi (2,900 foot depth) is obtained for the NEMO hull. The large margin is used in a first calculation to accommodate the degradation of penetrations, non-uniformities of thickness, deviation from sphericity, non-uniformities of loading and material creep.

MODELS

Six scaled hulls of 15 inch diameter and 1/2 inch wall thickness were constructed (Figure 3). The models included full-size NEMO features such as metal end plates with hatch or feedthroughs, and from the original concept, internal tie-rods. Table 1 shows the dimensional variations in the wall thickness and sphericity of the first two models. Although sphericity of the first model varied from +1.6 to -2.67 percent of radius, assembly techniques were improved on subsequent models such that their variation in sphericity was kept within $\pm$1/2 percent of radius. The weights and tie-rod forces for the models are shown in Tables 2 and 3.

The models were fabricated by the Technical Support Directorate of the Pacific Missile Range at Point Mugu using type G commercial grade acrylic sheet of 1/2 inch thickness. Bandsawed 10 inch diameter discs were heated in an oven to 310°F. Forming was performed in a 160°F aluminum mold using vacuum to pull the soft acrylic into the concave mold. Dimensions were controlled by mold contour and the inside surface was lightly touched during forming. Though mark-off from the mold was prevented, it is noted that slight blemishes on the outside surface of the hull will hardly be visible when submerged in water.

Formed spherical discs were sized to pentagon shape by milling the five edge surfaces whose plane coincides with a segment of a great circle on the spherical surface. The 12 pentagons were joined into a sphere using an assembly fixture (Figure 4) to ensure proper alignment of the pentagons and maximum adhesive penetration into the joint. A monomer-polymer PS-18 adhesive was used and the assembled hull was annealed at 160°F for 24 hours to completely cure the adhesive and to decrease the magnitude of residual stresses. Figure 5 shows a completed model including external lead ballast to simulate the mass of the service module.

a. Test Method

The models were subjected to hydrostatic tests at the facilities of NCEL, Port Hueneme, California. The model was held in a holder such that the buoyancy force was restrained through the bottom end plate. In some tests the model was inverted and held down by means of the hatch equipped end plate. This procedure was used to bring the feedthroughs on the bottom end plate close to the pressure tank cover when necessary. Figure 6 schematically shows a typical test set up prior to installation in the pressure tank. Strain gage readings were periodically taken while the pressure and temperature of the pressurizing medium, sea water, were continuously recorded.

b. Test Description

After several trial pressure cycles to 500 psi and 750 psi of varying duration, the first model was pressurized to 1,000 psi (2,200 feet) in

five minutes and held at this load until failure occurred at 10-1/2 hours. Strain readings from this test are shown in Figures 8 and 9 for the region around the end plates and the equator respectively. Figure 10 is a photograph of the reconstructed shell showing a triangular area at the equator measuring approximately 5 X 5 X 8 inch that had disintegrated. Figure 9 includes a strain reading the disintegrated area which indicates decrease in compressive strain on the interior surface of the sphere prior to collapse. This phenomenon plus the inwardly fractured edges at the failure zone indicated local plastic buckling rather than simple compressive failure of the acrylic shell. Buckling was apparently triggered in the meridional direction if the early reversal of compressive strain signal on the meridional direction was valid. It is noted that in most tests the circumferential strains were larger than the meridional ones. The spherical radius and thickness was 0.450 inch, thinnest of all pentagons comprising the model.

The second model is being subjected to a continuing test consisting of long-term pressure cycles, 500 psi pressure for an average of 125 hours followed by 125 hours of relaxation at atmospheric pressure. The rate of creep after 100 hours of 500 psi pressure loading was found to be less than 0.1 percent per hour of total strain reading (5,000 to 10,000 microstrains). At 500 psi the volume decreased 600 cc, equivalent to 1/8 inch diameter reduction. After relaxation, the gage readings returned to within 500 microstrains of their zero readings. Figure 7 shows typical strain during the long-term pressure cycle or creep test. During the first hour under pressure, 85 percent of the total strain (between 5,000 and 10,000 microstrains depending on location of gage) occurred. During the first eight hours of relaxation, 90 percent of the strain return took place. The second model is still being cycled and has undergone 10 cycles.

The third model is being used for short-term pressure cycles to 500 psi averaging five minutes per cycle. The hull will accumulate as many pressure cycles as time and pressure tank availability will allow. About 170 cycles have been imposed on the model without noticeable change in dimension or integrity.

The fourth model was a simplified version for hydrostatic compression test of the hull and was fitted with simple end plates which were held together with an elastic cord. It was pressurized to failure at a pressure loading rate of 100 psi per minute. The model was filled with water which was connected to an outside manometer to detect volume change in the model. Thus, the hull itself became slightly negatively buoyant and was rested on its end plate. It is noted that the bias pattern due to the uniform compressive force with respect to buoyancy during tests differed from the previous tests with unfilled pressure hulls. Figure 11 shows the pressure and volume change vs. time curves for the test where the collapse pressure was 3,700 feet (1,650 psi). Again the buckling

appeared to start at a small section of the shell at the equator which disintegrated into very small pieces with inward fragmentation at its edges.

The test was repeated with a fifth model, also a simplified version, and the collapse was at 3,600 feet, but this time the failure occurred when one of the steel end plates caved in. The stainless steel end plates were designed to fail at 3,000 feet.

The sixth model, a homogeneous acrylic hull of 12 spherical pentagons without end plates was hydrostatically compressed to failure at the same pressure loading rate as the previous two. The acrylic sphere was held down by means of a point load at the middle of a bottom pentagon through a cemented 3/8 square inch acrylic rod. The uniform compressive force due to pressure was thus biased by the buoyancy force at a singular spot. Collapse pressure depth for the homogeneous hull was 3,050 feet (1,360 psi).

Summary of Tests

Model	Loading Rate	Collapse Pressure	History
1.	200 psi/min hold @1,000 psi	1,000 psi	Several 500 psi to 750 psi cycles; 10-1/2 hours @1,000 psi before collapse
2.	Currently under slow cycling from 0 to 500 psi Duration of cycle - 125 hours at 500 psi & 125 hours at 0 psi		10 cycles already accumulated
3.	Currently under rapid cycling from 0 to 500 psi Duration of cycle - 5 min total		170 cycles already accumulated
4.	100 psi/min	1,650 psi	Elastic cord between end plates; simplified construction; no tether load other than wet weight of model
5.	100 psi/min	1,600 psi	Elastic cord between end plates; simplified construction; no tether load other than wet weight of model
6.	100 psi/min	1,360 psi	No end plates - tethered by 3/4" X 1/2" acrylic rod to a tie line

OBSERVATIONS AND PRELIMINARY CONCLUSIONS

The test on the 15 inch NEMO model of 10-1/2 hours at 2,200 feet (1,000 psi) indicates that it had a safety factor of 2.2 for 10-1/2 hours at 1,000 feet (445 psi). At 500 psi the model showed almost no creep rate after 100 hours and might indicate very long survival at this pressure. The acrylic hull returns almost exactly to original dimensions when the pressure is removed. For pressures between 500 and 1,000 psi, survival times longer than 10-1/2 hours are expected and conversely for durations less than 10-1/2 hours pressures can be expected to approach the theoretical collapse pressure. No high tensile stresses occurred in the shell.

For all real shells, variations exist in the tolerances on thickness, sphericity, and material properties with respect to location on the shell. Under high hydrostatic pressures, these variations determine the flow of material in pressure hulls made of materials that creep such as acrylic. Under continuing high pressure, a variation in shape thus takes place which ultimately results in shell failure by elastic and plastic instability.

Figure 12 shows the probable situation for materials such as acrylic in pressure shells. At low strain levels, the shell can be used for any practical time period; but as the strains increase, under higher hydrostatic pressures, the flow mechanism described previously results in plastic instability failure in shorter times. The position and shape of the instability failure curve is not known for acrylic in the NEMO hull configuration. If this view is accurate, it becomes necessary to define safety factor in terms of the difference between the pressure-dependent strain at the working pressure and the location of the instability failure curve at the maximum mission time. Similar load situations for cylindrical and conical shells of aluminum alloy at elevated temperatures have been reported (3).

Calculations of the theoretical collapse pressure, as shown in reference 4, apply to monolithic perfectly spherical shells. The NEMO 15 inch shell, on the other hand, consists of two very dissimilar materials (acrylic and stainless steel) with buoyancy force bias, tie-rod force bias, radius and thickness variations, joint imperfections, and unknown creep effects. Together these effects may have contributed to the time (10-1/2 hours) delayed buckling failure of the model at 1,000 psi.

However, acrylic, in a laboratory test, exhibited unusual toughness at room temperatures. A 1/2 X 2 X 4 inch coupon of type G acrylic was column-loaded and strained 10 percent (100,000 microstrains) without bending and upon release of load, found to gradually recover to its original size. When compressed beyond 20 percent, the coupon proceeded to bend into an S shape without fracture. Upon release of load, the distorted acrylic eventually recovered to its original shape but did not return to original dimensions.

It is believed that the unusual toughness of acrylic in compression allowed the acrylic spheres to withstand a collapse pressure of 3,700 feet (1,650 psi) where the time delayed effects of creep were minimized by rapid loading rate. Apparently the acrylic was able to distribute high local stresses by deforming plasticly without developing high stress concentration.

The strains at the equator were larger than those adjacent to the end plates, indicating that the metal-to-acrylic interface design was satisfactory. Generally, the circumferential compressive strains were larger than meridional strains but there were exceptions where the relationship was reversed.

Although acrylic is not normally known for its structural properties, its use as a transparent pressure hull material for NEMO may be justified. Its density (73.5 lbs per cu.ft.) is low and the resulting pressure hull has a weight-to-buoyancy ratio of .214 for an all acrylic hull, and .36 for an acrylic hull with metal end plates. The tests so far with the 15 inch diameter NEMO models have indicated positive results with regard to chemical and physical resistance to sea water under stress, and in ease of fabrication. The test results on the 15 inch diameter NEMO hull have shown no problems with the acrylic-stainless steel interface region.

These preliminary conclusions must be confirmed by further tests to establish a satisfactory confidence level.

FUTURE PLANS

Tests of the 15 inch diameter will be continued. Tests of acrylic material will be made to determine its properties as related to the integrity of an externally pressurized sphere.

These results will be incorporated in the design of an intermediate size sphere of 66" diameter. This sphere will be designed to house a two man crew at a depth of 1,000 feet for six hour periods.

The tests of the 66" sphere will provide data, in conjunction with data from the 15 inch sphere tests, to determine scaling factors for the design of the full scale NEMO.

Simultaneously, effort will be applied to the design of the interior fittings and the support module. Studies of the life support requirements and winch design will be completed. Communication, anchor design, and implantation problems will be investigated.

BIBLIOGRAPHY

1. Earth, Sea and Sky, A. Piccard, Oxford University Press, New York, 1956, pp 144-145.

2. Solid Glass and Ceramic External Pressure Vessels, J. D. Stachiw, NOW 63-0209-C-2, Ordnance Research Laboratory, Pennsylvania State University, 15 January 1964.

3. Studies in Creep Buckling of Circular Cylinders and Conical Shells, Thein Wah and R. K. Gregory, Southwest Research Institute, ARL 184, Aerospace Research Laboratory, Office of Aerospace Research, U. S. Air Force, December 1961.

4. Elastic Buckling Strength of Spherical Glass Shells, M. A. Krenzke and R. M. Charles, David Taylor Model Basin Report No. 1759, 1963.

5. Knickfestigkeit gerader Stabe, F. Engesser, Zeitschrift der Architektur und des Ingenieurwesens, 1889, p. 445.

6. Collapse of Tubes, R. V. Southwell, Phil. Mag., May 1913, pp 687-698; Sep 1913, pp 502-511; Jan 1915, pp 67-77.

7. General Instability of Circumferentially Stiffened Sandwich Shells Subjected to Uniform External Pressure, J. D. Stachiw, Master's Thesis, Department of Engineering Mechanics, Pennsylvania State University, 1961.

Table 1

15 inch Diameter NEMO Model

Pentagon Thickness and Deviation From Sphericity

(Diemnsions in Inches)

Pentagon	Thickness	Deviation From Sphericity	Thickness	Deviation From Sphericity
1	.468-.491	+.062	.457-.470	-.020
2	.480-.494	+.062	.468-.487	+.015
3	.465-.481	+.062	.474-.488	+.018
4	.467-.487	+.062	.452-.464	-.012
5	.454-.477	+.125	.459-.470	-.010
6	.452-.462	+.125	.465-.475	+.016
7	.450-.456	-.200	.454-.466	-.022
8	.466-.492	-.200	.450-.462	+.035
9	.455-.471	+.125	.458-.476	+.025
10	.450-.465	-.125	.466-.464	+.014
11	.475-.479	-	.455-.476	-
12	.475-.495	-	.460-.467	-

Table 2

15 inch Diameter NEMO Model Weight Distribution (lbs)

Weight of Sea Water Displaced	65.5
Weight of Model Including Innards	23.3
Buoyancy in Sea Water	42.2
Weight of Lead Ballast Used	46.5
Total Weight of Model and Ballast (dry)	69.8
Weight of Acrylic with Strain Gages	12.8
Weight of Steel Parts and Feedthroughs	5.6
Interior Lead Weight	4.9

Table 3

15 inch Diameter NEMO Model Tie-Rod Forces (lbs)

Tie-Rod Tension (Preload)	25 lbs
Total Tension (Preload)	100 lbs
Tie-Rod Spring Constant (Total)	400 lbs/inch

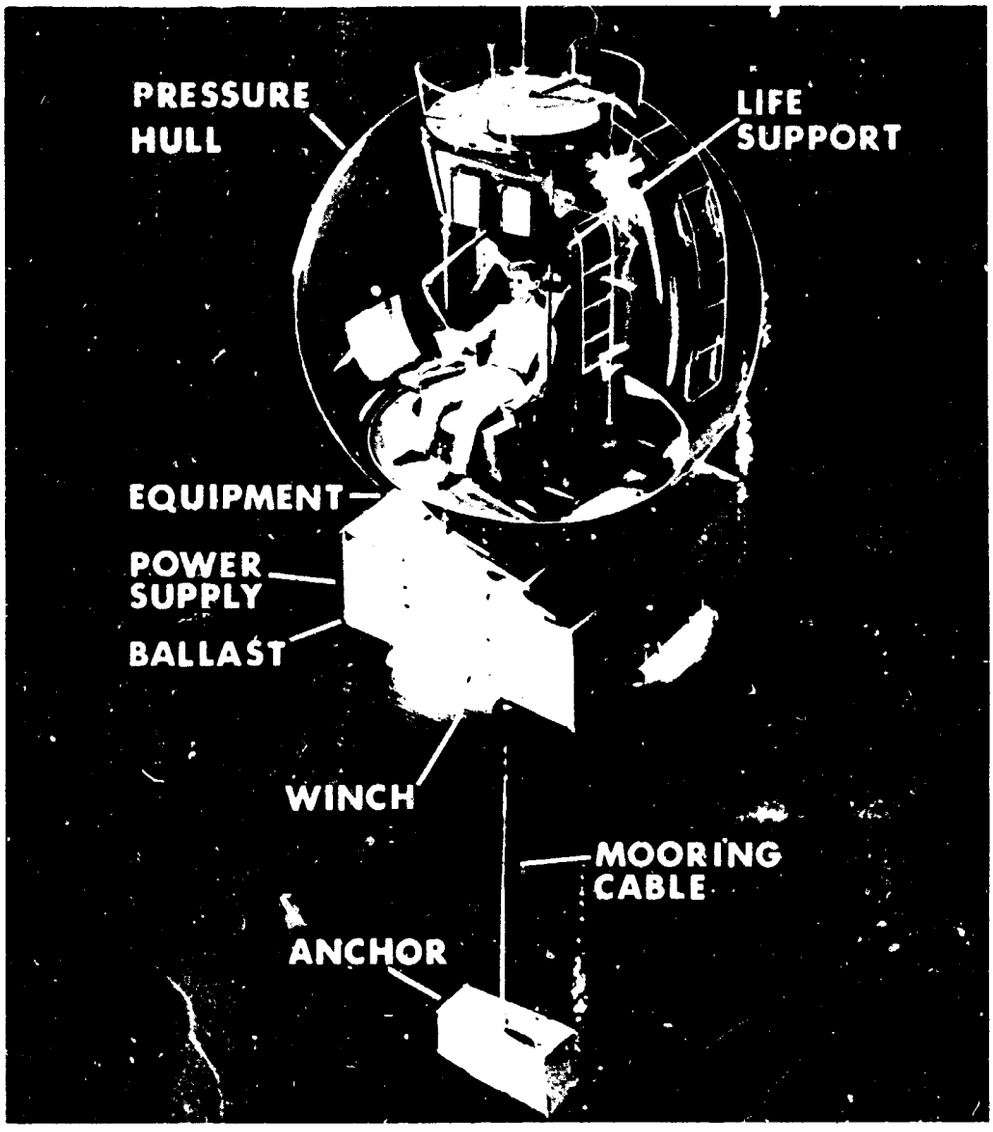

Figure 1

NEMO Design Concept

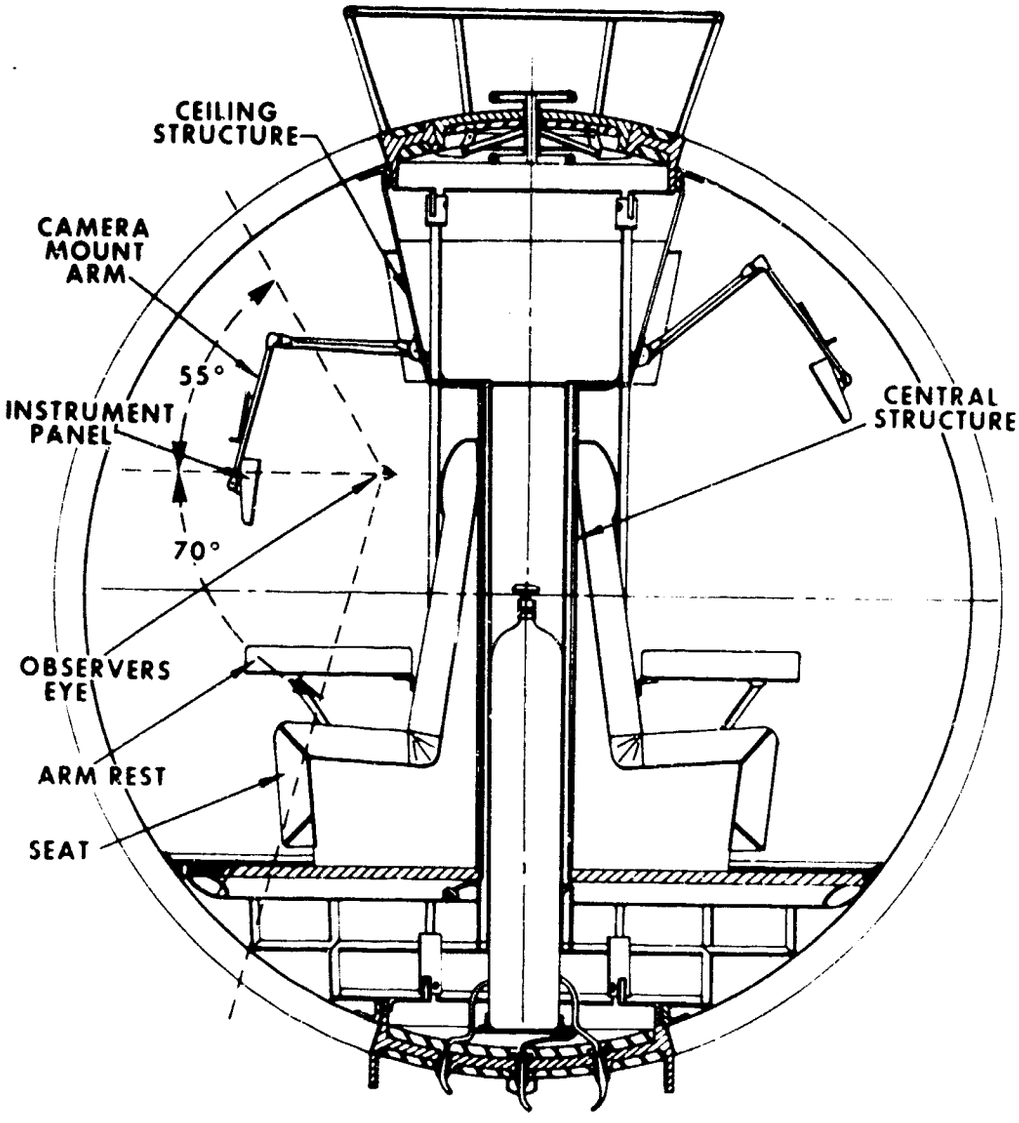

Figure 2

NEMO Capsule Interior

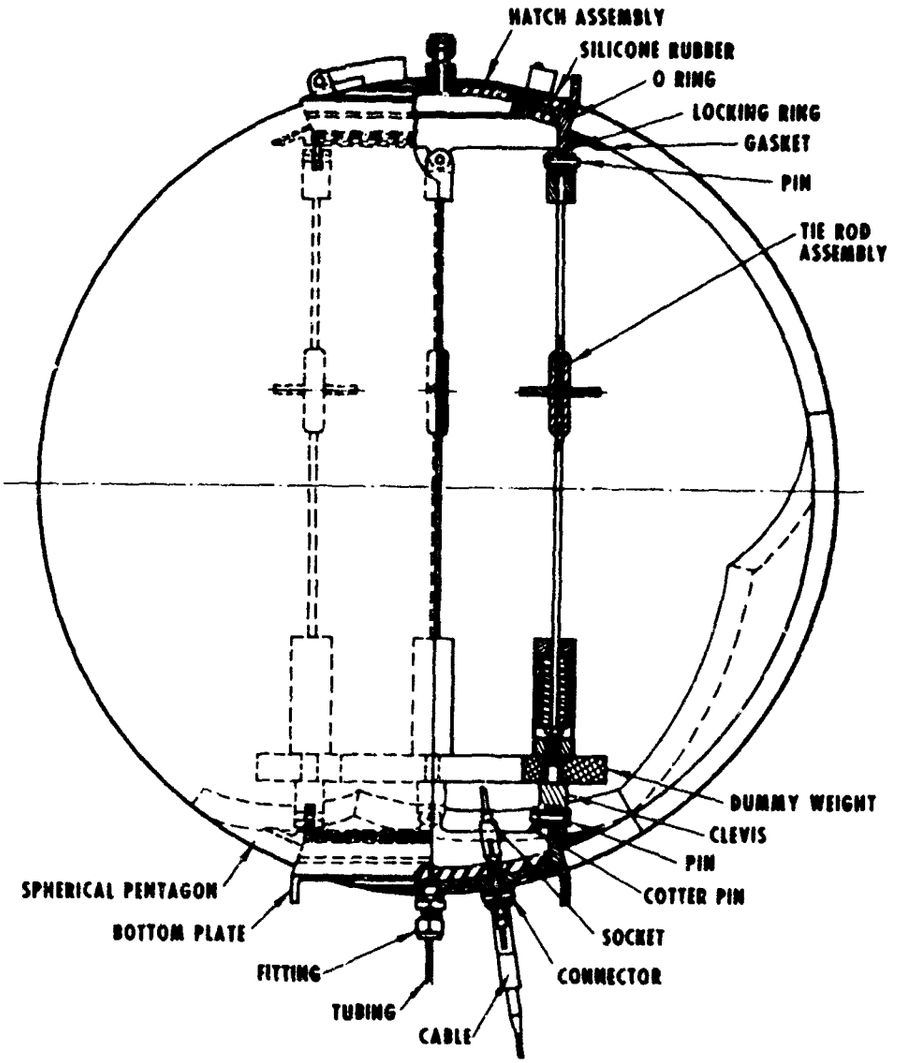

Figure 3

Details of 15 inch Diameter NEMO Model

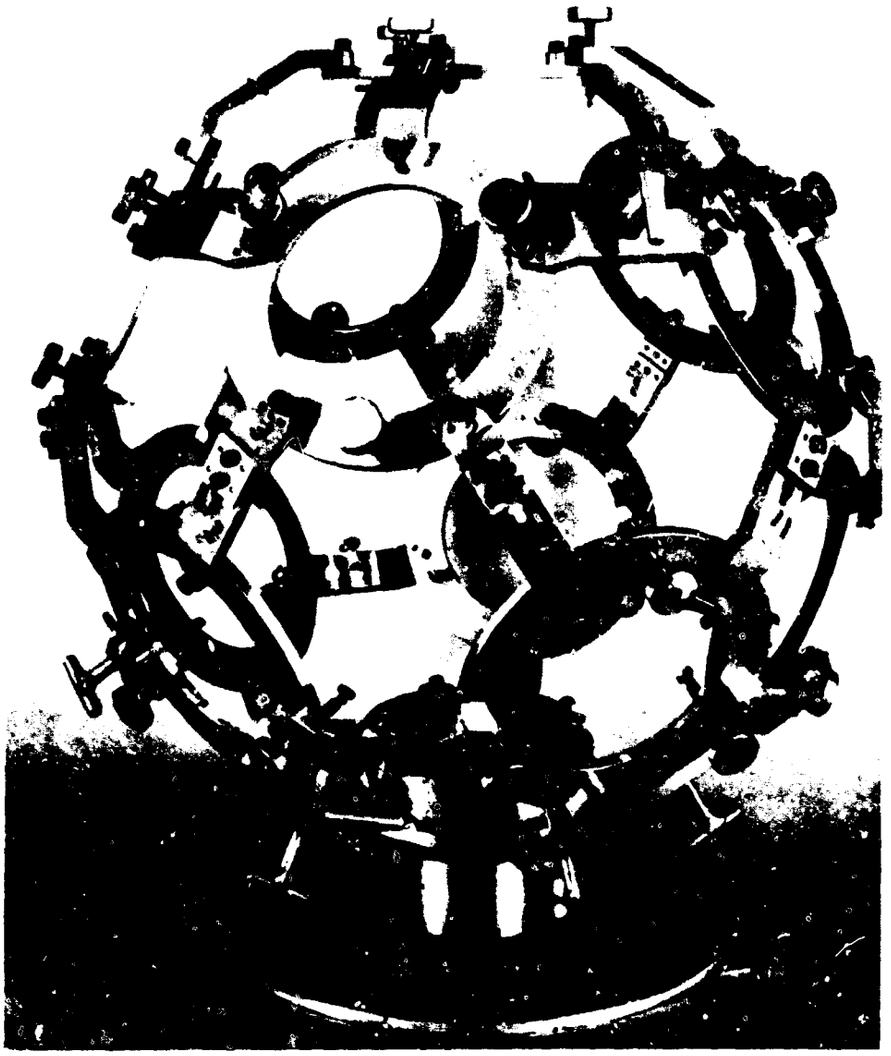

Figure 4

Assembly Fixture for 15 inch Diameter Model

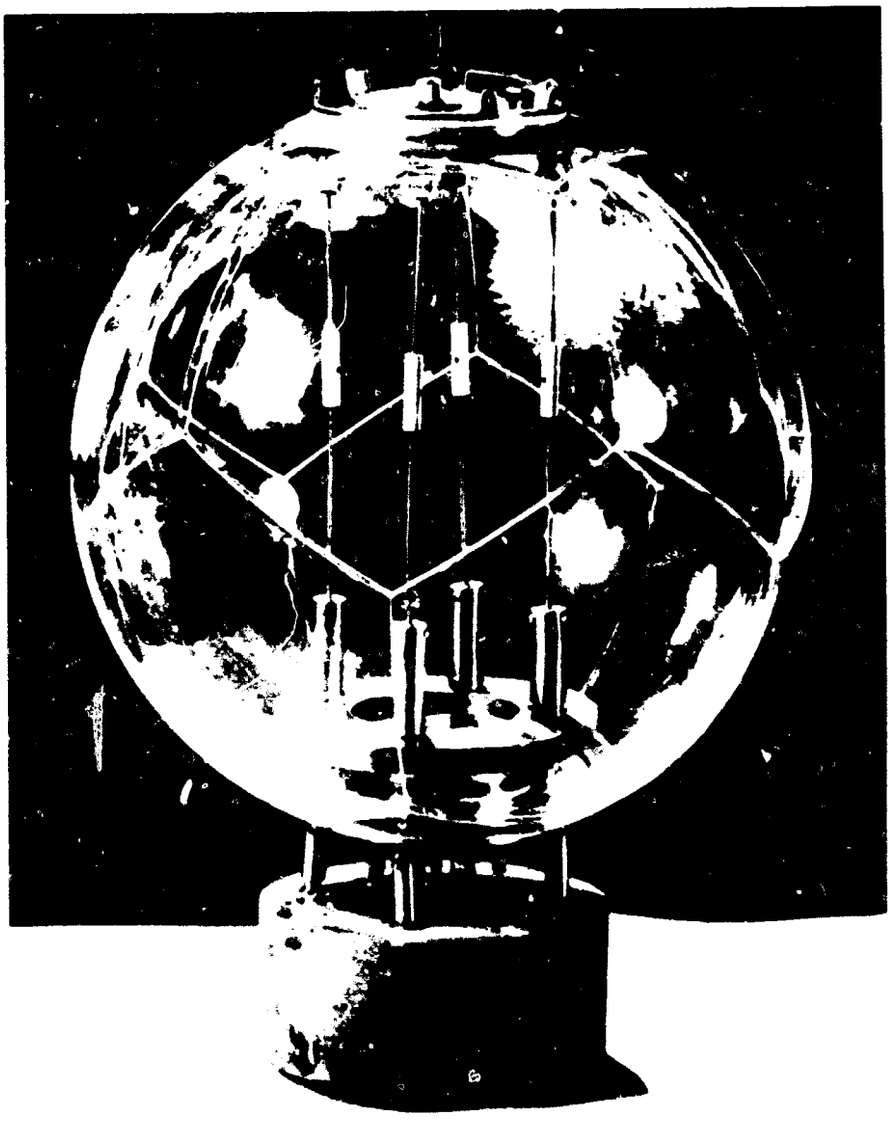

Figure 5

15 inch Model with Simulated Ballast

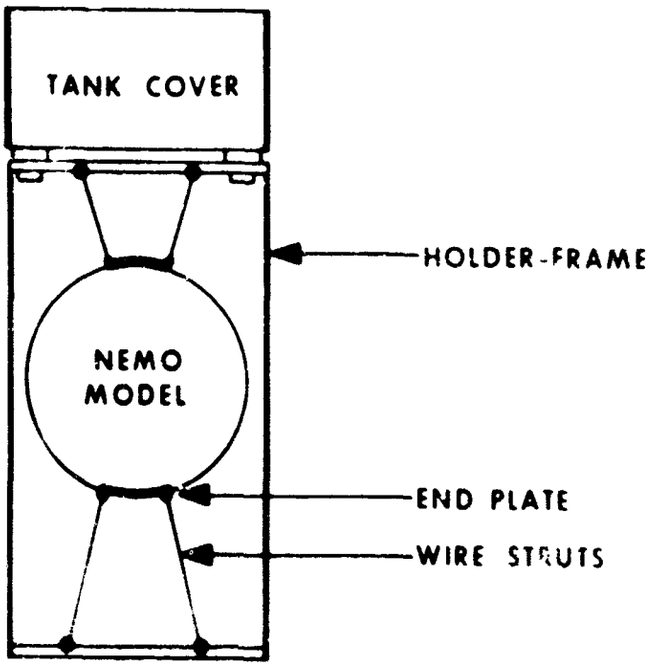

Figure 6

Hydrostatic Test Holder for NEMO Model

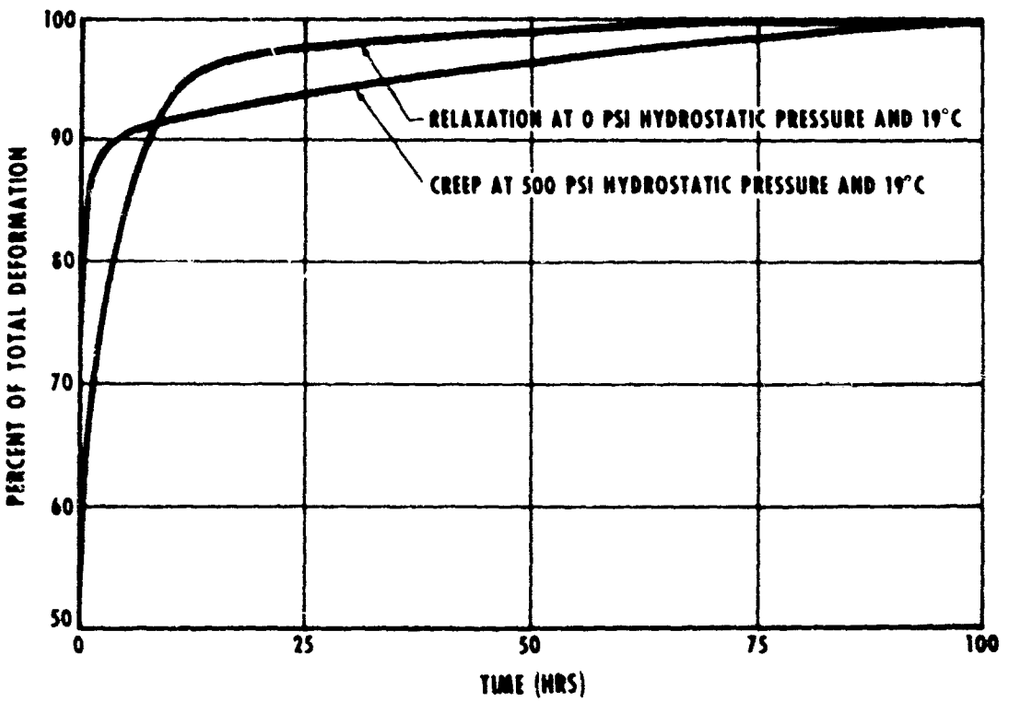

Figure 7

Typical Strain-Time Curves for Acrylic NEMO Hull

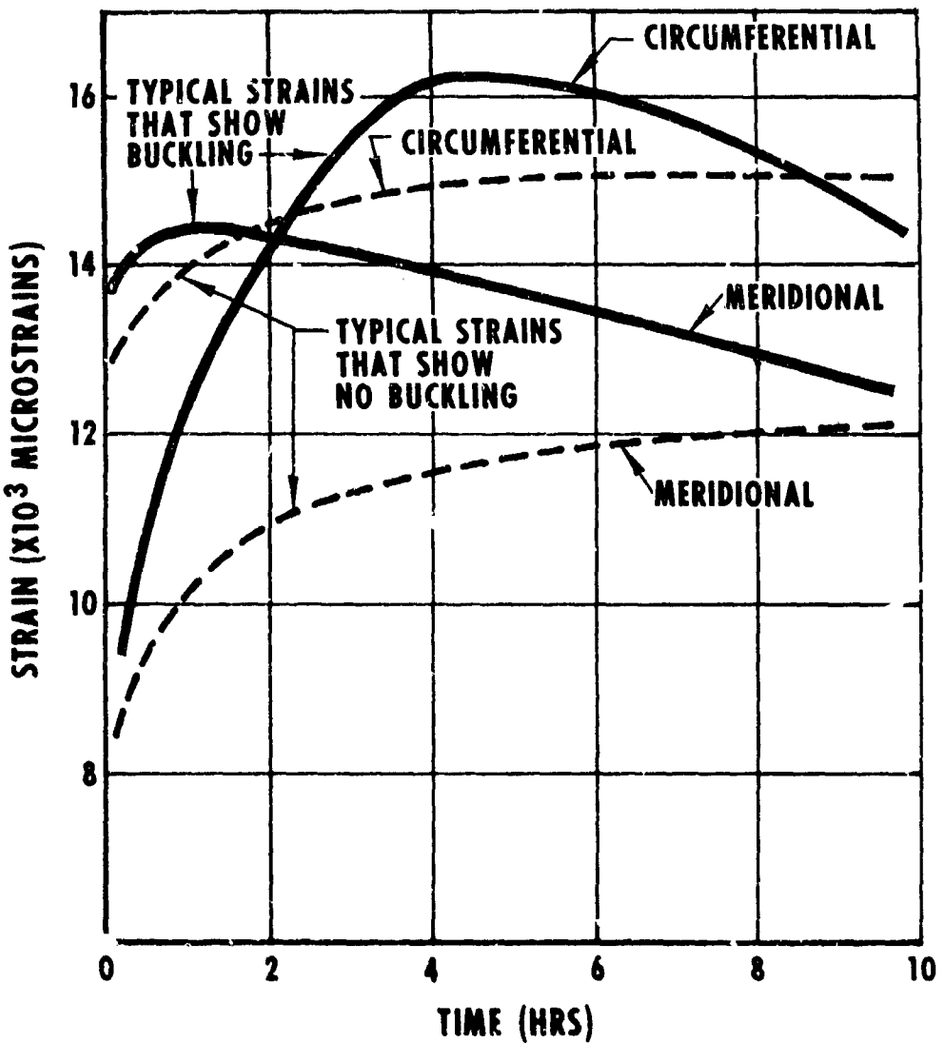

Figure 8

Typical Strain-Time Curves at the Equator of the Acrylic Hull Under 1,000 psi Hydrostatic Pressure

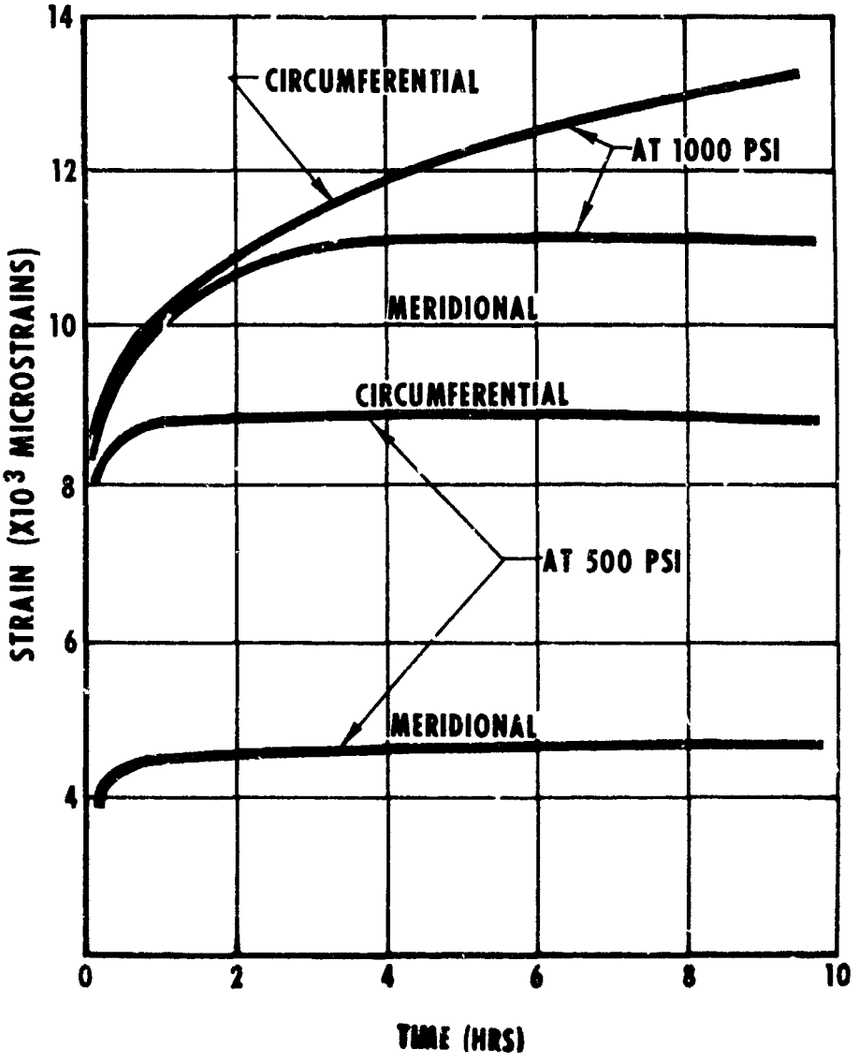

Figure 9

Examples of Strain-Time Curves in Acrylic Hull Near Steel End Plates

Figure 10

Reconstructed 15 inch Hull Showing Broken Out Area

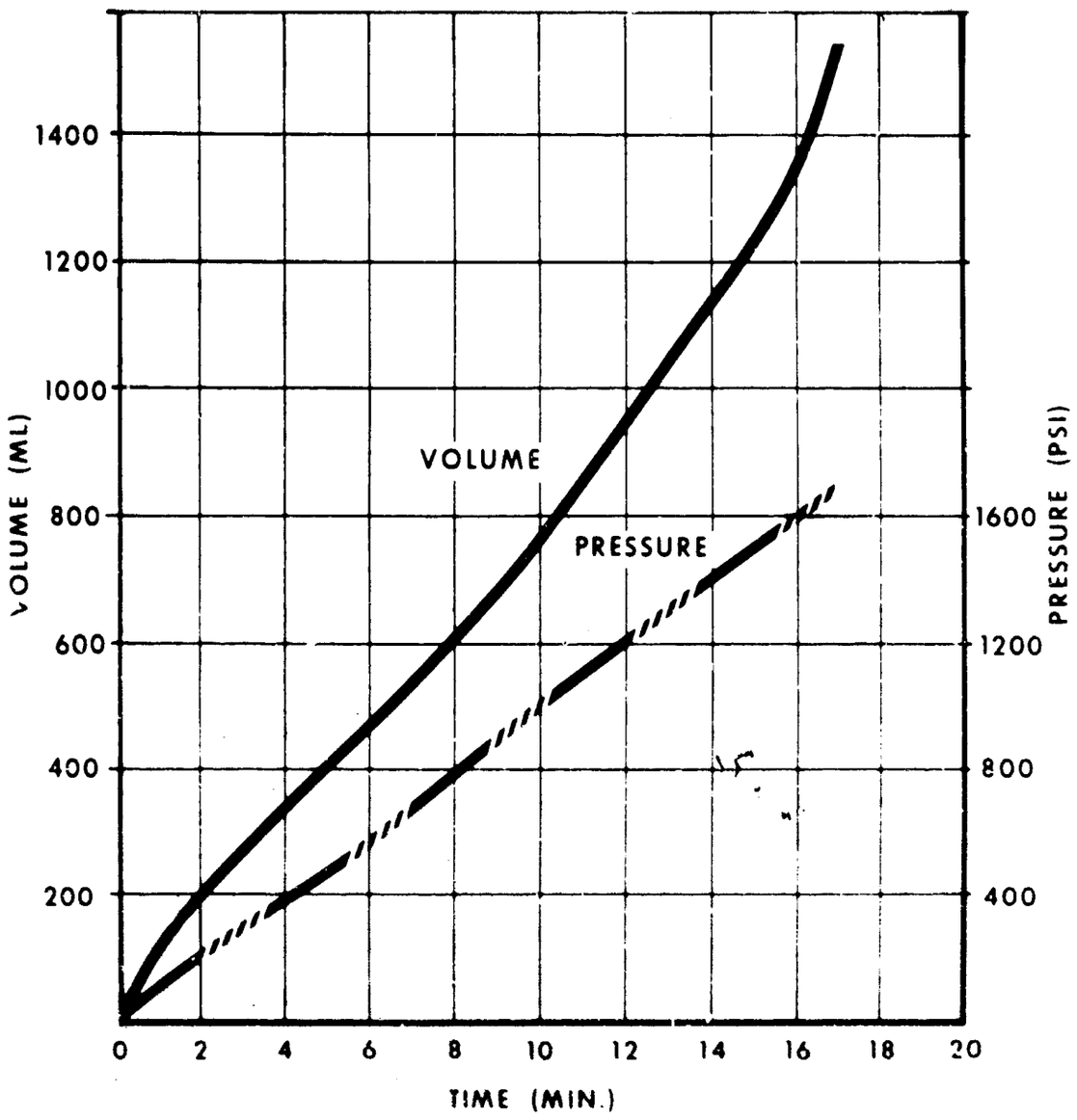

Figure 11

Volume Change and Tank Pressure as a Function of Time
For 15 inch Diameter NEMO Model (#4)

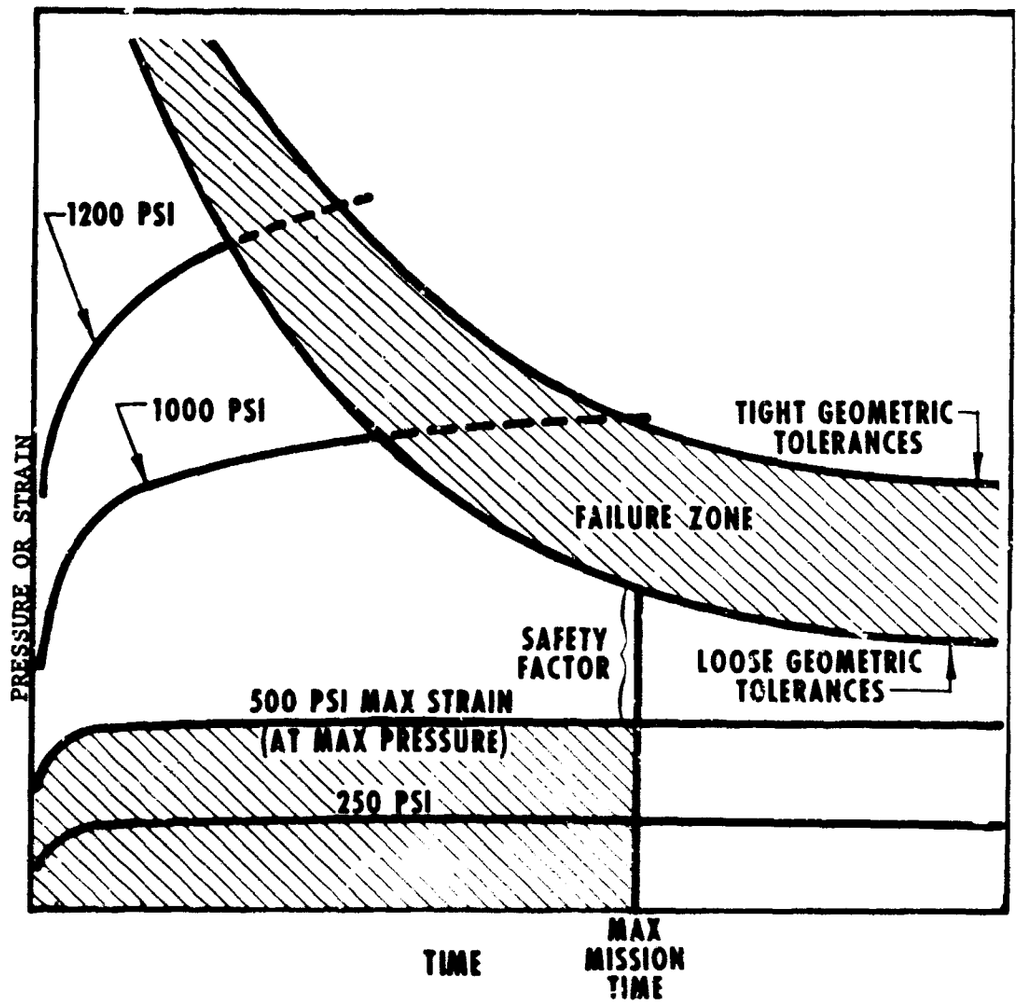

Figure 12

Structural Mission Envelope for Creep With Acrylic

COMPOSITE MODULES: A NEW DESIGN

FOR

DEEP OCEAN BUOYANCY APPLICATIONS

BY

Bernard Stechler and Israel Resnick
U. S. Naval Applied Science Laboratory

NOTE: The opinions or assertions contained in this paper are the private one of the authors and are not to be construed as official or reflecting the views of the Naval Service at large.

INTRODUCTION

Future exploration and exploitation of the ocean depends on the development of new vehicles capable of operating at great depths. One of the critical systems in such a vehicle is the buoyancy system. Without an adequate and dependable buoyancy system, the vehicle once submerged would not be able to return to the surface.

APPLICATIONS OF BUOYANCY MATERIALS

Since it does not seem reasonable to predict that within the next five years it will be practical to develop pressure hulls with sufficient positive buoyancy to operate safely with a pay load at depths as great as 20,000 feet, buoyancy systems must be devised that will both provide buoyancy and assure the structural integrity of the hull. The materials in such a system will probably constitute a large portion of the gross weight of the vehicle. As illustrated by the following examples from reference (1), the buoyant structure weight needed to provide net positive buoyancy for such vehicles with negatively buoyant hulls may be expected to vary between 15 and 50 percent of the vehicle gross weight, see Figure 1, depending upon the density of the buoyant structure. For the example shown in Table 1, syntactic foam with a density of 0.65 would constitute about 45 percent of the weight in a typical vehicle with gross weight of 66,700 lbs.

Development of lighter buoyant structures would provide substantial reduction in vehicle gross weight as shown in the above example using a buoyant structure with $(W/D)_B = 0.45$ instead of 0.65.

The saving in vehicle gross weight in this comparison equals the entire weight of the pressure hull and almost equals the assumed total weight of the external equipment. Development effort on buoyant materials thus appears to offer an attractive trade-off in terms of vehicle gross weight.

The relationship of buoyant structure volume to the total vehicle volume is another important consideration. For example, using the vehicle shown in Figure 1 with a W/D ratio of 1.2 for the pressure hull and 20,000 lbs of external equipment, the volume of the buoyant structure may vary from 19 percent to 30 percent of vehicle volume as seen in Table 2.

BUOYANCY MODULE FOR DSSV

*DEEP SUBMERGENCE SEARCH VEHICLE

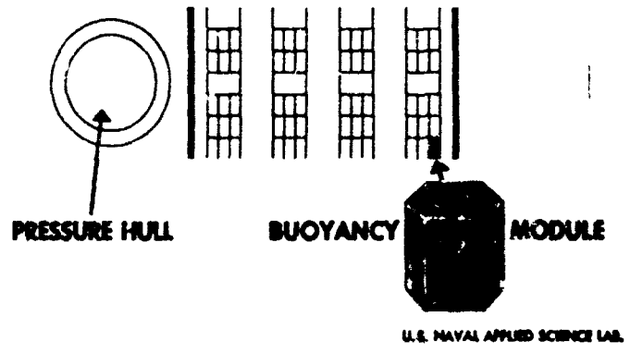

Figure 1

BUOYANCY REQUIREMENTS FOR TYPICAL VEHICLE

COMPONENT	WEIGHT, LBS.	DISPLACEMENT, LBS.	W/B RATIO
External Equipment	20,000	6,700	3.
Pressure Hull (7 1/2 ft. dia)	16,900	14,100	1.2
Total w/o Buoyancy Mat.	36,900	20,800	1.775
Total w/o Buoyancy Mat.	36,900	20,800	1.775
Syntactic Foam	29,089	45,900	0.65
Vehicle (Gross)	65,700	65,700	1 $W_w/W_a = 45\%$
Total w/o Buoyancy Mat.	36,900	20,800	1.775
Buoyancy Module	13,189	28,200	0.46
Vehicle (Gross)	50,000	50,000	1 $W_{sw}/W_a = 28\%$

U.S. NAVAL APPLIED SCIENCE LAB.

TABLE I

FUNCTION OF BUOYANT STRUCTURE FOR FAIL-SAFE OPERATION

The function of a buoyant structure, as discussed in reference (1), is "In addition to furnishing buoyancy or lift to compensate for the weight of the high density structures and equipment, the buoyant structure is a major factor in the design of a fail-safe search vehicle for operation at 20,000 ft. With respect to buoyant structure selection, two essential criteria for a fail-safe design are:

> The vehicle must have positive buoyancy, at any depth, sufficient to effect a safe return to the surface from any operating mode when all power, propulsion or ballast systems have failed or are inoperative.
>
> A buoyant structure failure shall not contribute to the failure of the pressure hull or other equipment that would result in catastrophic failure of the vehicle."

The buoyancy module containing syntactic foam meets both of the above criteria. See reference (2) for a comparison of syntactic foam with other low density liquids and solids considered for buoyancy applications.

BACKGROUND

The U. S. Naval Applied Science Laboratory has developed a candidate syntactic foam buoyancy material for deep submersible vehicles. This buoyancy material, which is identified as NASL ML-B3, consists of approximately 65 percent by volume of small hollow glass microspheres on the order of 10 to 100 microns (0.0004 to 0.004 in.) diameter embedded in a rigid epoxy resin matrix (see Figure 2). This material has a density of 0.6 to 0.7 gms/cm^3 (37 to 44 lbs/ft^3) and is capable of withstanding a uniform pressure of 10,000 psi for prolonged periods of time, as well as cyclic conditions over a range of hydrostatic pressure from atmospheric to 10,000 psi.

OBJECTIVE

Following the development of NASL ML-B3 syntactic foam, the Laboratory established a new objective - the development of a lower density, higher strength system of materials with a target density of 0.3

SYNTACTIC FOAM VS BUOYANCY MODULE IN TYPICAL VEHICLE

	BUOYANCY MATERIAL			VEHICLE		
	Weight, lbs	Density (W/D)	Volume, ft³	Gross Weight, lbs	Volume, %*	Weight, %
SYNTACTIC FOAM	29,800	.65	717	66,700	30	45
BUOYANCY MODULE	13,100	.45	457	50,000	19	26

*NOTE Based on 100% vehicle volume figure of 2400 ft³

U.S. NAVAL APPLIED SCIENCE LAB

TABLE 2

NASL DEVELOPED BUOYANCY MATERIALS

SYNTACTIC FOAM

Net buoyancy, pcf - 24

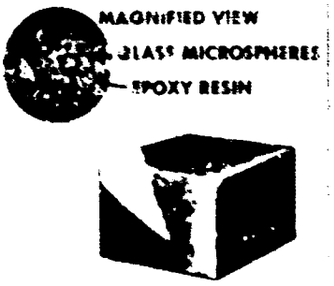

BUOYANCY MODULE

Net buoyancy, pcf - 36

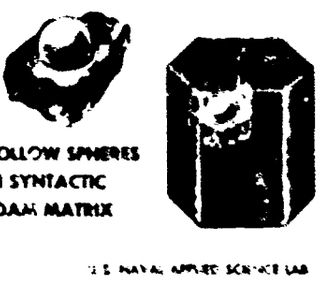

U.S. NAVAL APPLIED SCIENCE LAB

Figure 2

to 0.4 gm/cm^3 (19 to 25 lbs/ft^3) which will be able to withstand 13,500 psi hydrostatic pressure. This target system will consist of a module made of large hollow spheres contained in a syntactic foam matrix (see Figure 2).

APPROACH

In order to obtain higher strength, lower density materials, several approaches may be taken together or separately; these are:

a. Develop and use a lower density, higher strength resin matrix.

b. Incorporate lower density hollow microspheres in the existing or improved new matrix.

c. Incorporate high strength, large hollow spheres, one to four inch diameter, in a syntactic foam matrix thus making a composite module.

IMPROVEMENTS IN RESIN SYSTEM

The U. S. Naval Applied Science Laboratory has investigated and formulated high strength resin systems used in fabricating syntactic foam. Table 3 shows the properties of two of the many resin systems investigated. Originally ML-B3 was chosen because of its high strength properties, as seen in Table 3. Recently, both commercial and laboratory resins with higher strength have been developed. For example, the Applied Science Laboratory's new resin formulation, identified as NASL-GL-9 illustrates the increased resin compressive strength and modulus. Syntactic foam made with this resin system shows an almost 20% increase in compressive strength.

IMPROVEMENTS OF SMALL HOLLOW MICROSPHERES

Hollow microspheres of lower density are now becoming available. These should permit the development of lower density foams. These microspheres have a lower specific gravity than the high strength microspheres that are used in ML-B3 foam and will thus permit the development of lower density foams. Table 4 shows four foam materials made with the same resin system but with different types of hollow

RESIN DEVELOPMENT

Resin Designation	Epoxy	NASL-GL9
Compressive strength, psi	21,000	30,000
Compressive modulus, psi	5.5×10^5	7.6×10^5
Syntactic Foam Designation	**NASL-B4**	**NASL-B7**
Compressive strength, psi	16,000	20,000
Compressive modulus, psi	5.6×10^5	6.5×10^5

U.S. NAVAL APPLIED SCIENCE LAB.

TABLE 3

MICROSPHERE DEVELOPMENT

Nominal Sp Gr. of Microspheres	Syntactic Foam Designation	Foam Density lb/ft³	Compressive Strength, KSI Initial	Compressive Strength, KSI After Immersion*	Water Absorption, %*
0.45	NSL-B3	44.2	17.5	13.8	1.1
0.40	NASL-B11	42.	14.5	12.7	1.4
0.35	NASL-B12	38.5	12.4	10.5	3.0
0.35	NASL-B13	38.4	14.2	12.5	1.3
0.30 ←	Predicted	→ 36.			
0.25 ←	Predicted	→ 34.			

*NOTE: After immersion in water for 7 days at 10,000 psi

U.S. NAVAL APPLIED SCIENCE LAB.

TABLE 4

microsphere filler. As the specific gravity of the spheres decrease, the density of each corresponding foam decreases and the compressive strength is reduced. Formulation NASL-B13 was made with the same microspheres as formulation NASL-B12 except that the microspheres were pressure screened by subjecting them to 2,000 psi hydrostatic pressure, thus eliminating the weakest spheres. The unbroken floaters, which were the stronger microspheres, were used in formulation NASL-B13. The resulting foam shows a slight increase in density over the NASL-B12 but a compressive strength comparable to the NASL-B11 foam made with the higher density microspheres having a 0.4 nominal specific gravity. Two new lower density type hollow microspheres with nominal specific gravity from 0.3 to 0.25 are expected to be available in the near future. It may be expected that, if these microspheres follow the pattern shown in Table 4, the resultant syntactic foam will have a density of 34 lbs/ft^3.

LARGE HOLLOW SPHERES

Based on the existing state-of-the-art of glass and resin technology, the third approach offers the greatest immediate promise. Spheres have the best geometric shapes for resisting hydrostatic compression, and hollow shapes have the added property of very low density. Therefore, the large hollow spheres will make it possible to reduce the overall density of the system and still maintain the strength requirements.

A theoretical analysis of significant variables was conducted with glass, ceramic and hollow metal spheres to determine promising materials and sphere size for the module (see reference (3) for mathematical analysis). The assumptions upon which this mathematical analysis are based are listed in Figure 3.

An extensive group of materials was reviewed. The candidate materials selected are listed in the Nomograph, Table 5 under material density in ascending order. The selection of the optimum material was based on the need for:

High Modulus of Elasticity, and

Low Material Density.

APPROACH — IMPROVED BUOYANCY SYSTEM

- RESIN DEVELOPMENT
- MICROSPHERE DEVELOPMENT

→ IMPROVED SYNTACTIC FOAM

- INCORPORATE LARGE HOLLOW SPHERES IN IMPROVED SYNTACTIC FOAM MATRIX

U.S. NAVAL APPLIED SCIENCE LAB.

Figure 3

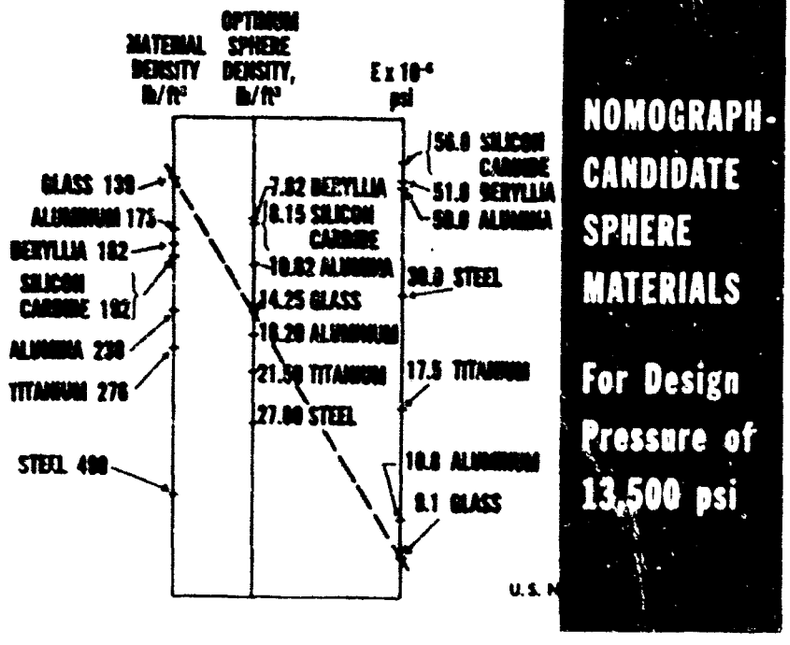

NOMOGRAPH-CANDIDATE SPHERE MATERIALS

For Design Pressure of 13,500 psi

TABLE 5

From the theoretical analysis, described in reference (3), the following conclusions can be drawn:

a. For a hollow sphere of a particular material at 13,500 psi external pressure the optimum sphere density is a constant for any outer diameter.

b. The candidate materials that are potentially suitable in sphere form are listed in the second column in Table 5 in order of ascending optimum sphere densities at 13,500 psi external pressure.

The preceding conclusions are based on an analytical solution of a hollow sphere and were used as the basic guideline for choice. The final selection of the optimum suitable candidate will be based on the factors listed in Figure 4. These factors are discussed below.

Beryllia and silicon carbide, though having the lowest hollow sphere density, see Figure 4, are at present, both expensive and difficult to fabricate in the spherical shape. It was therefore decided to evaluate glass and alumina spheres first because of their lower cost and greater availability. The state-of-the-art of fabrication of these materials as hollow spheres appears to be more advanced than that for other lower density materials.

Some development effort will be required to meet or closely approach the assumed conditions listed in Figure 3 since limitations of present production methods may introduce some variations from ideal conditions. Variations between actual and theoretical test results will be taken into account during the evaluation phase of the program. The intent is to approach the "ideal" conditions as closely as possible.

HYDROSTATIC TEST OF LARGE HOLLOW GLASS SPHERES

Tests were made to determine how close to the theoretical the actual failure pressures was for large hollow glass spheres. Three inch O.D. hollow glass spheres designed for the 3000 to 8000 psi range were used because of their availability and low cost. It is believed that information obtained from these 3-inch O.D. spheres can be extrapolated to design spheres suitable for use at 13,500 psi hydrostatic pressure.

A study was made to predict the actual failure pressure due to the variation of wall thickness in each sphere, which is one of the assumptions made in the theoretical analysis, see Figure 3. For each sphere, measurements were taken in both the latitudinal and longitudinal

directions, to determine actual wall thickness at each point and variations in wall thickness throughout the sphere. These spheres, although not perfect, showed a reasonably high degree of sphericity. Each sphere was put into a pressure vessel, and the pressure was increased at a uniform rate until the sphere failed. Preliminary studies, which require additional verification, indicated that the following equation explains about 60 to 65 percent of the variation in Failure Pressure (F.P.) results:

$$F.P. = 134.82\ x - 2S + 10496070\ (x^{-4}) + 42.69$$

F.P. - Failure Pressure

where: x = average thickness for specimen

S = within specimen standard deviation

Table 6 shows data for a selected group of spheres. It lists the theoretical and actual failure pressures, and the percentage deviation from the actual value for each sphere. The theoretical values shown are based on an Applied Science Laboratory developed equation for a hollow glass sphere with varying wall thickness, and differs from the theoretical equation reported and discussed in reference (3).

SYMPATHETIC IMPLOSION

When a hollow glass sphere fails in hydrostatic compression an implosion occurs. In working with glass and ceramic hollow spheres the phenomena of sympathetic implosion was observed and recognized as an important problem.

Sympathetic implosion may be defined as the effect of shock forces generated by the implosion of a shell causing implosion of another shell subjected to these forces either directly or by reflection. When a shell bursts abruptly inwardly, the potential energy in the shell coupled with the potential energy of the sea water in converting to kinetic energy, produces shock waves. The potential energy released at an environment

pressure P, due to collapse of a cavity which had a volume Vo, at the surface is represented by PV_o (references (4) and (5)).

The Applied Science Laboratory has conducted implosion tests on 3-inch O.D. hollow glass spheres of the type discussed under the previous section entitled Hydrostatic Test of Large Hollow Glass Spheres.

The test was performed on two spheres placed a specified distance apart in a pressure vessel. One thin walled hollow sphere, designed to fail at a low pressure was placed upstream. The second thicker walled hollow sphere, designed to fail at a higher pressure and proof tested was placed downstream. Pressure was applied and both spheres failed at the same low pressure. The assumption was that the failure of the "low pressure" sphere, by hydrostatic compression, produced a shock wave which caused the "higher pressure" sphere to fail. The phenomena of sympathetic implosion occurred at various distances between spheres up through 14 inches, which was the largest separation distance possible in the pressure vessel used.

The Applied Science Laboratory has tested a limited number of ceramic spheres and found that the problem of sympathetic implosion also exists with ceramic materials. The phenomena of sympathetic implosion occurring with spheres made of other materials has not yet been explored at the Applied Science Laboratory. From the literature and work conducted by other laboratories, references (6) and (7), this phenomena does not seem to be a problem with most metals. Thus the problem, if found critical enough in glass and ceramic types, may be a good reason for considering metal spheres as a component for the buoyancy module.

Underwater tests have been conducted at the Naval Ordnance Laboratory on large hollow glass spheres 10 inches in diameter, reference (8), which were exposed to explosions of Pentolite charges of T.N.T. at a range of depths. One of the results reported shows that at greater depths the implosion problem is less critical but still occurs. In general, it can be seen that the major obstacle to the use of glass and ceramic hollow spheres for buoyancy is the development of a suitable cladding or matrix material that will insure adequate shock protection.

As part of a future program the Applied Science Laboratory will investigate the effect of sympathetic implosion of hollow glass spheres as well as hollow spheres made of other materials embedded in a syntactic

LARGE HOLLOW SPHERE

ASSUMPTIONS

- UNIFORM EXTERNAL PRESSURE
- UNIFORM INNER & OUTER RADII
- NO CONSTRAINTS
- FAILURE BY ELASTIC BUCKLING

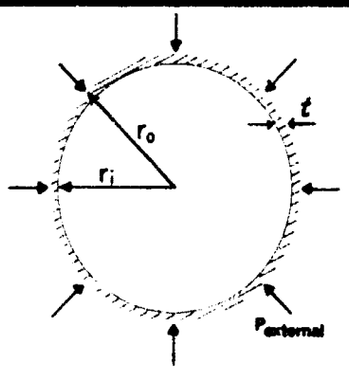

U.S. NAVAL APPLIED SCIENCE LAB.

Figure 4

FINAL BASIS FOR SPHERE MATERIAL SELECTION

- ANALYTICAL SOLUTION
- AVAILABILITY AND COST OF MATERIALS
- FABRICATION TECHNIQUES
- EXPERIMENTAL RESULTS
- UNIFORMITY OF WALL THICKNESS
- SYMPATHETIC IMPLOSION
- INTEGRATION INTO MATRIX

U.S. NAVAL APPLIED SCIENCE LAB.

Figure 5

HYDROSTATIC TESTS - HOLLOW GLASS SPHERES

FAILURE PRESSURE, psi		
THEORETICAL*	ACTUAL	% DEVIATION
4,392	4,486	2.08
4,770	4,650	2.57
5,290	5,410	2.24
4,140	4,420	6.32
4,380	4,450	1.57
5,500	5,420	1.47
3,880	3,820	1.57
4,820	5,190	5.05
4,720	4,900	3.67
4,220	4,390	3.88

*NOTE: Based on NASL developed equation for a hollow glass sphere with nonuniform wall thickness.

U.S. NAVAL APPLIED SCIENCE LAB.

TABLE 6

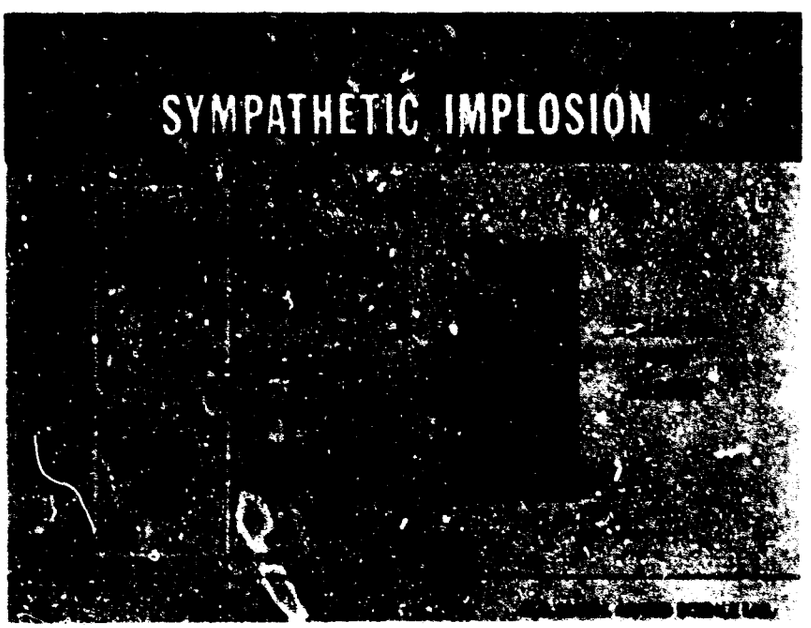

Figure 6

foam matrix, see Figure 7. The initial study will be concerned with the critical spacing of two spheres in a syntactic foam matrix (a one dimensional array). This initial phase will be followed by a study of the spacing in a two or three dimensional array.

THE COMPOSITE MODULE

The integration of hollow spheres of glass or other materials in an array and the optimum design of the array are complicated and difficult problems. In this design the two important criteria are density and strength. Figure 8 shows an exploded view of a composite module. It may seem from the figure that a composite module has a particular size and geometry, size and material of hollow sphere and spacing in the matrix. If only the spacing is changed the corresponding changes in buoyancy can be determined from the parametric curve in Figure 9. Although it is not shown in Figure 9, changes in spacing would also produce changes in strength. Likewise, variations in diameter and material of the sphere, and geometry and size of the composite module will result in changes of buoyancy and strength. In evaluating the above criteria the following design parameters must be considered critical:

a. Failure Mode of Components. Determination of the best components which will yield the maximum strength and lowest density based on component material design failure mode and failure pressure.

b. Interaction of Components. The effect of interaction between two or more materials thus changing properties and possibly failure modes.

c. Stress Considerations. The design of a composite module using stress analysis to determine modes of failure for a multi-component system.

d. Packaging. The design of a geometric shape or shapes which would facilitate the best volume usage and be capable of being easily positioned and replaced.

e. Fabrication. Different methods of fabrication would result in different stress considerations and interaction of components.

f. Sympathetic Implosion. The determination of critical distances due to the shock wave problem for a particular level of reliability.

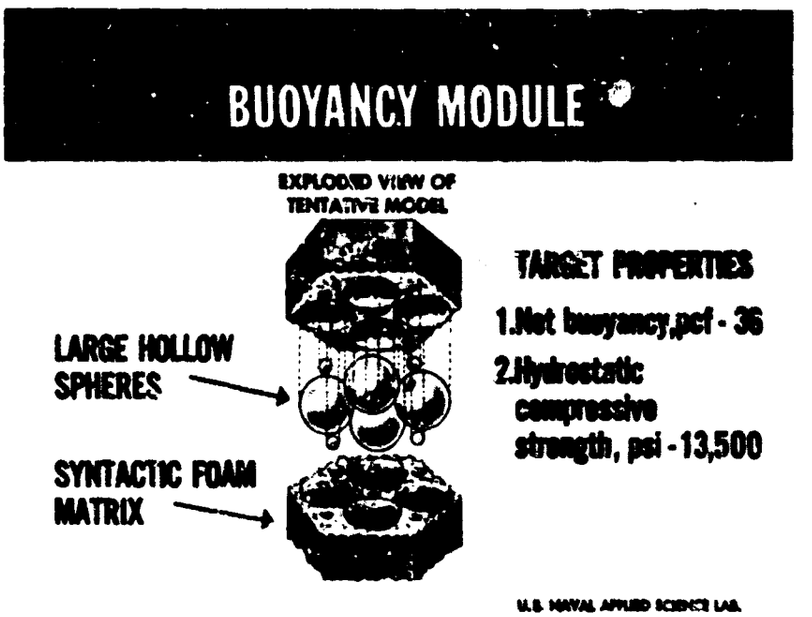

Figure 7

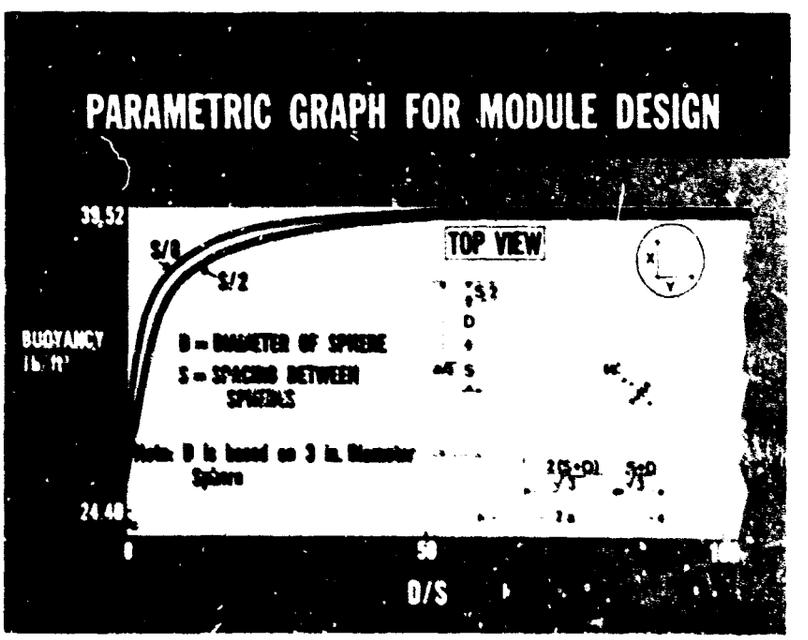

Figure 8

The final optimum system will only be optimum for a particular application; there will be different tradeoff points for different applications. In general the optimum system should be able to meet the particular strength application and have the lowest density possible for that application.

FORECAST OF FUTURE PROPERTIES

The Applied Science Laboratory prepared a report in 1964, reference (9), which presented the 1964 properties and costs for syntactic foam and forecast the values to be expected in 1970. Figure 10 shows three of the most important of these properties which are:

a. Ultimate compressive strength.

b. Net buoyancy, and

c. Cost per pound of buoyancy.

For each of the three properties shown are their corresponding values predicted at that time (in 1964), for 1970 as well as the present (1966) values. It can be seen that during the past two years the following occurred:

Ultimate compressive strength has increased from 18,000 psi to 20,000 psi because of improvement in resin strength. This is half-way to the 1970 goal of 22,000 psi.

The net buoyancy of syntactic foam has increased from 20 to 24 lbs/ft^3 because of the availability of lower density microspheres. This goal forecast for 1970 has been reached in 1966.

The cost per pound of buoyancy has been reduced from $13 to $9 because of the reduction in cost of both the resin and the microspheres. The cost today is slightly less than that predicted for 1970.

It can be seen that the NASL forecast prepared in 1964 was conservative since for each of the values, the rate of improvement in properties is greater than the original forecast. Figure 11 shows the

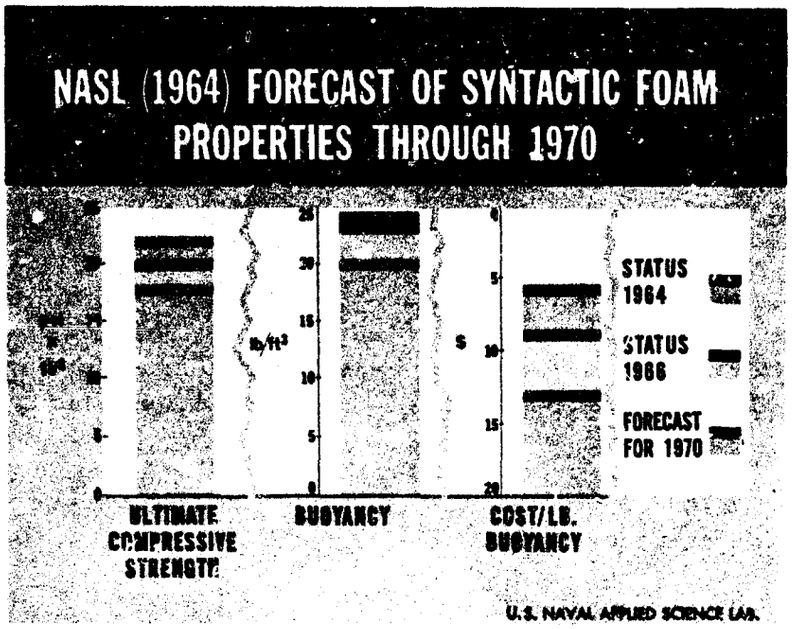

Figure 9

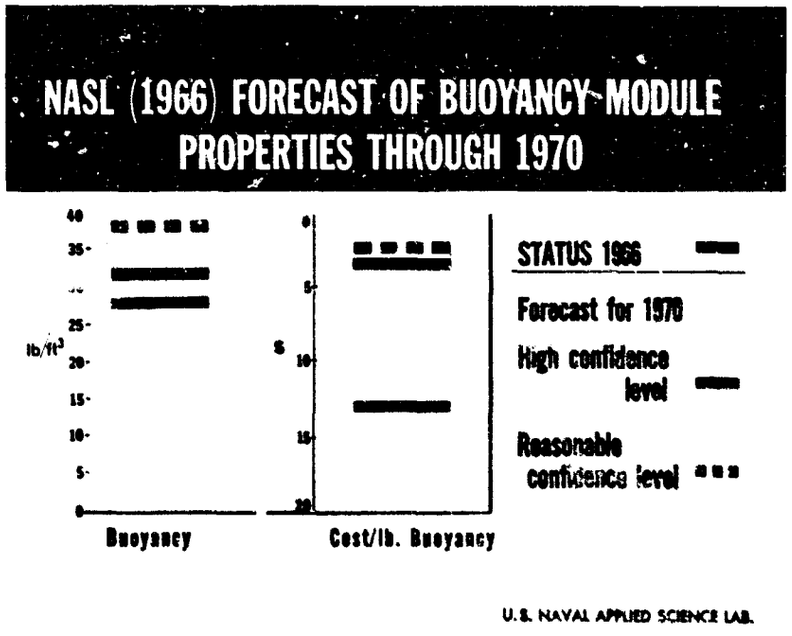

Figure 10

(ART NOT AVAILABLE)

Figure 11

buoyancy and cost per pound of buoyancy which may be realized in a buoyancy module now. The figure also shows forecasts for both properties based on high and reasonable confidence levels. By 1970 it is expected, with a high level of confidence, that a module will be available which will supply 32 lbs/ft^3 of buoyancy and will be priced at about $3.50 per pound of buoyancy.

SUMMARY

Buoyancy materials are required to permit deep submersible vehicles to carry a payload and remain buoyant. At the 2nd U. S. N. Symposium on Oceanography, the U. S. Naval Applied Science Laboratory discussed the development and properties of syntactic foam which has a net buoyancy of 20 lbs/ft^3 and is capable of withstanding service pressures of 10,000 psi. With the new emphasis on greater depth oceanography a new target of strength and buoyancy is necessary. To meet this need, the Applied Science Laboratory is developing buoyancy modules consisting of large hollow spheres contained in a syntactic foam matrix.

The target buoyancy module will provide 36 lbs/ft^3 of net buoyancy and be capable of withstanding service pressures of 13,500 psi; it will be designed to withstand the effects of shock and sympathetic implosion. The properties and behavior of the syntactic foam matrix material after exposure to high pressure hydrostatic exposure is given. Also, a study was made of glass, ceramic and metal hollow spheres to establish criteria for candidate sphere materials. Hollow glass spheres were evaluated to determine the relationship between theoretical and actual collapse pressures. Analytical studies of optimum sizes and geometry of modules were initiated. Based on an analysis of the hollow sphere and matrix materials, significant improvements in increased buoyancy, strength, and reliability over present buoyancy materials may be expected.

ACKNOWLEDGMENT

The authors are indebted to Mr. C. K. Chatten, Head of the Plastics and Elastomers Branch of the U. S. Naval Applied Science Laboratory for his encouragement, advice and assitance in preparation of this paper.

REFERENCES

1. Irgon, J. and Davidson, W. H., Final Report on Selection of Buoyant Materials for Deep Submergence Search Vehicle to Special Projects Office. Proteus Report No. SP-651F of 1 October 1965

2. Resnick, I., Syntactic Foam Buoyancy Materials for Submerged Research Vehicle. U. S. Naval Applied Science Laboratory, Vol. 1, Proceedings of the Second U. S. Navy Symposium Military Oceanography, 5-7 May 1965. Published by U. S. Naval Ordnance Laboratory

3. Stechler, B. G. and Resnick, I., Analytical Studies of Hollow Spheres for Lower Density Higher Strength Buoyancy Materials, SF 020-04-05, Task 1013, U. S. Naval Applied Science Laboratory Project 9300-57, Progress Report 1 of 16 August 1965

4. Lamb, H., Hydrodynamics, 6th Ed. 1930, Dover Publications

5. Cole, R. H., Underwater Explosions, 1948, Princeton University Press

6. Krenzke, M. A., Tests of Machined Deep Spherical Shells under External Hydrostatic Pressure. Report 1601, dated May 1962. David Taylor Model Basin

7. Krenzke, M. A. and Kiernan, T. J., Tests of Unstiffened Machined Spherical Shells under External Hydrostatic Pressure, Report 1741, dated August 1963, David Taylor Model Basin

8. Faux, W. H., and Niffennegger, C. R., The Resistance of Hollow Glass Models to Underwater Explosions at Great Depths, Part I Spheres, Report NOLTR 65-145 dated 30 September 1965, U. S. Naval Ordnance Laboratory

9. Bukzin, E. A. and Resnick, I., Buoyancy Materials, from NRL Report 6167, Status and Projections of Developments in Hull Structural Materials for Deep Ocean Vehicles and Fixed Bottom Installations, Edited by W. S. Pelleni, Underwater Sound Reference Laboratory dated 4 November 1964

PROTECTIVE COATINGS IN SHALLOW AND DEEP OCEAN ENVIRONMENTS

C. V. Brouillette, R. W. Drisko, and R. L. Alumbaugh
U. S. Naval Civil Engineering Laboratory, Port Hueneme, California

INTRODUCTION

Numerous activities in the Naval Shore Establishment have encountered difficulties in protecting from corrosion steel structures exposed to a submerged marine environment. Until comparatively recently, almost all attempts at corrosion control were directed to structures located at very shallow depths. The Navy is now paying increased interest to protection at greater ocean depths.

Submerged steel structures are frequently protected by cathodic protection when a source of electrical power is readily available. Protective coatings are generally used in conjunction with cathodic protection to reduce current requirements. They are almost always used on steel structures in the tidal area where cathodic protection is ineffective and at geographical locations where electrical power is unavailable.

The U. S. Naval Civil Engineering Laboratory has conducted several studies[1,2] into protective coatings for steel located in a submerged marine environment. One such study utilized coated steel piling and angle iron driven into surf and harbor areas at Port Hueneme, California and Guam, Marshall Islands, another utilized coated steel panels ten feet long, four inches wide, and one-fourth inch thick suspended from piers at two locations, and a third utilized mooring buoys serving the fleet at San Diego Bay. The data to be presented on the performance of protective coatings at shallow depths were taken from these studies.

Coated steel specimens exposed at greater depths were twelve inches long, six inches wide, and one-eighth inch thick. These were placed in racks and secured to a submersible test unit (STU)[3] exposed at various bottom depths off the coast of Southern California.

Exposed specimens in all environments had been coated under the direction of application specialists. Sandblasted steel surfaces were coated in accordance with the best recommended practices at a temperature greater than 60°F and a relative humidity less than 85%. Surfaces were primed immediately after sandblasting to white metal, and additional coats were applied after undercoats had completely dried. Total dry film thickness was determined by magnetic gage.

All test specimens were carefully installed to avoid coating damage and permit meaningful conclusions to be made. This paper will compare the performance of a number of protective coatings in shallow and deep ocean environments.

ORGANIC COATING SYSTEMS

Ten coating systems, nine completely organic and one containing a zinc inorganic silicate, were exposed in one deep ocean exposure program. These systems were exposed on pairs of panels, one scribed and the other unscribed. Test panels were first exposed for four months at 5,600 feet. When found to suffer no deterioration in this environment, they were exposed at a depth of 6,800 feet for an additional thirteen months. The performance of these systems at 6,800 feet and in a shallow ocean environment will be discussed individually.

Mica-filled asphalt emulsion - This system consists of one coat of pretreatment primer MIL-P-15328B, two coats of phenolic primer MIL-P-12742A, and three coats of mica-filled asphalt emulsion giving a total dry film thickness of 20-21 mils. At shallow depths the soft asphaltic topcoats were subject to abrasion damage and penetration by barnacles. The underlying zinc chromate-pigmented primer provided protection where much of the asphaltic topcoat had been lost by barnacle attack.

This system performed well at 6,800 feet. The only deterioration was a very slight rusting and tuberculation at the scribe. It should be noted that there was practically no fouling on any of the panels at great depth, the only occasional organisms present being identified as small hydroids and porifera (sponges).

Coal Tar - This system consists of three coats of cold-applied coal tar coating MIL-C-18480A to a total dry film thickness of approximately 40 mils. The soft coating was very susceptible to abrasion damage and penetration by barnacles at shallow depths in the same manner as the asphaltic topcoat of the previous system. This usually led to early failure in the tidal zone.

At 6,800 feet there was no coating damage and only slight rusting at the scribe.

Coal Tar Epoxy - This system consists of two coats of catalyzed coal tar epoxy primer and one aluminum-filled catalyzed coal tar epoxy topcoat giving a total dry film thickness of 15 mils. This system had provided excellent protection for steel specimens at shallow depths up to three years.

At 6,800 feet this system performed well with only slight rusting and tuberculation at the scribe.

Epoxy - This system consists of one coat of catalyzed epoxy primer and three catalyzed epoxy topcoats giving a total dry film thickness of 10 mils. It has given very good protection to steel specimens for three years at shallow depths.

At 6,800 feet the unscribed panel showed no deterioration, but the scribed panel had medium blistering, and tuberculation at the scribe.

Epoxy-Phenolic - This system consists of one coat of catalyzed epoxy primer and two catalyzed epoxy-phenolic topcoats giving a total dry film thickness of 15 mils. It has given excellent protection to steel specimens for two years at shallow depths.

At 6,800 feet the unscribed panel showed no deterioration, and the scribed panel had only two blisters at the scribe.

Phenolic Mastic - This system consists of one coat of catalyzed mica-filled phenolic primer and one catalyzed phenolic topcoat giving a total dry film thickness of 18-20 mils. This hard, smooth coating system has provided very good protection for steel panels at shallow depths but has suffered moderate amounts of abrasion damage on test mooring buoys.

At 6,800 feet there was no coating damage and only slight rusting at the scribe.

Saran - This system consists of alternate coats of vinylidene chloride resin lacquer, MIL-L-18389, Types I and II (white and orange) giving a total dry film thickness of 6-8 mils. It has given excellent protection to steel panels for four years at shallow depths. Slight pinpoint rusting and blistering was noticed after four years exposure.

At 6,800 feet the unscribed panel showed no deterioration, but the scribed panel had medium blistering near the scribe and rusting and tuberculation in the scribe.

Vinyl - This system consists of one coat of pretreatment primer MIL-P-15328B, five coats of vinyl primer MIL-P-15929A, and two coats of either vinyl-alkyd enamel, MIL-P-15936B (gray) or vinyl-alkyd enamel MIL-P-16738B (white), giving a total dry film thickness of 10-12 mils. It has provided very good protection for steel specimens at shallow depths for two years. It has also performed well on Coast Guard navigational buoys and navy vessels for two or more years.

At 6,800 feet the unscribed panel showed no deterioration, but the scribed panel had considerable blistering and lifting of coating at the scribe.

The framework of a STU unit exposed at 5,300 feet for three years was coated with the vinyl system. This coating showed no deterioration other than a slight pin-point rusting and very slight blistering.

Urethane - This system consists of one coat of catalyzed urethane primer and three catalyzed urethane topcoats giving a total dry film thickness of 10-11 mils. In some cases, it has performed satisfactorily for two years before light blistering occurred and in other cases moderate blistering was noted after one year.

At 6,800 feet both panels had extensive blistering and pin-point rusting.

Zinc Inorganic Silicate - Vinyl Mastic - This system consists of one coat of post-cured zinc inorganic silicate, one coat of vinyl-phenolic primer, and two vinyl mastic topcoats giving a total dry film thickness of 13-14 mils. It had extensive blistering and loss of the organic coatings on panels at shallow depth and on a mooring buoy, but the underlying zinc inorganic silicate has provided excellent protection from corrosion for two years.

At 6,800 feet both panels showed no coating deterioration, and there was only light rusting at the scribe.

Panels coated with the above ten coating systems were exposed in a 5% salt spray cabinet for 3181 hours. The test results were listed in Table 1. There was no apparent correlation between performance under salt spray and under field exposure conditions.

The pressure at 6,800 below the ocean surface, approximately 3,000 psi, exerted considerable force on the coated panels. The scribed panels had much more coating deterioration than the unscribed panels. All scribed panels with coating thicknesses at least 13 mils had little, if any, deterioration, and those with coating thicknesses less than 13 mils had significant amounts of deterioration. Thus, one requirement for good performance of an organic coating at great ocean depth may be a minimum dry film thickness of 13 mils. Any coated structure to be placed at depth must be able to perform well when bare steel is exposed by abrasion or impact damage.

The soft asphaltic and coal tar coatings performed better in a deep than in a shallow ocean environment because of susceptibility to barnacle damage in surface waters. In general, however, the organic coating systems performed similarly at shallow and deep ocean environments except for the latter scribed panels described above.

Table 1. Size and Frequency of Organic Coating Blisters After Salt Spray Exposure

Coating System	Blistering Ratings,* Size/Frequency			
	216 hrs	456 hrs	1,117 hrs	3,181 hrs
Mica-filled asphalt emulsion	6/F	4/M	2/M	2/MD
Coal tar	10/N	10/N	10/N	10/N
Coal tar epoxy	10/N	2/F	2/F	2/MD
Epoxy	6/F	4/M	2/M	2/MD
Epoxy-phenolic	10/N	2/M	2/M	2/M
Phenolic mastic	10/N	10/N	10/N	10/N
Saran	6/M	2/MD	2/MD	2/D
Vinyl	10/N	2/MD	2/MD	2/D
Urethane	10/N	2/MD	2/MD	2/D
Zn Silicate-Vinyl Mastic	10/N	10/N	10/N	10/N

* The rating method was ASTM Designation D-714-56. The size ranges from no blistering (1) to large blisters (2). The frequency of blistering was none (N), few (F), medium (M), medium dense (MD), or dense (D).

ZINC INORGANIC SYSTEMS

Three proprietary post-cured and six proprietary self-cured zinc inorganic coatings were applied to steel panels, and overcoated with the proprietary coatings recommended by the supplier. In addition, one of each type was overcoated with the vinyl system described in the previous section of this paper. Sets of these coated panels were exposed in a salt spray cabinet for 3181 hours, at shallow depths for six months, on the ocean floor at 2,340 feet for six months, and on the ocean floor at 6,800 feet for thirteen months. All specimens had either no or only slight rusting after exposure. The blistering of the overcoating, along with a description of each coating system, is given in Table 2.

As with the organic coated panels, the scribed panels with inorganic zinc coatings had more blistering at 6,800 feet than the unscribed panels. Those coating systems that performed well at shallow or deep environments performed well when exposed to salt spray. It should be noted that Systems using zinc inorganic coatings B and R performed well in salt spray testing but did not perform well in deep exposure. Performances were generally comparable in a shallow and deep ocean environment.

The post-cured coating systems generally had less blistering at all exposures than the self-cured systems. Since the observed blistering was probably accelerated by the presence of soluble zinc salts on the over-coated surface, it appears that the thorough hand scrubbing and washing of the post-cured zinc inorganic coatings (probably much better than would be received in field applications) removed most of these salts. The post-cured zinc inorganic coatings were found after exposure to be generally harder than those self-cured. The system with product Q performed well in spite of its relative thin film thickness. The other systems were of approximately the same dry film thickness, and thickness could not be related to performance.

SPLASH ZONE COMPOUNDS

Four two-component splash zone compounds (underwater-curing epoxy coatings) were applied to four panels coated with some of the previously described organic coating systems. Two 2½-inch square areas were sand-blasted to white metal on one side of each of the coated panels. A 3½-inch square of splash zone compound was placed by hand over each sand-blasted area so that there was a ½-inch overlap over each side. The test pattern is shown in Table 3 where Epoxy I has an asbestos filler added to the catalyst, Epoxy II was prepared directly from the Shell formulation, Epoxy III has a very fluid catalyst, and Epoxy IV has copper oxide added to the epoxy resin to retard marine fouling. After thirteen months exposure at 6,800 feet, all epoxy patches were adhering tightly to the panels with the exception of Epoxy IV that had a slight lifting at the edges that permitted rusting of the underlying steel. Epoxy IV was

Table 2. Size and Frequency of Blisters on Zinc Inorganic Panels

Coating System				Blistering Ratings[b]						
Coating[a]	Thickness (mils)	Description of Overcoating	System Thickness (mils)	Hours in Salt Spray				At Shallow Depth	At 2,340 Feet	At 6,800 Feet
				216	456	1,117	3,181			
A	2½	3 coats epoxy	12½	10/N	4/F	2/F	2/MD	4/F	10/N	10/N
B	2½	3 coats vinyl	10½	10/N	10/N	10/N	10/N	4/F	2/MD	2/MD
C	2½	1 tie coat + 3 Al-filled hydrocarbon coats	11½	10/N	10/N	10/N	10/N	10/N	10/N	4/D[c]
C	2½	Spec. vinyl system of previous section	12	10/N	10/N	10/N	10/N	10/N	10/N	2/D[c]
M	2½	1 coat coal tar epoxy	12	6/F	2/M	2/MD	2/MD	10/N	4/F	4/F
N	5	3 coats epoxy	13	10/N	4/F	2/F	2/MD	2/F	2/F	2/F
O	5	3 coats epoxy	14½	10/N	10/N	10/N	10/N	10/N	6/F	2/M[c]
P	3½	1 anti-corrosive coat + 1 coat epoxy	15	10/N	10/N	10/N	2/F	2/F	10/N	8/F[d]
Q	2	3 inorganic coats	5½	10/N	10/N	10/N	10/N	--	10/N	10/N
R	3½	1 tie coat + 3 Al-filled hydrocarbon coats	12	10/N	10/N	10/N	10/N	4/F	2/D	2/MD[c]
R	2½	Above spec. vinyl system	14	2/F[c]	2/F	--	--	2/F	2/D	4/D

a Coatings A-C were post-cured and M-R self-cured.

b See Table 1 for method of rating.

c At scribe only.

d The topcoats of both panels had loss of adhesion.

rather easily chiseled from the test panels, and there was rusting of the underlying steel. Epoxies I and II were chiseled from the panels with considerable difficulty, and it was virtually impossible to remove the Epoxy III patches in one piece. The surface under these three epoxies were free of corrosion. All four splash zone compounds tested have performed well in patching damage coatings on mooring buoys.

Table 3. Pattern of Splash Zone Compound Testing

Panel Coating	Splash Zone Compound Used
Mica-filled asphalt emulsion	I, II
Epoxy	II, III
Urethane	III, IV
Coal tar epoxy	I, IV

ACKNOWLEDGEMENT

Mr. A. F. Curry of the U. S. Naval Civil Engineering Laboratory was most helpful in the monitoring of coating applications, placement of coated specimens, and rating of coating conditions.

REFERENCES

1. R. W. Drisko. A study of coatings in a marine environment. Official Digest Journal of Paint and Engineering Technology, 36, 767-778 (1964) July.

2. R. L. Alumbaugh. Field test data on coatings for steel piling in sea water. Materials Protection, 3, 34-35 (1964) July.

3. K. O. Gray. Materials testing in the deep ocean. Materials Protection, 3, 46-53 (1964) July.

4. ASTM Designation: D-714-56, Standard Method for Evaluating Degree of Blistering of Paints. 1964 Book of ASTM Standards, Part 21, 138-147. American Society for Testing and Materials. Philadelphia, Pennsylvania, 1963.

AN AUTOMATIC OCEANOGRAPHIC DATA COLLECTION SYSTEM FOR USE IN AN ARCTIC ENVIRONMENT

by P.C. Stahl
The Bissett-Berman Corporation
San Diego, California

ABSTRACT

This paper describes an Arctic Oceanographic Data Collection System developed for the U.S. Navy Electronics Laboratory under Contract No. N123-(953)50172A. The equipment consists of seven underwater packages and two automatic winches and data handling equipment sets that are to be housed on two barges. Five of the sensor packages are located at fixed positions on the bottom, and the other two continuously profile below each barge at a very slow speed. Parameters measured are salinity, water temperature, current speed, current direction, and depth. All sensors are designed for long life, stable operation, and minimum power consumption, and are protected from the effects of corrosion and biological fouling.

All data are sampled once each minute and recorded on magnetic tape. At the option of the operator, data may be printed out on a small digital printer. In addition to actual parameter measurements, individual calibration data for each sensor and the telemetry link is recorded once each hour.

The inherent flexibility of the system permits fully automatic unattended operation with optional semiautomatic control by an operator. The system is designed for continuous operation for a minimum of one year.

INTRODUCTION

The methods of collection, reduction, and storage of oceanographic data sometimes take as many forms as there are people directly concerned with the individual facets of ocean science. However, even though detailed concepts and final hardware may vary widely, the basic requirements are very similar. Particular oceanic parameters must be sensed, data generally must be telemetered to a convenient location, and finally, data must be converted to a form for presentation and/or storage in a manner suitable for visual or machine interpretation. This process is essentially the same for all technical disciplines.

The automatic system described here utilizes state-of-the-art concepts, and through the use of a wide variety of techniques, provides an overall system that offers the accuracy, reliability, and flexibility deemed necessary for general use. In addition, since this particular system will be placed in the Arctic in an environment which will deny access to the underwater equipment once it is installed, continual operation is guaranteed only by virtue of adequately tested components and built-in redundancy.

SYSTEM DESCRIPTION

Two individual, completely isolated systems comprise the overall installation. The major difference between the two self-contained systems is that one of them collects data from three sensor stations, and the other collects data from four. Because the differences are minor, only one system will be fully described. The overall system is shown in simplified block diagram form in Figure 1. A typical underwater sensor package, a winch, and the barge-mounted data conditioning and recording equipments are illustrated in Figures 2, 3 and 4 respectively.

The bottom-mounted sensor packages each contains an in situ salinometer, a water temperature sensor, a current speed and direction sensor, and an underwater signal mixer. The output signal of each sensor is a FM analog of the sensed phenomenon. These FM signals are combined in the mixer and transmitted by means of a two-conductor cable (isolated return) to the barge-mounted deck terminal equipment. In addition to the sensors previously mentioned, the profiling sensor package also contains a pressure (depth) sensor.

Each sensor package is physically connected to the deck electronics by an insulated, armored, two-conductor oceanographic cable. This cable is constructed to meet the rigors of submersion at very low temperatures for long periods without degradation.

At the barge end of the oceanographic cables, the multiplexed FM signal is separated, digitized, and recorded. Sequencing and timing logic automatically scan each sensor signal once per minute. In addition to the raw sensor data, heading data consisting of station identification and a time code (year, day, hour, minute, and second) are recorded on tape. Every hour a standard three-quarter inch gap is generated. Every six hours, an individual record containing standard heading information and calibration data for each sensor is recorded on tape. The calibration data consists of 0%, 50% and 100% indications of the full-scale value of each parameter. Data may also be displayed in real-time on the digital printer under control of the operator. This output is identical in form to that which is recorded on magnetic tape.

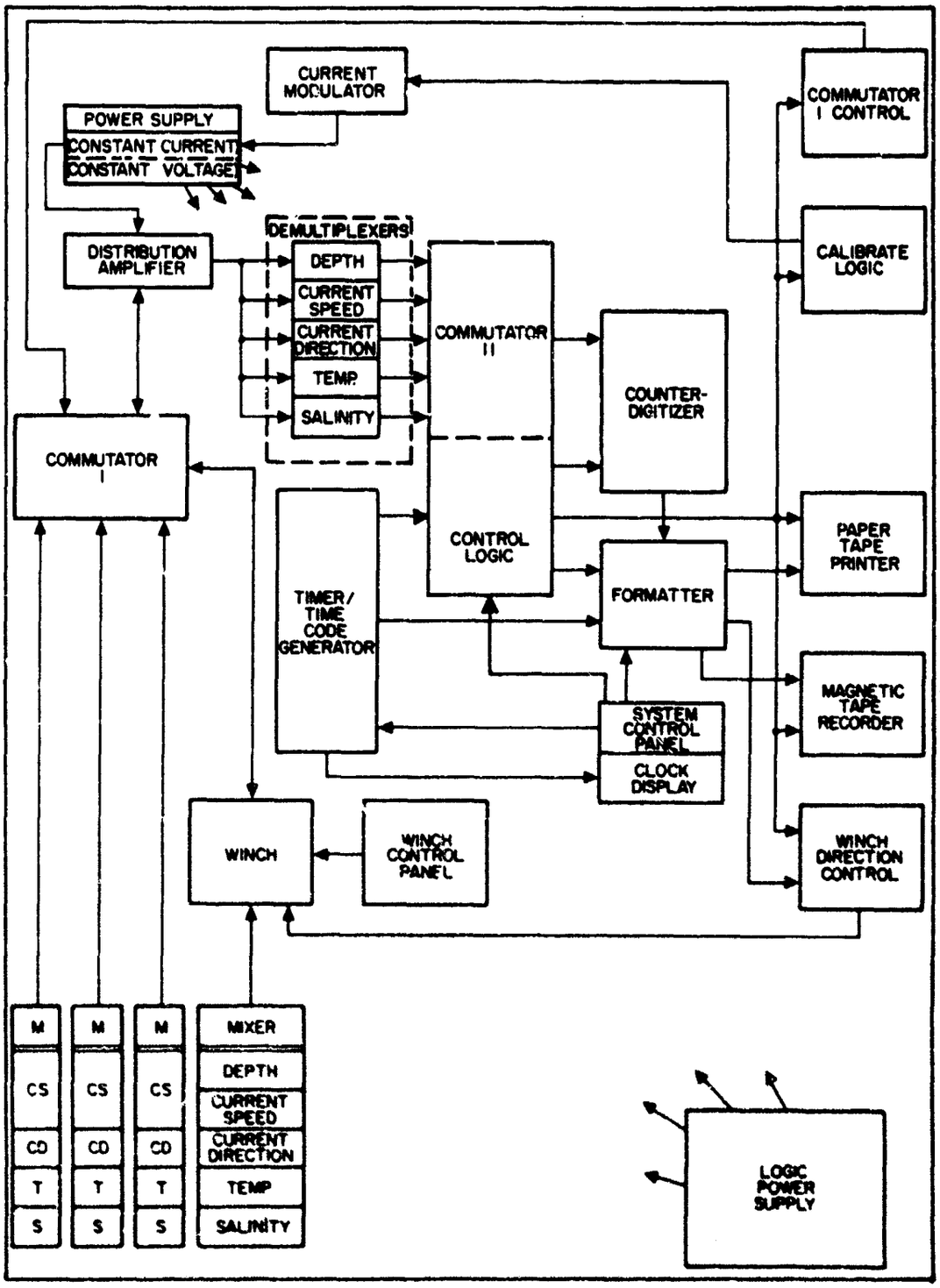

Figure 1. System block diagram.

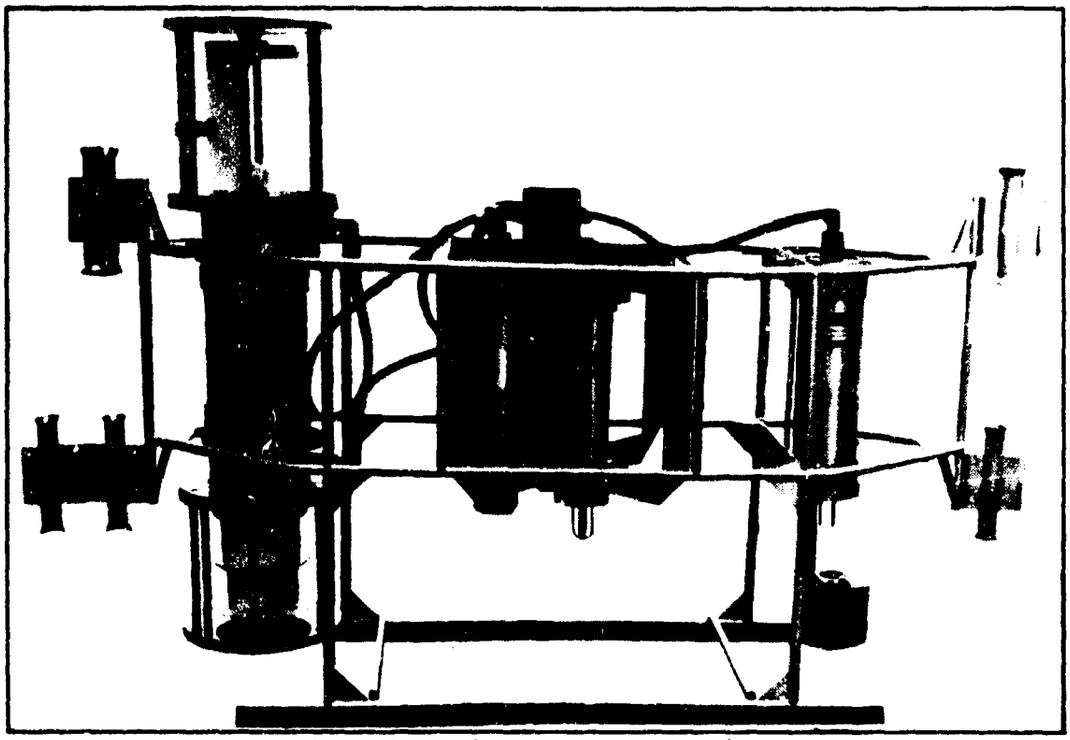

Figure 2. Underwater sensor package.

The major components included in each barge-mounted electronics complex are: power supplies for the underwater units; a distribution amplifier; a frequency demultiplexer for each parameter channel; an operator control panel; an input power chassis; an incremental magnetic tape recorder; an electronic counter; a digital printer; control and timing logic; a logic power supply; and a time code generator and system clock.

UNDERWATER INSTRUMENTATION

As mentioned, two different types of underwater subsystems are provided with the data collection system. One is the profiling subsystem shown in Figure 2, and the other is a fixed position type that is identical to the profiling unit except that it does not have the hinged guide ferrules and the depth sensor, and it has a stainless steel plate at the bottom of the underwater rack for mounting on a tripod. Each underwater rack contains an in situ salinometer, a temperature sensor, a current speed and direction sensor, an underwater signal mixer, and the depth sensor for determining the position of the unit at all times.

Functionally, all sensors except current speed convert a transducer response to a frequency analog of the measured parameter within a PARALOC® oscillator.

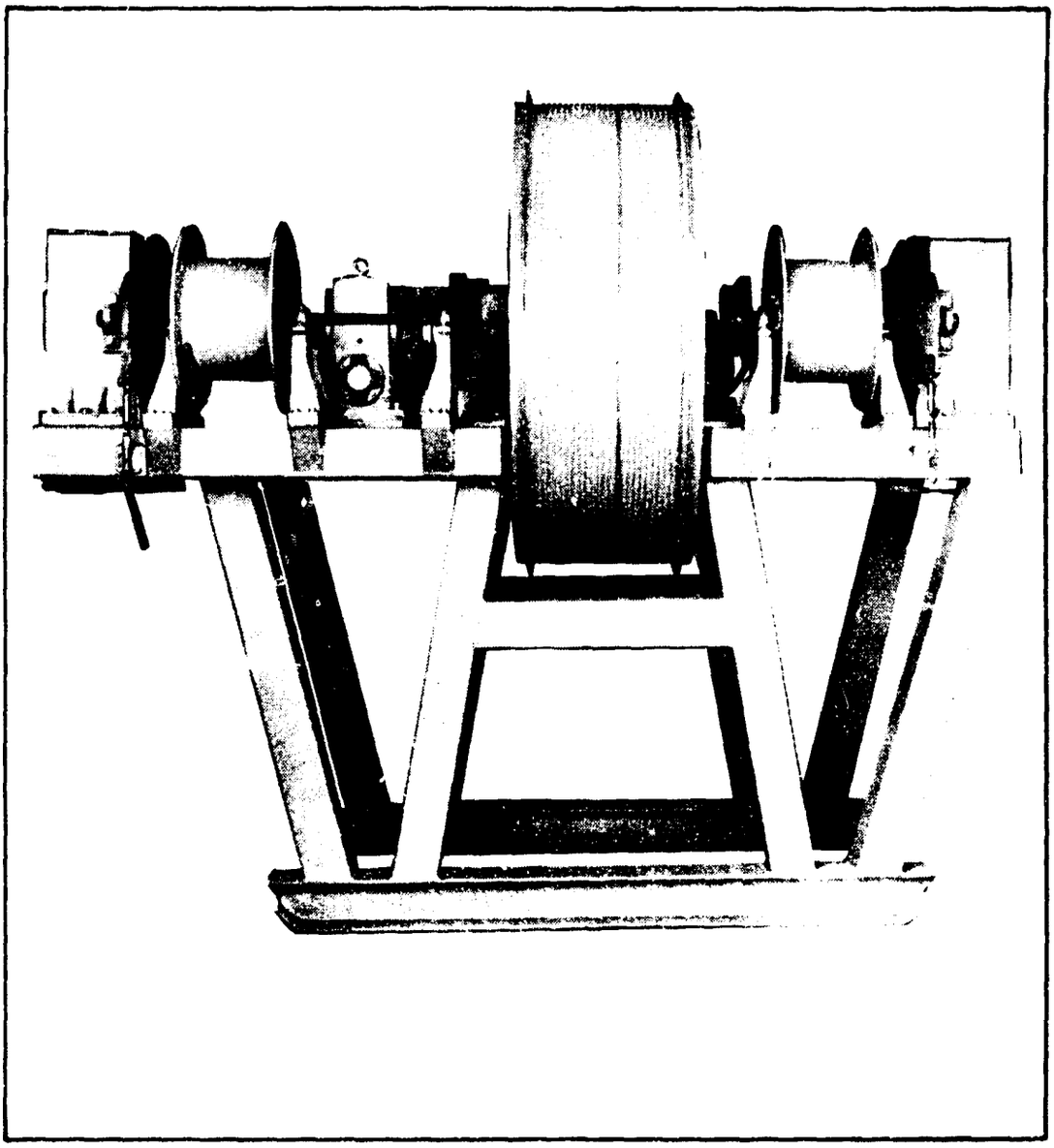

Figure 3. Tide compensating automatic winch.

In the PARALOC, the transducer element reactance, an analog of the measured variable, is translated directly into a proportionate frequency. This method of measurement eliminates errors that are normally associated with dc transducer excitation. Oscillator stabilities of ±0.03% of center frequency are typical over extended operating periods. The current speed sensor provides an FSK signal in which the duration of each frequency group is proportional to the speed of the savonius rotor.

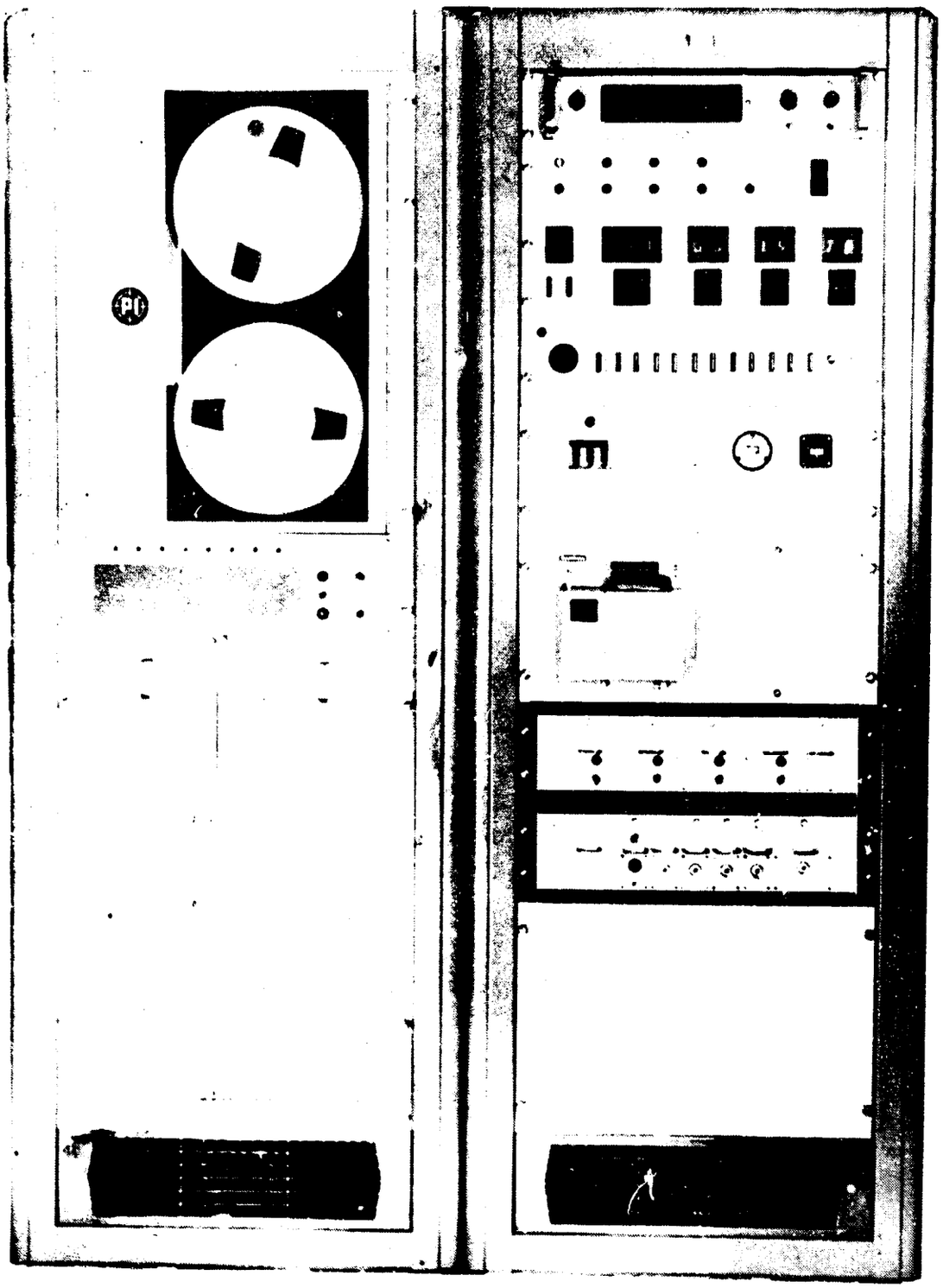

Figure 4. Data conditioning and recording equipment.

A unique feature of each of these sensors is the inclusion of circuitry which permits remote "confidence" testing of the instrument. When this test is initiated, the individual sensor transducers are replaced by known components which accurately simulate each transducer output at selected values of its range. This technique enables verification of proper operation of the sensor electronics, the complete telemetry link, and the barge-mounted electronics.

SENSOR SPECIFICATIONS

Detail specifications, which were either met or exceeded for each of the individual sensors, are provided in Table 1. The maximum error in salinity

TEMPERATURE SENSOR	
Range	-4°C to 15°C
Accuracy	± 0.02°C, including nonlinearity and repeatability
Output Frequency	2,127 to 4,193 Hz
Output Amplitude	1.4 volts rms ± 20%
Output Impedance	10,000 ohms
Time Constant	Approximately 0.3 seconds

DEPTH SENSOR	
Range	0 to 100 meters
Accuracy	±0.25% of full-scale including nonlinearity, hysteresis, repeatability and temperature effects.
Output Frequency	1,572 to 1,628 Hz
Output Amplitude	1.4 volts rms ± 20%
Output Impedance	10,000 ohms

IN SITU SALINOMETER	
Range	0 to 40 ppt
Accuracy	±0.02 ppt over the range from 20 ppt to 35 ppt and ±0.04 ppt over the ranges from 0 ppt to 20 ppt and 35 ppt to 40 ppt. (These accuracies are obtained after corrections are applied.)
Repeatability	0.01 ppt
Output Frequency	4,996 to 11,288 Hz
Output Amplitude	1.4 volts rms ± 20%
Output Impedance	10,000 ohms

A typical set of calibration curves for the in situ salinometer is shown in Figure 5.

CURRENT DIRECTION SENSOR	
Range	0-360° (fixed reference)
Threshold	0.1 knot
Accuracy	±5°
Output Frequency	1,202 to 1,396 Hz (0° is equivalent to 1,292 Hz)
Output Amplitude	1.4 volts rms ± 20%
Output Impedance	10,000 ohms.

CURRENT SPEED SENSOR	
Range	0.05 to 6 knots
Accuracy	±0.05 knots from 0.05 to 2.5 knots and ± 2% of full-scale over the range 2.5 to 6.0 knots
Output	IRIG channel 14-FSK (13,412 or 15,868 Hz)

TABLE 1. SENSOR SPECIFICATIONS.

over the entire range from zero to 40 parts per thousand and from -4 to 15°C is ±0.1 ppt, as shown in Figure 5. However, it should be noted that this relationship is repeatable within ±0.01 ppt, enabling correction of the raw data after recovery. All other sensors meet the stated specifications without correction and are, therefore, completely interchangeable.

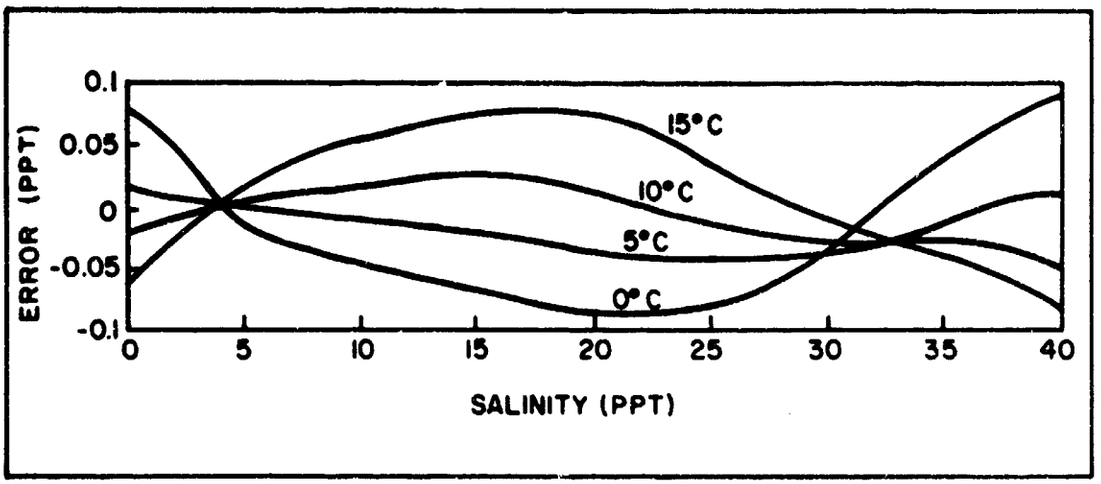

Figure 5. Typical calibration curves for in situ salinometer.

UNDERWATER SIGNAL MIXER

The underwater signal mixer is a multipurpose device which separates the dc power transmitted to the sensors from the multiplexed telemetry signal sent up the cable, and provides local regulation of dc power. It accepts audio signals from as many as six telemetry sensors, and generates a frequency-multiplexed summation signal of low impedance which is suitable for driving the sea cable. The mixer also decodes the current-level calibration signal that is transmitted down the line, and provides the signals to the individual sensors that steps them through the "confidence" checks.

TIDE COMPENSATING WINCH

The automatic winch shown in Figure 3 consists of a main cable drum, two guide line drums, two tidal compensators, and a dc motor with a reversible worm gear reduction drive and controller. The winch is mounted on a welded steel frame equipped with skids for ease of movement and firm attachment to the barge deck. The main cable supports the profiling sensor package which is guided by two stainless steel guide lines that are fixed between the surface and the relatively

shallow bottom. The main cable drum holds 100 meters of 9/16 inch neoprene jacketed, armored cable. The running end of the cable is fitted with a mechanical termination and electrical connector that mates with the underwater sensor package. The fixed end of the cable terminates under the surface of the drum and connects electrically to slip rings at the end of the hollow shaft.

During normal operation, commands from the data handling subsystem control the direction of drum movement. These signals are derived from the depth output of the pressure (depth) sensor. As a precautionary back-up, limit switches are installed on the face of the drum periphery. These switches are actuated by the weight of the cable as it winds and unwinds from the drum. These switches provide an automatic stop should the sensor package come either too close to the surface or too close to the bottom.

The tidal compensator is a constant torque device driven by a steel ribbon spring that operates between a storage drum and a driven drum. During installation, the anchoring clumps on the guide lines are lowered until they rest on the ocean floor. Slack in the guide lines is taken up manually. The compensator is wound until a dial-type tide indicator installed on it corresponds to actual tide condition. The compensator is then engaged to a gear in the guide line drum, and a tension of approximately 150 pounds is applied to the guide lines. As the tide raises and lowers the barge, the guide line drum winds and unwinds under the constant tension provided by the compensator.

The winch is normally operated by automatic commands from the data handling subsystem. However, a manual control panel (Figure 6) provides necessary control during installation and checkout, and for manual operation when desired. A mode selector switch permits the operator to select either manual control (from the local control panel) or automatic control (from the data handling subsystem). A START-STOP switch offers immediate control over the entire system in either the manual or automatic mode. In manual mode, the operator may actuate an UP or DOWN switch to change

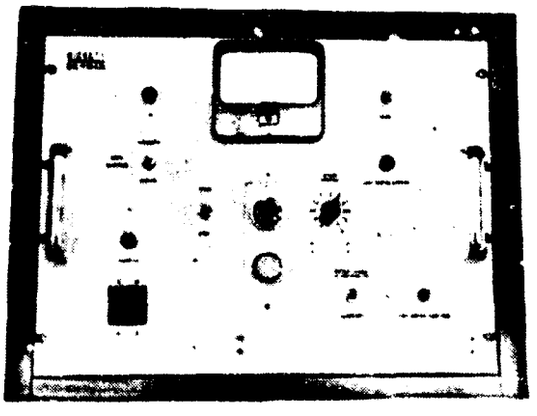

Figure 6. Winch control panel.

the state of several signal switching relays which in turn change the direction of movement of the main drum. In the automatic mode this signal relay switching function is controlled from the data handling subsystem. Winch speed is set manually by speed control regardless of the operating mode. This control establishes a reference voltage that is a direct analog of the required motor speed (which is variable from zero to approximately 10 feet per minute). If either limit switch on the drum periphery is closed, a warning light and an alarm are actuated at the control panel; a limit switch override must then be closed to enable further winch operations.

DATA HANDLING AND RECORDING EQUIPMENT

The barge-mounted electronics consist primarily of power distribution and signal conditioning circuitry, control and logic, a time code generator and system clock, a frequency counter, a system control panel, a magnetic tape recorder, and a digital printer. These equipments are housed in the two single bay cabinets shown in Figure 4. Overall dimensions of a single bay, including lifting eyes and casters, are 24 inches wide by 25 inches deep by 77 inches high.

Complete system operation may be controlled from the system control panel except for those few winch controls previously mentioned. Table 2 lists all control panel controls and indicators and their functions.

The primary storage media for data in the system is the magnetic tape recorder. All data are recorded in IBM 729 Mod II format as shown in Figure 7. A quick-look capability is provided by means of the manual switch which enables real-time printout of heading and sensor information on the digital printer.

SYSTEM OPERATION

The system is configured for fully automatic operation. This means that once the complete system is installed each sensor is scanned once each minute and the data are recorded on magnetic tape. In addition, total excursion of the profiling sensor package is automatically controlled, i.e., the winch reverses when the package reaches a prescribed depth when traveling downward and reverses again near the surface at a prescribed setting when traveling upward. Calibration data (confidence check) are recorded automatically every six hours.

Optional controls allow the operator to step from one sensor to another, to step through a calibration cycle, and to printout information on the digital printer.

CONTROL OR INDICATOR	SETTING OR INDICATION	FUNCTION	CONTROL OR INDICATOR	SETTING OR INDICATION	FUNCTION
STATION NUMBER, thumbwheel switch	0-9	Selects STATION NUMBER heading	A1, Light	SENSOR SELECTED, SENSOR PACKAGE	Light illuminates when sensor package 1 is selected for data recording
	TIME				
YEAR, two thumbwheel switches	0-9 0-9	Select YEAR heading information	A2, Light		Light illuminates when sensor package 2 is selected for data recording
DAY, three thumbwheel switches	0-3 0-9 0-9	Selects DAY information to set the System Clock	A3, Light		Light illuminates when sensor package 3 is selected for data recording
HOUR, two thumbwheel switches	0-2 0-9	Selects HOUR information to set the System Clock	A4, Light System A only		Light illuminates when sensor package 4 is selected for data recording
MINUTE, two thumbwheel switches	0-5 0-9	Selects MINUTE information to set the System Clock		SENSOR SELECTED, __ SENSOR __	
SECOND, two thumbwheel switches	0-5 0-9	Selects SECOND information to set the System Clock	Depth, Light		Light illuminates when the depth sensor is selected for data recording
SET TIME, momentary switch and light	SET TIME	Resets System Clock to zero and enters new time from control panel thumbwheel switches	Current Speed, light		Light illuminates when the current speed sensor is selected for data recording
	OPERATING MODE		Current Direction, light		Light illuminates when the current direction sensor is selected for data recording
Mode Selector, three position rotary switch	NORMAL TAPE ON	Puts subsystem in normal running mode and selects magnetic tape recording	Salinity, light		Light illuminates when the salinometer is selected for data recording
	NORMAL TAPE OFF	Puts subsystem in normal running mode and inhibits magnetic tape recording	Temperature, light		Light illuminates when the temperature sensor is selected for data recording
	MANUAL	Puts subsystem in manual mode and inhibits magnetic tape recording		TIME	
			DAY, three Binary Readouts	0-3 0-9 0-9	Displays Day of the Year as stored in the System Clock
MASTER RESET Momentary switch and light	MASTER RESET	Resets all logic except the System Clock			
NORMAL SCAN momentary switches and lights	START	When depressed allows automatic start of a scan cycle. Illuminates when depressed and remains illuminated until STOP switch is depressed.	HOUR, two Binary Readouts	0-2 0-9	Displays Hour of the Day as stored in the System Clock
	STOP	When depressed causes subsystem to stop at the following completed scan. Illuminates when depressed and remains illuminated until the START switch is depressed.	MINUTE, two Binary Readouts	0-5 0-9	Displays Minute of the Hour as stored in the System Clock
	MANUAL				
STEP, momentary switch and light	STEP	Operative only in MANUAL operating mode. When depressed will cause the subsystem to advance and if the sensor is selected, to print heading data or sensor data	RECORD, two Binary Readouts	0-5 0-9	Displays Second of the Minute as stored in the System Clock
CALIBRATE, momentary switch and light	CALIBRATE	Operative only in MANUAL operating mode. When depressed will initiate a calibrate scan cycle at the beginning of the following scan cycle. Illuminates while in the calibrate scan cycle		STUCK	
			UP light		Light illuminates when the switch is selected for travel in the UP direction
PRINTER, alternate action switch and light	ON-OFF	Selects paper tape printer ON light illuminated when printer is selected. OFF light when not selected	DOWN light		Light illuminates when the switch is selected for travel in the DOWN direction

TABLE 2. OPERATING CONTROLS AND INDICATORS.

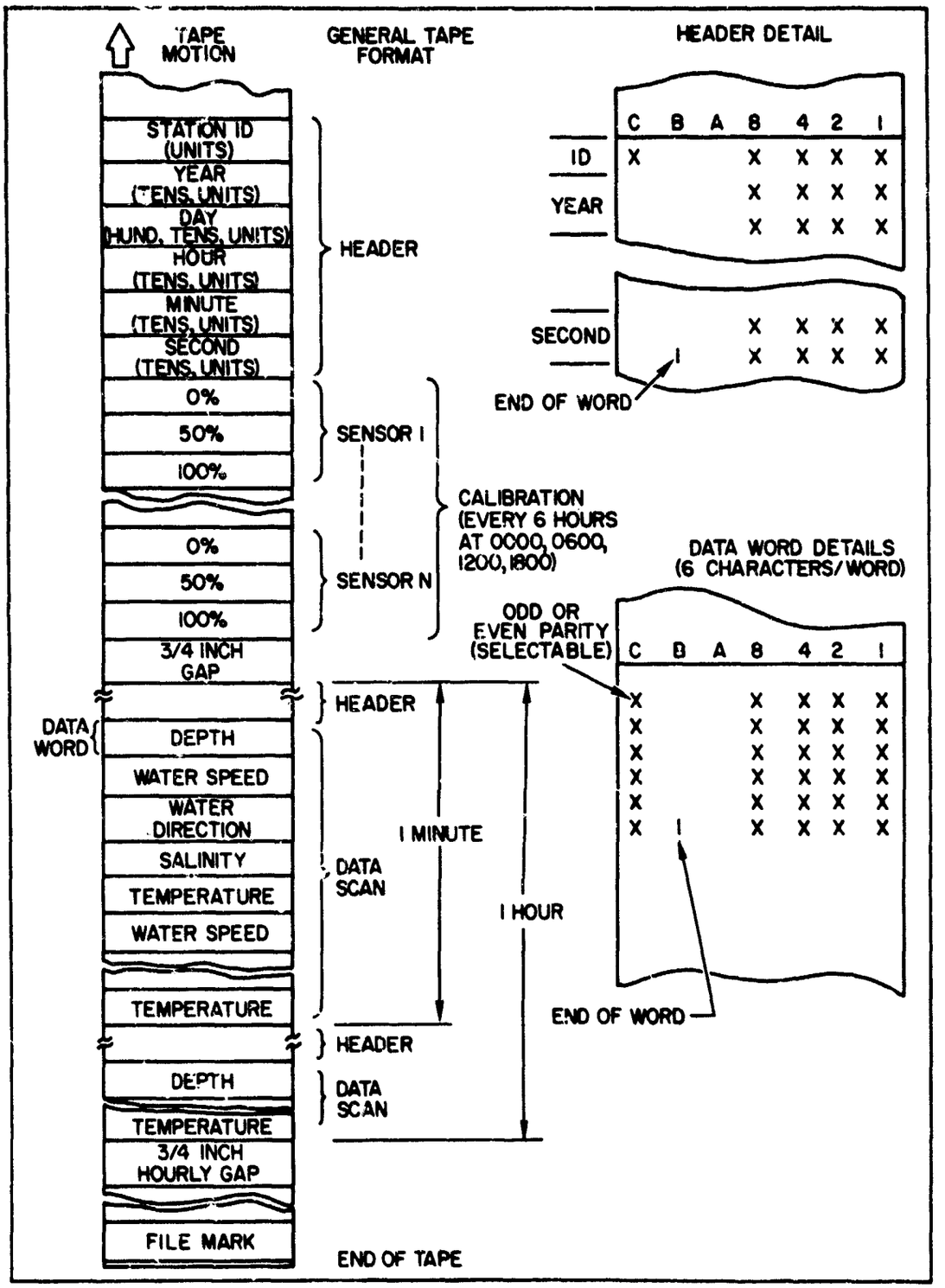

Figure 7. Magnetic tape format.

TEST RESULTS

Initial calibration and testing indicated consistent recovery of data to a greater accuracy than specified as shown below:

Temperature:	±0.01°C
Depth:	±0.10% of full-scale
Current Direction:	±2°
Current Speed:	As specified
Salinity:	±0.02 ppt over the range from 0 to 40 ppt (after corrections)

Further laboratory testing after delivery of the system has verified proper operation for a period of 4 months on a nearly continuous basis. Further testing, with implantment of the sensor packages in the Sea Ice test tank at the Navy Electronics Laboratory, is scheduled during the next few months.

SUMMARY

Operational ease, simplicity of installation, and flexibility characterize this Arctic Oceanographic Data Collection System. The complete systems approach has enabled an interaction of disciplines required to produce a truly operational system. Utilization of proven underwater sensors, electrical terminations, and oceanographic cable has strengthened reliability. In addition, minimizing the amount of underwater electronics and an adequate testing program has enhanced the probability of long-term use without failure.

ENGINEERING FIELD TEST RESULTS OF AN EXPENDABLE SOUND SPEED PROFILING DEVICE

Bernard K. Swanson
U.S.Naval Oceanographic Office, Washington,D.C. 20390
and
Raymond A. Stahl
American Bosch Arma Corporation, Tele-Dynamics Division
Philadelphia, Penna.

INTRODUCTION

In order to provide a fleet sonar ship with a real time sound speed profile, the U.S. Naval Oceanographic Office (NAVOCEANO), working with American Bosch Arma Corporation, has developed and field tested an expendable profiling device. This device, called an Aquasonde, has been in the research stages for three or four years and in the exploratory development stages during the past year. During next fiscal year it is anticipated that advanced development as well as some operational tests and evaluations will be possible. The desirability and the requirements for such a device to enhance sonar operations and improve detection capabilities have been documented elsewhere (Swanson, et al.,1965).

The logical development of such a device stems from advances in sonar design and extensions of sonar ranges in recent years. With these advances, historic environmental data have obvious limitations for providing exact solutions to operational problems. This paper will describe the field test results, instrument characteristics, and Aquasonde system adaptations for a multitude of uses.

FIELD TEST

Preliminary tests were conducted by NAVOCEANO and American Bosch Arma personnel in the Tongue of the Ocean near New Providence Island, Bahamas. The tests were made during April-May 1965 from the USS LITTLEHALES (AGSC-15) and MAS R/V LORD RAYLEIGH. Figure 1 shows the instrument package and attached battery simulator being tested for watertightness prior to a lowering, using a wire link during one of the engineering tests. A variety of configurations were tested during the survey. Figure 2 shows one of the instruments at the moment of release while underway using a sonic link. Two instruments were expended in this manner at the close of the survey. Figure 3 shows the fantail

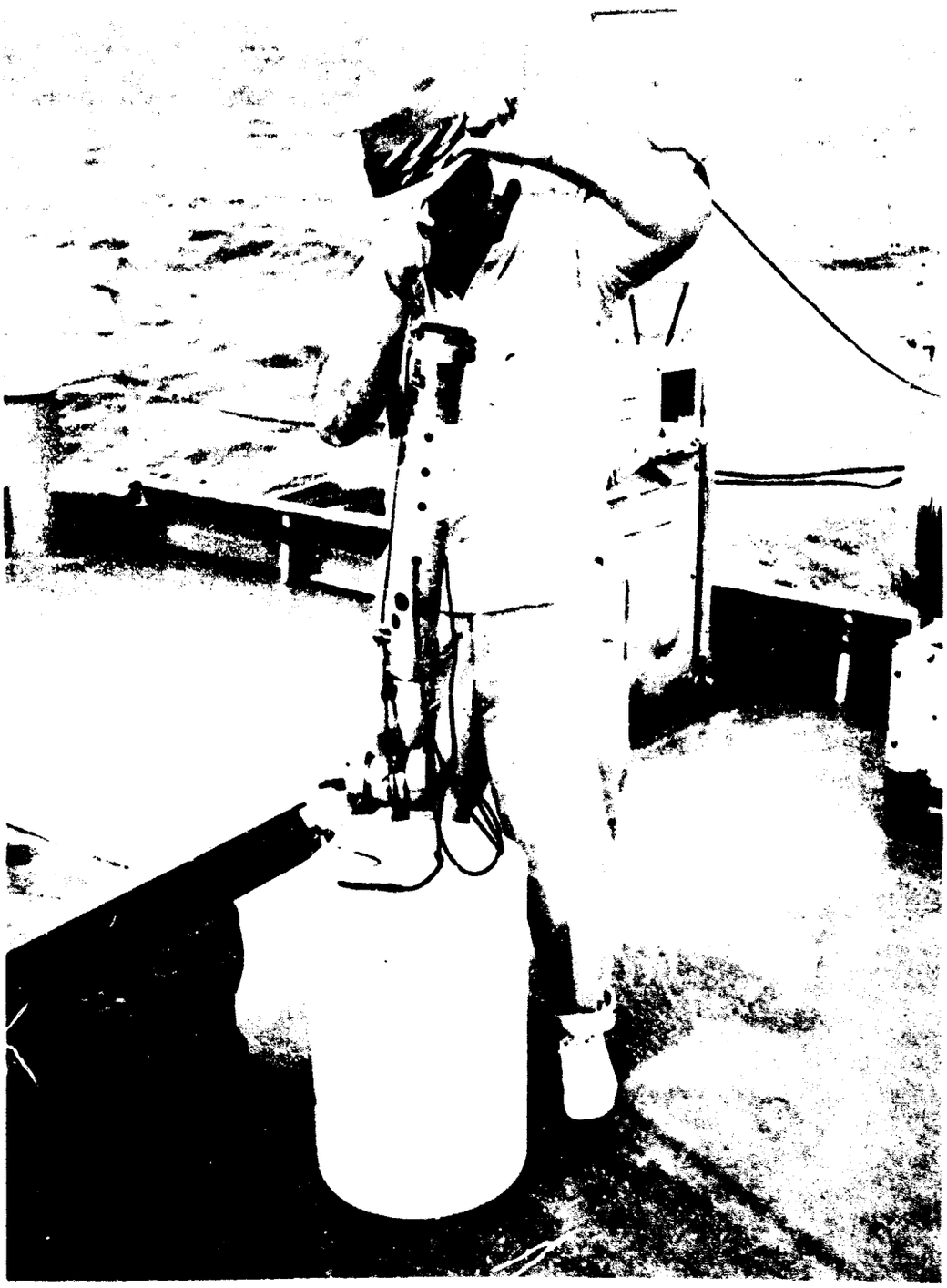

Figure 1 Aquasonde Wire Link and Battery Simulator Test Assembly

Figure 2 Underway Expendable Release of an Aquasonde

Figure 3 The Towed Hydrophone System

arrangement on the USS LITTLEHALES (AGSC-15) of the towed hydrophone system. Progress has been made to adapt the present echo-sounding transducer to serve the dual function of receiving soundings from both 12 kc for depths and 21 kc for sound speed profiles.

Briefly, the field test instrumentation consisted of a towed hydrophone system, analog recording instrumentation, and oceanographic winches for the various instrument test lowerings. Both sonic and wire links were tested in an assortment of lowerings, i.e., at the end of the oceanographic wire, tethered sliding down the oceanographic wire, and expendable free fall. Some tests were made while the ship was on station, and others while underway. The 2-ship operations simulated a high speed destroyer obtaining expendable operational data, but permitted recovery of the test instrument. The above tests provided the necessary data and controls for systematic analysis for engineering improvements and final design configuration.

The five Aquasondes used in the tests were developmental models and differed from true expendables in that they could be recovered, analyzed, and reused. This permitted disassembly, repair, and modification during the tests as results dictated.

An oversize sea battery provided extended operating life necessary for the winch lowerings and on the 2-ship operation. A battery simulator was used on many tests early in the program to conserve the rather costly supply of sea water activated silver chloride batteries.

Analysis of the field test to date show that:

1. The sonic communication link in the ocean is not only feasible but also appears to be reliable.

2. The instrument functioned during free fall to depths of 8400 feet and to slant ranges in excess of two miles.

3. Errors in the instrument, hydrophone, and receiving system can be eliminated or compensated without major re-engineering problems.

4. The expendable must incorporate a reference signal to compensate for errors in the long sonic path.

5. The expendable must contain a discrete time-depth measurement such as a pressure switch.

6. The device should incorporate a turn-off switch after reaching the bottom or a desired depth.

7. The receiving system can be materially improved, thereby improving the quality of the data.

DATA ANALYSIS

Standard oceanographic Nansen cast stations were occupied during the field tests. These data were compared to historical Nansen cast data in nearby areas and found to be in close agreement. These data were then converted to sound speeds, and smoothed profiles were drawn for comparison with the corrected Aquasonde data. Although this comparison is still in progress, the results to date show close tracking of the profiles even though several of the comparisons were made with data separated by several days in time. The most synoptic data available are separated by 24 hours and show departures of as much as 5 feet per second at several intervals to depths of 2300 feet, a fairly constant and systematic departure of about 10 feet per second from 2300 feet to 3500 feet, and then close tracking to 5000 feet. In most instances, the Nansen cast data displayed sound speed values lower than the Aquasonde data. Comparison of the tethered Aquasonde profiles only, show much better agreement among the profiles; however, comparing tethered lowerings to wire lowerings, both using the sonic link the departures are as much as 40 feet per second. No explanation is offered for this departure at this time; however, the data were taken four days apart and in different areas. The four wire lowerings were made within an 8-hour period in the same area and tracked almost perfectly. Maximum variations of only about 3 feet per second were found.

Although all of the systematic errors and noise have not been eliminated from the Aquasonde records, random variations in the profiles indictative of microstructure have been noted. After some smoothing and averaging to eliminate minute microvariations, there remained variations in the sound speed profile of between 2 to 8 feet per second in depth intervals of 10 to 20 feet. Further smoothing of one profile between 2100 and 2200 feet resulted in variations of about 5 feet per second in this depth interval. Variations of this magnitude have been reported previously by other workers (Piip, 1964). In particular, variations at these depths are in accord with profiles taken within 750 miles of the Aquasonde data by Piip using back-to-back sound velocimeters and pressure depth sensors.

THE OPERATIONAL SYSTEM

The historical development and description of the present Aquasonde has been reported previously (Stahl & Miller, 1965). The advantages of obtaining accurate sound speed profiles to great depths without interrupting ship routines and in rough weather without personnel hazards are attractive from a cost effectiveness standpoint provided the expendable instrument cost can be made low enough. For oceanographic research or on surveys, a moderately-sized vessel can acquire manyfold more profiles covering a larger area and in a timely and economic manner. Although the fleet operational units have problems that differ from the oceanographer's, past experience has shown that the fleet is quick to adopt oceanographic hardware if it has immediate application, even though incomplete solutions may result. The development of the Aquasonde is continuing in an orderly but unhurried pace to meet oceanographic needs, but in the process the design is such that only the processing and recording subsystems need be altered to obtain advancement in operational capability. The expendable instrumentation remains unchanged in either instance.

The Aquasonde is designed to fall at a constant rate of about 20 ft/sec through the water column. The unit comes complete with an integral rapid activated silver-chloride sea water battery and calibration data. Real-time data are relayed via a sonic link on a 21 kc signal. Sound speed is measured using the accepted sing-around technique. A stable audio reference signal is multiplexed with the carrier signal to accommodate errors due to fall rate, sonic path variations, or ship speed variations. An accurate and repeatable pressure switch closure at a predetermined and calibrated depth provides a final check on depth as the profile is formed. Sound speed data are taken at a rate of over 20,000 samples per second. Table 1 lists some of the important characteristics of the sensor.

The receiving system can be modified readily to suit user needs. Essentially the receivers are portable, modular, easily powered by available ship power, and consist mostly of commercially available shelf items integrated into a functional system. Briefly, the basic receiving system consists of a hydrophone, amplifiers, filters, AM demodulator, digital circuits including a card reader, a digital tape recorder and an analog display. This design is based upon results of the field tests. Each Aquasonde has a calibrated card which is fed to the system to correct for errors inherent in any assembly line product. Local information such as position, time, ship speed, etc. are entered manually. Thus, from the drop signal to the end of the profile, the system receives, demodulates, normalizes format, and records data in real time digital tape with a quick look analog trace. Investigations are now underway to provide a

TABLE 1 AQUASONDE CHARACTERISTICS

Accuracy of Sound Speed Measurement:	5 ft/sec*
Resolution of Sound Speed Measurement:	1 ft/sec
Center Frequency of Sonar Data Link:	21 kc ± 5%, Frequency Modulated by Sound Speed Value
Reference Frequency:	730 cps Amplitude Modulating the Sonar Frequency
Reference Accuracy:	100 ppm*
Reliable Operating Depth:	6,000 ft
Crush Depth:	12,000 ft
Depth Switch Accuracy:	1%*
Switch Operate Depth:	About 2,500 ft*
Size:	3" Dia X 16" Long with a Separately Attached 5 "Dia X 1" Fin
Activation Time:	1 Second
Sonic Output Level:	About +88db

*When corrected with individual punched card data furnished.

hull-mounted hydrophone to replace the towed assembly used in the field tests. To date, it appears feasible to modify the present standard echo-sounder transducer such that both depth and sound speed signals can be accepted, and that these modifications can be made at dockside.

A simplified version of the shipboard receiving system could be assembled by eliminating the digital components and instead provide only an analog display. A more complex system than the basic system could be assembled such that it would process the digital tapes through an on-board computer to a display of sound intensity and detection probabilities for specific sonars. This system would be essentially automatic from start to finish, and would entail considerable initial expense unless coordinated with planned computer capabilities aboard ships. Telemetering of data to shore stations for processing would be an alternative for any of the above methods.

There are many possible adaptations of the Aquasonde for either oceanographic or operational applications. Some of these are shown in Table 2. The majority of these applications are available with a minimum of alteration to the basic system. For example, the teflon slip ring used in the tethered tests proved so successful that with slight changes could

TABLE 2 POSSIBLE ADAPTATIONS OF AQUASONDE

1. On Station - Retrievable
   a. Sonic Link - Tethered Drop on Ocean Wire, Core Cable, Camera Cable, etc.
      - Time-Series Data
      - Pop-Up System
   b. Wire Link - Submarine Hull-Mounted: Real Time Data on Command
      - Submarine: Float to Surface or Lowered
      - Ship: Time-Series Data
2. On Station - Expendable
   a. Sonic Link - Ship or Submarine: Areal Sound Speed Profile Data
      - Ship or Submarine: Time-Series Data
3. Underway - Retrievable
   a. Sonic Link - Submarine or Ship: Ocean Wire Lowering for Profile
      - Ocean Wire Lowering and Towed for Continuous Data
   b. Wire Link - Same as Above
4. Underway - Expendable
   a. Sonic Link - Submarine or Ship: Operational Real-Time Data
5. Buoy Applications
   Multitude of Possible Configurations and Adaptations
6. Aircraft
   a. Sonobuoy Piggy-Back Adaptations

be adapted for use in conjunction with cable supported core samples, underwater cameras, or other lowered devices. The 3" diameter of the Aquasonde fits both submarine flare tubes as well as aircraft "E" size sonobuoys. Wire link for submarine use may be preferred for quiet situations. Buoyed systems often unintentially become expendable systems, so incorporation of the Aquasonde for time-series data becomes especially attractive.

SUMMARY

The results of the field test on the Aquasonde have provided insight into engineering improvements in design and data flow. Although preliminary analysis of the data obtained are encouraging, it is anticipated that test results of the next generation system will be even more favorable. Especially important is the essentially "hands off" feature of the entire data acquisition procedure which drastically effects cost effectiveness considerations. The versatility and adaptability of the system to various oceanographic and operational requirements is considered worthy of special note.

BIBLIOGRAPHY

Piip, A. T. A Survey of the Sound Velocity - Depth Structure Around the Sound Channel in the Bermuda-Barbados Area (U). First U.S. Navy Symposium on Military Oceanography, Vol. II, p.197, June 1964. CONFIDENTIAL

Stahl, R. S. Properties of a 22KHz FM Sonar Telemeter. Paper presented at 1966 National Telemetering Conference, May 1966.

--- and Miller, R. S. The Aquasonde. Proceedings of the Third National Marine Sciences Symposium, Vol. III, Marine Sciences Instrumentation, Instrument Society of America, April 1965.

Swanson, B. K., Atkocius, D.A., and Fenner, D. F. A System Concept for Rapid Retrieval and Display of Static and Dynamic Environmental So. r Information (U). Paper presented at 23rd U.S. Navy Symposium on Underwater Acoustics, December 1965. CONFIDENTIAL

SEDIMENT SOUND SPEED MEASUREMENTS USING A PULSE TECHNIQUE

Robert S. Winokur
U. S. Naval Oceanographic Office
Washington, D. C. 20390

INTRODUCTION

Since September 1964 the U. S. Naval Oceanographic Office has been using a pulse technique to measure sound speed in cored ocean bottom sediments. As the pulse method is the most favored technique for making sediment sound speed measurements and has been successfully used by Paterson (1956), Laughton (1957), Sutton et al. (1957), Abernethy (1965), and many others, it is the purpose of this paper to only describe the pulse equipment and technique presently being utilized at the Oceanographic Office and to present a limited amount of sediment sound speed data.

The pulse equipment, referred to as a sediment velocimeter, described in this paper was developed by the Oceanographic Office as part of a program to investigate the acoustic properties of the ocean bottom. The system was designed and fabricated under contract by Underwater Systems, Inc. The sediment velocimeter has been successfully used, both in the laboratory and aboard ship, to measure sediment sound speeds of cores collected from the North Atlantic Ocean, Pacific Ocean, Gulf of Mexico, and Caribbean Sea. The results of these measurements and statistical studies relating the acoustic and physical properties of the sediments will be the subject of future reports now in preparation.

GENERAL CONSIDERATIONS AND EQUIPMENT

The pulse method involves measuring the travel time of a transmitted wave over a known path length. The technique employed with the sediment velocimeter is similar to the method used by Laughton, but differs from direct measurements of travel time, in that sediment sound speed is determined by comparing the travel time through a sediment sample to the travel time through a reference sample having a known sound speed. Distilled water is usually used as the reference and the sound speed determined from Wilson (1959). The comparison method eliminates the need for absolute measurements of transit time.

The sediment velocimeter was designed to be a compact portable system capable of making sound speed measurements on a saturated core, with minimum disturbance to the core. These objectives are accomplished by making the measurements immediately after a core comes aboard ship and by means of a specially constructed tank, illustrated in Fig. 1, equipped

with portholes and calibrated transducer positioning rods. These features permit sound speed measurements to be made across the diameter of the core, without cutting or extruding the core, or through the length of a core sample contained in the core liner, but cut from the overall length of the core. By making measurements across the diameter, it is possible to make continuous measurements along a core as the core is moved through the tank via the portholes. The only limitation on core length is ease of handling. Operational experience has shown that 10 feet is a practical limit and sound speed measurements are routinely made at 10 cm intervals along the length of the core.

Since measurements made across the diameter permit a long core to be handled with minimum distrubance or cutting, this mode of operation is preferred; however, for extremely short cores or for special laboratory studies sound speed measurements can be made through the length of the sediment sample. For this measurement, the tank can accomodate samples varying in length between 1 and 10 inches.

The sediment velocimeter is illustrated in a block diagram in Fig. 2. Barium titanate transducers are excited to emit ultrasonic pulses in the compressional mode. A General Radio 1217 B pulse generator, followed by an Underwater Systems, Inc. pulse amplifier, is used to excite the transmitting crystals at their natural resonant frequency of 400 kilocycles per second. A 250 volt pulse of .5 microseconds duration is used to obtain the sonic ring. The transmitted pulse is also used to trigger the sweep of a dual trace oscilloscope. The signals are simultaneously transmitted through the sediment and reference samples and detected on crystals identical to those used for transmission. The received signals are amplified by Scott 140 B decade amplifiers and then displayed on a Tektronix 535 A dual trace oscilloscope.

SOUND SPEED MEASUREMENT ACROSS THE DIAMETER OF THE CORE

Sediment sound speed, measured across the diameter of the core, is determined by measuring the difference between the transmission time through the core sample and the transmission time through the reference sample. The core is inserted into the tank via the portholes located on the sides of the tank, as illustrated in Fig. 3. The sample tank is then filled with distilled water, which acts as an acoustic coupling medium between the transducers and the core. The transmitting and receiving crystals, in both the core and reference tanks, are set at identical separations and an empty core liner is placed on v-blocks in the reference tank. The empty core liner is used to compensate for the contribution of the liner, surrounding the sediment sample, to the measured sound speed, so that the only difference between the tanks is the presence of the sediment itself. The transducers do not have to be in contact with the sediment sample and the transducer separation is not readjusted until the measurements on the entire core are completed. Both the sample and

reference signals are displayed on the oscilloscope and the oscilloscope time delay is adjusted so that the difference in travel time between the signals can be determined. The difference in travel time then corresponds to sediment sound speed as follows

$$C_S = \frac{C_W}{1 - \frac{C_W (T_W - T_S)}{d}} , \qquad (1)$$

where:

C_S = sediment sound speed,
C_W = sound speed of reference sample (distilled water),
T_W = transit time through reference sample, including empty core liner, and electronic delay time,
T_S = transit time through sediment sample, water couple, core lin r, and electronic delay time, and
d = inside diameter of core liner.

MEASUREMENT OF SOUND SPEED THROUGH THE LENGTH OF SAMPLE

Sound speed measured along the longitudinal axis or length of a sediment sample is determined by comparing the length of the sample with the length of a column of distilled water for which the transmission times are equal. The measurement is made with the entire sample immersed in water or by placing a small amount of water between the sediment and the transducers to insure proper contact. There is usually no need to seal the bottom of the sample; however, should the sediment run out of the liner or should the sample start to lose water, the bottom of the liner is sealed. A temporary seal may be used until the sample is properly positioned. Once positioned, the seal (plastic disc) can be removed or, if a permanent cap is used, a duplicate cap is placed in the reference tank to compensate for its effect. The length of the distilled water column is adjusted until the reference signal, displayed on the oscilloscope, can be superimposed on the received signal transmitted through the sediment sample. The lengths of the sediment sample and the reference water column are determined by the positioning rods which are calibrated to ± 0.001 inch.

Thus, knowing the length of the sediment sample, the length of an equivalent distilled water column, and the speed of sound of the distilled water, the sediment sound speed is determined by using the following equation

$$C_S = C_W \frac{d_S}{d_W} , \qquad (2)$$

where:

C_S = sediment sound speed,
C_W = speed of sound of reference sample (distilled water),

d_s = measured length of sediment sample, and
d_w = measured length of reference sample.

MEASUREMENT ACCURACY

The overall estimated accuracy for the measurement made across the diameter of the core depends on: 1) the accuracy to which C_w is known, 2) the accuracy in measuring $(T_w - T_s)$, 3) the accuracy in measuring the diameter of the core liner, 4) the oscilloscope incremental time delay error, and 5) the difference in electronic delays between the two circuits.

The estimated total error is determined by taking the square root of the sum of the squares of the individual errors. While it is difficult to assess the individual errors, the following factors must be considered: 1) C_w is known from Wilson's tables and is subject to error in determining the reference temperature and possible contamination of the distilled water, 2) the travel time difference $(T_w - T_s)$ can be measured with a maximum error of 0.02 microseconds, 3) the inside diameter of the core liner can be measured to $\pm$ 0.001 inch, although some errors may result from possible variations in the thickness of the core liner, 4) maximum oscilloscope incremental time delay error of 0.4%, and 5) negligible difference in electronic delays between both circuits in comparison to the travel time through the sediment. Considering these factors the overall estimated accuracy is about $\pm$ 0.5%.

The total estimated error for the sound speed measurement made through the length of a sediment sample is dependent on: 1) the accuracy to which d_s and d_w are measured, 2) the proper alignment of the received signals, 3) the difference in electronic delays between the two circuits, and 4) the accuracy to which C_w is known. It can be seen that time is missing from equation (2) and, consequently, length is the only accurate physical measurement that must be made.

The following factors must be considered in determining the overall accuracy: 1) both d_s and d_w are measured to $\pm$ 0.001 inch; however, some degradation of this accuracy may result from compaction in the upper surface of the sediment sample in contact with the positioning rod, 2) improper alignment of the superimposed signals may result in an error in d_w of $\pm$ 0.001 inch, 3) and 4) the errors in C_w and electronic delay as previously mentioned. Although it is again difficult to assess the exact error in each case, as the magnitude of the errors depends on sound speed and sample size, the total estimated error is about $\pm$ 0.2%. The greater accuracy for this method is to be expected since the incremental time delay of the oscilloscope is not required for measurements of travel time.

To verify the aforementioned accuracies, sound speed measurements were made on four primary alcohols for which the speed of sound had been accurately measured by Wilson (1964). These measurements verified the stated accuracies and have shown the feasibility of applying correction factors to the measurements, which should yield an overall accuracy of about ± 0.1%.

RESULTS OF SEDIMENT SOUND SPEED MEASUREMENTS

As previously mentioned, measurements of sediment sound speed have been made on cores collected from a variety of locations; however, only the results of measurements made on a 13 foot core from a depth of about 2400 fathoms in the western Yucatan Basin (19°38'N, 86°01'W) will be reported on in this paper. The measurements were made across the diameter of the core at intervals of 10 cm. As shown by Hamilton (1963) the measured sound speeds were corrected to estimated in situ values by applying corrections for differences in temperature and pressure between measurement conditions and in situ conditions. Wilson's tables for the speed of sound in sea water were used to make these corrections. Corrected laboratory (in situ) sediment sound speed versus depth is illustrated in Fig. 4. The sound speed of the water just above the bottom was computed by utilizing temperature and salinity data collected at the core location and by using Wilson's equation. Except at depths of 90, 290, and 350 - 390 cm the sediment sound speed is less than that of the bottom water. The low-velocity nature of the ocean bottom has been established by Katz (1956), Hamilton (1956), Shumway (1960), Fry and Raitt (1961), and others and is, consequently, not surprising.

SEDIMENT SOUND SPEED AND RELATED PHYSICAL PROPERTIES

The relationship between sound speed and porosity is illustrated in Fig. 5. Shumway's porosity-sound speed relationship is included for comparison and has been corrected to in situ. In general, Shumway's curve forms the lower limit to the measured data and there is a grouping of data that falls within ± 10 m/sec of Shumway's curve. It can also be observed that when the measured sound speed exceeds about 1523 m/sec, Shumway's curve does not agree with the measured data; however, it generally appears that these points form a curve which parallels Shumway's, but is shifted towards higher sound speed. This difference may be due to the interdependence between various variables, such as porosity, grain size, and carbonate content. Sutton et al. determined a multiple linear regression equation relating sound speed to phi median grain diameter, carbonate content, and porosity:

$$C_s = 2.093 - .0414\phi + .00135\gamma - .44\eta, \qquad (3)$$

where:

C_s = sediment sound speed,
ϕ = phi median grain diameter,
γ = carbonate content, and
η = porosity.

Fig. 6 is a composite of sound speed, porosity, phi mean grain diameter, and carbonate content versus depth below the top of the core. It can be seen that for the 40 cm thick layer at the bottom of the core the increase in sound speed is associated with a decrease in porosity, an increase in grain size, and an increase in carbonate content. This behavior is expected from equation (3); however, at 130 cm, for example, the decrease in carbonate content and grain diameter are associated with an increase in sound speed, which is not predicted from the Sutton et al. equation. As a third example, consider the increase in sound speed at 290 cm. At this depth, there is a significant increase in grain diameter and decrease in carbonate content and it appears that the sound speed is controlled by grain diameter. Again, this is in general agreement with equation (3), as it can be seen that sound speed is more sensitive to changes in grain diameter than to changes in carbonate content.

It is beyond the scope of this paper to determine exact interrelationships between the variables illustrated in Fig. 6, but it appears that, for this set of data, porosity alone cannot explain the measured sound speed values. It would seem that a multiple linear regression equation, similar to equation (3), would be more useful than a relationship utilizing a single variable. As has been pointed out by various investigators, an ocean-wide sediment sound speed-physical properties relationship probably does not exist and it is not surprising that sound speed data from the Yucatan Basin in the Caribbean Sea do not agree exactly with relationships derived from data from mainly the continental shelf off the West Coast of the United States (Shumway) or data mainly from the eastern Atlantic Ocean (Sutton et al.).

Fig. 7 is a composite of sound speed, cohesion, and modulus of elasticity versus depth. Cohesion represents shearing strength per unit area under zero externally applied load and is directly proportional to compressive strength or the load per unit area required to shear an unconfined, natural, or remolded sediment mass. The modulus of elasticity is the ratio of stress to strain under given loading conditions and is numerically equal to the slope of the tangent of a stress-strain curve. In general, an increase in cohesion or shear strength and modulus of elasticity reflects an increase in sound speed; however, the exact relationship is not immediately obvious. It can be seen that for a similar increase in sound speed, as occurs at 90 and 290 cm, there is a considerable difference between the respective values of cohesion and elasticity.

The Shumway sound speed-porosity curve illustrated in Fig. 5 is, in fact, a plot of Shumway's equation (7) (1960), which relates sediment sound speed to rigidity, porosity, and density. As mentioned, an increase in sound speed is usually accompanied by an increase in elasticity; however, the modulus of elasticity is extremely variable and does not appear to be as reliable an indicator as cohesion. In addition, for those measured sound speed values that did not agree with the Shumway sound speed-porosity curve (Fig. 5) it can be observed that there is a measurable increase in cohesion. It can be inferred that an equation similar to Shumway's, relating sound speed to porosity and cohesion or shear strength, would be an effective indicator of sediment sound speed.

ANOMALOUS RESULTS

While general relationships between sound speed and physical properties exist for the limited data presented, one notable exception is obvious. That is, at 30 cm there are significant increases in cohesion, elasticity, grain size, and a decrease in porosity, but there is only a very slight increase in sound speed. The sediment at this depth is a very fine to fine-grained calcareous sand. Since the sound speed measurements were repeated to insure repeatability in the measurement technique, it can be assumed that there is no error in the measurement. While the lithology and physical properties indicate that there should be an increase in sound speed, there is no apparent reason for this exception, particularly in view of the fact that the 350 - 390 cm high-velocity layer is similarly a fine-grained calcareous sand. It should also be noted that the increase in grain diameter at 50 cm is due to the presence of a layer of shells (coquina) that does not have the rigidity of the fine-grained sand layers in the core. The lack of change in sound speed for this coarse-grained material has been observed by the author while making other measurements on cores containing significant amounts of coquina.

SEISMIC DETERMINATION OF SURFACE SEDIMENT SOUND SPEED

Seismic reflection data records collected at a location about 30 miles from the core reveal a phase reversal or change in the direction of first motion of the bottom reflected signal with respect to the incident signal. The observed phase reversal, which is theoretically predicted for low-velocity sediments at the angle of intromission, permits the in situ surface sediment sound speed to be computed. The angle of incidence which is equal to the angle of intromission is given by Rayleigh (1945) to be

$$\cot^2 \theta_I = \frac{(C_w/C_b)^2 - 1}{(\rho_b/\rho_w)^2 - (C_w/C_b)^2}, \qquad (4)$$

where:

C_w, ρ_w - the sound speed and density, respectively, in the water, and

C_b, ρ_b = the sound speed and density, respectively, in the bottom.

Using temperature and salinity data collected at the seismic station to compute the sound speed of the bottom water, the laboratory measured sediment density, and the observed angle of intromission, the calculated in situ sound speed is 1502 m/sec. This value is about 11 m/sec less than the in situ corrected laboratory measurement at 20 cm; however, considering that the seismic station and the core location do not coincide, the overall agreement appears to be quite good and does verify the low velocity nature of the bottom.

SUMMARY AND FUTURE EFFORTS

The U. S. Naval Oceanographic Office, as part of a continuing program to investigate the acoustic and physical properties of the ocean floor, is making measurements of sediment sound speed using a compact portable sediment velocimeter capable of making measurements on a saturated core with a minimum amount of disturbance to the core. It is planned to expand the measurement program by utilizing the variety of cores collected as part of various oceanographic programs in progress at the Office. These data will be used to seek sediment sound speed-physical property relationships for various geological and physiographic provinces and to expand those relationships already available. In addition, a pressure tank is being added to the velocimeter to make shear wave sound speed measurements as well as compressional wave measurements under pressure.

The limited amount of data presented in this paper does not permit definite conclusions to be made, but it is apparent that the relationships between sediment sound speed and physical properties are complex. It is obvious that while general relationships already exist, as derived by various investigators, their usefulness is limited to the environment from which the sediments came or for sediments having similar properties.

ACKNOWLEDGEMENTS

The author gratefully acknowledges the assistance of Messrs. J. Coleman, P. Beckman, D. S. Hill, and Miss L. K. Glover for performing the physical properties analyses and Mr. S. Chanesman for his assistance in preparing this paper.

REFERENCES

Abernethy, S. H., 1965, Improved equipment for a pulse method of sound velocity measurement in water, rock, and sediment, U. S. Navy Electronic Laboratory, Technical Memorandum 824.

Fry, J. C. and Raitt, R. W., 1961, Sound velocities at the surface of deep-sea sediments, Journal of Geophysical Research, vol 66, p. 589-597

Hamilton, E. L., 1956, Low sound velocities in high-porosity sediments, Journal of the Acoustical Society of America, vol 28, p. 16-19.

_____, 1963, Sediment sound velocity measurements made in situ from bathyscaph Trieste, Journal of Geophysical Research, vol 68, p. 5991-5998.

Katz, S. and Ewing, M., 1956, Seismic refraction measurements in the Atlantic Ocean, Part VII: Atlantic Ocean Basin, West of Bermuda, Bulletin of the Geological Society of America, vol 67, p. 475-510.

Laughton, A. S., 1957, Sound propagation in compacted ocean sediments, Geophysics, vol 22, p. 233-260.

Paterson, N. R., 1956, Seismic wave propagation in porous granular media, Geophysics, vol 21, p. 691-714.

Rayleigh, J. W. S., 1945, The theory of sound, vol II, reprinted, Dover, New York, 504 p.

Shumway, G., 1960, Sound speed and absorption studies of marine sediment by a resonance method, Parts I and II, Geophysics, vol 25, p. 451-467, p. 659-682.

Sutton, G. H., Berckheimer, H., and Nafe, J. E., 1957, Physical analysis of deep-sea sediments, Geophysics, vol 22, p. 779-812.

Wilson, W. D., 1959, Tables for the speed of sound in distilled water and in sea water, U. S. Naval Ordnance Laboratory, Report No. 6747.

_____, 1960, Speed of sound in sea water as a function of temperature, pressure, salinity, Journal of Acoustical Society of America, vol 32, p. 641-644.

_____, 1964, Speed of sound in four primary alcohols as a function of temperature and pressure, Journal of the Acoustical Society of America, vol 36, p. 333-337.

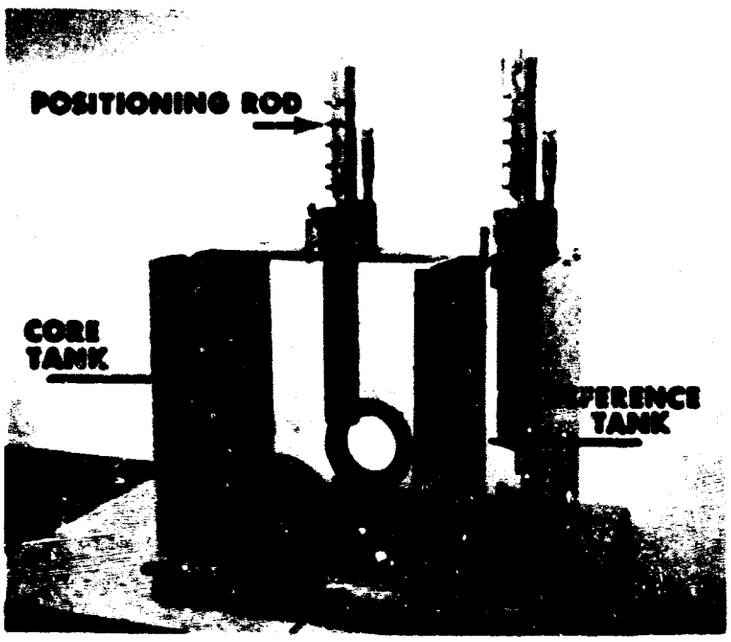

Figure 1. Sediment velocimeter tank.

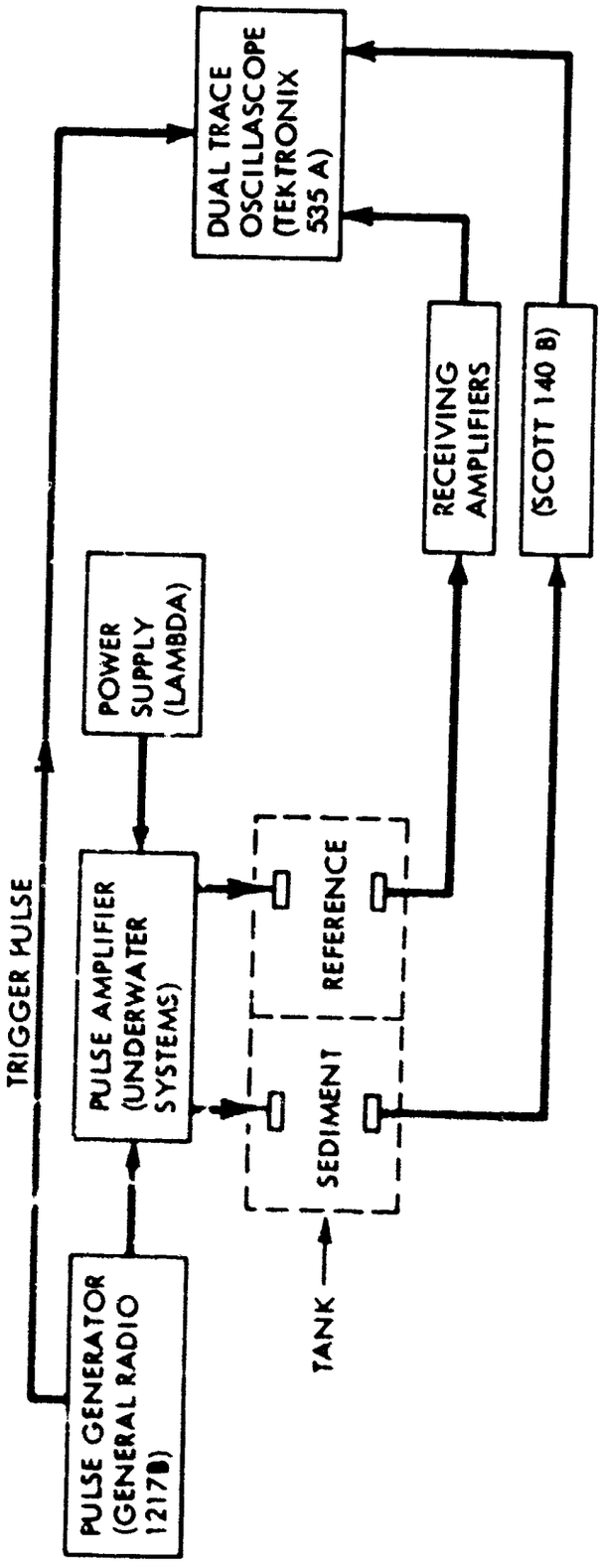

Figure 2. Block diagram of sediment velocimeter.

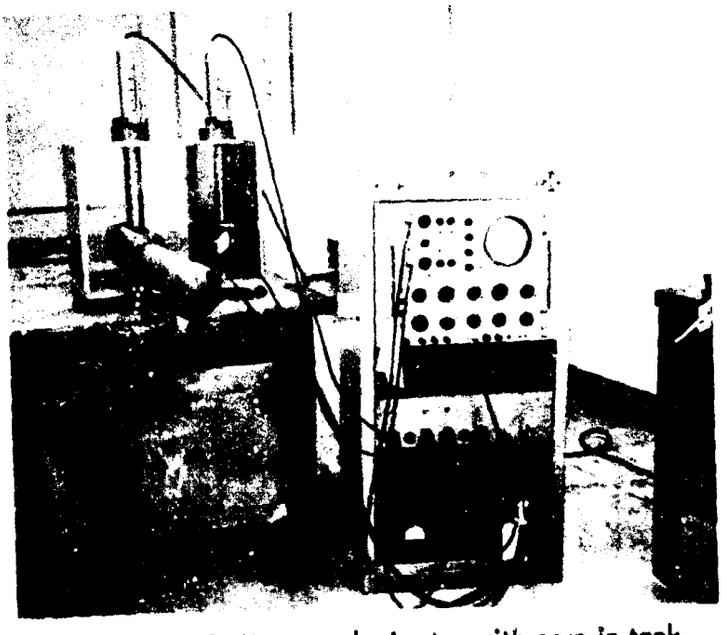

Figure 3. Sediment velocimeter with core in tank.

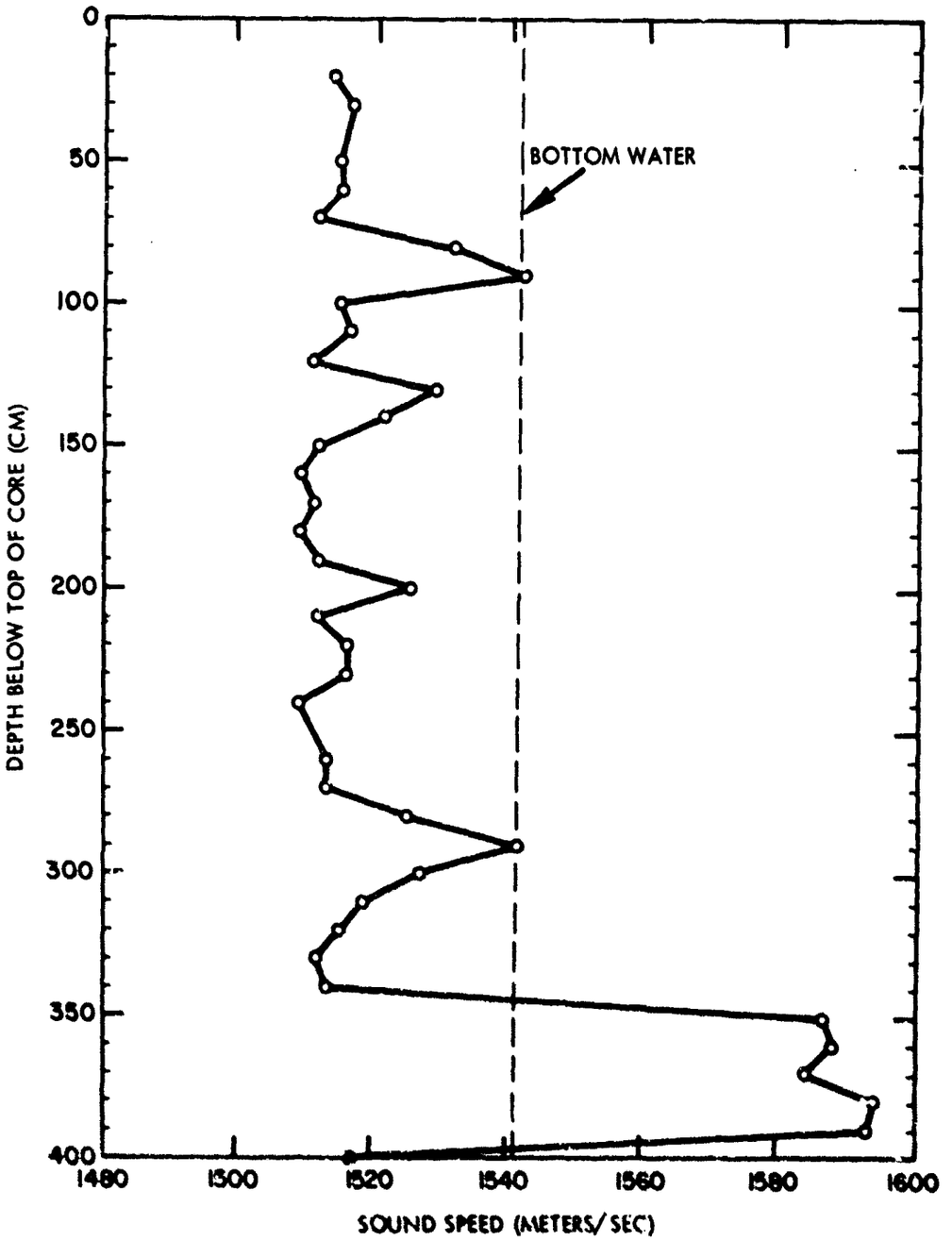

Figure 4. Sediment sound speed versus depth below top of core.

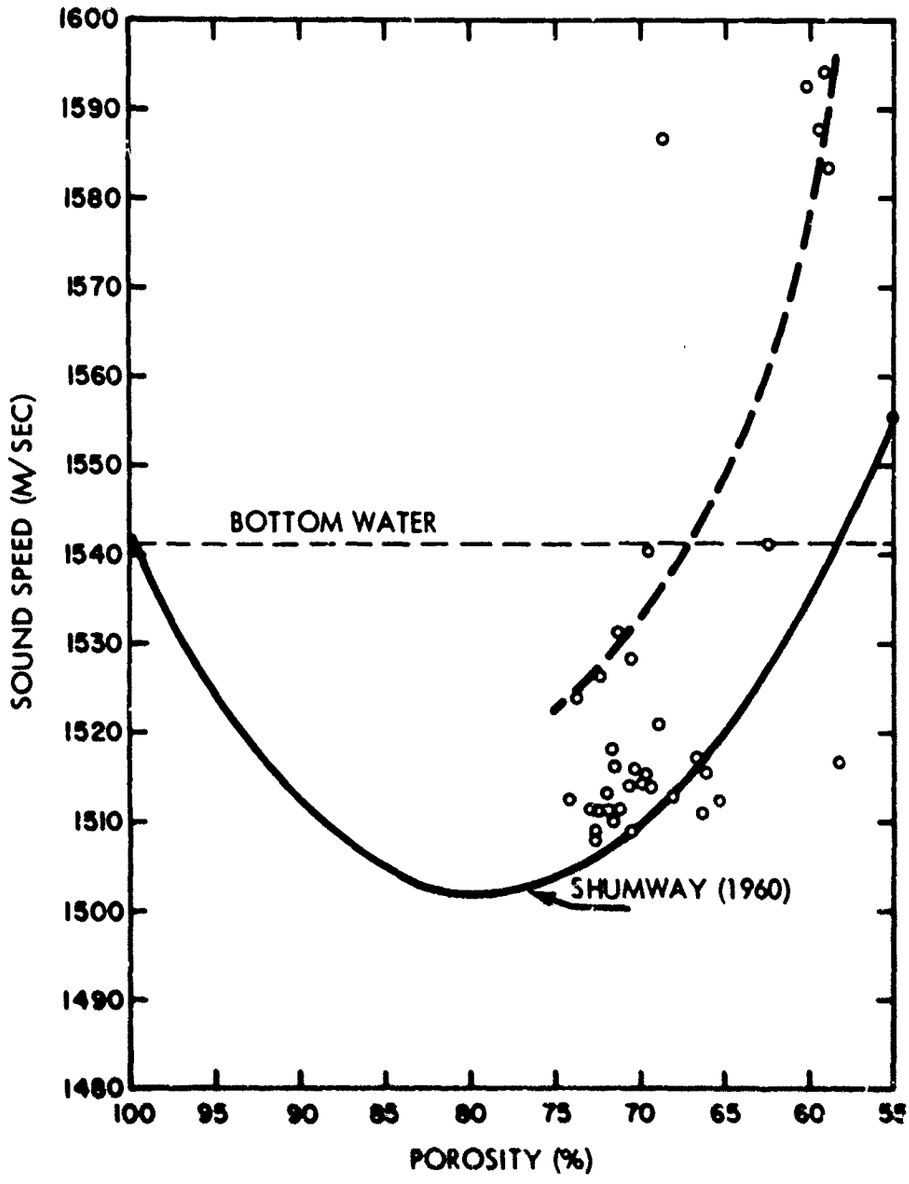

Figure 5. Sediment sound speed versus porosity (Shumway's empirical curve is corrected to in situ).

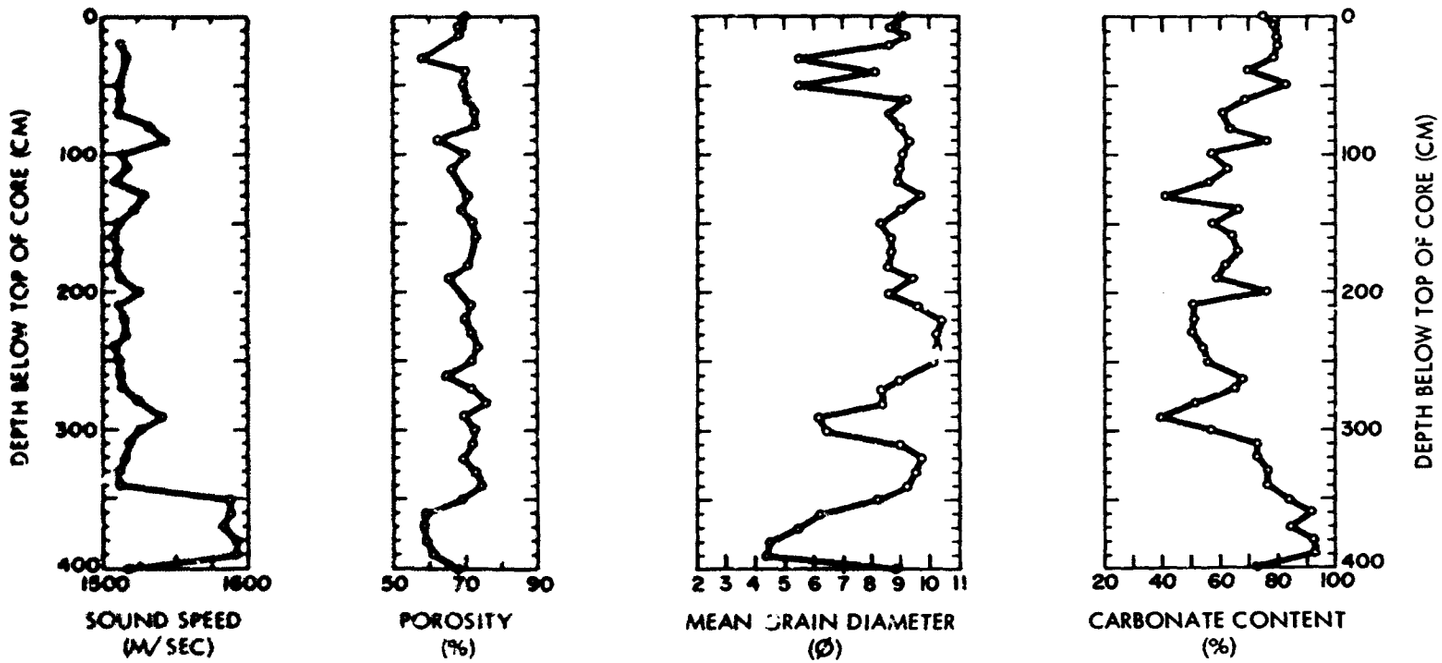

Figure 6. Composite of sound speed, porosity, mean grain diameter, and carbonate content versus depth below top of core.

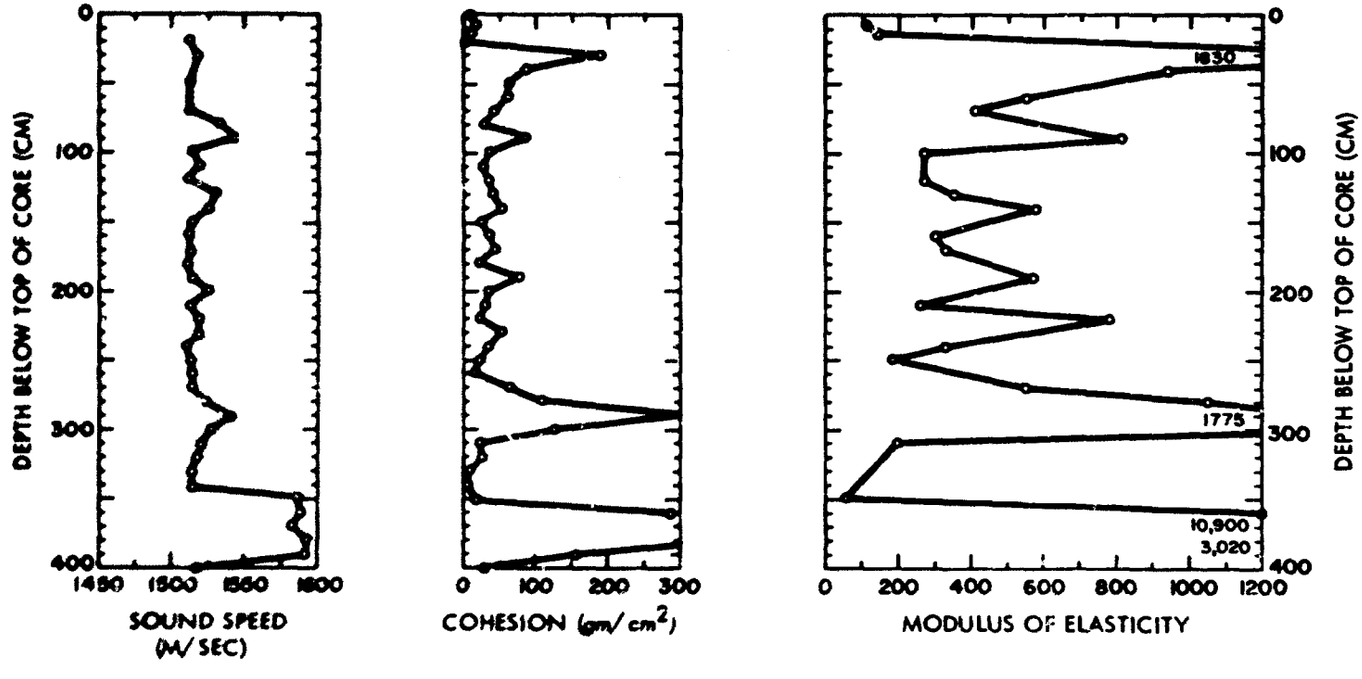

Figure 7. Composite of sound speed, cohesion, and modulus of elasticity versus depth below top of core.

EFFECTS OF EXPLOSIVE LOADING ON THE STRENGTH OF SEA-FLOOR SANDS

by

Robert F. Dill
U.S. Navy Electronics Laboratory
San Diego, California 92152

INTRODUCTION

The use of explosives to compact certain loosely packed sea-floor sediments has been reported for Norwegian fjords.[1] The purpose of this paper is to present new shear strength data acquired by diving, and thus supplement the existing information on the effects of explosive loading on sediment strength. The subject is restricted here to data taken in sediments found in depths above 80 meters and in channels where the movement of objects like marker stakes show that the sediments are unstable prior to explosive loading. In the open sea, bottom sediments are usually subjected to periodic, storm-induced currents capable of moving, by traction, the uppermost layers of sand grains. Ripple marks are common, and the sand movements create laminations that separate heavy minerals and micas from predominantly quartz grains. Dense or loose packing seldom exists on the sea floor surface because of constant agitation by currents. In confined areas the pore spaces between grains may contain gas generated by the decay of organic material. Most of the long term data in this report are from submarine canyons where marker stakes placed in the fill are observed to move down-slope,[2] thus proving the instability of the sandy sediments in the tested areas.

LA JOLLA REGION

The main area where the effects of explosions on the strength of sea floor sands has been measured is in Scripps Submarine Canyon off La Jolla, California. This canyon intercepts, and diverts seaward, the sand moved south along the coast by the prevailing northwest swell (fig. 1). Throughout most of the year coarse sand is transported inside the surf zone. Fine grained sediment carried to the coast by rivers also moves alongshore in the zone outside the breaker line spreading seaward at the bottom or along the coast until intercepted by the nearshore heads of the canyon.[3,4] Density flows of fine

Table 1. DENSITY, POROSITY, SHEAR STRENGTH, AND VOLUME CHANGE OF A FINE GRAINED MICACEOUS SAND FROM THE HEAD OF SCRIPPS CANYON.

Normal Stress (lb/in^2)	Peak Shear Strength, s_m, (lb/in^2)	Residual Shear Strength, s_u, (lb/in^2)	Wet Density (gm/cm^3)	Porosity P, (%)	Change in Volume during Shear: ΔV, (in^3)
0.10	0.36	0.30	1.849	55.31	+0.044
0.13	----	----	1.850	54.17	+0.026
0.37	----	----	1.823	54.52	+0.024
0.86	0.82	0.73	1.804	55.79	+0.030
1.73	1.40	1.20	1.810	55.29	+0.024
2.96	2.25	1.95	1.806	55.45	+0.030

Average in situ density 1.848 gm/cm^3; porosity 50.09%. Increase in volume indicates all samples were denser than the critical density prior to shear. Densities were measured after direct shear test and represent the critical density of the sediment. ΔV is volume change during shear. Positive values indicate an increase.

grained material set in suspension by storm swells, move both sand and mud sized sediment down-slope into the canyon. The coarse sand rapidly settles on a predominantly-micaceous, fine-grained sand that slowly accumulated throughout most of the year. This underlying unstable and weaker fill (fig 2) then fails. Slumps, slides, and sand flows result.

Investigators[5, 6] believed that explosives could trigger slides in such marginally stable sediments and that the collapse of a meta-stable sediment would cause the fill to liquefy and flow down the canyon as a turbidity current. An attempt to initiate such a current by explosion was made in 1964.

Measurements of the mass physical properties of the canyon fill showed that explosions would not liquefy the sediments. Therefore a special series of measurements of the sediment in the proposed explosion area were made prior to the tests.[4]

A small, vane-shear instrument was used to determine relative shear strength values before the charges were set off. Small brass cylinders were inserted into the bottom to obtain undisturbed samples of bottom sediment. Encapsulated samples were returned to the laboratory under sea water for standard density determination. Direct shear-box measurements of canyon sand, compacted to the same density as that found in situ, were made to determine the shear strength of the canyon sediments and whether or not they expanded or contracted when stressed (table 1).

Before the charges (14 pounds of TNT) were exploded, the in situ peak shear strengths of the sediments were measured with a vane-shear instrument. Values, 6 inches below the bottom, ranged between 0.4 and 0.7 pound/inch^2 (28 to 49 gm/cm^2) and had residual strengths of about 0.2 pound/inch^2 (14 gm/cm^2). The average wet density was 1.85 gm/cm^3 ; porosity ranged between 48.8 and 62.9 percent and averaged 50.0 percent. The grain size varied between 0.098 and 0.119 mm and averaged 0.11 mm in diameter.

After the charges were exploded, the sediments were found to be extremely dense in the immediate area surrounding the crater formed by the explosion. All vane-shear measurements exceeded the range of the test instrument and were thus above 2.4 pounds/inch^2 (169 gm/cm^2). A dense sand plug or dam had been created in the canyon fill instead of a liquefaction that could have developed into a

turbidity current. Temporary stability had thus been achieved in a sediment that had previously been creeping down-slope.

JAMAICAN REGION

Additional data on the effects of explosive loading on sea floor sands could be tested near Jamaica as a result of industrial activity in that area. TNT charges of up to 2000 pounds were used to break through a limestone ridge blocking Discovery Bay on the north coast. The near shore buttress reef off the Jamaican site is cut by a series of channels partially filled with a deposit of calcareous sand. The sandy debris which accumulates at the head of channels and in a depressed terrace area between depths of 40 and 60 feet is unstable and moves downslope. Large objects such as fish traps are carried down slope by the moving sediment similar to stakes placed in Scripps Submarine Canyon.

The Jamaican sands had an average grain size of 0.18 mm, an average porosity of 47.4 percent, and average densities of 1.99 gm/cm^3. As in Scripps Canyon, most vane-shear strength measurements were made 6 inches below the bottom surface. The average value of vane-shear strength obtained in four locations is shown in table 2. Measurements made where sediments were compacted by explosive loading showed a sediment peak strength twice as strong as in uncompacted areas.

An important aspect of the field measurements was the abrupt increase in shear strength at about 6 inches below the sediment surface. Vane-shear measurements taken at 2 inches below the sediment were very low in all areas. At 4 inches the sediment in most regions usually showed some increase of strength. Some zones of weakness were found throughout the upper 6 inches and were apparently caused by weak sediment at slip surfaces. Similar zones of weakness were found in the upper layers of sediment in Scripps Canyon and in the submarine canyons of Baja California, Mexico that are filled with a coarse arkosic sand.

CONCLUSIONS

Explosive loading of unstable sandy sediment deposited under open sea conditions has been shown to render them stable. In Scripps Submarine Canyon this stability created a sediment mass that blocked the normal down slope creep of the fill until it was eroded away by

Table 2. RELATIVE CHARACTERISTICS AND LOCATION OF SEDIMENTS INVESTIGATED OFF NORTHERN JAMAICA.

Location	Distance from Blast Area (miles)	Depth of Water	Average Bottom Slope	Average Vane-Shear Peak Strength (lbs/in^2) 2"	4"	6"	Vane-Shear Residual Strength at 6" (lbs/in^2)	Type of Failure	Ave. Md. Dia. (mm)	Sediment Type
Discovery Bay	0	140 feet	29°	--- 0.4	1.6 1.1	--- 2.5	0.4 0.4	Abrupt	0.41	Medium Sand
Runaway Bay	5	100 feet	30°	---	---	1.0	0.3	Average	Surface 0.056 at 2" At 6"	Very Fine Sand Medium Sand
Pear Tree Bay	4	175 feet	28°	---	0.7 - 0.8	1.4	0.4	Slow Failure	0.50	Medium Sand
"The [illegible]"	1	150 feet (slump zone)	10° - 15°	---	---	0.7	0.2	Average	0.41	Medium Sand

Note: All sediments were similar in average grain size, sorting, and composition. Vane-shear instrument was calibrated both before and after expedition and found to be accurate to within ± 0.1 lbs/in^2.

ABSTRACT

EFFECTS OF EXPLOSIVE LOADING ON THE STRENGTH OF SEA-FLOOR SANDS

by

Robert F. Dill
U. S. Navy Electronics Laboratory
San Diego, California 92152

Explosions can increase the capacity of unstable sea floor sands to support heavy structures. Sand bottoms are in most instances made significantly stronger and stabilized by blasting. Shear strength values for sandy sediments near their critical density 6 inches below the sea floor can be increased from 1.0 pound per square inch to between 2.0 and 2.4 pounds per square inch by the use of underwater explosives.

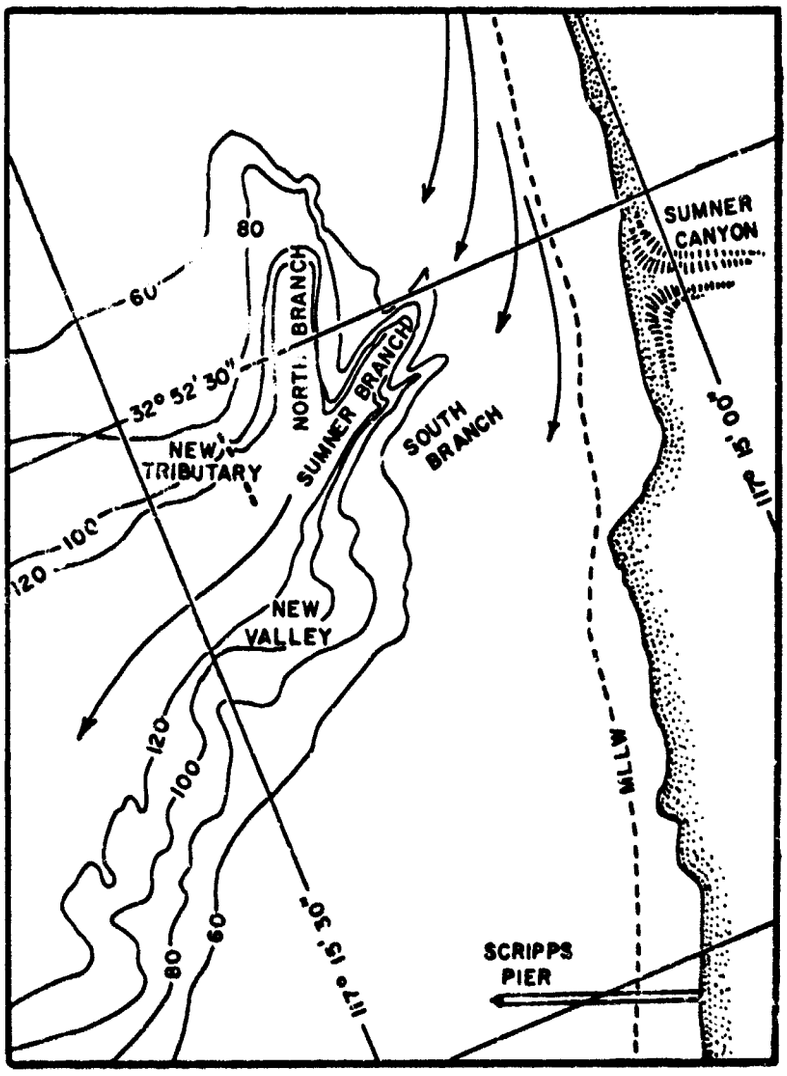

Figure 1 Chart of the head of Scripps Canyon, off La Jolla, California where observations on sediment movement and stability were made. Arrows depict direction of sediment movement into the canyon head. Depths are in feet (from Dill, 1964).

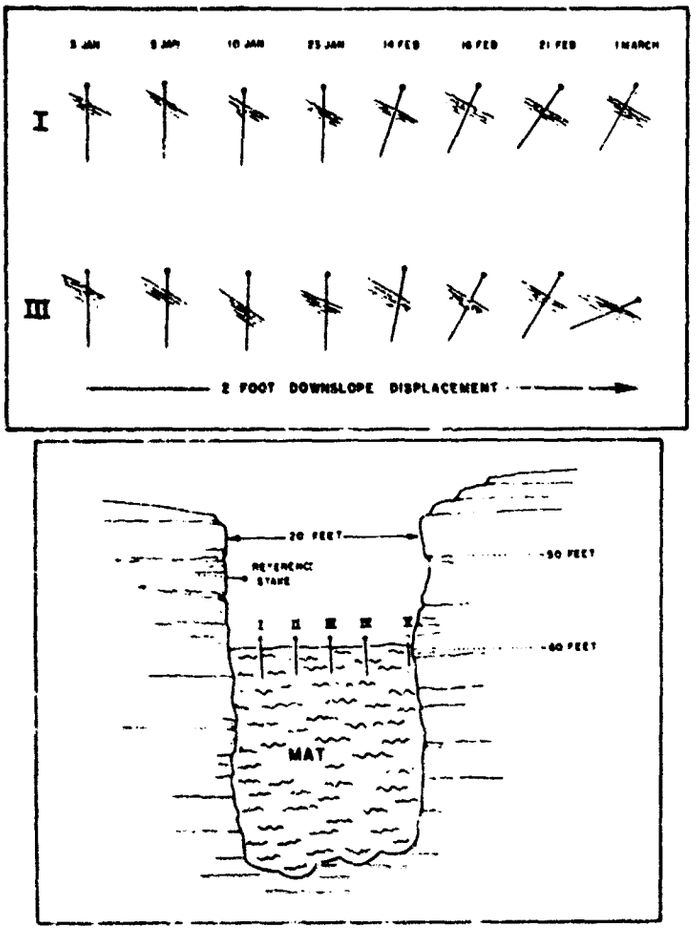

Figure 2 Slope angle, down slope movement and tipping of 4-foot stakes placed 3 feet in the sediment in head of Sumner Branch. Stakes, sediment levels and tip angles are at true scale (from Dill, 1964).

PERFORMANCE OF A NEWLY DEVELOPED SHIPBOARD WAVE HEIGHT SENSOR FOR USE IN OBTAINING WAVE MEASUREMENTS IN THE DEEP OCEAN

by Duncan B. Ross
U. S. Naval Oceanographic Office
Washington, D. C. 20390

INTRODUCTION

Obtaining meaningful measurements of ocean surface waves has presented problems to oceanographers and mariners for many years. Ship routing, fleet exercises, carrier operations, refuelings and logistic transfer procedures, and sea plane operations are a few of the activities which could benefit from on-the-spot information concerning surface wave conditions.

Technological advances in recent years have led to various free floating buoys and several shipboard and airborne wave measuring devices. Use of electronic and numerical methods to obtain statistics of waves measured with these devices have, in many cases, given conflicting results. These inconsistancies have been introduced through instrument drift because of fluctuations of power in the field, inability of numerical methods to handle available signals, inability of the instrument to respond accurately to the medium itself, and modification of the waves by the presence of the instrument or its carrier.

The Radio Corporation of America, under contract to NAVOCEANO, designed and built a shipboard sonic ranging device to obtain ocean wave measurements in the open ocean. This system displays a time history of surface wave displacement by removing ship motions from relative motions of a bow-mounted, echo-ranging, sonic altimeter. A brief description of the system, during early stages of development, was given by Mark (1962).

INSTRUMENTATION

The shipboard wave height sensor consists of a sonic scanner and heave accelerometer mounted in a roll stabilized package attached to a boom at the bow of the ship, Figure 1.

The bow-mounted package, Figure 2, consists of a vertical gyro which roll-stabilizes the transducer and heave accelerometer. In addition, the accelerometer is pitch stabilized. The transducer signal, a 38KC CW Pulse with a 16 degree beam width, is fed into the summing amplifier. The vertical accelerometer output is integrated twice electronically and also fed into the summing amplifier where it is algebraically added to the transducer signal, Figure 3. The output of the summing amplifier, together with the heave velocity, heave displacement, and transducer signals, are

FIGURE 1 MOUNTING STRUCTURE FOR TRANSDUCER PACKAGE

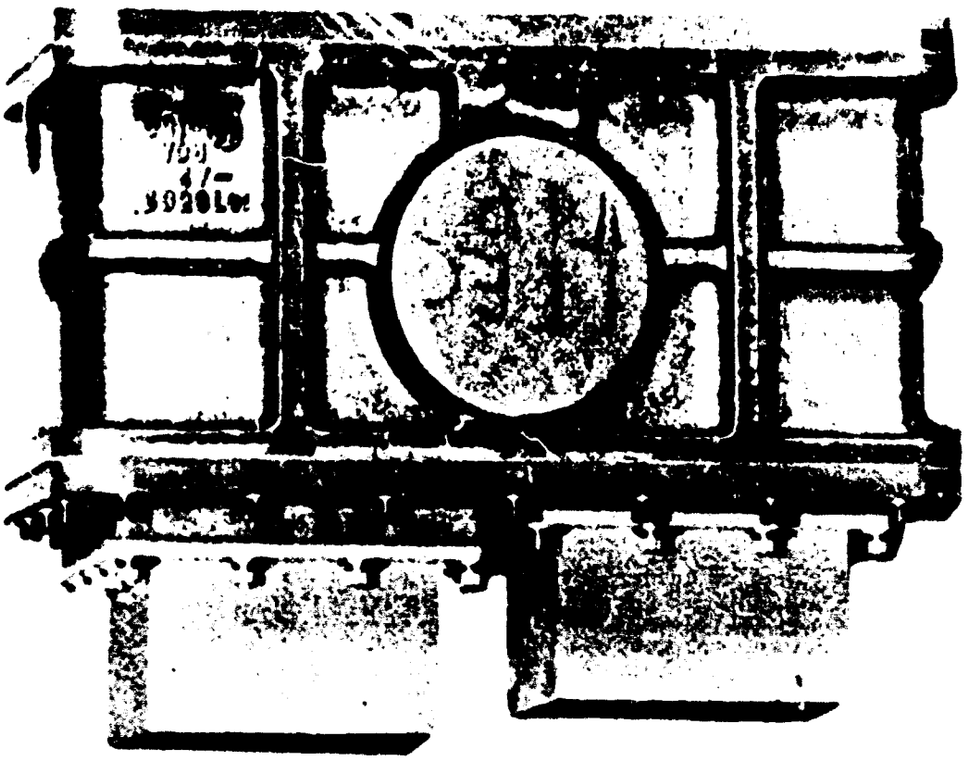

FIGURE 2 TRANSDUCER PACKAGE

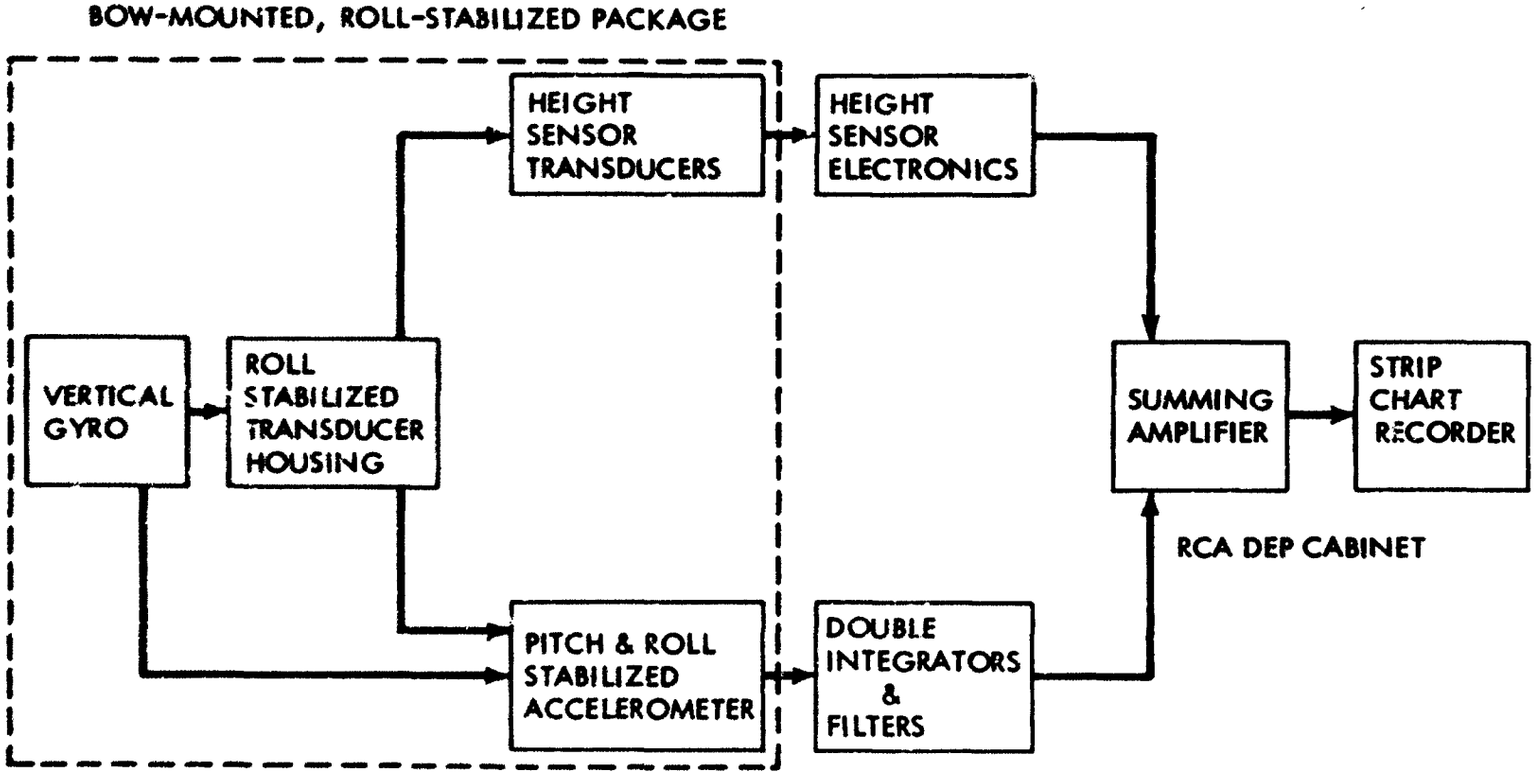

FIGURE 3. BLOCK DIAGRAM OF SHIPBOARD WAVE HEIGHT SENSOR

displayed on a 4-channel Sanborn recorder housed in an RCA Deck Electronics Package together with the integrating and summing amplifiers shown in Figures 4 and 5.

Prior to shipboard installation, the system was statically tested aboard the ARGUS ISLAND tower (31°57'N, 65°11'W) using a fixed resistance-wire wave staff as a reference. Comparison of power spectral estimates computed from the two time series is shown in Figure 6 which indicates very good agreement over the entire frequency band.

The unit was then mounted on a Coast Guard Cutter and test runs were conducted near the ARGUS ISLAND tower, again using the resistance-wire wave staff as a reference. Power spectra of data obtained from runs of various speeds and headings were computed, mapped to fixed coordinates, and compared to the spectra obtained from the wave staff.

Figure 7 presents spectral comparisons obtained with a ship's speed of two knots, and a heading, relative to the predominant wave direction, of 000°T. A comparison of significant wave heights indicates the shipboard wave meter to be approximately 15 percent too high.

A similar run, again at 000°T, at a speed of five knots, Figure 8, resulted in a discrepancy of less than 10 percent, again on the high side.

Significant height comparisons from other runs were generally 5-10 percent too high. A complete summary of the system and spectral data, illustrating results of four field tests, has been presented by Moskios and DeLeonibus (1965).

NUMERICAL INTEGRATION

One of the problems associated with the shipboard system was excessive drifting attributed to overheating as a result of poor ventilation. In order to determine to what extent, if any, drifting of the integrating circuits and the summing amplifier would bias the resultant spectral estimates, the use of numerical techniques operating on the heave acceleration and transducer time histories was indicated.

Numerical integration of a time series representation of acceleration may be accomplished by two methods. The first is a well known algebraic process operating in the frequency domain whereby the spectral estimates per unit band width of the acceleration, or velocity, time series are simply divided by the fourth, or second, power of the frequency interval in radians per second. For example:

$$A^2_{hd}(N) = \frac{A^2_{hv}(N)}{k^2} = \frac{A^2_{ha}(N)}{N^4}$$

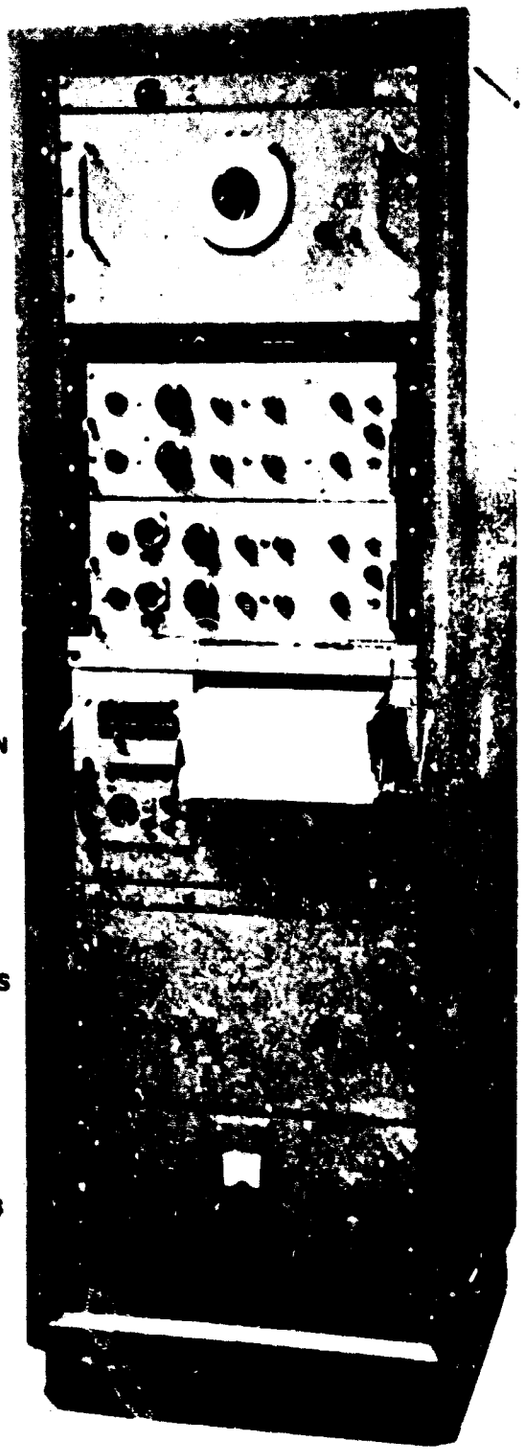

FIGURE 4 DECK ELECTRONICS PACKAGE (DEP)

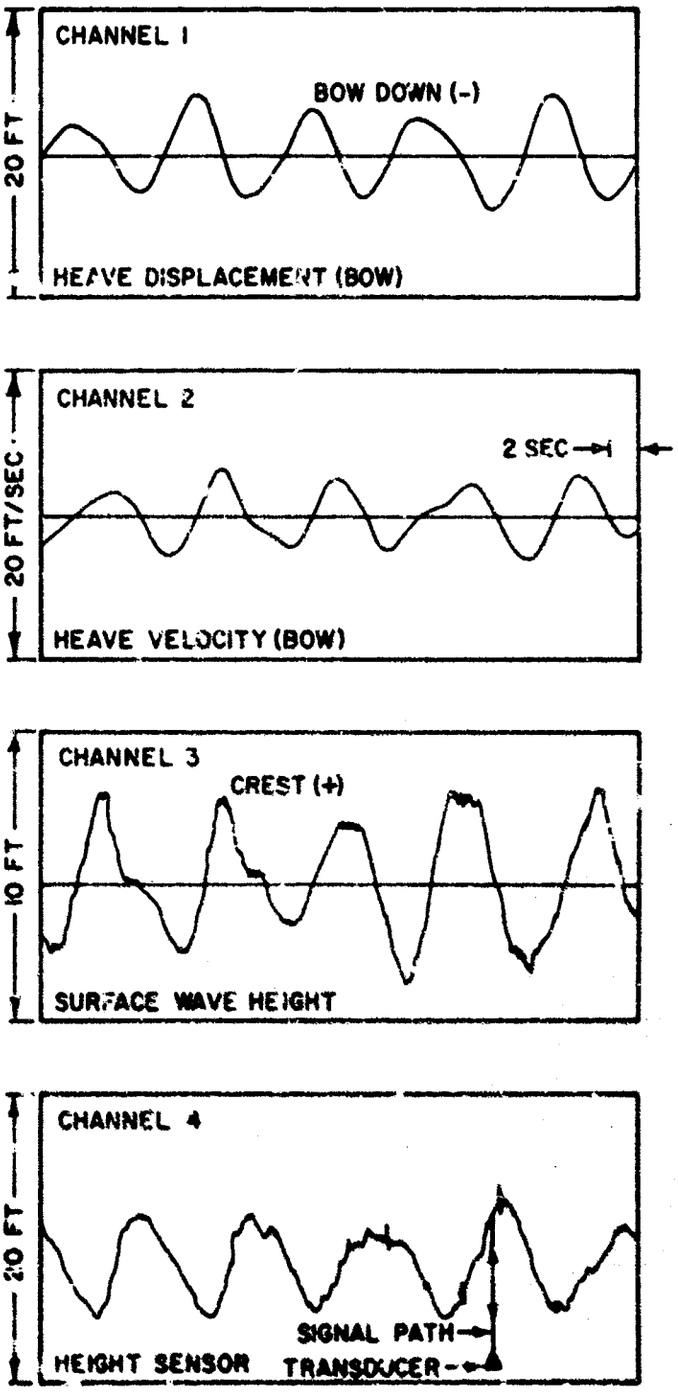

FIGURE 5. EXAMPLE OF RECORDING FROM SHIPBOARD WAVE METER.

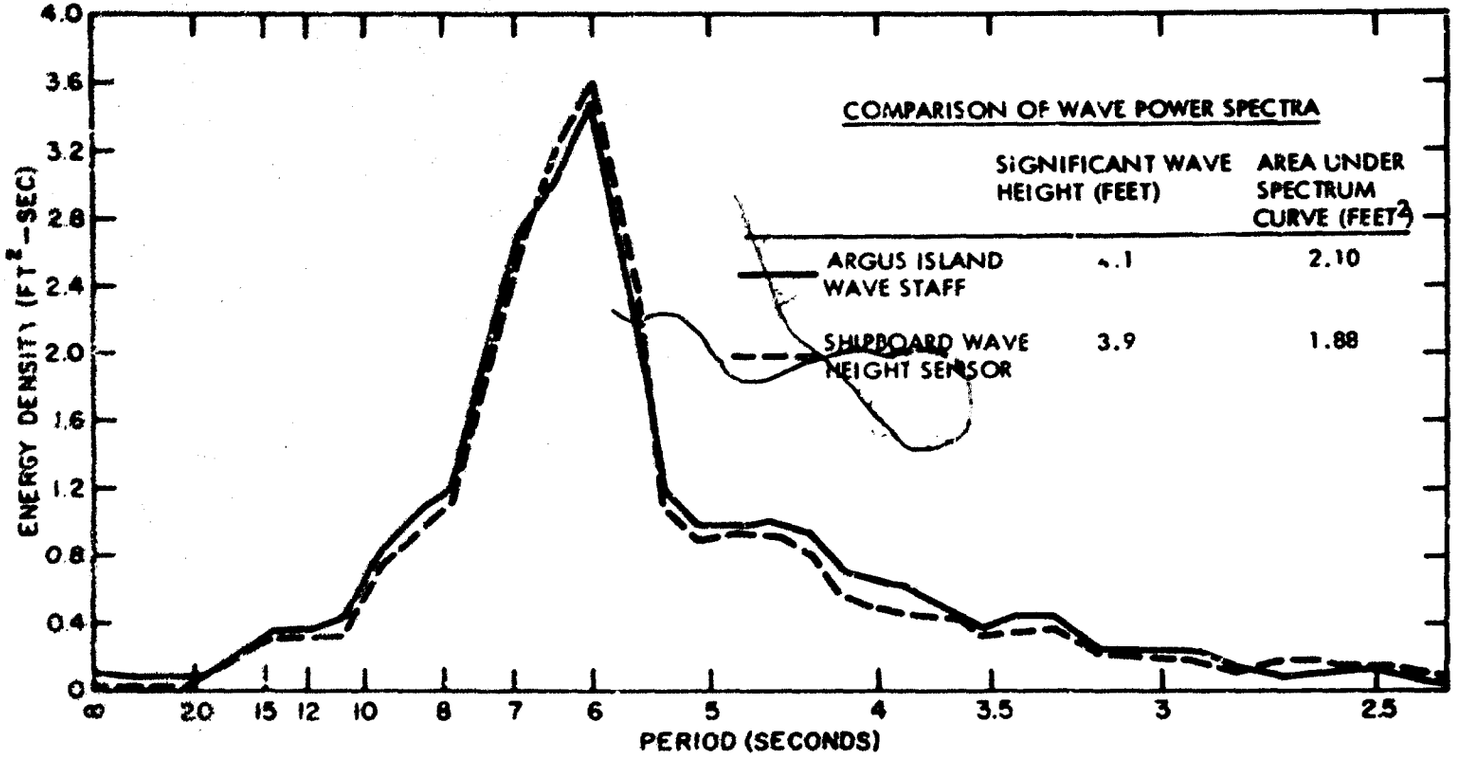

FIGURE 6. STATIC TEST OF SHIPBOARD WAVE HEIGHT SENSOR AT ARGUS ISLAND. SENSOR CLAMPED 35 FEET ABOVE MEAN SEA LEVEL.

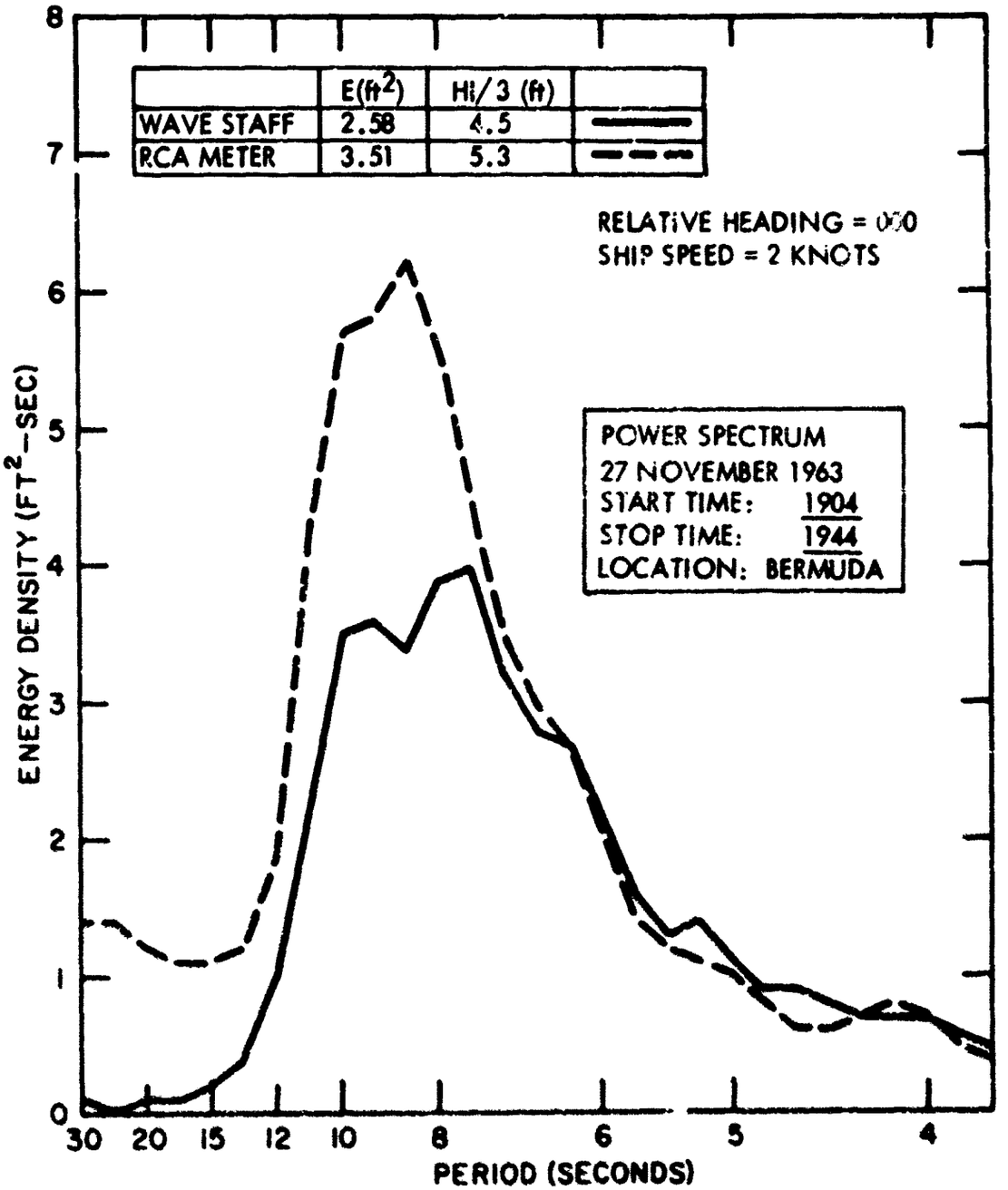

FIGURE 7. COMPARISON OF WAVE HEIGHT SPECTRA, SHIPBOARD WAVE SENSOR AND ARGUS ISLAND WAVE STAFF.

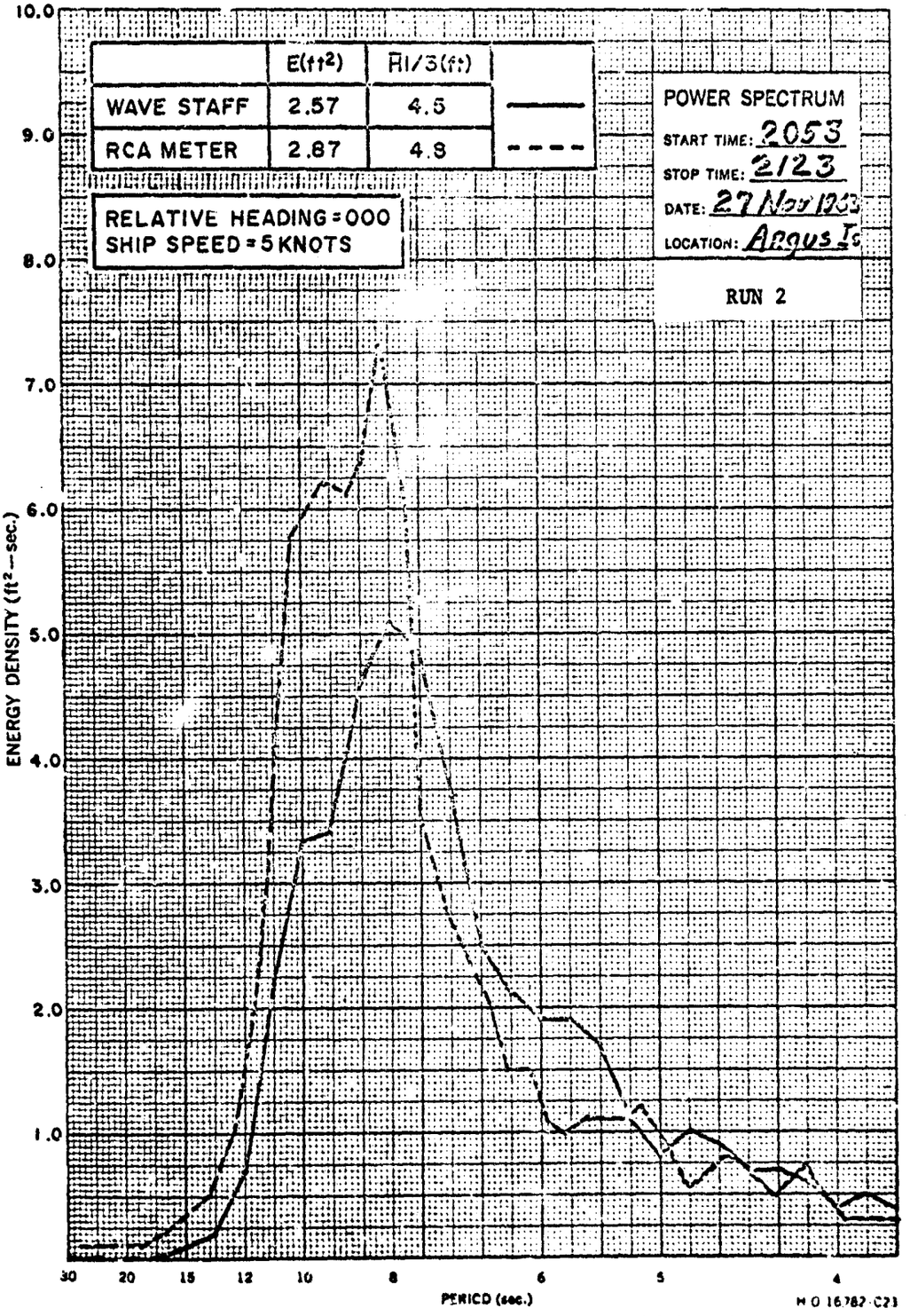

Figure 8 · Comparison of Wave Height Spectra, Shipboard Wave Sensor and ARGUS ISLAND Wave Staff, 2053-2123, 27 November 1963

Where $A^2_{hd}(W)$ = spectral estimate of heave displacement

$A^2_{hv}(W)$ = spectral estimate of heave velocity

$A^2_{ha}(W)$ = spectral estimate of heave acceleration

$$W = \frac{2\pi}{f}$$

Also well known are the problems involved with the algebraic process. That is, the tendency for the spectrum to blow up at the low frequency end. This "blow up" energy is introduced through a trend or drift in the mean values of the signals. Such trends could be introduced by a drift in the reference voltage of the integrating circuits.

Obtaining a time series representation of heave displacement from heave acceleration may be obtained by several numerical methods. A method which shows good response characteristics over a wide range of frequencies is that of Tick (1961) and Tick (unpublished) and is as follows:

$$Y_{n+1} = Y_{n-1} + h(.3584Y'_{n+1} + 1.2835Y'_n + .3584Y'_{n-1})$$

Where Y denotes the antiderivative
Y' denotes the derivative
h denotes the sampling interval

Integration in the time domain, as in the frequency domain, introduces energy at the low frequency end of the spectrum. However, numerical filtering techniques provide a method of removing this trend in a convenient manner. A procedure by Linette (1961) is very efficient and involves deriving a series of weights which are added to each computed point.

Since the acceleration output was not recorded, the product of the first integration, velocity, was selected for analysis. Figure 9 is a comparison of spectral estimates obtained from the algebraic and the electronic techniques. In both cases the time series were filtered prior to computing power spectra.

Figure 10 is a comparison of power spectral densities obtained from electronic integration to that obtained from the numerical procedure of Tick. Good performance by the electronic integrated circuits is immediately evident. Not so evident, but of equal importance, is the powerful tool of numerical integration and filtering techniques in time series analysis.

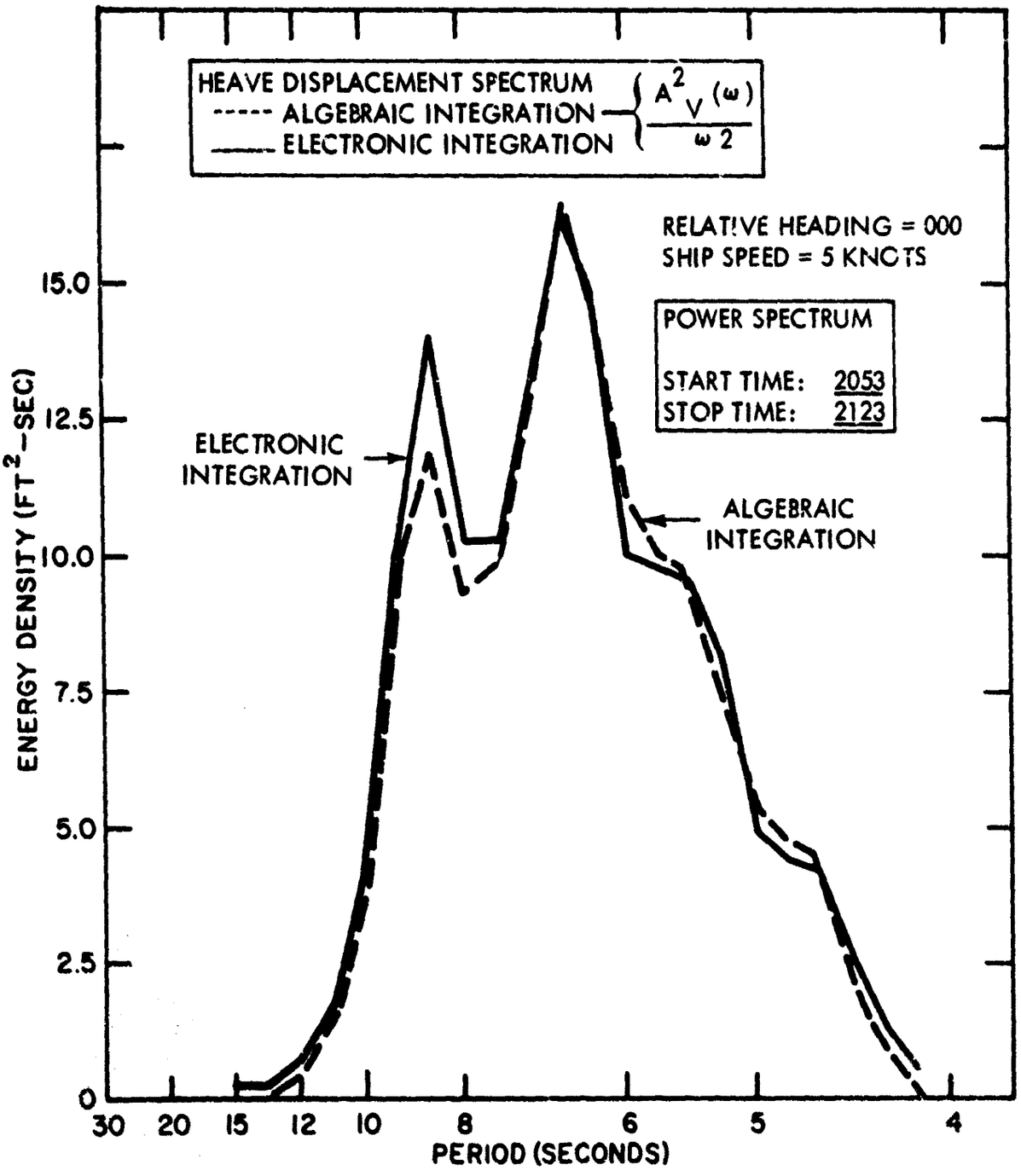

FIGURE 9. ALGEBRAIC INTEGRATION VS ELECTRONIC INTEGRATION

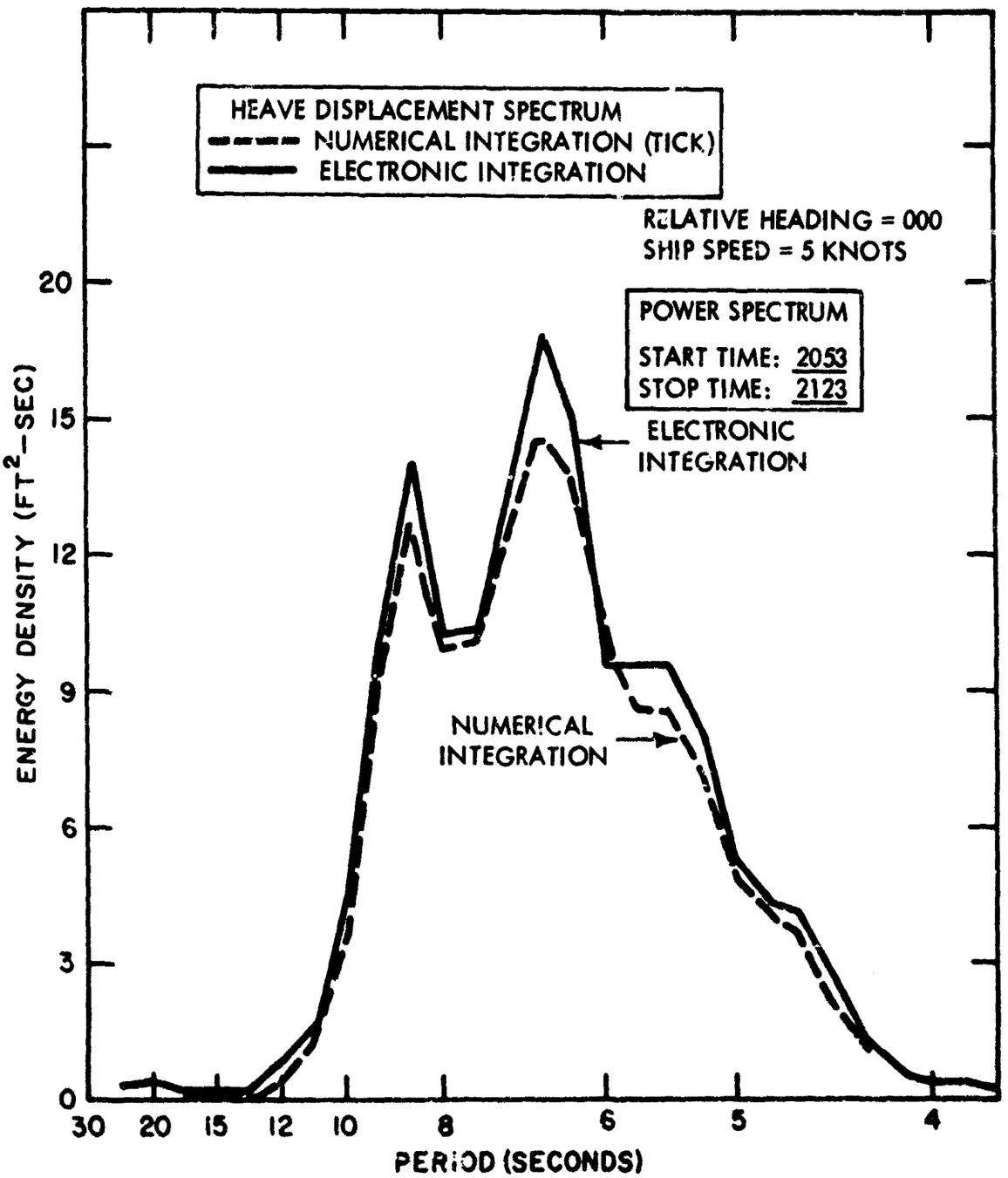

FIGURE 10. NUMERICAL INTEGRATION VS ELECTRONIC INTEGRATION

CROSS-SPECTRUM ANALYSIS

In order to obtain an estimate of the power spectrum of the apparent wave heights a cross spectrum analysis was performed, bypassing the summing amplifier entirely. Twenty-minute samples of heave velocity and transducer time history were digitized and filtered numerically and were subjected to cross-spectrum analysis.

The cross-spectrum technique involves adding the power spectrum of heave displacement to the power spectrum of the transducer time history and subtracting twice the cospectrum of the heave displacement and the transducer time series:

$$A^2_{wh}(W) = A^2_T(W) + A^2_{hd}(W) - 2Cos_{ht}(W); \text{ where}$$

$A^2_{wh}(W)$ = Spectral density of wave height

$A^2_T(W)$ = Spectral density of transducer time series

$A^2_{hd}(W)$ = Spectral density of heave displacement

$Cos_{ht}(W)$ = Cospectral density of transducer and heave displacement

A similar technique was used by Marks (1964) to study the motions of a hydrofoil craft.

Figure 11 presents a typical example of spectral estimates obtained from the time series output of the summing amplifier and that obtained from the cross-spectrum technique compared to the wave staff. Here we can see an error introduced by drift of the summing amplifier.

The spectral estimates obtained from the shipboard wave meter using the cross-spectrum technique fall within the confidence limits of the spectra obtained from the wave staff. The analysis indicates that the summing amplifier contributed the relatively minor discrepancies observed and that the technique of obtaining accurate information of surface wave conditions from a remote sensor on a ship at sea is valid and one that will lead to increased knowledge of wave mechanics, ship motion studies and to more efficient and safe maritime operations.

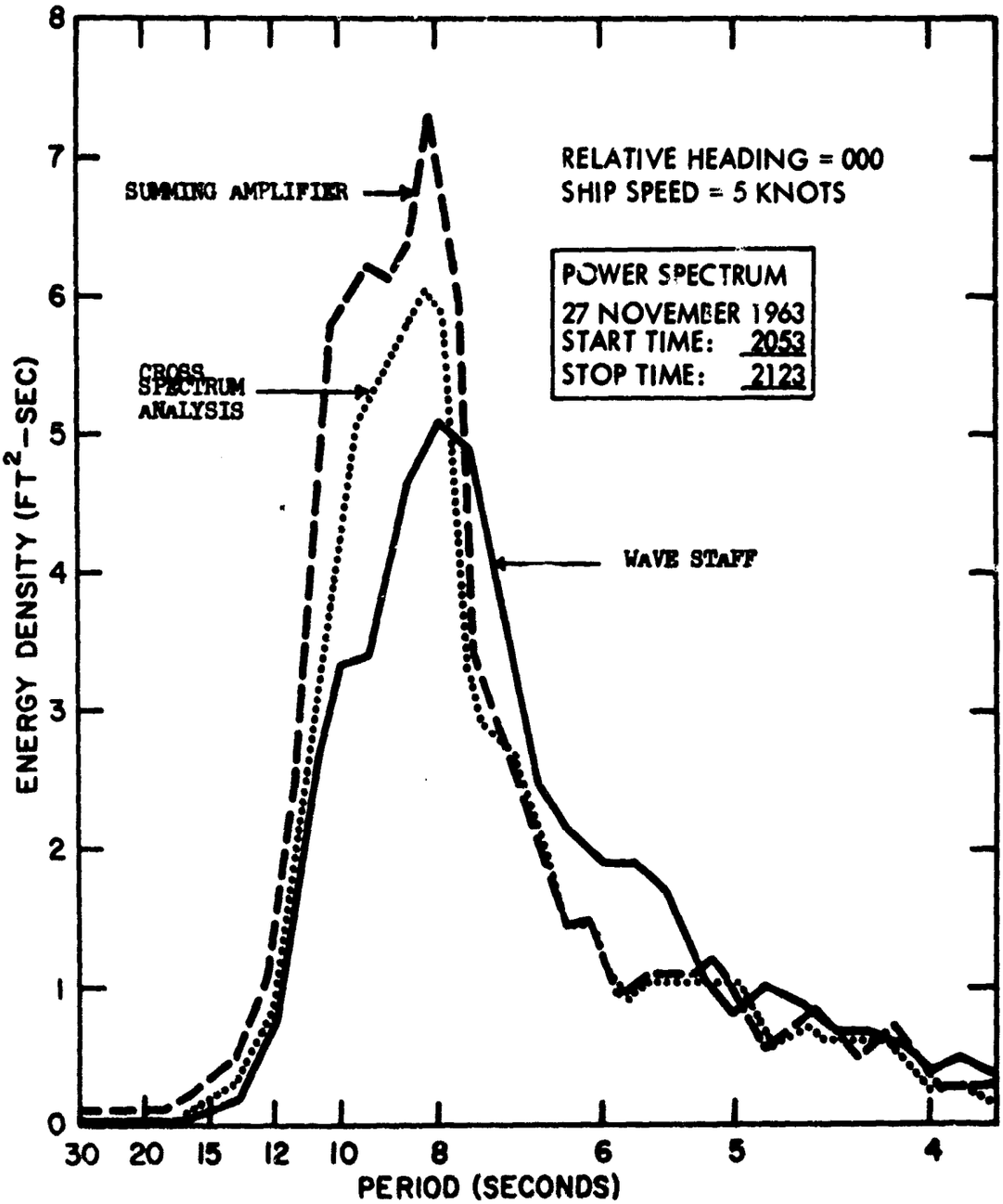

FIGURE 11. COMPARISON OF SPECTRA OBTAINED VIA SUMMING AMPLIFIER WITH THAT OBTAINED VIA CROSS SPECTRUM ANALYSIS AND THE ARGUS ISLAND WAVE STAFF.

REFERENCES

1. Blackman, R. B. and Tukey, J. W. "The Measurement of Power Spectrum," Dover Publications 1958.

2. Linnett, H. M. "Statistical Filters for Smoothing and Filtering Equally Spaced Data," Research Report 1049, U. S. Navy Electronics Laboratory, San Diego, California (1961).

3. Mark, R. B. "Shipboard Ultrasonic Wave Height Sensor," Marine Sciences Instrumentation, Instrument Society of America, Volume II, New York, Plenum Press, 1962.

4. Marks, W. "Determination of the Wave Spectrum from Observed Motion of a Vehicle in a Seaway," Oceanics Inc., Sep. 1964.

5. Moskios, A., DeLeonibus, P. "Performance of a Shipboard Wave Height Sensor," U. S. Naval Oceanographic Office Informal Manuscript, Report 0-4-65 (Unpublished Manuscript, March 1965)

6. Tick, L. J. "Integration of Stationary Time Series," Engineering Research Division, New York University, Statistics Laboratory, July 1961.

7. - - - "Integration of Time Series II," Task Report No. 2, College of Engineering Research Division, New York University, New York, New York. (Internal Unpublished Report)

AMBIENT THERMAL NOISE IN THE SEA AND THE INSTRUMENTAL AND OBSERVER ERRORS AND BIASES OF SEA TEMPERATURE MEASUREMENTS

Paul M. Wolff, Captain, USN
and
N. M. Stevenson, Commander, USN

ABSTRACT

Frequent observations of sea surface bucket temperatures and bathythermographs by a mine division during a transit to the Western Pacific Operating Area have provided a unique opportunity to determine the thermal ambient noise level and instrumental and observational errors and biases.

It is demonstrated that it is not possible to determine, with any certainty, the dimensions of minor thermal patchiness in the sea, except as well marked water type boundaries (i.e. fronts). Therefore, the variability that is observed is termed "thermal ambient noise." Its magnitude in different areas is determined by the range of two standard deviations.

From a time series of simultaneous observations, taken from identical ships, the instrumental and observational errors and biases are determined statistically.

From a comparison of synoptic messages and initial communications drafts, the types and frequency of transmission error are determined. Finally, some shortcomings of present instrumentation in regards to sea surface temperature and bathythermographs are described.

1. INTRODUCTION

Through coordination with Commander Thomas N. Nutt, Commander Mine Division Seventy-One, a specially designed environmental observation plan was executed by Mine Division Seventy-One during a transit of the Pacific Ocean - February/March 1966. The five ships, identical in size and traveling in company in a relatively close but variable formation, offered a unique opportunity to study the space and time variability of the environment as well as establish, qualitatively, the observer bias and error, and, quantitatively, the instrument bias and error.

The results of this study are applicable for improving existing and future oceanographic models for synoptic analysis and forecasting. Furthermore, it is possible to point out several shortcomings in instruments, data transmissions, collections, and retransmissions, and recommend observational procedures. It was therefore decided to publish the results of the first segment of this transit without delay. The final report will contain further statistical evaluation as well as a complete analysis and description of the environment (in space and time) during the transit.

The following ships of Mine Division Seventy-One participated in the oceanographic sampling exercise. The officers and men of this division contributed much toward improving our knowledge of the ocean.

USS FORTIFY (MSO 446)
USS LOYALTY (MSO 457)
USS ENGAGE (MSO 433)
USS INFLICT (MSO 456)
USS IMPERVIOUS (MSO 449)

2. OBSERVATIONAL PLAN AND INSTRUMENTATION

While transiting the Pacific, the five minesweepers of Mine Division Seventy-One recorded the following observations in addition to prescribed, routine environmental reports: Sea Surface Temperature - BT casts - Wind Wave and Swell Height and Direction - Wind Speed and Direction - Wet and Dry Bulb Temperatures. During this transit at least two ships were making continuous observations (ranging from quarter-hour to hourly observations) of SST and BT soundings and three-hourly observations of other selected environmental parameters (i.e. Barometric Pressure Cloud Cover - Present Weather - etc.). In addition, during selected 15 hour periods, all five ships made SST observations and BT casts every 15 to 30 minutes depending upon a prearranged schedule and hourly to three-hourly observations of the other selected environmental parameters. These special data collections were conducted with the ships in formation, line abreast, with a spacing interval of 1/2, 1, 2 and 4 miles between individual ships. This formation was maintained throughout the 15 hour period.

Part of the track of Mine Division Seventy-One is shown in Figure (1), illustrating that their course was south of the main shipping route in relatively sparse synoptic data areas. The SST measurements were recorded utilizing a plastic bucket designed specifically for SST observations and obtained from the U.S. Fish and Wildlife Service, Bureau of Commercial Fisheries through the cooperation and help of Dr. Flittner, Tuna Resources Laboratory, La Jolla. The designed reading accuracy for these thermometers was $\pm 0.1^{\circ}F$ and they were uncalibrated as are all thermometers in general use for SST observations at present. However, due to the state and direction of the sea, many of these specially designed thermometers were soon broken when the bucket would strike the side of the ship during an excessive roll. Replacement thermometers utilized were the thermometers furnished with the BT instrument (reading accuracy $\pm 0.5^{\circ}F$). Wet and dry bulb sling thermometers were procured through standard Navy Supply channels and were also uncalibrated. Twenty-five additional BT instruments were obtained on a loan from BUSHIPS.

3. SEA SURFACE TEMPERATURE (SST)

The deficiencies in instrumentation are described, in general, in Chapter 6, and the results of this preliminary analysis are reported here in summary form.

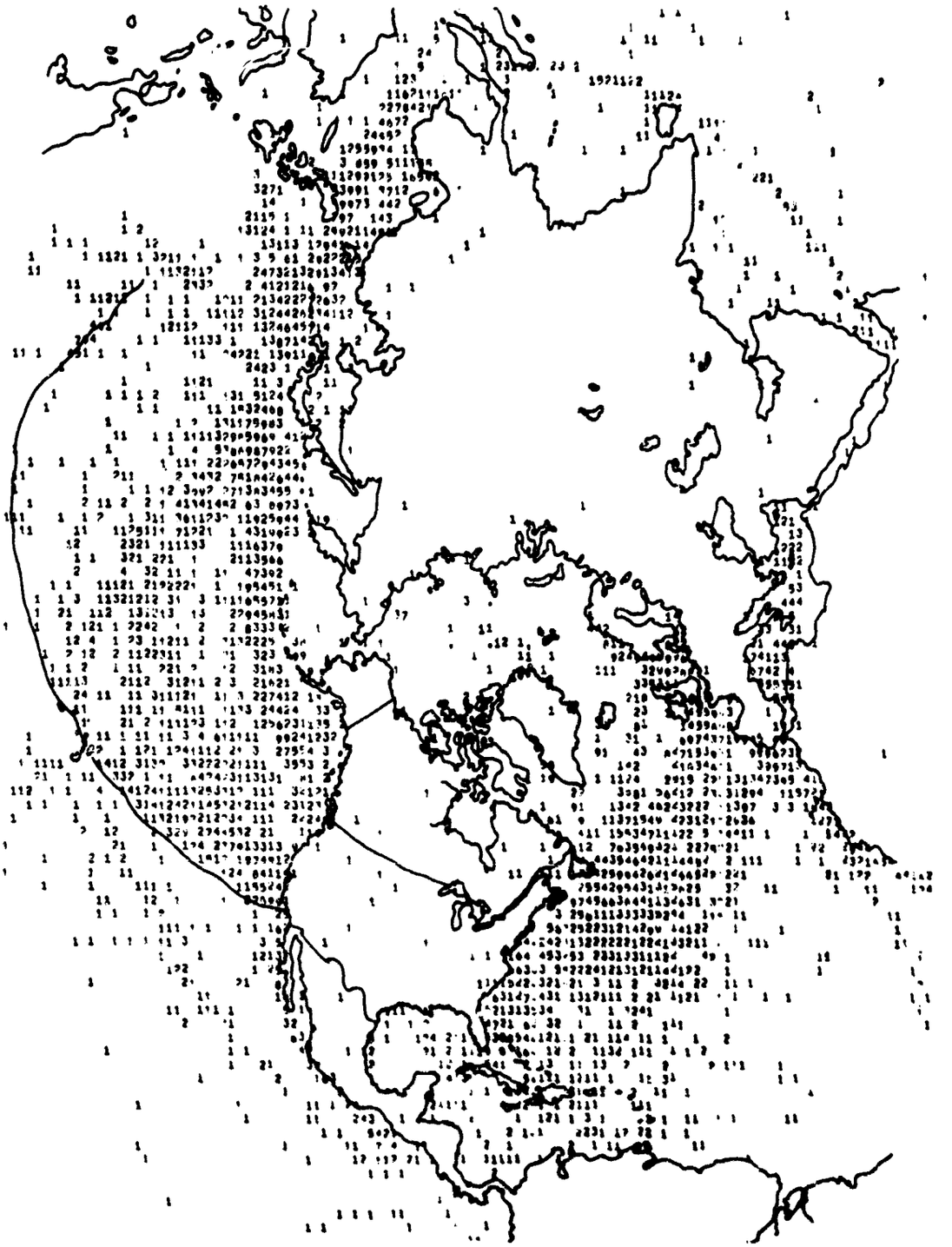

FIGURE 1. TYPICAL DENSITY OF SST REPORTS DURING 3½ DAYS IN LATE WINTER AND THE TRACK OF MINSWEEPERS

3.1 Fluctuations in space and time

3.1.1 The mean SST of the five ships changed an average of 0.25°F in 15 minutes (approximate distance of two miles), the maximum and minimum changes were 0.6° and 0°F respectively. (Table I)

3.1.2 The more pronounced changes occurred at water type boundaries off the California Current and the Central Pacific Water boundaries. Both boundaries are indicated normally in FNWF Ocean Frontal Analyses. (Figure 9)

3.1.3 Individual ships observed a number of SST changes with an average range of 0.4°F per 2 hours (approximately 16 nautical miles). Except for the two changes at the oceanic fronts, mentioned in 3.1.2, these changes could not be correlated from ship to ship, despite the small distances between ships (1/2 to 4 nautical miles). Thus thermal tongues could not be substantiated in this part of the ocean and these small variations must be ascribed to turbulent "thermal noise" and to observation error. (Figure 2)

There are a number of reasons for this irregular, unpredictable and changeable thermal noise and thermal turbulence, such as insolation affected by clouds and changeable wind currents. One example of irregular, day to day surface wind current variations is shown in Figure (3) for two adjacent 2-1/2° squares in the Central Pacific from 12 January to 13 February 1963.

3.1.4 To obtain a measure of the thermal noise, the instrumental bias of individual ship SST observations was removed and the standard deviation computed for SST in two hour blocks along the track (or approximately 16 nautical miles). The average thermal noise (range) defined in this manner was smaller than 0.4°F. (See Table I.) Obviously, these values are variable in space and time, but the results appear to be characteristic for the greatest part of the offshore ocean areas.

3.1.5 For comparison, some values on thermal noise are quoted from recent literature. Paul's (1965) data from the Gulf of Alaska indicates that thermal noise of approximately the same order of magnitude (i.e. 0.3°F) was present in May during a special detailed survey. Owen (1966) also describes a similar spotty distribution of SST, attributing this mainly to patchiness in transient thermoclines and heat exchange.

3.1.6 The difference between the SST reported by the minesweepers and the 12 hourly SST analyses made at FNWF is shown on Figure (4). The mean difference is about 1.0°F; this is smaller than the expected standard error due to analysis method. Larger differences are observed from 23 to 24 February in the area of the FNWF analysis boundary and from 10 to 12 February at the boundary of the California Current. This agrees

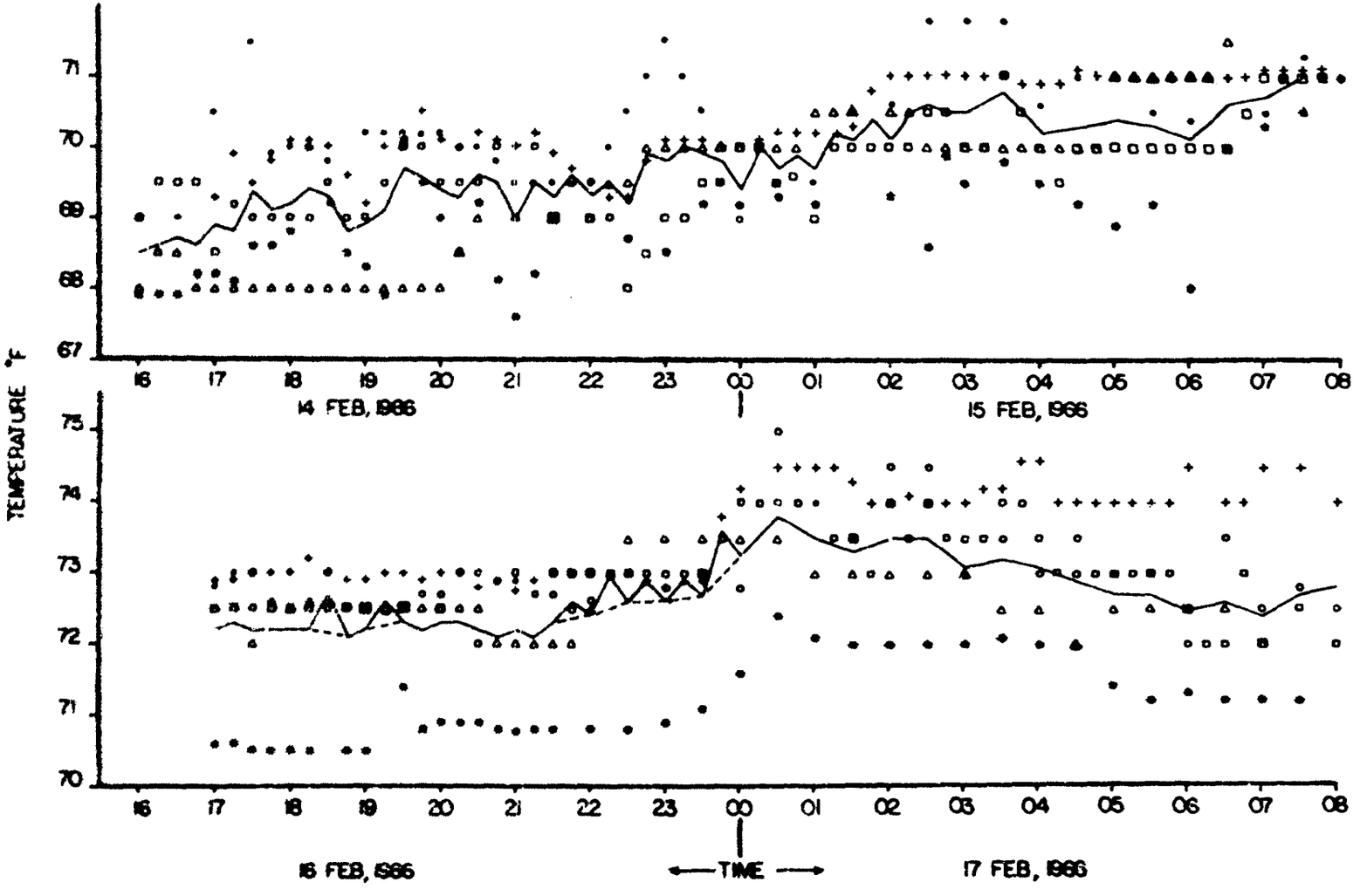

FIGURE 2. EXAMPLES OF SST OBSERVATION DURING TWO PERIODS (14-15 FEB AND 16-17 FEB 1966)
MEAN SST OF THE FIVE SHIPS WITH INDIVIDUAL OBSERVATIONS ARE SHOWN

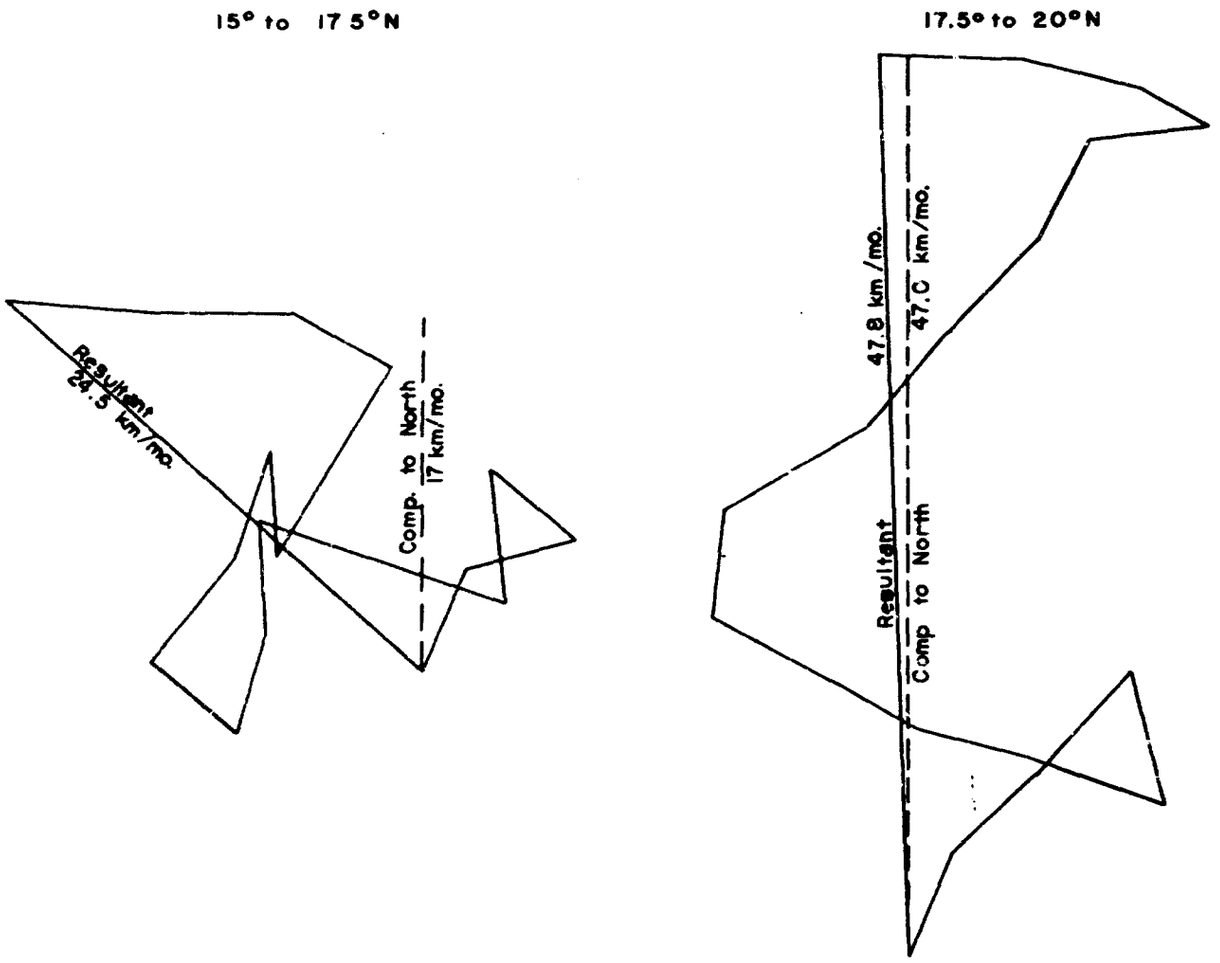

COMPUTED AVERAGE WIND CURRENTS FROM 12 JAN 63 TO 13 FEB 63
IN TWO ADJACENT 2½° SQUARES ALONG 150°W
(AFTER LAEVASTU AND ROTHSCHILD)

FIGURE 3

Table 1

Preliminary statistical summary of SST and BT observations (^{o}F)

	Av.	Max.	Min.
Change of 5 ship mean SST			
in 15 min (2 n. miles)	0.25	0.6	0
in 1 hour (8 n. miles)	0.3	0.8	0
Change of individual ship SST (those reporting with $\pm$ 0.1^{o}F)			
in 15 min.	0.2	1.2	0
in 1 hour	0.35	2.5	0
in 2 hours	0.50	2.5	0
in 4 hours	0.65	2.5	0
Bucket thermometer bias	0.35	2.5	0
Reading accuracy	$\pm$ 0.2	$\pm$ 0.5	$\pm$ 0.1
(Reporting accuracy)	1.35	--	--
Defined thermal noise (20 miles) (2 σ) ca.	0.4^{o}F		
Instrumental and observational range (2 σ)	> 2^{o}F		
Difference between bucket SST and BT SST (errors over 4^{o}F removed)	1.1	(4)	0
Defined thermal noise, instrument bias, instrumental and observational range and reporting accuracy for SST messages	> 3^{o}F		

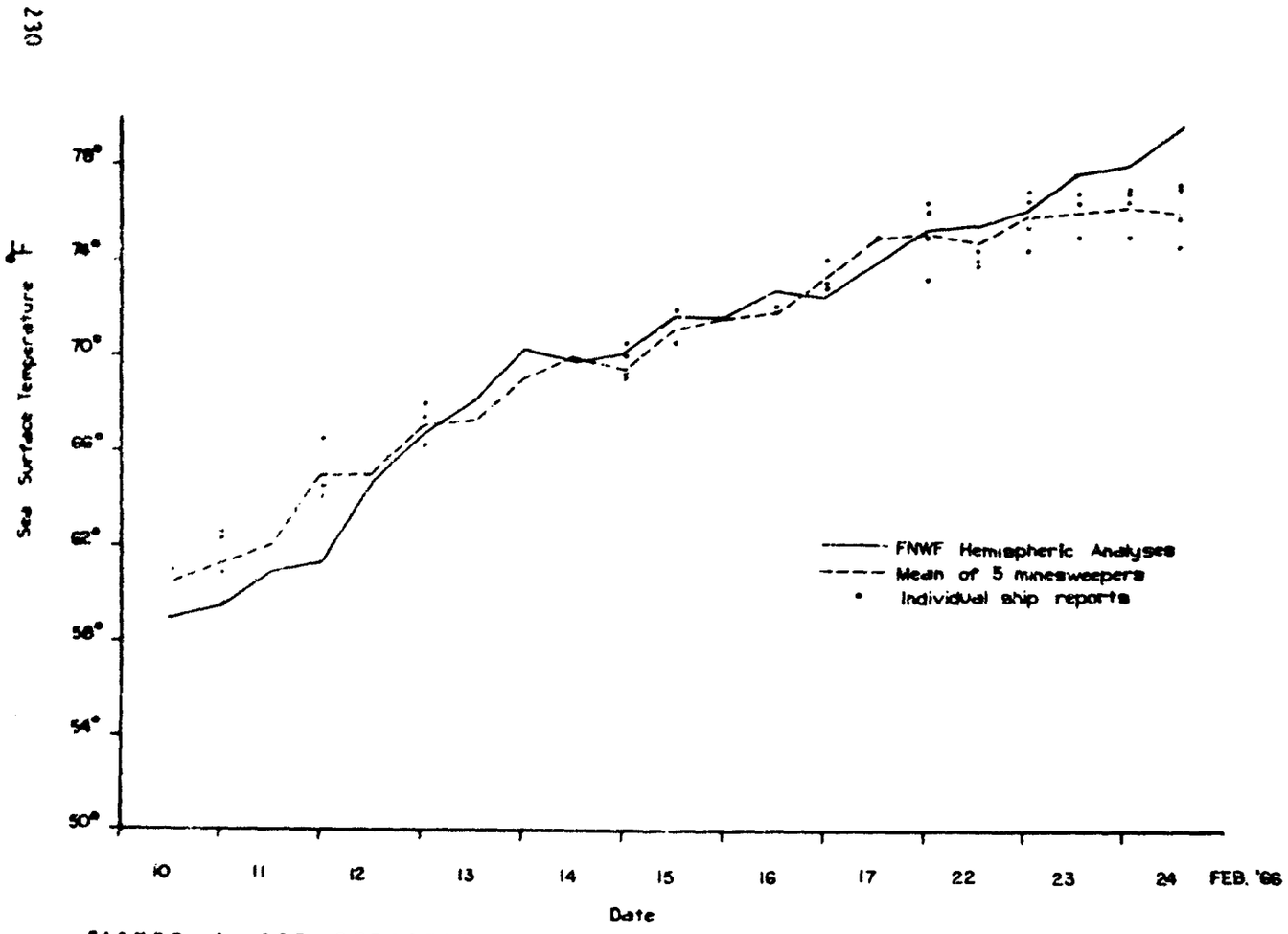

FIGURE 4. SST REPORTED BY MINESWEEPERS AND 12 HOURLY FNWF HEMISPHERIC SST ANALYSES FROM 10 TO 24 FEB 1966

well considering the conservatism in FNWF analyses in sparse data areas, and the fact that heavy winds in this area during the transit of Mine Division Seventy-One caused advective changes.

3.1.7 LaFond and Moore (1964) also found that the subsurface thermal structure fluctuations decreased with increased distance from the California Coast.

3.1.8 No true diurnal variations of SST were discernible in these data (none were expected on the basis of physical considerations).

3.2 Observational and Instrumental Biases and Errors

3.2.1 The bucket thermometer bias averaged 0.35°F, ranging from 0.0°F to 2.5°F. One group of thermometers had biases within the range of ± 0.3°F and a few thermometers had biases in the order of 0.2°F. The results here are, in general, higher than in condenser intake thermometers utilized for routine SST observations.

3.2.2 The reading accuracy ranged from ± 0.1°F to ±0.5°F. In routine SST observations the reporting accuracy is ±0.75°C (±1.35°F) due to present code limitations. Superimposed upon this are instrumental errors and biases.

3.2.3 In summary, the observational reporting errors and instrument biases exceeded considerably the thermal noise in most sea areas. Consequently, there is an urgent need for code format revision and instrument calibration and testing for reliable SST observations.

4. BATHYTHERMOGRAPH OBSERVATIONS

4.1 Difference between reference temperature and BT surface temperature

4.1.1 The difference between SST and BT surface temperature averaged 1.2°F (ranging from 0.0°F to 4.0°F. BT's with differences in excess of 4.0°F were not included in this sample).

4.1.2 The difference between SST and surface temperature for a given BT is not a constant value but shows erratic movements as well as some steady drift (Figure 5). The main causes of these differences and their fluctuations are the change in calibration of the instrument and improper positioning of the BT slide into the reader.

4.1.3 The BT surface temperatures were in general higher than the bucket temperatures. This positive bias has been observed before in lower latitudes. This can be attributed to operational procedures since the BT instrument temperature sensor tends to stabilize to the ambient temperature of the launching area of the ship; when the instrument is lowered in the ocean, sufficient time is not allowed for cooling in the surface water

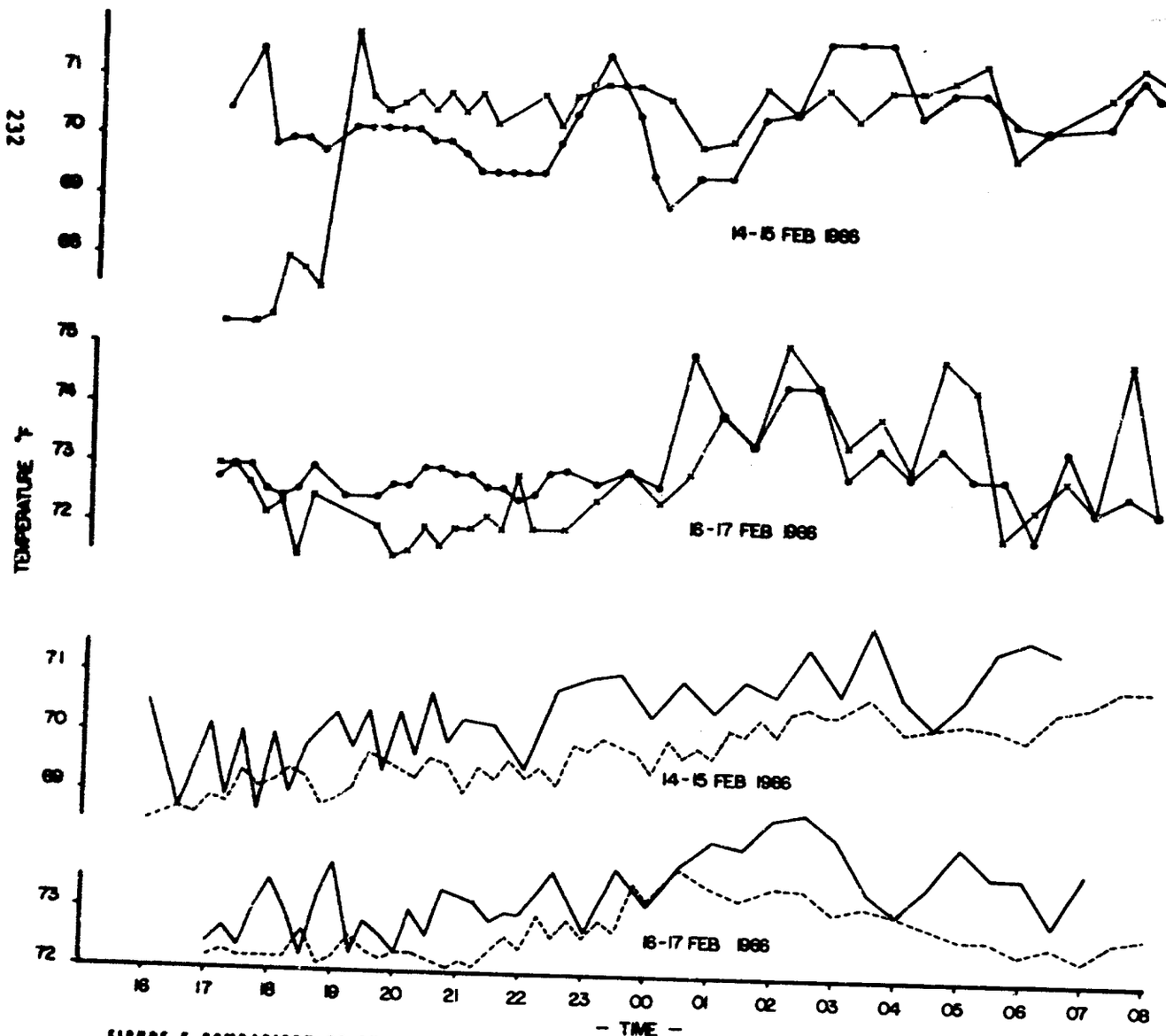

FIGURE 5. COMPARISON OF AN INDIVIDUAL SHIPS SST VERSUS HER BT SURFACE TEMPERATUE ON 14 TO 15 FEB AND 16 TO 17 FEB 1966 AND 5-SHIP MEAN SST VERSUS MEAN BT SURFACE TEMPERATURE DURING SAME PERIOD

(several minutes) prior to completing the BT cast. This cooling procedure is particularly difficult for fast moving platforms. Therefore, BT's should be brought to surface temperature by utilizing a running water bath if possible.

4.2 Differences in subsurface thermal structure between different ships

4.2.1 The greatest differences in subsurface thermal structure are caused by the off-calibration of the BT instrument.

4.2.2 There are also differences in the details of the subsurface thermal structure with depth (Figure 6). These differences could be caused by (a) small-distance real differences in the sea (LaFond 1964), (b) variations in BT response from instrument to instrument, (c) BT temperature and/or depth sensors not within calibration limits, and (d) different interpolation criteria used by individual operators.

4.2.3 The differences of subsurface thermal structure in very small time-distance intervals have been observed on a number of other occasions. This fact led Canadian authorities on the West Coast to conclude that a single BT observation is of little value. Canadian OCEAN procedures require 8 BT's at 15-minute intervals from station vessels or within 5 minute intervals from moving vessels. In addition, a catalogue of the means and approximate standard deviations of their individual operators is maintained to facilitate BT correction.

4.3 Differences in reporting BT soundings

4.3.1 In the area and season along the route of Mine Division Seventy-One, the inflections of thermal structure were not well pronounced. In addition, lack of standardization throughout the Navy in regards to interpretation and coding creates a problem in communications and synoptic utilization. Some ships overdo, some underdo the reporting of inflection points in a BT trace.

4.3.2 At FNWF the best analyses are derived from BT's which report temperatures at standard levels (at 100 ft intervals from 0 to 400 ft and at 200 ft intervals below 400 ft) and at significant inflection points between these levels. In other words, the coding of BT's should be analogous to upper air sounding procedures. The nations of the world, in cooperation with the World Meteorological Organization (WMO) have, through years of experience in recording, processing, training, and communications, devised a system to adequately report the earth's atmosphere that is reliable and universal. A similar coding system should most certainly be adopted for BT observations.

4.4 Transmission errors and other obvious errors in BT messages

It would be extremely time consuming to determine where transmissions errors occurred - from log to radioman, in first transmission, in retransmission, etc. Some errors are easy to recover in original messages without comparison with original logs (such as errors in tens of degrees, etc.). Other errors can only be discovered in comparison with original

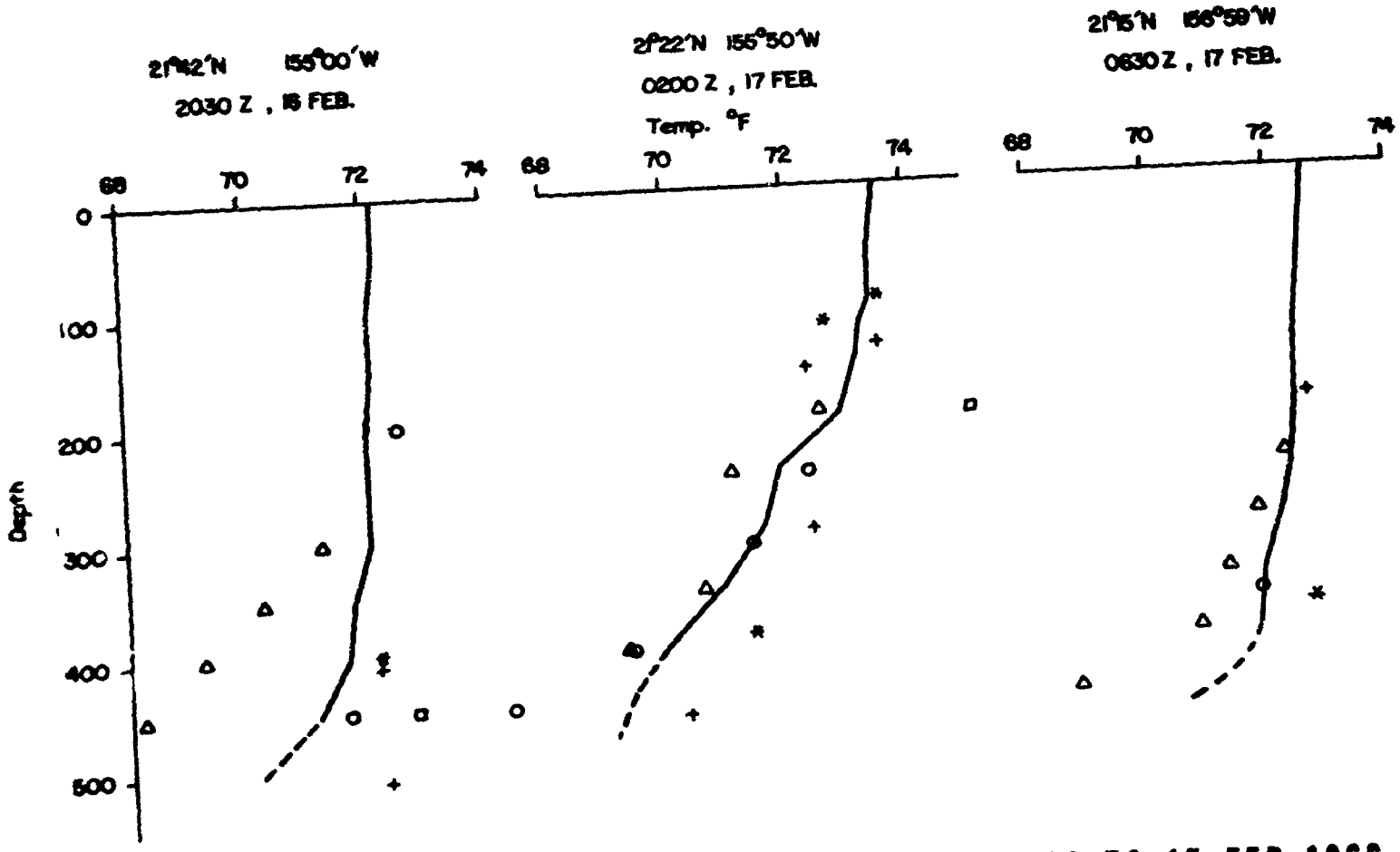

FIGURE 6. BT MESSAGES AT THREE LOCATIONS ON 16 TO 17 FEB 1966

logs, as was attempted in this exercise. In many cases a single error in a group makes the whole group useless and often a single error in the message, such as in the position group, makes the whole message useless. Almost 7% of all groups contained errors. There were more than 2 errors in one message in about 10% of the cases studied. (See Table II) These percentages are representative of the errors found in most BT messages received at FNWF.

In general, little specialized training in operational BT procedures is given to cognizant personnel; BT operations are considered a secondary speciality. Therefore, before any improvement in BT soundings can be realized, training and instruction in BT operational procedures must be instituted.

5. DEFICIENCIES IN INSTRUMENTS, INCLUDING OPERATIONAL PROCEDURES AND UTILIZATION

From the present study as well as from the general experiences at FNWF, the following recommendations are made covering instrumentation and procedures:

5.1 All thermometers used for environmental observations should be tested and calibrated periodically. For comparison, the BT's placed on the fishing boats by the Tuna Resources Laboratory, La Jolla, California are recalibrated approximately every 120 days.

5.2 Bucket surface temperatures with tested thermometers should be required until improved instrumentation is available. On such ships where bucket thermometers cannot be used, intake thermometers graduated in half degree increments should be installed. (At present most intake thermometers are graduated in two degree increments.)

5.3 BT operational procedures should be distributed and BT's which are more than three degrees from a calibration standard should not be used.

5.4 Shallow BT's (450 ft or less) should be converted to a deep sounding (900 ft) vehicle. Experience has shown that these BT's are harder to keep in calibration primarily due to operator error.

5.5 The construction of BT winches should be modified. The winches on board the minesweepers had only free fall, stop, and haul-in at full speed. This resulted in the loss or damage of many BT's. It is necessary that the winch provide gradual friction braking of the free fall and at least two hauling speeds.

6. SUMMARY AND CONCLUSIONS

This report has been prepared in summary form. Therefore, only the most important results are re-emphasized below.

Table 2

Types and frequency of more obvious errors in BT messages

Number of messages considered	321
Total number of groups	2253
Number of groups containing errors	152
Number of position groups containing errors	48
Two or more errors in one message	33

6.1 The procurement of instruments (thermometers, BT's, etc.) on short notice or for purposes above the authorized allowance established for a class of ship is too tied up in administrative red tape. Some activities do not consider the BT to be an expendable item despite the fact that many are lost or damaged. A pool of calibrated BT's for utilization in future exercises such as this should be established to reduce lead time in procurement.

6.2 The ambient thermal noise between Long Beach and Honolulu (in about 20 nautical miles) averaged less than 0.4°F. The observational range with bucket thermometer recordings was about 2.0°F in the same space scale. Thus the observational range was considerably higher than the thermal noise. In normal synoptic observations (vessels reporting intake temperatures) the observational noise is greater than 3.0°F.

6.3 The average difference between FNWF analyses and the recorded SST observations was 1.0°F (less than the observational noise).

6.4 No patterns could be recognized in thermal noise, except at the two oceanic frontal crossings.

6.5 The difference between SST and BT surface temperature is not fixed, but drifts with the instrument. It is in general positive in lower latitudes (BT temperature higher).

6.6 Subsurface thermal structure shows thermal noise and observational noise of the same or higher magnitude than SST observations.

6.7 BT observational procedures as exercised by the Canadian Navy (OCEAN Procedures) reveal several possible areas for adoption by our Navy.

6.8 BT slides should be read at standard levels (at 100 ft intervals down to 400 ft and at 200 ft intervals below 400 ft with significant inflection points included as required to define the structure).

6.9 Transmission errors cause considerable information loss in synoptic BT reports.

6.10 Instruments utilized in measuring SST should be calibrated periodically.

6.11 Shallow BT's should be converted for utilization to greater depths.

6.12 BT winch design should be improved.

6.13 Personnel should be trained to effect better quality control for all environmental observations (especially BT's) on board Navy vessels.

REFERENCES

ASWAC	Oceanography Subcommittee Report of the NSIA Fleet Measurement and Use of Oceanographic Temperature-Depth Profiles, Procedures and Recommendations.
LaFond, E. C. and A. T. Moore 1964	Measurements of thermal structure between Southern California and Hawaii with the thermistor chain.
Laevastu, T. and B. J. Rothschild Ms.	Movement of a water type boundary, persistence of water types and heat exchange along 150°West 15° to 25° North during January and February 1963.
Owen, R. W., Jr. 1966	Small-scale, horizontal vortices in the surface layer of the sea. J. Mar. Res. 24(1):56-66.
Pauls, K. H. 1965	A comparison of sea surface temperatures obtained by infrared radiation and in situ thermometers. Pacific Naval Laboratory, Esquimalt, Techn. Memo No. 65-5.
Saur, J. F. T. 1963	A study of the quality of sea water temperatures reported in logs of ships' weather observations. J. Appl. Met. 2(3):417-425.

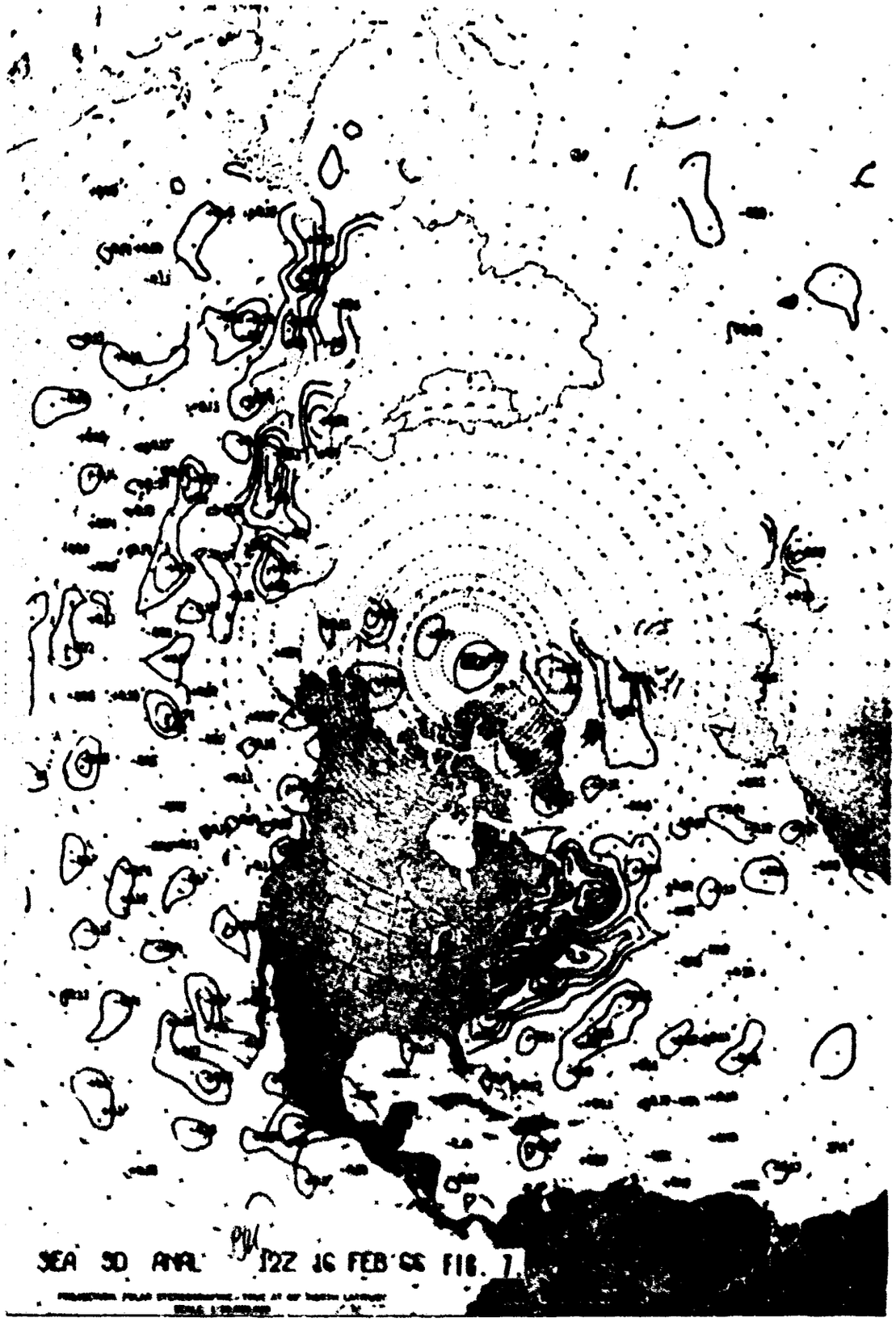
SEA SD ANAL 12Z 16 FEB 68 FIG. 1


SEA T ANAL 00Z 17 FEB 66 FIG. 1.
PROJECTION: POLAR STEREOGRAPHIC - TRUE AT 60° NORTH LATITUDE
SCALE: 1:60,000,000

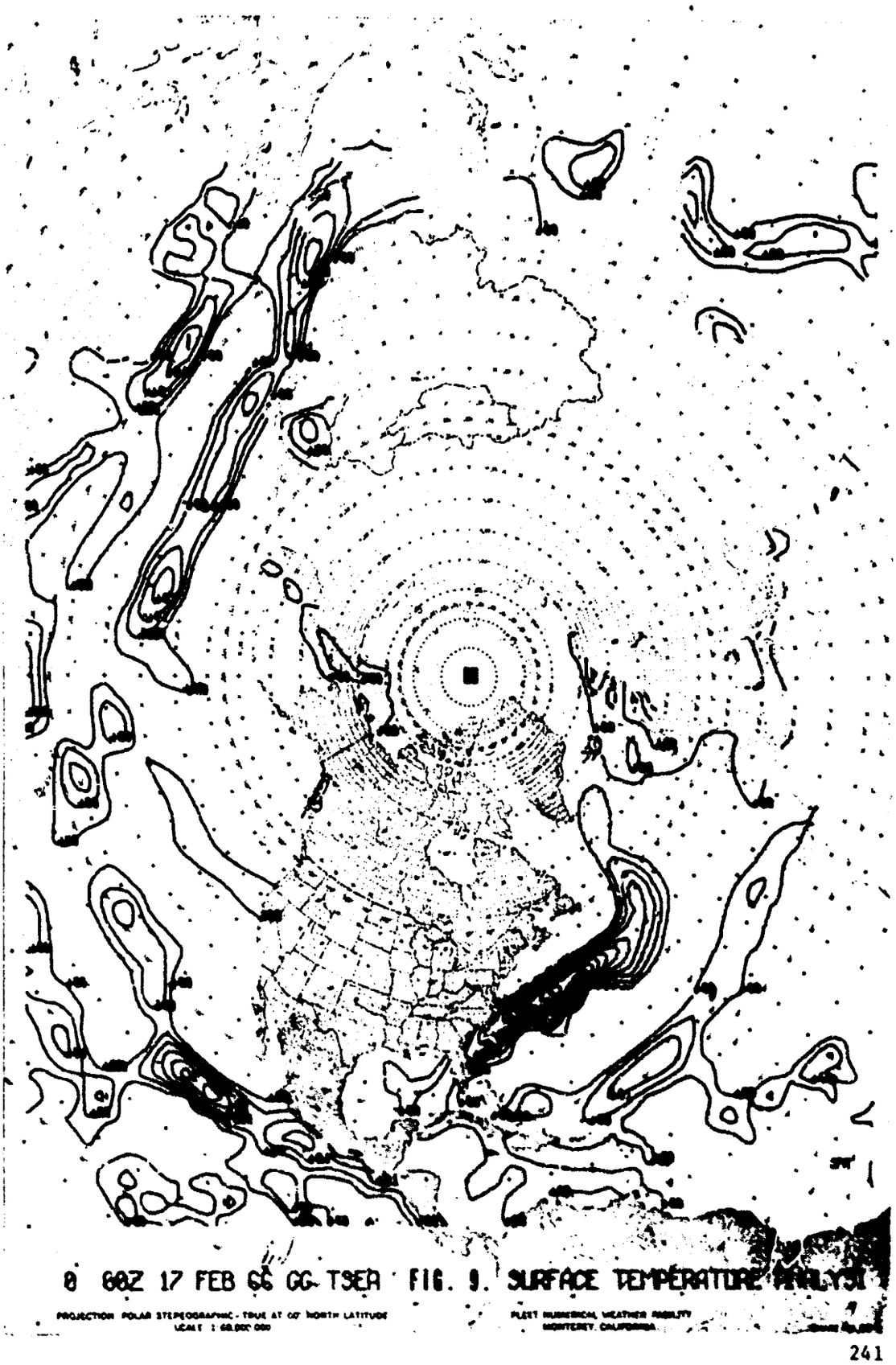

FIG. 9. SURFACE TEMPERATURE ANALYSIS

SUMMARY OF COMPUTER-ANALYZED TEMPERATURE DATA FOR PACIFIC AND ATLANTIC OCEANS

Margaret K. Robinson
Scripps Institution of Oceanography, La Jolla, California

INTRODUCTION

The BT Analysis Group at Scripps Institution of Oceanography is completing a computer analysis of bathythermograph (BT) and hydrographic station data in the Pacific and Atlantic Oceans. The Atlantic Ocean analysis has been done in collaboration with Elizabeth H. Schroeder, Woods Hole Oceanographic Institution. BT processing and analysis at Scripps Institution of Oceanography and Woods Hole Oceanographic Institution have been supported by the Office of Naval Research for many years. The National Science Foundation supported the development of the computer programs, and the U. S. Fleet Numerical Weather Facility provided the necessary funds for the analysis of the Pacific and Atlantic temperature data. The numerical values are already in use as the climatic guess-field for the oceanographic computer analyses and forecasts of the U. S. Fleet Numerical Weather Facility. Monthly charts of average temperatures for the surface, 100, 200, 300 and 400 ft., and average thermocline depths are being prepared for publication in atlas format by the U. S. Naval Oceanographic Office.

In practice, mean temperature distributions at selected levels are more useful to oceanographers than to the men in the fleet. However, climatological summaries of the ocean environment are of potential value for operational planning, or for tactical use on shipboard to supplement on-the-spot observations and short-term forecasts, or when such information is not available to the ship. A major concern to the oceanographer is how best to describe the oceanic environment in the way most useful to the Navy user. In addition to atlases of mean temperatures, a real need exists to publish mean temperature data in graphical formats to meet specific Navy purposes. Suggested formats are illustrated, and their potential application to Navy problems discussed.

METHOD OF ANALYSIS

The mean temperature values are based on available BT and/or hydrographic station data. Mean temperatures by 1° squares at selected depth levels are first computed. Then, a space interpolation is performed which computes approximate temperature values for all 1° squares where no data existed. The 2-dimensional space interpolation program used is a solution of Laplace's equation. The interpolated values, together with observed values, are smoothed by successive averaging along latitudinal and longi-

tudinal axes in the second step of the analysis. The third step performs an harmonic analysis of the 12 monthly values obtained by the space-smoothing. A truncated summation over the annual, semi-annual and ter-annual harmonics is made, and it is these space- and time-smoothed mean values which we propose to publish in atlas format.

The next step in the analysis computes several quantities along the temperature depth curve for all months for each 1° square. These include (1) temperature differences between 100 ft. levels, (2) temperature differences between the surface and 400 ft., (3) cumulative temperature differences by 100 ft. intervals between the surface and 400 ft., and (4) the depth at which the temperature is 2°F less than the surface temperature.

TOP OF THERMOCLINE (Depth of T_0 -2°F)

Knowledge of the mean depth of the thermocline is essential for prediction of sonar performance in the surface layer. We have chosen to define the depth of the top of the thermocline as that depth at which the mean temperature is 2°F less than the mean surface temperature. This definition is somewhat different from that of "mixed layer depth". The averaging and smoothing processes to which the temperature data have been subjected minimize the effect of internal waves at the thermocline but cannot eliminate the effects of transient heating and cooling at the surface from the average temperature values. Therefore, in order to distinguish between small transient negative gradients and the large gradients in the seasonal and permanent thermoclines, we have selected minus 2°F as the critical temperature difference for deriving the top of the thermocline from smooth average temperatures.

In summer, in northern latitudes where a seasonal thermocline is well developed and the break in slope is very sharp, the bottom of the mixed (isothermal) layer and the surface temperature minus 2°F depth are close together. However, in the tropics, and in winter and spring in northern latitudes, when the top of the thermocline is ill-defined and small transient negative gradients may occur throughout the water column, the surface temperature minus 2°F depth can be expected to be found at the top of the permanent thermocline. The thermocline top, as derived by this method, is the net effect of the dynamics of the current systems and the local heat budgets.

In Figure 1, the depth of the top of the thermocline by this definition is shown for the Pacific Ocean in the region of the Kuroshio for the months of March and August, and in Figure 2, for the Gulf Stream area of the Atlantic Ocean for the same two months. The stippled areas in March indicate areas where the temperature did not decrease 2°F in 400 ft. Not portrayed by this type of presentation is the increase of temperature with depth which is found in the north. The thermocline topography in the Pacific, in March, is more irregular than in the Atlantic. Numerous islands and irregular bottom topography of the Western Pacific give rise to more irregular thermocline topography--both in winter and summer--than

is found in the Western Atlantic. Irregular bottom topography, and the intrusion of warm water of the Tsushima Current into the Sea of Japan results in the shallow thermoclines in this region in winter. The ridge along the left side of the Kuroshio is less well-defined by the selected contour intervals than that along the Gulf Stream. The synoptic picture would find the mean thermocline topography perturbed by internal waves of at least 25 feet in amplitude, and the general configuration would be altered by eddies or waves along the current axes.

MAGNITUDE OF THE THERMOCLINE

The magnitude of the thermocline determines to what extent sound waves are bent by the temperature gradient and how large the shadow zone is. We represent the magnitude of the thermocline by the mean temperature difference between the surface and 400 ft. This definition is based on the assumption that there is a mixed layer above the thermocline, and, therefore, the surface temperature is a good estimate of the temperature at the beginning of the thermocline. The interpretation of these differences, however, must be governed by the fact that the 400 ft. level is not the bottom of the thermocline--particularly, in subtropical and tropical regions. Seasonal variation below 400 ft. is minimal, and a single difference chart will be prepared to describe the additional decreases in temperature between 400 ft. and the bottom of the permanent thermocline.

Figure 3 presents the temperature difference (°F) between the surface and 400 ft. for March and August for the Kuroshio Region of the Pacific, and Figure 4 shows this difference for the Gulf Stream region of the Atlantic. Plus numbers indicate an increase of temperature with depth. The 37°F temperature difference in August in the Japan Sea, and the 29°F difference east of Honshu are the outstanding features of the Pacific Region. The large area north of the Gulf Stream, where positive gradients up to 8°F are found, is the principal feature of the March Atlantic chart. Maximum differences in the Atlantic, in August, are 21°F.

TEMPERATURE DIFFERENCES BETWEEN 300 AND 400 FEET

A knowledge of the temperature gradient at mid-depths is of importance in the use of variable depth sonars. These gradients are approximated by the mean temperature differences between 300 and 400 ft. and are presented for March and August in Figure 5 for the Pacific, and in Figure 6 for the Atlantic. The stippled areas in the two charts indicate that the gradient is less than $\pm$ 0.5°F per 100 ft. Gradients are somewhat less in the Bermuda, Sargasso Sea area, in August, than in similar regions of the Pacific. In the southeastern portions of the Japan Sea and west of the Ryukyu Chain, the gradients are large and variable in both March and August.

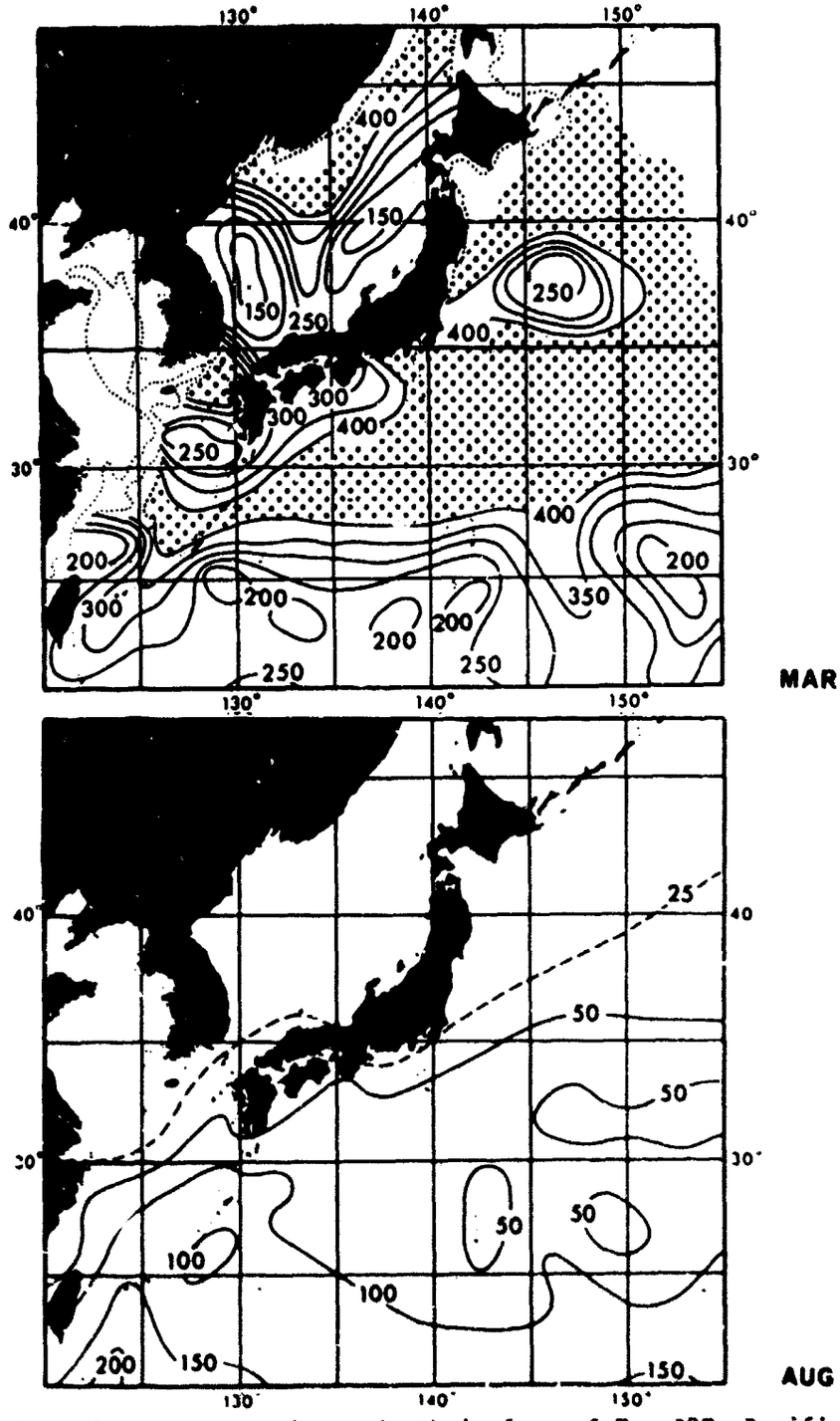

Fig. 1 Top of the thermocline - depth in feet of T_0 -2°F, Pacific. Stippled areas indicate temperature did not decrease 2°F in 400 feet.

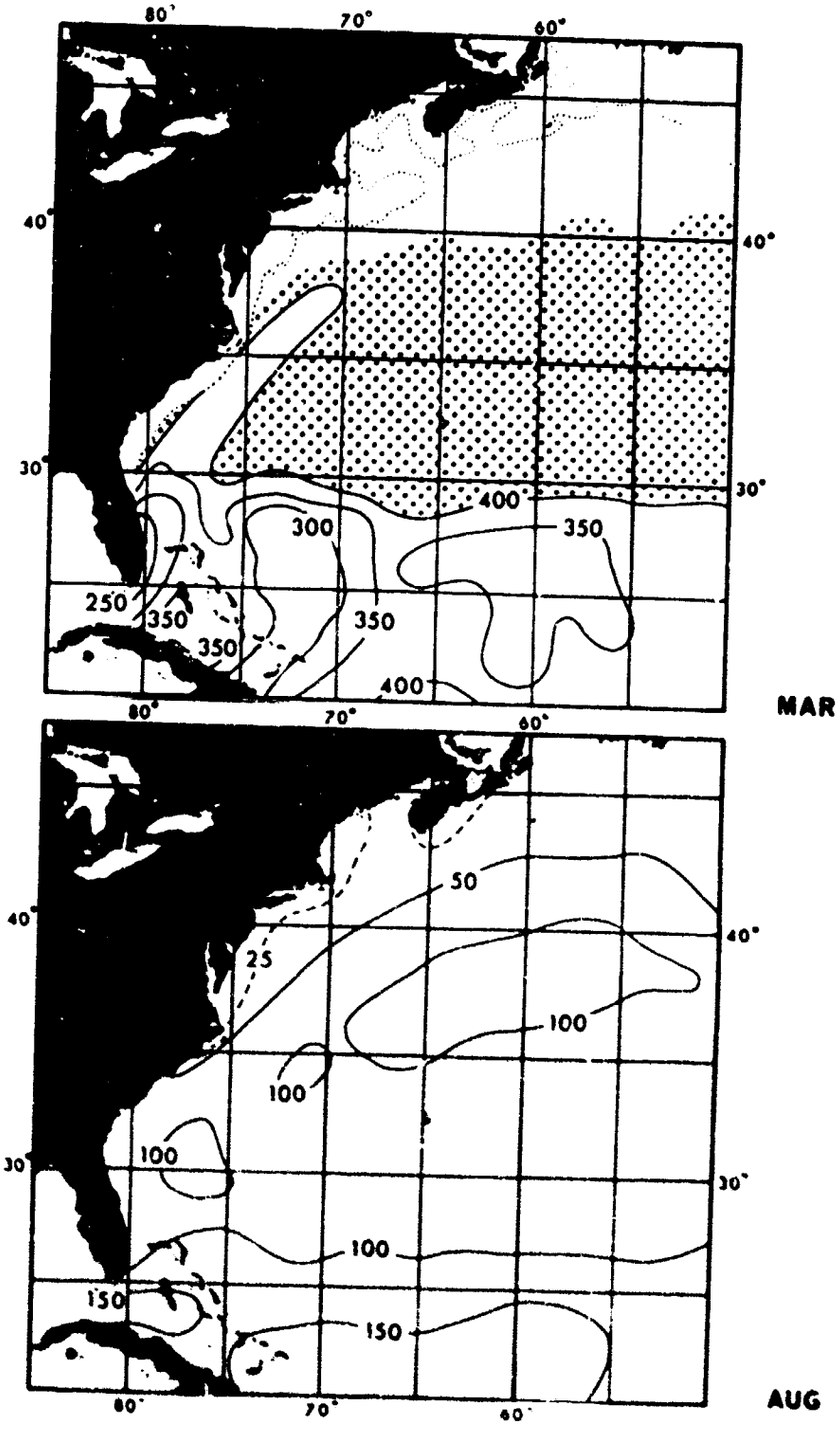

Fig. 2 Top of the thermocline - depth in feet of T_0 -2°F, Atlantic. Stippled areas indicate temperature did not decrease 2°F in 400 feet.

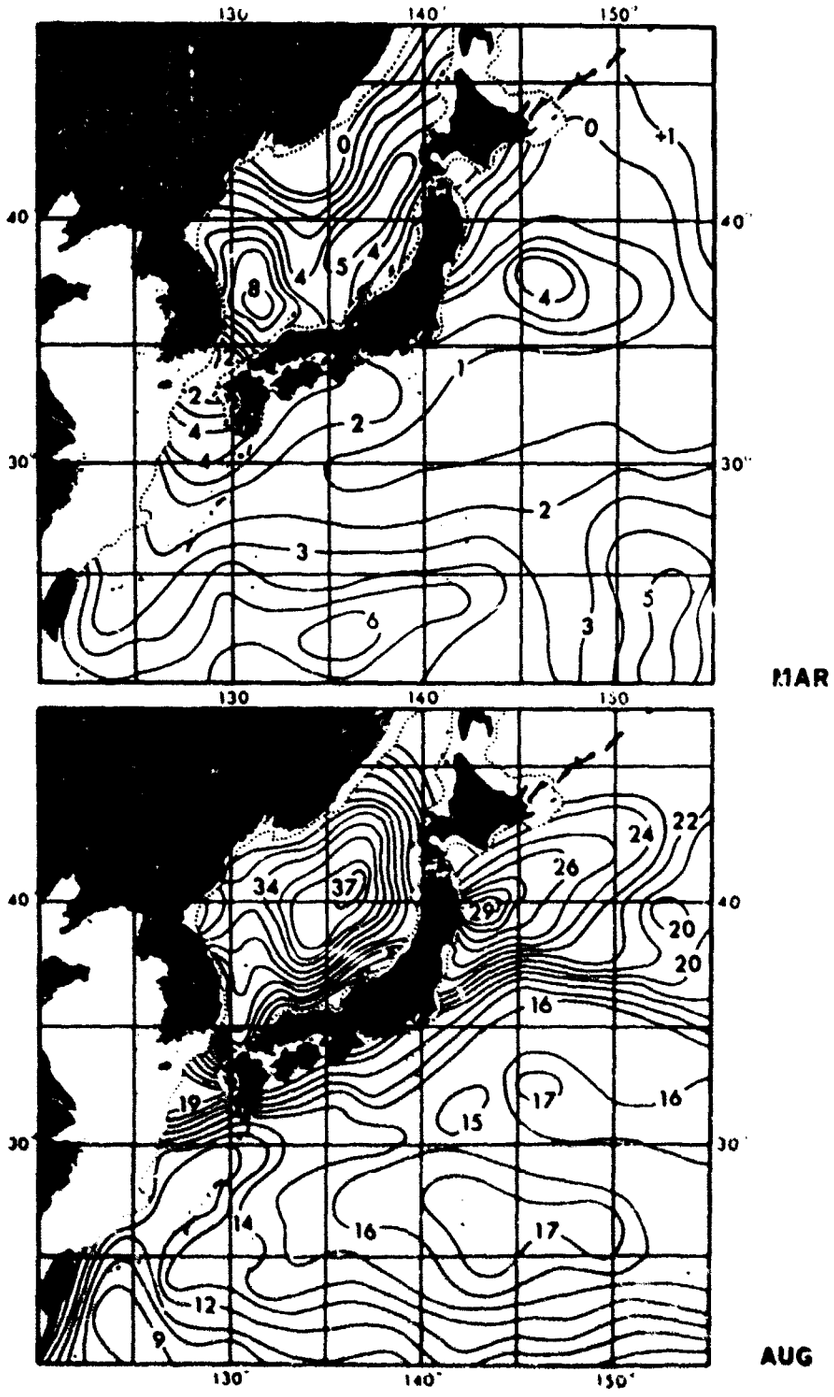

Fig. 3 Magnitude of thermocline - temperature differences in °F between the surface and 400 feet, Pacific. Plus numbers indicate increase of temperature with depth.

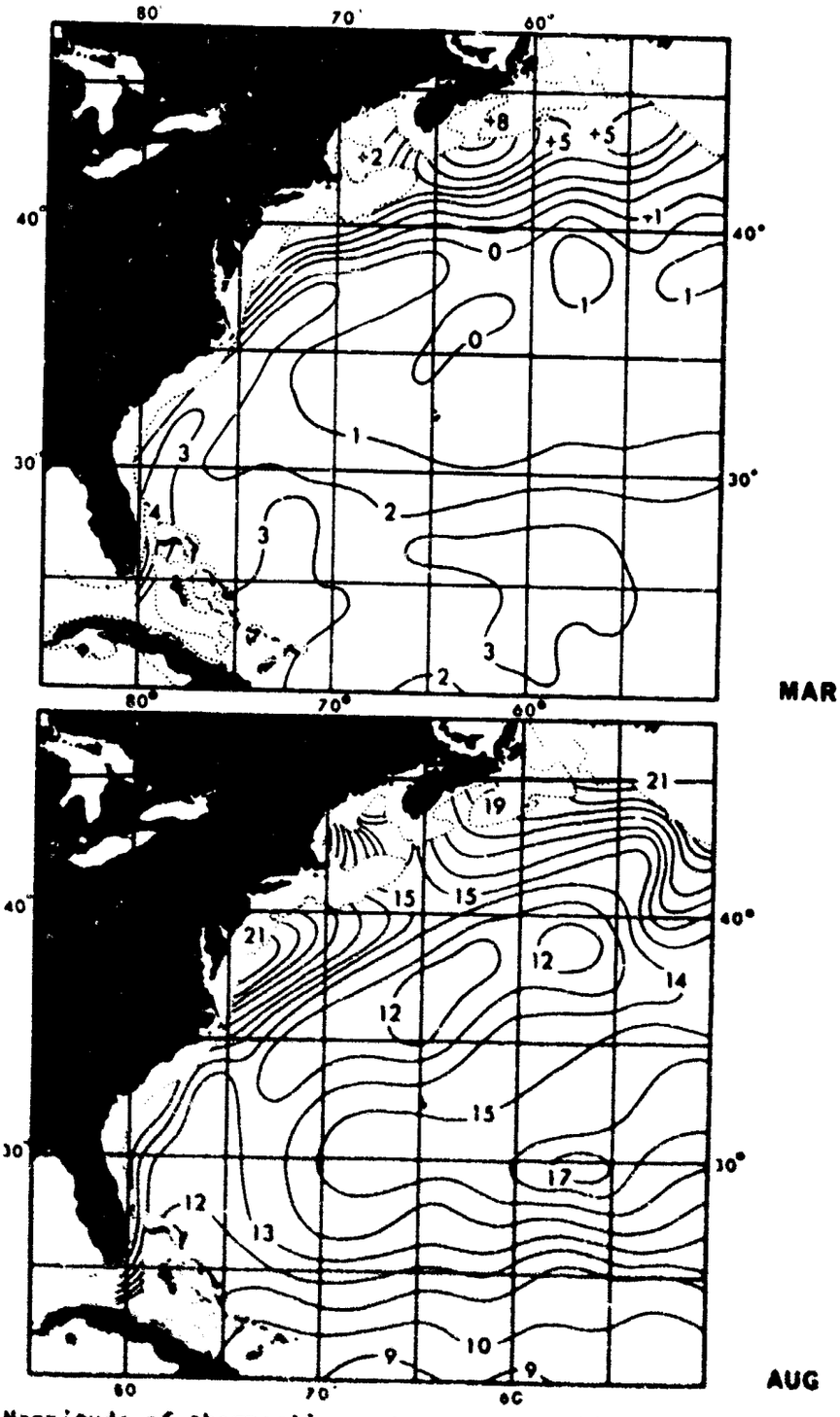

Fig. 4 Magnitude of thermocline - temperature differences in °F between the surface and 400 feet, Atlantic. Plus numbers indicate increase of temperature with depth.

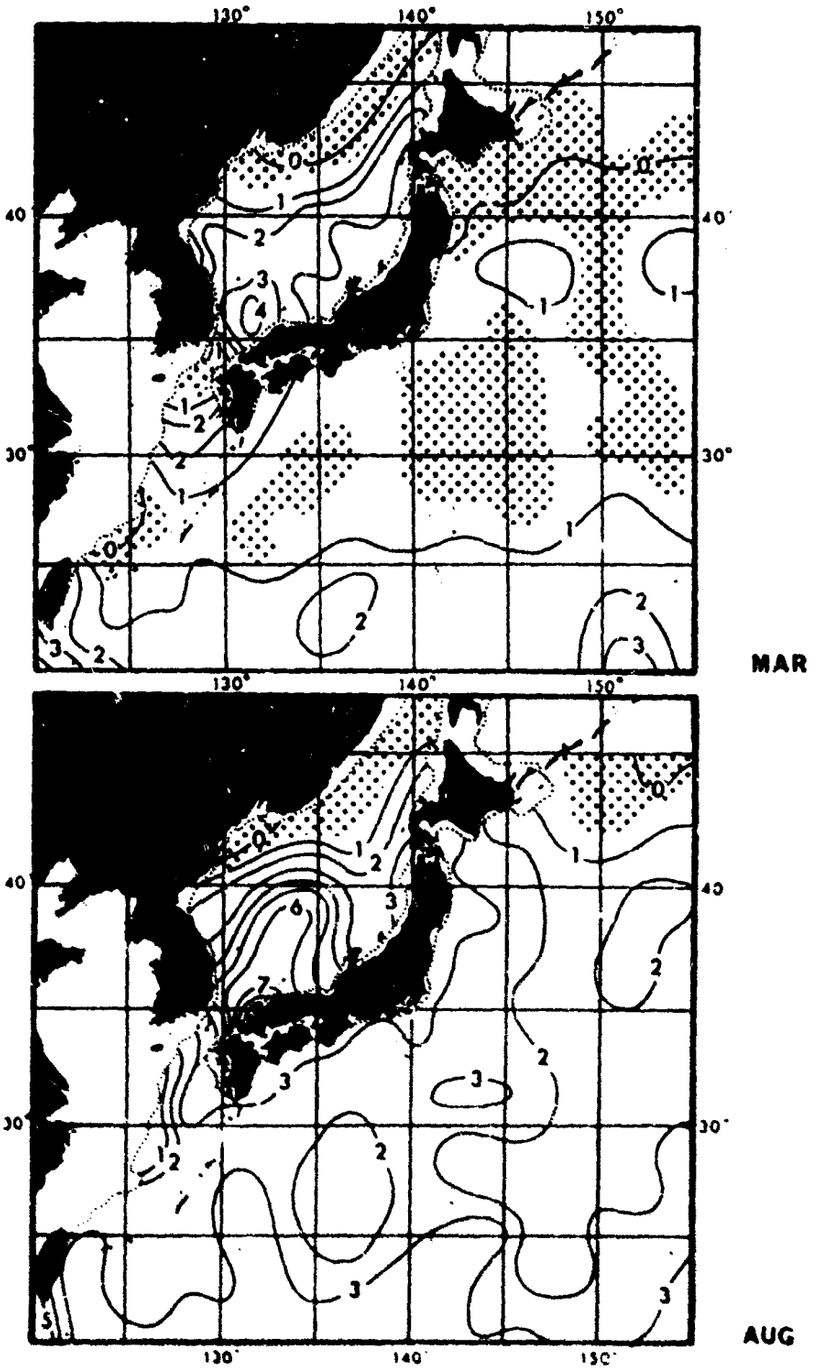

Fig. 5 Temperature differences between 300 and 400 feet, Pacific. Stippled areas indicate gradient less than ± 0.5°F.

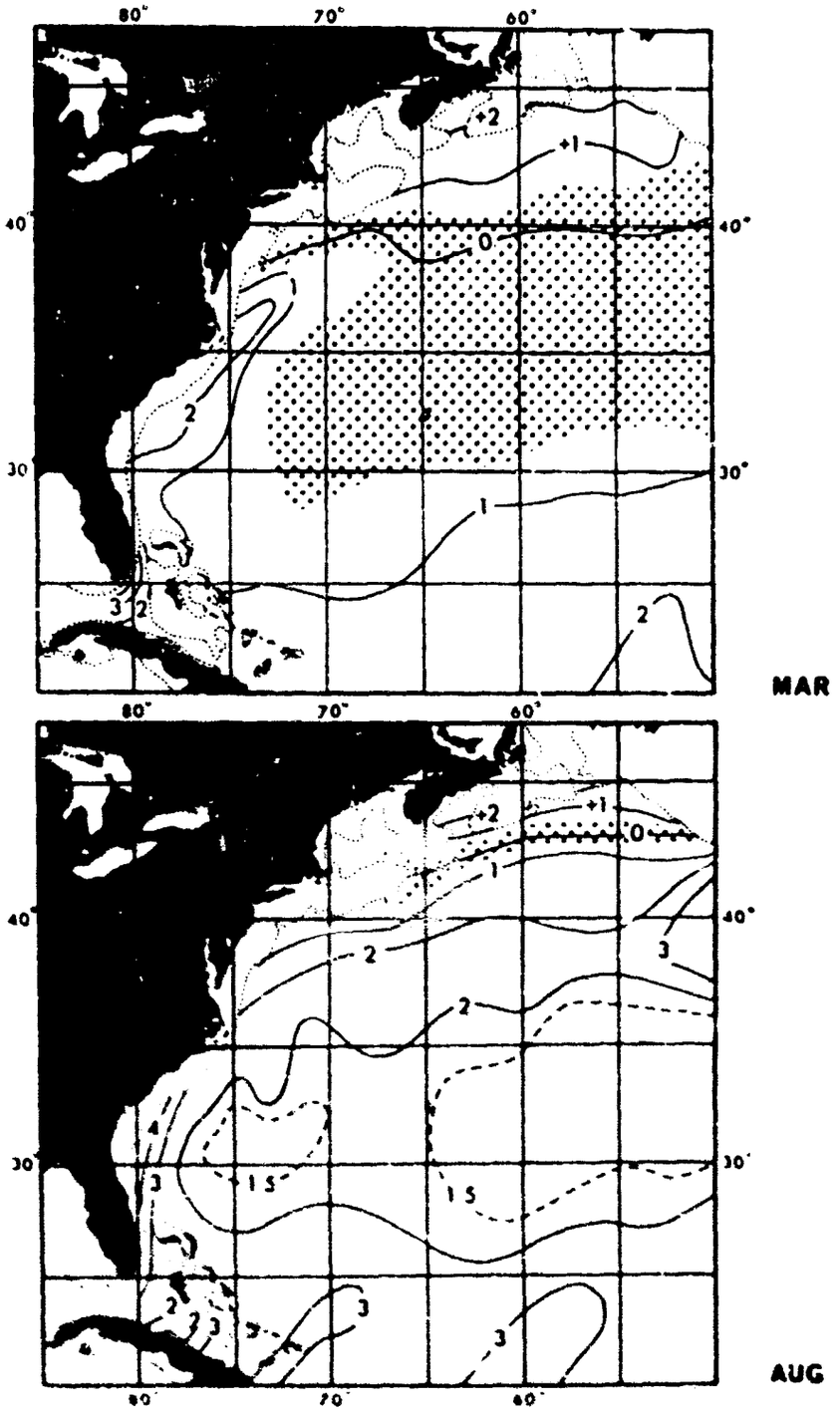

Fig. 6 Temperature differences between 300 and 400 feet, Atlantic. Stippled areas indicate gradient less than ± 0.5°F.

AVERAGE TEMPERATURE-DEPTH SECTIONS

Average temperature-depth sections along selected routes provide indications of sonar conditions to be encountered and permit selection of best submarine cruising depth and other criteria. Such sections can be readily constructed, in any direction for any month, from average temperature charts at the surface and at selected depth levels. The mean temperatures which will be published in atlas format will be on the Mercator projection, and any track laid out on these charts will be proportional to actual distances traveled. Figure 7 is an illustration of the graphical construction of a vertical temperature section from the Coast of California toward Hawaii. The proposed course is marked on the temperature charts for the surface and each depth level. On a transparent overlay, a grid is drawn whose horizontal distance equals the length of the proposed track. The vertical scale is arbitrarily chosen; for example, 1" = 100'. The grid is completed by drawing depth lines at appropriate spacing for each temperature chart (i.e., 100, 200, 300 and 400 ft.)

The overlay is then placed on the surface temperature chart, with the surface grid line lying on the ship's proposed track line. Ticks are made at points where isotherms cross the track. The value of each tick should be labeled on the grid. Next, the transparent grid is placed on the 100 ft. temperature chart. This time, the 100 ft. grid line lies on the ship's track. Again, ticks are made for each isotherm, and its value labeled. The same procedure is followed for successive depth levels, with grid line depth and temperature chart depth always corresponding. When all levels have been ticked, ticks of equal value are connected to complete the vertical section.

gure 8 compares average vertical sections, constructed as described above, with sections based on actual BT observations. These two sections cover approximately the same track as that used in Figure 7; namely, San Francisco to Hawaii. The BT observations were taken by the U.S.S. NEREUS in July 1947, and the U.S.S. MAURY in September 1947, at 2-hour intervals. For simplicity, only every fifth isotherm is shown. There is good agreement in both sections between the average location of the isotherms, both at intermediate depths and at the point where the isotherms intersect the surface; however, the isothermal surfaces are perturbed in the actual BT observations by as much as 75 feet. Oscillations in the depth of the thermocline due to internal waves can be deduced from the oscillations in depth of isotherms. It is not possible, as yet, to predict the amplitude of these oscillations. In any given synoptic situation, however, one must realize that the observed depth of an isotherm or thermocline will not remain constant. The probable variability in depth of the thermocline must be considered in dealing with both the synoptic and the mean values. Thermocline depths may differ greater between successive synoptic observations than either observation may differ from the mean value. An observed thermocline depth may, therefore, be more misleading than the estimated mean thermocline depth.

DETAIL OF THE TEMPERATURE STRUCTURE AT SINGLE LOCATIONS

For operational planning, it may be necessary to look at the details of the temperature-depth structure at selected locations. To demonstrate the capability now existing to adapt the graphical presentation of the average temperatures to specific Navy requirements, we have selected from Figures 3 and 4 the one-degree square area 39°N, 143°E in the Pacific, and 38°N, 73°W in the Atlantic. These are areas having large temperature differences, surface to 400 ft.

a. In Figure 9a is presented the annual cycle of cumulative temperature differences between the surface and 400 ft. at 39°N, 143°E, and Figure 9b is a similar graph for the Atlantic area, 38°N, 73°W.

Figures 10a and 10b present temperature gradients per 100 ft. in the same two areas.

Both presentations emphasize time changes. The cumulative differences stress total changes surface to 400 ft. The gradients stress individual layers and clearly represent the change of depth of maximum temperature gradient with season. The thermocline structure is more readily seen in gradient graphs, but it is not convenient to pick off scalar quantities from either representation.

b. In Figures 11a and 11b, in polar coordinates, we have plotted the annual cycle of cumulative temperature differences at the same two locations. In these graphs, one can easily scale either cumulative differences or gradients, but the thermocline structure, itself, is not evident.

c. In none of the previous presentations are absolute temperatures made available. In Figures 12a and 12b, the mean temperatures at the selected 100 ft. intervals are plotted as continuous annual cycle curves. These curves are generated from the harmonic coefficients derived in the original temperature analysis program. The plots are based on weekly values and the figures are photographed directly from the machine plots. In addition to the absolute values, these annual cycle curves can be scaled to give both cumulative differences and gradients per 100 ft. These curves are perhaps of more interest to the oceanographer than to the Navy man because in no other format is the change in the seasonal cycle with depth so evident.

At 39°N, 143°E, a marked double cycle develops below the surface which is only slightly developed in the curves at 38°N, 73°W. In spring, there appears to be warming throughout the column but when the thermocline becomes well-defined and stability in the layer increases, transport of heat across the thermocline appears to be

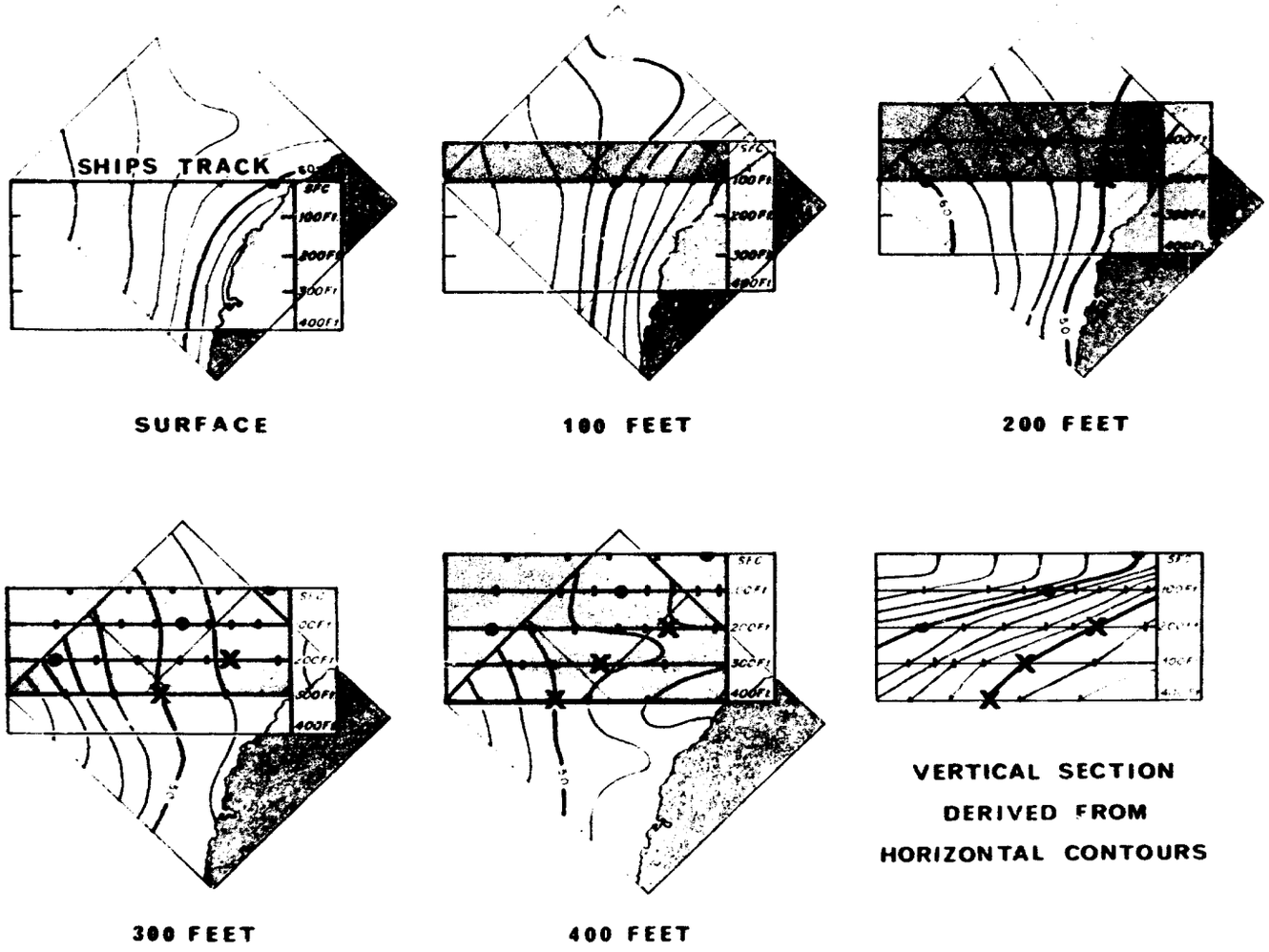

Fig. 7 Graphical method for constructing vertical temperature sections.

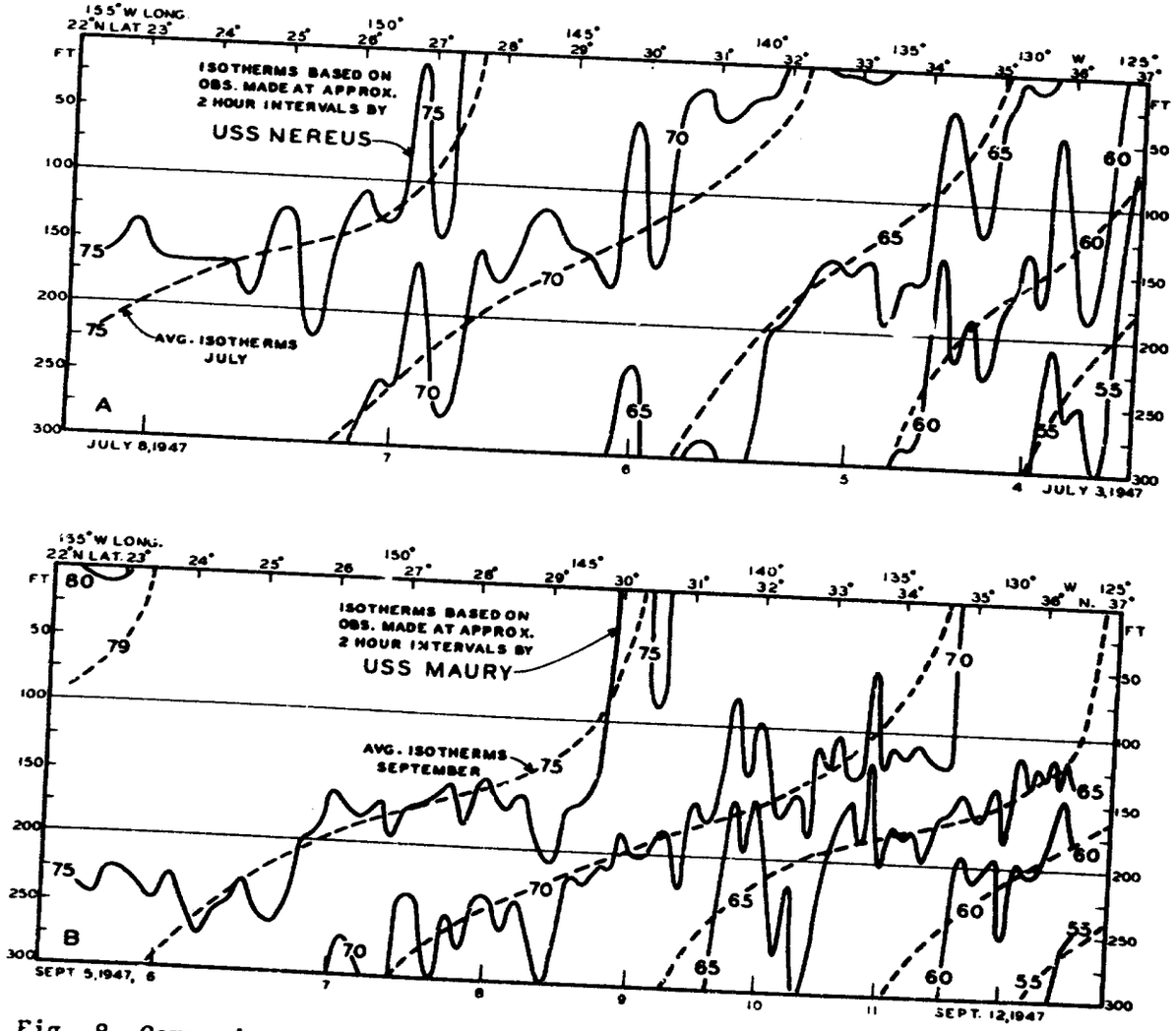

Fig. 8 Comparison of vertical sections based on individual and smoothed average BT temperatures.

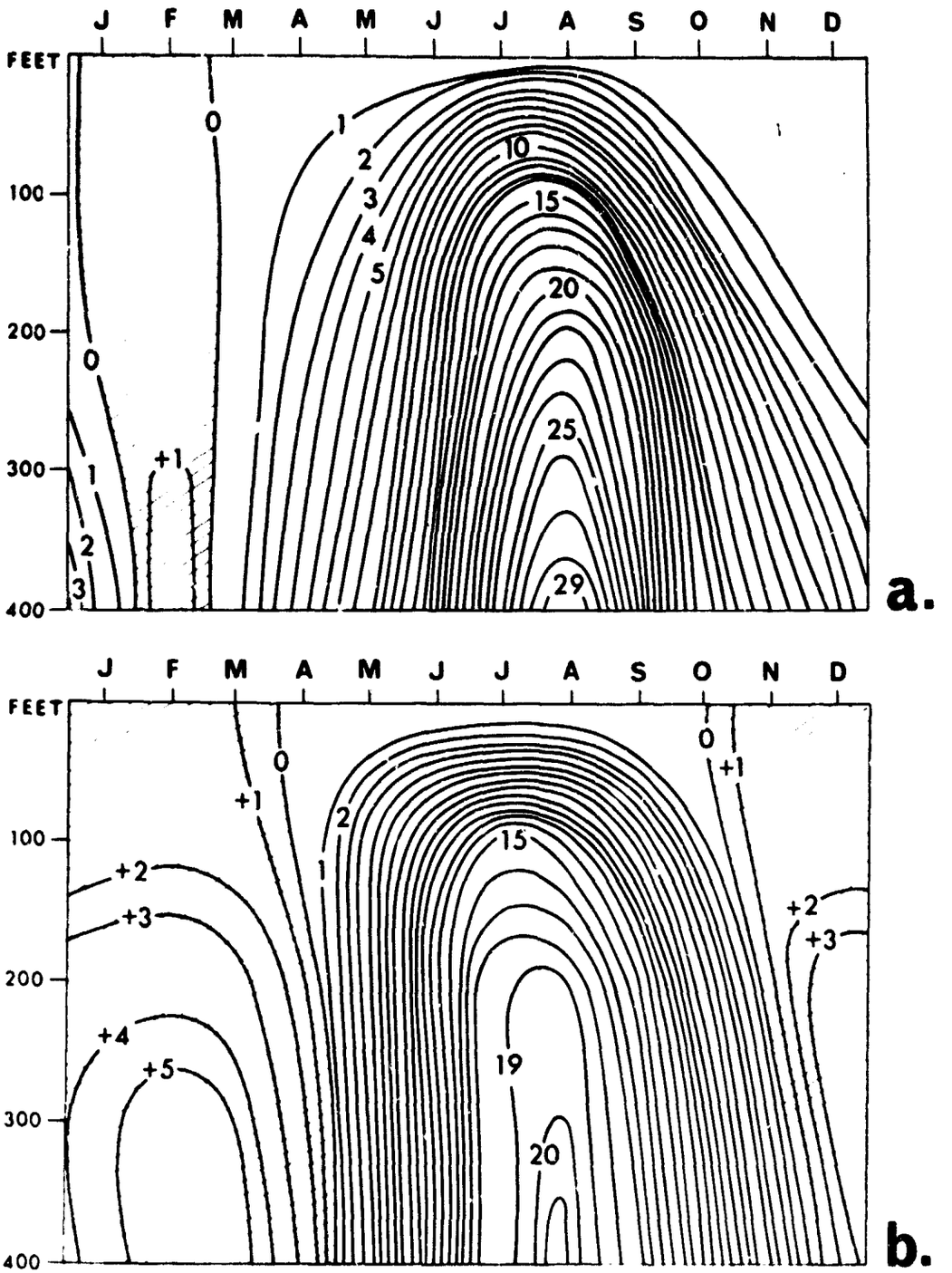

Fig. 9 Annual cycle of cumulative temperature differences: a. 39°N, 143°E; b. 38°N, 73°W.

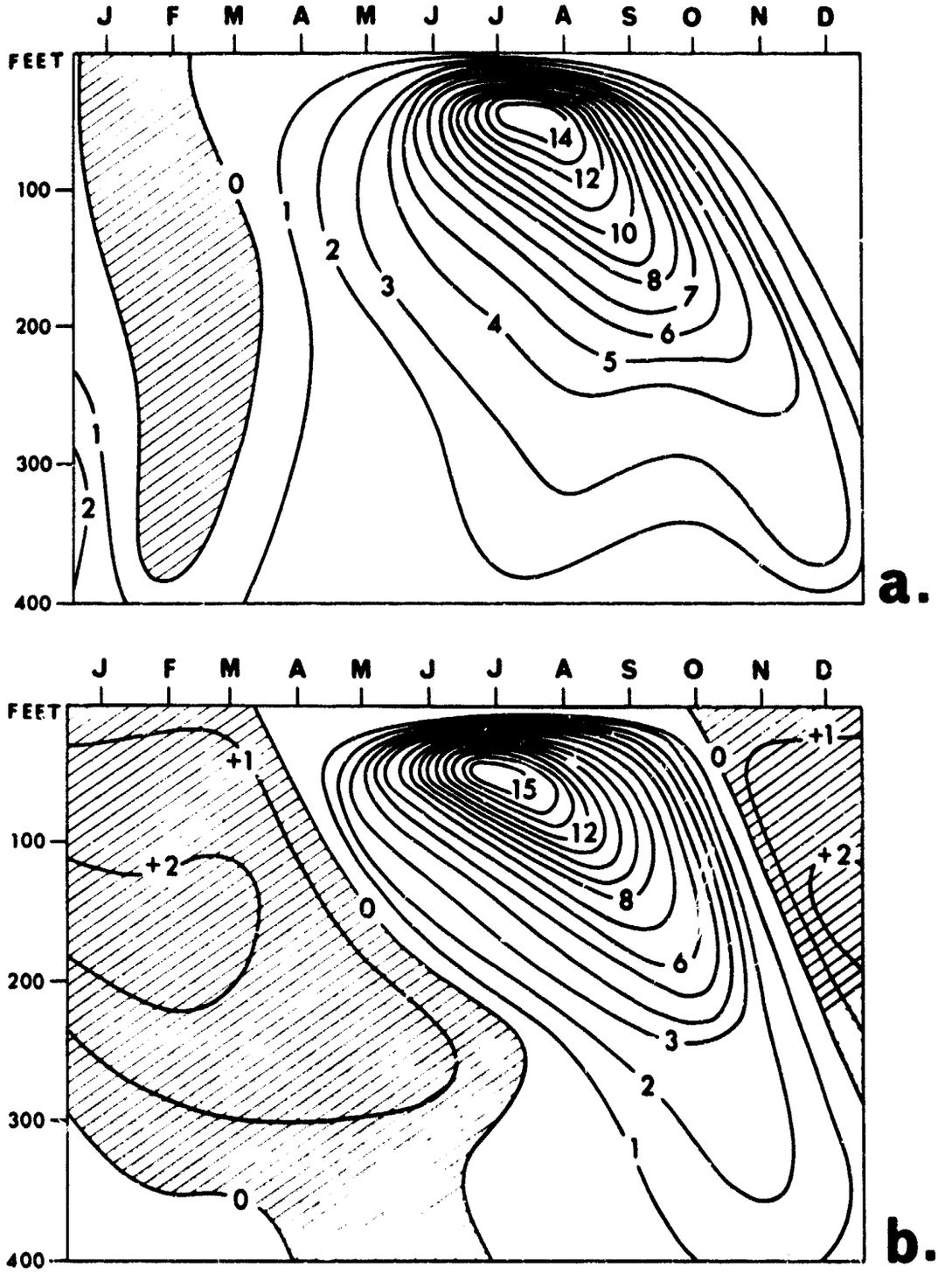

Fig. 10 Annual cycle of gradients per 100 feet:
a. 39°N, 143°E; b. 38°N, 73°W.

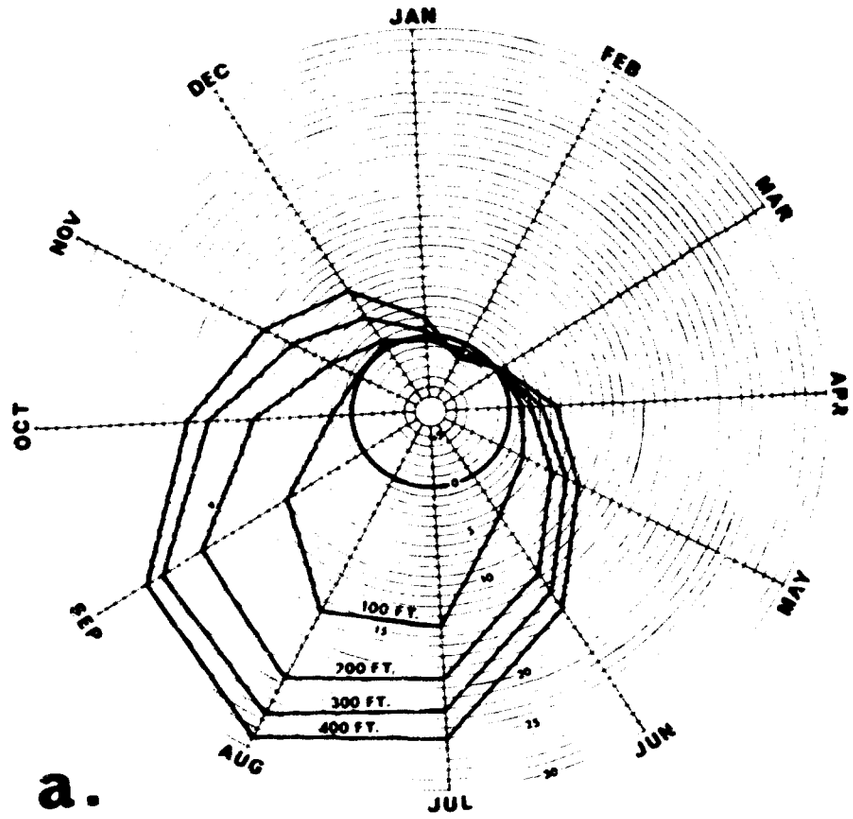

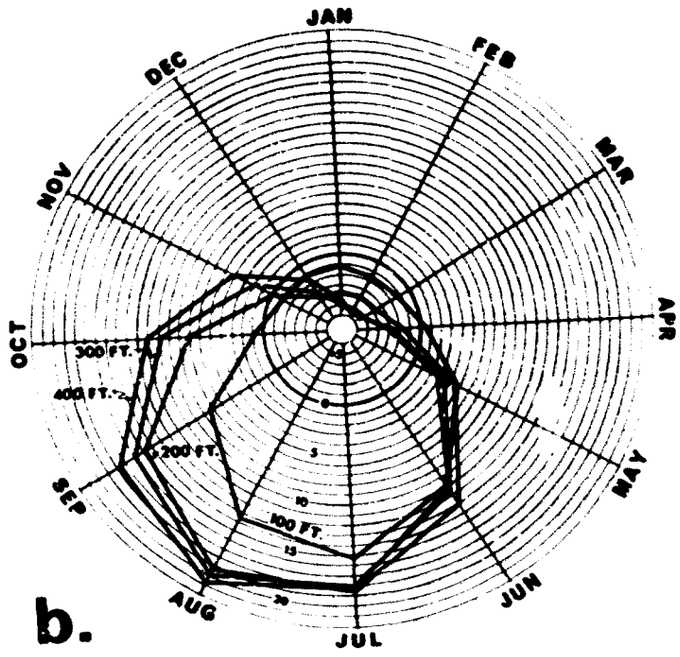

Fig. 11 Annual cycle of cumulative temperature differences in polar coordinates:

a. 39°N, 143°E; b. 38°N, 73°W.

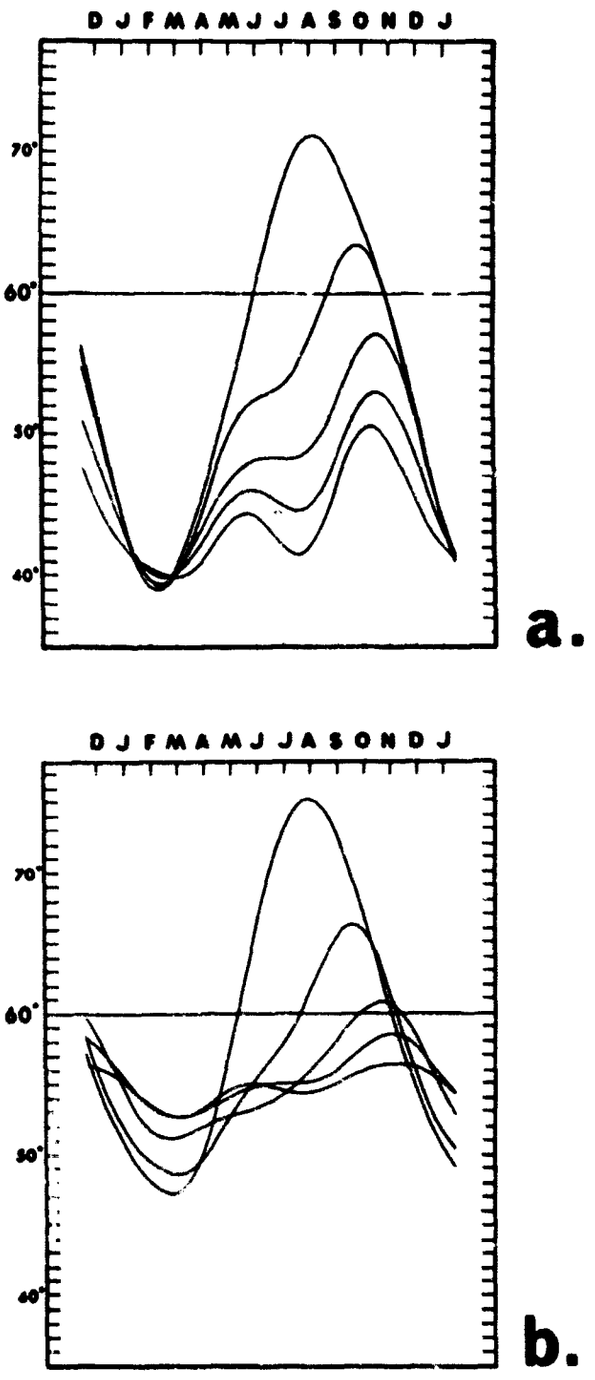

Fig. 12 Annual cycle temperature curves:
a. 39°N, 143°E; b. 38°N, 73°W.

impeded, and beneath the thermocline the temperature may actually decrease by either of two mechanisms--advection, or mixing with the cooler water below. When cooling at the surface begins in the fall, and convective mixing takes place, temperatures increase at the deeper levels until winter isothermal temperatures are reached.

At 38°N, 73°W, in winter, cold, low salinity water lies above warmer, high salinity water, and convective mixing is limited. The extension of the Continental Shelf and Grand Banks shallow areas as far as 50°E prevents the flow of deeper, cold Labrador Current water into the region, and the increase of temperature with depth occurs as shallow as 100 ft. This is not the case off Japan where cold, low salinity Oyashio water is found down to depths greater than 300 ft. at 39°N, 143°E in winter, and the first indication of an increase of temperature with depth is on the 400 ft. mean charts.

The higher Atlantic temperatures at all times and depths cannot be accounted for by the 1° difference in latitude at the two locations. The greater mass transport of the Gulf Stream system carries warmer water farther north than does the Kuroshio.

THE RELATION OF AN INDIVIDUAL TEMPERATURE-DEPTH OBSERVATION TO THE MEAN TEMPERATURE-DEPTH STRUCTURE

It is necessary to know to what extent the averaging processes alter the temperature-depth structure and how well the average structure represents what is found in a synoptic observations.

In August 1964, the FASOR Expedition of the U.S.S. DAVIS made observations in the Western Pacific. In Figure 13, an inner envelope is drawn showing the range of the BT curves for four BTs taken in a 3-hour period by the FASOR Expedition. The outside envelope is based on four BTs taken in three different years. The mean temperature at this location, derived from these data by our computer analysis, is portrayed by dots at selected levels. The outer BT envelope indicates that there are very large year-to-year differences in absolute temperatures in this area. However, the mean temperature values did not depart more from the FASOR envelope than the FASOR BTs did from each other in three hours. The important point is that the sonar conditions did not change significantly with shifts in the temperature-depth curves, and the computed average values remained typical of sound conditions to be encountered.

A similar situation is shown in Figure 14. In this figure is shown the envelope of 1,000 BT observations taken on the FLIP Expedition, between September 2 and September 29, 1963 within the one-degree square, 39°N, 69°W. Within the envelope is shown a curve for one of the BTs taken on September 15, the mid-month point. Also shown are the average temperatures for this square from the computer analysis. Only one [illegible] observation had previously been taken at this location. In this [illegible] average temperature is higher at the surface but falls almost

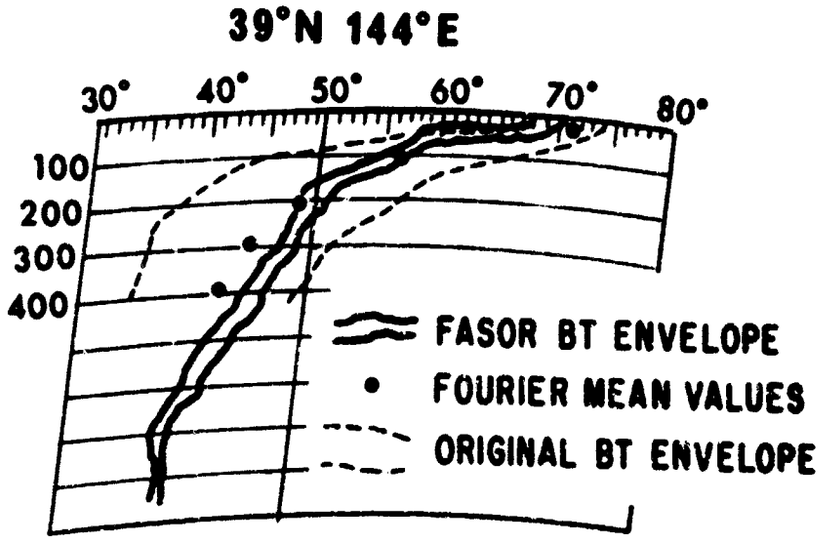

Fig. 13 Comparison of individual BT observations with mean BT temperatures, August 1964.

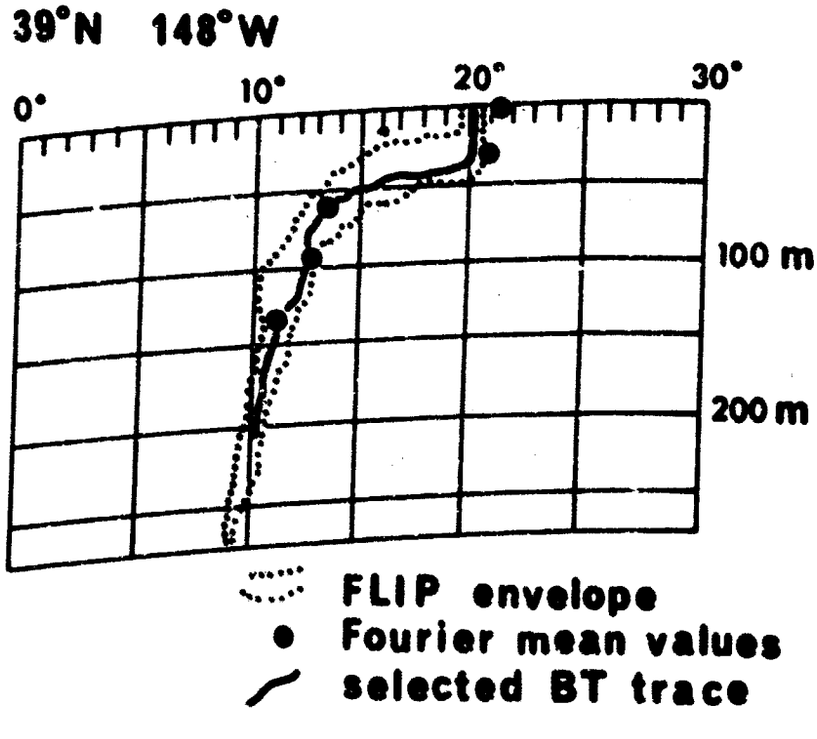

Fig. 14 Comparison of individual BT observations with mean BT temperatures, September 1963.

exactly on the September 15 BT curve beneath the surface.

The important implication of these two comparisons is that the mean temperature-depth structure is probably reproducible from year to year, if one considers the gradients represented by the mean differences. The continuous oscillation alters the depth but not the gradient of the thermocline, and the gradients appear to be similar from year to year.

STATISTICS

One product of the computer analysis is the computation of standard deviations of individual observations around their own mean. The standard deviations give measures of variability and reliability in areas where there are sufficient numbers of observations. We have no measure of reliability in areas where the means are based on interpolation. We are planning to set up a system of evaluation of the reliability of the interpolated mean temperatures by using the synoptic observations transmitted to the U. S. Fleet Numerical Weather Facility. When sufficient numbers of new observations are received, we can re-compute means easily and quickly for new data areas.

CONCLUSION

For the first time, we now have completed seasonal temperature models for the North Pacific and North Atlantic. In areas of sparse data, these results must be considered to be first approximations only.

These seasonal models can provide useful oceanographic information to the Navy for a variety of special purposes. Their usefulness is an adjunct to, not a replacement for, synoptic observations and daily forecasts.

ACKNOWLEDGEMENTS

This project is supported by the Office of Naval Research, the National Science Foundation, the U. S. Fleet Numerical Weather Facility, and the U. S. Naval Oceanographic Office. The author also wishes to acknowledge the assistance of Dr. C. Fremont Sprague, III, in the development of the computer programs, and Commander Roy C. Atkinson, USN, for suggestions concerning the Navy's special oceanographic data requirements

SHALLOW WATER SOUND TRANSMISSION PATHS FROM THE USNEL OCEANOGRAPHIC RESEARCH TOWER OFF MISSION BEACH

by

Palle G. Hansen and Owen S. Lee
U. S. Navy Electronics Laboratory, San Diego, California

INTRODUCTION

For several years the Navy Electronics Laboratory has experimented with fixed path acoustic transmission in shallow water. In recent years experiments have been conducted from a fixed platform, the NEL Oceanographic Research Tower, which permits laboratory-like controls over measurements. This report is concerned with the physical interpretation of some of the experimental observations.

Ufford (1945) apparently was first to recognize the significance of internal waves in acoustic transmission in the ocean. He, and later Sperger (1957) and Lee (1961), computed sound fields on the basis of ray theory to explain some of the acoustic variations caused by transmission through a natural field of internal waves. Barkatov and Cherkashin (1963) experimented with acoustic transmission in a small laboratory tank wherein a two-layer system was maintained. Their result essentially was a laboratory demonstration of the lens effect of internal waves on sound beams. The internal wave slopes and refractive index ratio of the two layers used in all of these experiments are much higher than those observed in the ocean. Lee and Batzler (1964) recorded sound transmitted over a fixed path, and ocean temperature, in shallow water. Simultaneous spectra derived from these experiments showed sound-pressure-level fluctuations at frequencies equal to those of free internal waves. Barakos (1965) mathematically analyzed the problem of acoustic transmission across a sinusoidal boundary between two infinite layers. He found two cases that are of practical importance: (1) low-frequency sound incident upon an interface perturbed by an internal wave of low amplitude, and (2) high-frquency sound incident upon an interface perturbed by high-amplitude internal waves. The subject matter of this report deals with the latter.

EXPERIMENTAL PROCEDURES AND EQUIPMENT

The NEL Oceanographic Research Tower is situated 0.5 nautical mile off San Diego, California, in approximately 60 feet of water. The bottom consists of coarse sand and is featureless except for ripples caused by surface waves. The stability of the water column varies over wide ranges, but a two-layer system is often approximated. High amplitude internal waves commonly occur at frequencies near the stability frequency at this location. Internal waves with amplitudes

of 10 feet and wave lengths of 300 feet are common, and these dimensions have been considered for purposes of interpreting the observations. The waves are observed to progress toward shore with a speed of about 0.3 knot from a range of directions between west and southwest. The wave specified herein can be assumed to cause maximum disturbance in the sound-pressure-level record.

All equipment used in conjunction with the experiments was installed within a short distance of the NEL tower as shown in the elevation in Figure 1 and the plan view in Figure 2. The source was fixed to the NEL tower at a depth of 10 feet and trained on any one of three targets, each consisting of one reflector and one receiver to facilitate simultaneous records of one-way and two-way transmission. Records of 30 hour duration were made with the source trained on each. The three targets were placed so that the sound beam axis could be oriented parallel, perpendicular and at 45° to the crest line of the internal wave.

A Minneapolis-Honeywell Sea Scanar was used as a source for one-way transmission and as a source and receiver for two-way transmission. The transducer of the Sea Scanar consists of a circular disc of barium titanate.[1] Its resonance frequency is 178 kHz, and the 3-dB downpoints are ± 4° from the axis of symmetry. The receiving hydrophone is a barium titanate cylinder about one-half inch long and one-fourth inch in diameter; these dimensions are of the same order of magnitude as the wavelength of sound used.

The reflector used in two-way transmission was developed especially for these experiments. Experience with corner reflectors, air-filled spheres, and water-filled spheres showed that it was difficult to maintain a high stable target strength for the duration of the experiments. The water-filled sphere presented recording difficulties because of multiple echoes (Batzler (1959)). The reflector most satisfactory for these experiments is shown in Figure 3. The new reflector is a half sphere with a center disc removed. This configuration eliminates unwanted echoes but retains the desired echo. Solid lines in Figure 3 illustrate an incoming and desired reflected ray, and dashed lines show an eliminated ray that would occur in a water-filled sphere.

The acoustic signals were simultaneously displayed on two cathode ray oscilloscopes. The oscilloscope traces were photographed on two continuously running 35 mm films. Noise, such as returns from spurious targets, was removed by masking unwanted parts of the trace before it was recorded on film.

Time-series observations of temperature were recorded on an array of six thermistors spaced at equal intervals of depth. The direction of internal waves was recorded immediately with an array of 48 thermistors arranged in a 450-foot-diameter circle. The circle of thermistors was

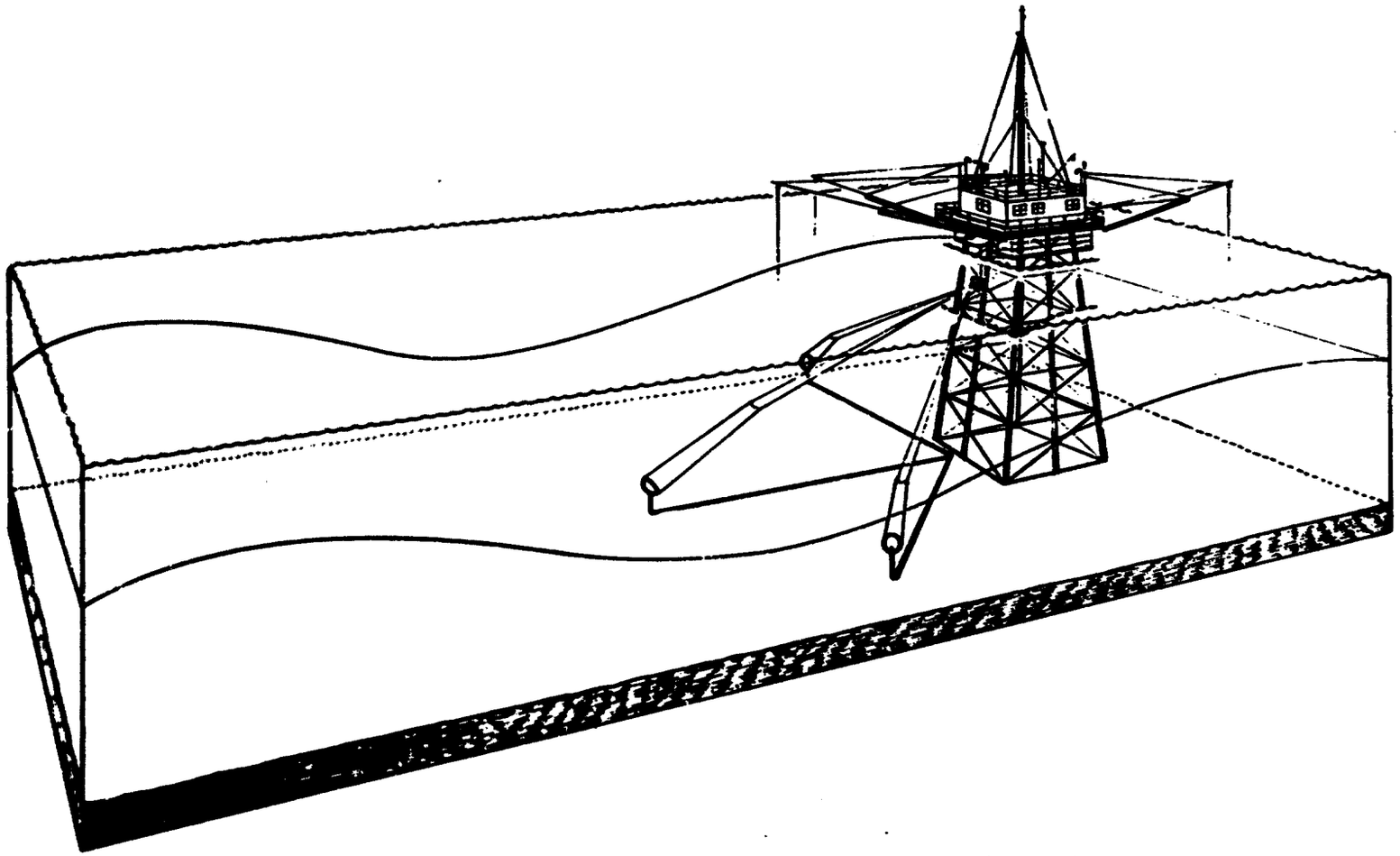

Figure 1 Elevated view of the experimental arrangement depicting a two layer system perturbed by an internal wave.

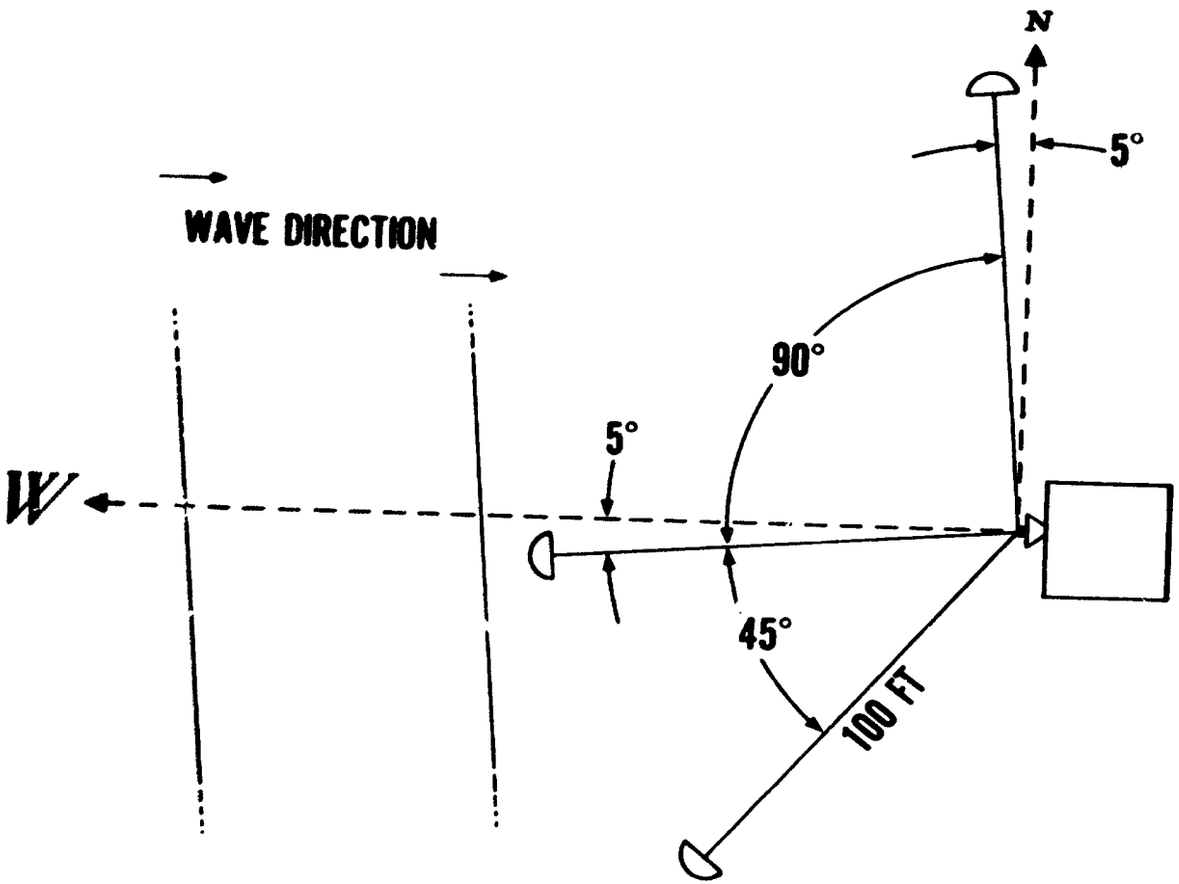

Figure 2 Plan view of the experiment showing internal wave crests and direction of propagation.

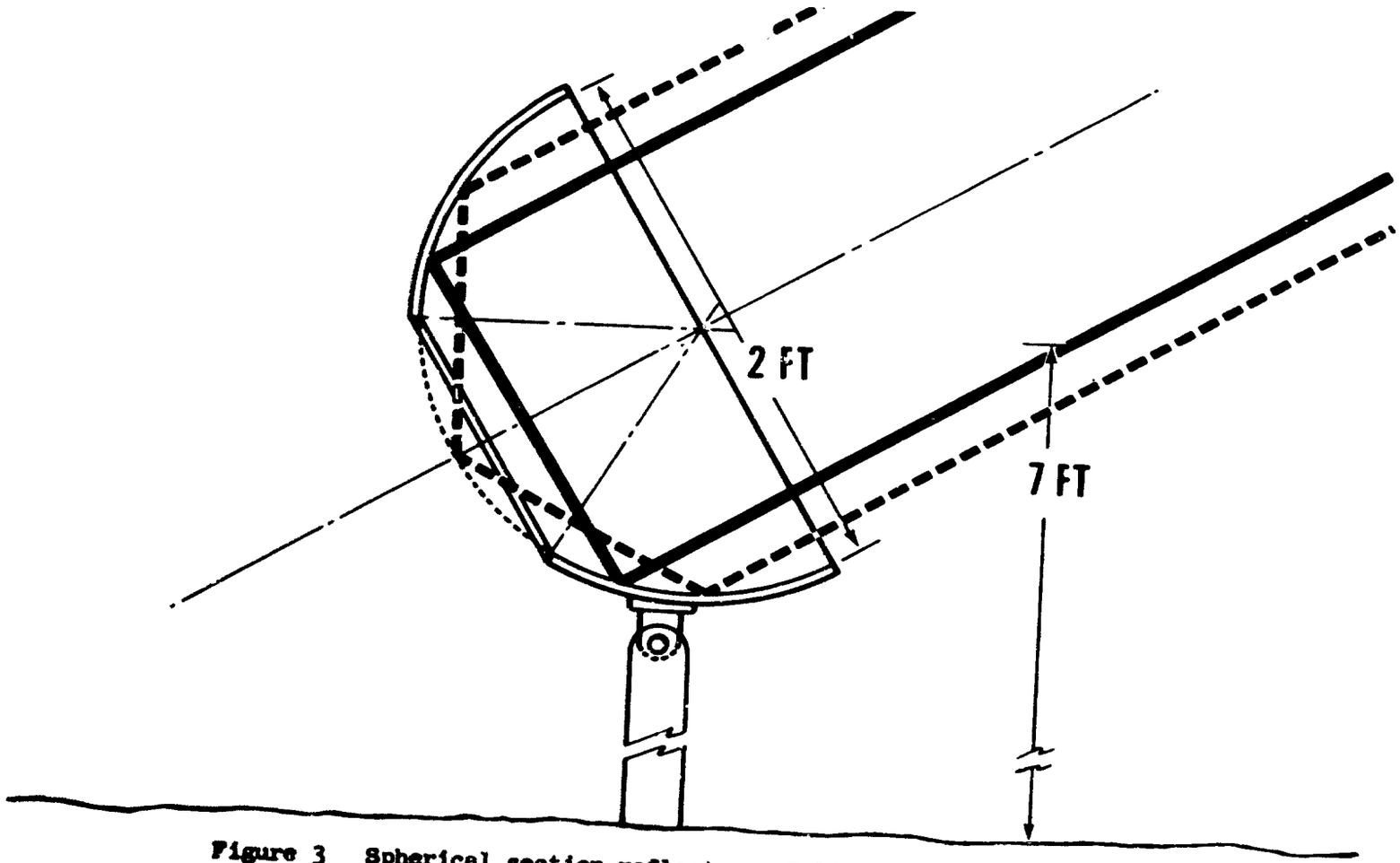

Figure 3 Spherical section reflector. Solid lines show the path of the returned echo and dashed lines show the rejected echo.

placed in a horizontal plane at a depth of 30 feet. The thermistors were scanned frequently and recorded. As an internal wave traveled across the circular array, its associated changes in temperature could be discerned. Direction was determined by noting the thermistor which first picked up the temperature perturbation.

ACOUSTICS

Two processes act to modify sound when it passes from one medium through an interface into another. These processes are reflection and refraction and were treated by Rayleigh (1878). His formulae are well known in one form or another. All fluctuations in sound-pressure-level recorded during the course of the experiments can be interpreted in terms of the two processes.

Rayleigh's formulae have been applied to a two-layer system consisting of 65°F water above the interface and 60°F below the interface. Computation indicates that reflection at the interface does not contribute significantly to fluctuation in sound-pressure-level. The reflected wave amplitude is less than one-quarter percent of the incoming wave amplitude when the angle of incidence is 0°. The reflected wave amplitude rises with increasing angle of incidence, but it does not become appreciable until the ray is almost at the grazing angle. This, however, assumes that the interface is absolutely sharp (a step change in sound velocity) and only an approximation to the real ocean. When the transition between warm and cold water takes place over a few wave lengths of the sound, reflection of sound energy is materially reduced. The wave length of sound used in the experiments was about one centimeter; consequently, reflection is of little importance with the possible exception of almost grazing incidence.

The records of sound-pressure-level derived from both one-way and two-way transmission show a broad spectrum of fluctuation in sound level. The amplitude spectra are peaked, but the amplitudes at the peak frequencies are of the same order of magnitude, i.e. the high-frequency fluctuations have amplitudes about as large as the low-frequency fluctuations. High-frequency fluctuations are apparently caused by turbulence and spurious targets such as fish. Most of the variance in sound-pressure-level at low frequencies is believed to be caused by internal waves although large, turbulent eddies may contribute. Only sound-pressure-level changes caused by internal waves are considered in this report and in that context a physical interpretation of low-frequency fluctuation is sought.

Four cases that lead to low-frequency fluctuation in sound level are considered. A composite of these four cases is schematically illustrated in Figure 4. The upper portion in each block of Figure 4 represents the two-layer medium separated by a sinusoidal interface indicated by the heavy solid lines. The lower portion of each block is a sketch of the

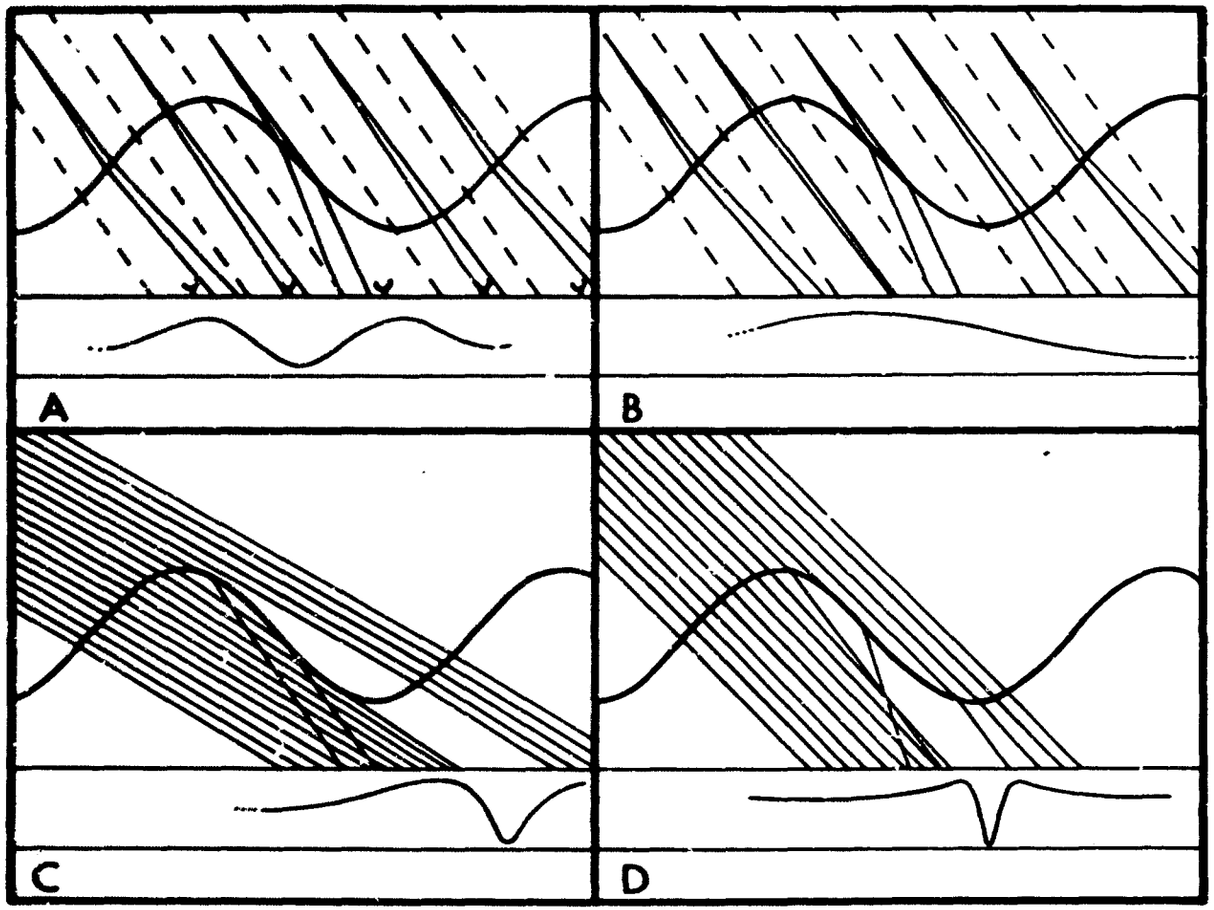

Figure 4 Block A: Simple refraction of sound beam. Block B: Simple refraction and focusing of sound beam. Block C: Shadow zone effect with ray slopes smaller than maximum internal wave slope. Block D: Shadow zone effect with ray slopes equal to maximum internal wave slope.

envelope of sound-pressure-level resulting from transmission within the medium. The vertical scale in the upper portion of each block represents depth and the horizontal scale represents time. By proper choice of scale, the abscissa can also represent distance in blocks C and D (Fig. 4). The dashed lines in the upper block set off a bundle of rays at any instant in time; consequently the region between two neighboring dashed lines can be interpreted as a space plot. The series of space plots across the upper blocks shows the effect on a stationary sound beam when an internal wave passes across it. None of the dimensions in Figure 4 are drawn to scale, and the plots have been distorted as necessary to emphasize the four cases under consideration.

In the discussion of the four cases it will be convenient to refer to the slope of the sound beam and the maximum slope of the internal wave. The sound beam slope is the angle the beam axis makes with a horizontal surface, and the maximum slope of the internal wave is its amplitude multiplied by its wave number. The experiments reported here made use of beam slope angles about 12° larger than the maximum slope angle of the internal wave already specified. Experiments reported by Lee and Batzler (1964) used beam slopes lower than the maximum internal wave slope.

Block A (Fig. 4) depicts a case of simple bending of a sound beam by refraction. The beam axis is swept back and forth across the reflector, which is drawn as a tiny semicircle at the bottome. The end result of this process in both one-way and two-way transmission is to cause a low-frequency change in sound-pressure-level as sketched in the lower portion of block A. The frequency of the sound level fluctuation is twice that of the internal wave.

Block B (Fig. 4) illustrates the same king of refraction as in the first case but here beam focusing is added. A sinusoidal interface results in a lens effect that causes a beam to focus and diverge, depending on sign of the curvature. Curvature goes through one complete cycle within one period of the internal wave and a corresponding cycle in sound pressure level occurs. The focusing effect alone causes a sound level fluctuation with frequency equal to the internal-wave frequency.

Block C (Fig. 4) depicts a third case in which sound ray slopes are smaller than the maximum internal-wave slope. The sharpness of the interface, and the near equality of the sound beam slope and maximum internal wave slope, are important considerations. The effect is a shadow zone below the interface. The shadow zone is basically a lens effect that is accentuated by grazing or almost grazing incidence. This causes severe refraction and secondary reflections. Block C (Fig. 4) leads to an area of intense insonification followed by a low-intensity zone as shown in the lower part of the block. The resulting sound-pressure-level fluctuation has a frequency equal to that of the internal

wave, but its envelope is considerably distorted compared to the perturbation on the interface.

Block D. (Fig. 4) is very similar to block C and, although actually not distinct, has been separated for clarity. The difference is that sound ray slopes are equal to the maximum internal wave slope in block D and no secondary reflections occur. When the rays approach the interface at grazing angle, a more pronounced dip in sound-pressure-level results. Block D introduces a sound level fluctuation at a frequency equal to that of the internal wave.

The cases just described give a physical description of what happens during the passage of an internal wave through a fixed sound beam. Although experimental studies of oceanic turbulence have been infrequent, there is no reason to believe that turbulence is any less common than internal waves. The data from these experiments show fluctuations that are undoubtedly caused by turbulent motion in the medium. The sound level signatures caused by turbulence apparently do not differ from those of internal waves. Free internal waves do not exist above the stability frequency, but the experimental data contain fluctuations in this range with amplitudes as large as those occurring below the stability frequency. For internal waves and turbulence at greater distances from the source, internal waves will probably have the greater effect on sound level fluctuation.

A sample of sound pressure level data is reproduced in Figure 5. The two traces in the upper block represent approximately 15 minutes of two-way transmission, and the two traces in the lower block represent one-way transmission for the same 15-minute period. The interval between two consecutive timing marks above each trace is 6 minutes. No logarithmic amplifiers were used anywhere in the system; consequently the vertical scale in Figure 5 is linear.

The two-way transmission provides a very distinct record because (1) there is only one return echo of appreciable magnitude, and (2) the large reflector (Fig. 3) effects an average over many acoustic paths. The small size of the hydrophone causes it to receive a very narrow pencil of rays; thus there is a frequent fading of the signal when two slightly different sound paths arrive out of phase at the hydrophone. This results in an indistinct envelope characteristic of the lower block in Figure 5.

Although the two time-series observations in Figure 5 are not copies of each other, there is general agreement between them. The long-period change evident in both records corresponds to the passage of an internal wave as determined from the temperature record. The short-period changes must be caused mainly by turbulence. Both the long and short-period changes have the same general signature shape as those shown in blocks C and D (Fig. 4).

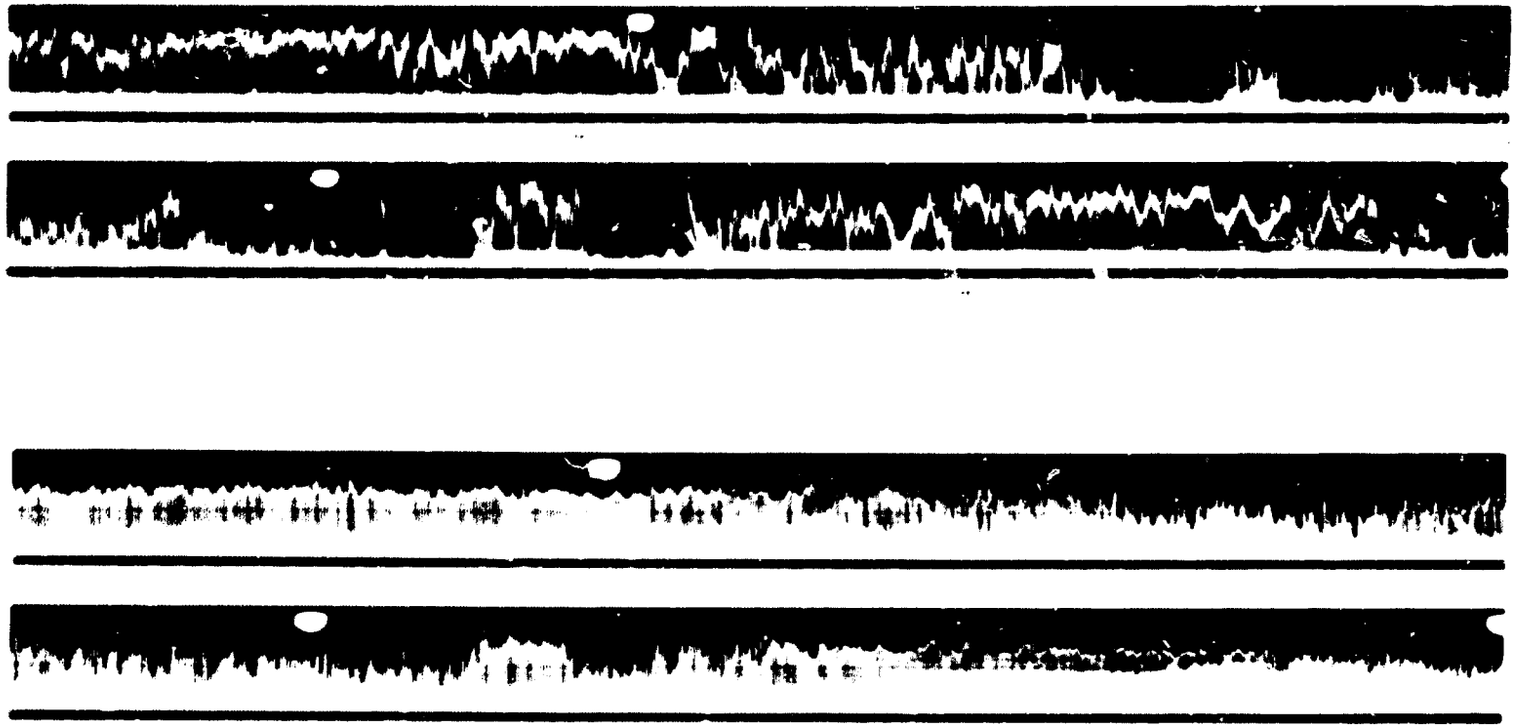

Figure 5 Upper block: Two-way sound transmission data of about 15 minutes duration. Lower block: One-way sound transmission data from the same time interval.

The numerical results of this study are not yet tabulated, but some qualitative results are clear at this time. Cases shown in 4A and 4B cause low-frequency sound level fluctation, but the amplitude is small. In the experiment described here, these cases introduce a sound level variation of the order 1 dB or less whereas cases 4C and 4D cause sound level changes of the order 10 dB or larger. The importance of the effects of all cases rises with increasing range.

Frequency doubling is more pronounced when the beam axis is trained parallel to the wave crest. The major effect is still the shadow zone even when conditions shown in blocks C and (Fig. 4) are only approximately achieved.

In the ocean where the transition between two layers is continuous. conditions approaching those in block C (Fig. 4) can occur for relatively short ranges. Ray theory indicates that the cases shown in blocks A and B (Fig. 4) introduce a very small shift in sound level, yet significant changes at twice the frequency of the internal wave occur in actual transmission parallel to the wave crest. This is especially so when longer ranges of transmission are involved. Under these circumstances, the maximum slope of the internal wave and the slope of the sound beam axis are often nearly the same. The results of sound beam slopes being sometimes a little above or below the internal wave slope are (1) a maximum frequency doubling effect and (2) a maximum frequency coupling effect.

CONCLUSIONS

The passage of an internal wave through a stationary sound beam causes a sound level variation at twice the frequency of the internal wave, but the amplitude is ordinarily small. Shadow zones occur when the sound beam slope approaches the slope of a scalar surface perturbed by internal waves or turbulence and cause a large change in sound level. With transmission perpendicular to the wave crest this effect introduces a sound level fluctuation with the same frequency as the internal wave. With transmission parallel to the wave crest an analogous shadow zone causes variation in sound level with twice the frequency of the internal wave.

BIBLIOGRAPHY

Ufford, C. W., Internal Waves off San Diego, California, UCDWR Report M 290, 1945.

Sparger, C. R., An Example of Sound Ray Focusing by Internal Waves, Navy Electronics Laboratory Report 760, January 1957.

Lee, O. S., Effect of an Internal Wave on Sound in the Ocean, Journal of Acoustical Society of America, v. 33, pp 677-681, May 1961

Barkatov, A. N. and Y. N. Cherkashin, Deformation of a Beam of Sound by an Internal Wave at the Boundary between Two Liquids, Soviet Physics -Acoustics v.9, p 86--87, July-Sept 1963.

Lee, O. S. and W. E. Batzler, Internal Waves and Sound-Pressure-Level Changes, Proceedings of the First U. S. Navy Symposim on Military Oceanography, pp 47-67, June 1964.

Barakos, P. A., On the Theory of Acoustic Wave Scattering and Refraction by Internal Waves, Navy Underwater Sound Laboratory Report 649, Feb. 1965.

Rayleigh, Lord, The Theory of Sound, Dover Publications, v. 2 pp 78-86, 1945 (first printing 1878).

Batzler, W. E., The use of Free-flooding Spherical Shells as Standard Acoustic Targets, U. S. Navy Journal of Underwater Acoustics, v. 9 No. 3, pp 547-552, July 1959.

U. S. NAVAL ACADEMY OCEANOGRAPHY CURRICULUM AND SOME PRELIMINARY SCIENTIFIC/TECHNICAL RESULTS

Commander Donald C. Bayly, U. S. Navy
U. S. Naval Academy, Annapolis, Maryland

The immense volume, revealing content and potential naval importance of the knowledge which is spewing from the thousands of dedicated scientists probing the air-ocean environment today partially provides for our continued control of the seas. I say partially because control also involves leadership and leadership involves the practical utilization of knowledge. It is therefore appropriate here, at the close of this third Symposium on Military Oceanography, to pose the question, "Are we providing our future naval leaders with the knowledge, ability and determination to properly evaluate and use effectively this available mass of data to our Navy's advantage?" Not long ago an affirmative reply could be made by providing graduate programs for educating specialists capable of meeting the needs of service agencies and bureaus as well as staffs throughout the Navy. The U. S. Navy Postgraduate School Program, which responds to this need, was described by Dr. Glenn Jung at the second symposium last year.

An affirmative answer to the posed question is no longer as simply stated. Science and technology, particularly that which provides useful and up-to-date data to the fleet, have now advanced to a sophistication and detail which dictate that others besides specialists must be classed as users. This is especially true in the case of environmental data. Vital information flowing from analysis centers is available to all: Weather information for officers of the deck and supply officers; layer depth predictions for ASW officers; air density data and winds for weapons officers; botton conditions, scattering layers, refraction zones, sea heights, surf and swell, optimum track, deep currents, ice, infra red, satellite readouts, sound paths, and so on. All of this information is or soon will be available to all, those on independent ships, submarines or aircraft as well as staff specialists. Raw and refined data, continuously modulating over, on and under the seas, is available at the turn of a hand. At the present time much of this information falls on deaf ears. The Navy, aware of this lag between information and its use and recognizing that specialists alone will not suffice, has launched a program of environmental education for more of its future officers. This new program has been initiated at the Naval Academy.

This course incorporates the study, in descriptive form, of the interrelationships of the two environments stressing the effects of heat balance, turbulence and circulation systems as well as the causes and effects of currents, tides and winds.

The second objective, that of providing a sound background for graduate study and specialization, is the goal of the Oceanography major and minor programs. Integrated closely with the Naval Postgraduate School in Monterey, these courses may lead to advanced standing upon graduation. A very brief summary of the six course minor will demonstrate its general content.

N603 - Introduction to Oceanography. This course is an introduction to basic oceanography including marine geology, biology, chemistry and the physical aspects. The origin, form and structure of ocean basins and margins, geomorphic features and sediments are included. An examination is also made of the biomass in terms of classification, distribution, nutrient cycles and interaction. An elementary consideration is made of forces and motion in the ocean.

N607 - Introduction to Meteorology. An introduction to the basic principles of meteorology, this course covers the structure and composition of the atmosphere, weather elements, instruments and observations and the nature and dynamics of air masses, fronts and storms. The physical principles governing heat budget, equations of motion, stability, turbulence and mixing are treated with emphasis on the interactions at the air-sea interface.

N705 - Ocean Waves, Tides and Ice. The basic consideration of classical wave theory is contrasted with the modern approach in this course. Relationships between wind and sea phenomena, swell, breakers, internal waves, tides and tidal currents, seiches and tsunami are included along with the description, formation, melting and movement of ice.

N708 - Synoptic Meteorology. This course is a study of atmospheric systems on a synoptic scale. Elements of map analysis and forecasting from a marine viewpoint are included along with motion and evolution of weather systems, storms at sea and the relationship of upper flow to surface systems.

N821 - Nearshore Oceanography. The shallow water environment is the subject of this course. It includes geology of the continental shelves, types and formations of coastlines, sediments, beaches and beach erosion, swell, surf and wave refraction, the littoral biomass and studies of harbors, river mouths and estuaries. Aerial coastal field trips are included.

N826 - Oceanographic Applications. This is the terminal course of the oceanography program and includes a laboratory. The application of the principles and methods of oceanography and meteorology to naval operations and problems is highlighted. Topics include problems in forecasting weather, surf and wave, optimum track routing, factors in ASW as well as amphibious and mine warfare. The student is familiarized with the national, international and U. S. Navy Oceanographic programs and requirements through study and field trips to The Navy Oceanographic Office, The Navy Oceanographic Data Center, ICO, The Bureau of Commercial Fisheries, The Oceanographic Instrument Center and other agencies.

Completion of the six courses constitutes a minor in Oceanography. Students qualifying for a major must complete the minor program and in addition must take two semesters of biology or geology, two semesters of advanced mathematics and two semesters of advanced physics. Provision is also made for exceptional students to undertake two semester research projects for additional credit.

A number of closely oriented courses in other diciplines are also provided within the environmental framework. Since documented environmental information is dependent upon accurate position, a course in basic navigation and a second covering the latest advanced systems are offered. A new course on the Aerospace Environment, supporting the aerospace major, was inaugurated this year with assistance from the Goddard Space Flight Center.

One may well question how undergraduate students are capable of undertaking such an ambitious elective concentration. We at the Naval Academy are convinced that not only is it possible, but also that for gifted students, such a program is vital and highly motivating. Its success of course depends upon increasing sophistication and advanced teaching programs in elementary and secondary schools. Such advances are not dreams but reality today in increasing numbers of schools. As a consequence, entering fourth classmen are validating increasing numbers of courses each year, and are commencing work towards major and minor areas of interest at an earlier point in time.

The Naval Academy environmental facilities are expanding in proportion with the academic programs. An Environmental Data Center is receiving weather information by facsimile recorders directly from the National Weather Network and by late summer will receive oceanographic data via X-Y plotter from the Numerical Analysis Facility in Monterey. A modest laboratory is presently being equipped and a 75 foot patrol craft is being instrumented for orientation as well as student and faculty research.

The success of any educational program can only be measured by the performance of its graduates. The present program has not been in existance long enough for us to use this measure. However, one early test of how well students are being motivated and educated is in terms of the individual research they conduct. At the present time two Trident Scholars are conducting extensive investigations in oceanographic areas. Midshipman Ian S. Gordon has been conducting a project titled "A Study of Sound Energy Losses in the Deep Scattering Layer." This original work has utilized raw data from Oceanographic Office tapes of surveys previously conducted in bottom scattering investigations. It has been performed in three phases. The first consisted of a thorough investigation into similar related works as well as studies outside the classroom in underwater acoustics, biology and data processing. The second phase has been the processing of the tape information to show sound losses with respect to frequency of sound energy, as well as the depth and thickness of the scattering layer. The Naval Academy IBM 1620 computer has been utilized to process the large volume of raw material which has resulted from a sound spectrum analysis of these charges through various band pass filters. The third phase, which is now underway, involves the derivation of an empirical relationship to give a scattering coefficient which is a function of frequency, as well as depth and thickness of the scattering layer. This relationship is expected to be suitable for inclusion in the general sonar equations and will hopefully assist in predicting the performance of the very high powered bottom bounce sonars. Midshipman Gordon's work will be published late this month.

A second Trident Scholar project has just been commenced by Midshipman Linton Wells entitled "The Effects of Internal Waves on Underwater Sound Propagation." The purpose of his original work will be to investigate the effects of internal waves on sound propagation across the maximum density change interface. The effects will be studied in two particular areas. The first will examine short period sound intensity fluctuations due to the changing angle of the interface and the second will investigate long period changes resulting from a strenghening or weakening of the interface by wave and current action. Midshipman Wells also anticipates that sufficient information will be gathered during the second phase to permit an additional analysis of the influence of these waves and currents on mixing between the two adjacent water masses. A wave tank has been constructed and Midshipman Wells is presently investigating conditions in the interface between pure water and a saline solution. The investigation will utilize conductivity as a measure of mixing and time lapse and slow motion photography of light refraction shadows as a measure of movement. This project hopefully aims to assist in predicting sonar performance where internal waves are significant and may help to explain the in and out nature of sonar contact under certain conditions.

The sudden surge of man's knowledge and the acceleration of science and technology are producing revolutionary changes in segments of our society besides the Navy. Educational institutions in particular have responded to the impact and the impetus is filtering down through primary and secondary schools. The Naval Academy, responding to these academic stimuli as well as those from sophisticated engineering and weapon systems which are appearing in the fleet, began a major academic overhaul in 1959. A number of the more important changes that have been made are worth noting. Provision is now made for incoming midshipmen to validate previously completed college level work. This enables the student to commence work earlier on courses leading towards fields of concentration. Simultaneously, the academic program was liberalized, providing a core curriculum of 34 courses devoted to basic study in science, naval science, engineering, social science and humanities. These required courses are oriented toward naval applications and are designed to provide all midshipmen with the educational background required for effective naval leadership. Augmenting the core is an elective program of over 200 courses encompassing majors and minors which lead either toward graduate work in a wide variety of diciplines or provide intellectual enrichment for those capable of taking additional loads. In most cases the core courses plus six electives make up a minor and provide the 137 semester hours required for graduation. An additional six courses qualify as a major.

An important change to the Naval Academy organization was made in 1963 with the appointment of a civilian Academic Dean. At the same time several special programs for exceptional students were established. The Trident Scholar program enables a small number of specially selected midshipmen to pursue independent research during their senior year. I will return to this program later. Means is now provided for other selected students to proceed directly upon graduation to an institution of their choice for continued work leading to the doctorate.

Environmental Science, including Oceanography, occupies a conspicuous position within this new academic program. In response to the environmental needs of the fleet, the objectives of this curriculum at the Naval Academy provide for two distinct avenues leading toward separate goals. The primary objective is to familiarize all midshipmen with the marine environment. For this purpose a core course titled Air-Ocean Environment is provided during the fourth class (freshman) year. This orientation course introduces the effects of the natural environment on naval operations. Key parameters of importance are presented, along with their related naval applications, in terms of the air column, air-ocean interface, water column and water-bottom interface. Statistical and analytical information available to the fleet, its sources and uses, is included. A broad description is given of the environmental properties of the ocean and atmosphere including the topography and biological characteristics of the sea.

It is apparent that the Navy is moving to insure that future officers receive a sound education in environmental science; an education which will keep pace with the long range advances in science and technology. This effort not only involves the Naval Academy but also the many other institutions of learning across the country, graduate, undergraduate, secondary and primary. Although the impact of the new environmental programs will not be fully realized in the fleet until 1968, I feel confident in stating that the preliminary effects are already being favorably noted.

SOUND VELOCITY PROFILES IN AN AREA SOUTH OF BERMUDA

by

William A. VonWinkle and Linda Mary Jones
U. S. Navy Underwater Sound Laboratory
New London, Connecticut

The determination of the velocity structure of a given volume of the ocean is basic to important studies of the propagation of sound through sea water. A particular application is that such data afford valuable information for the design and use of underwater acoustic systems.

The Underwater Sound Laboratory has been fortunate in obtaining from the Bermuda Biological Station[1] eleven years of Nansen cast data taken approximately every two weeks by the vessel PANULIRUS. These measurements were made about 15 nm southeast of St. David's Light, Bermuda, in water 1500 to 2400 fathoms deep and are judged to be typical of the deep ocean immediately south of Bermuda.

Velocity profiles were calculated from the data by use of Wilson's formula.[2] From these individual profiles, monthly and seasonal profiles were obtained and, to give a general picture of the limits of the sound velocity structure for this location, a composite profile was made.

The mean monthly profiles have been plotted with their corresponding extreme profiles. (See Figure 1.) Each month's distinct profile is apparent. Since the Nansen cast data were not always taken at exactly the same depth, depths at which to plot these combined profiles were selected for points at which distinctive characteristics occurred. More points were chosen, of course, in the first 500 meters than in the deeper water. These monthly profiles should prove to be the most useful combinations of the data, since the area between the extremes is reasonably small so that the need for evaluating each individual profile is reduced.

To show the time variation of sound velocity by months through the year, the mean velocities for several depths are shown in Figure 2. For each point, the distribution of the sound velocity data about each mean is shown in the bar graphs in bands of 2 meters/second. These distribution data are quite useful in evaluating the extremes shown previously. Note that the distribution widens from the surface down to 600 meters; it becomes less at 1000 meters and continues to narrow as the depth increases.

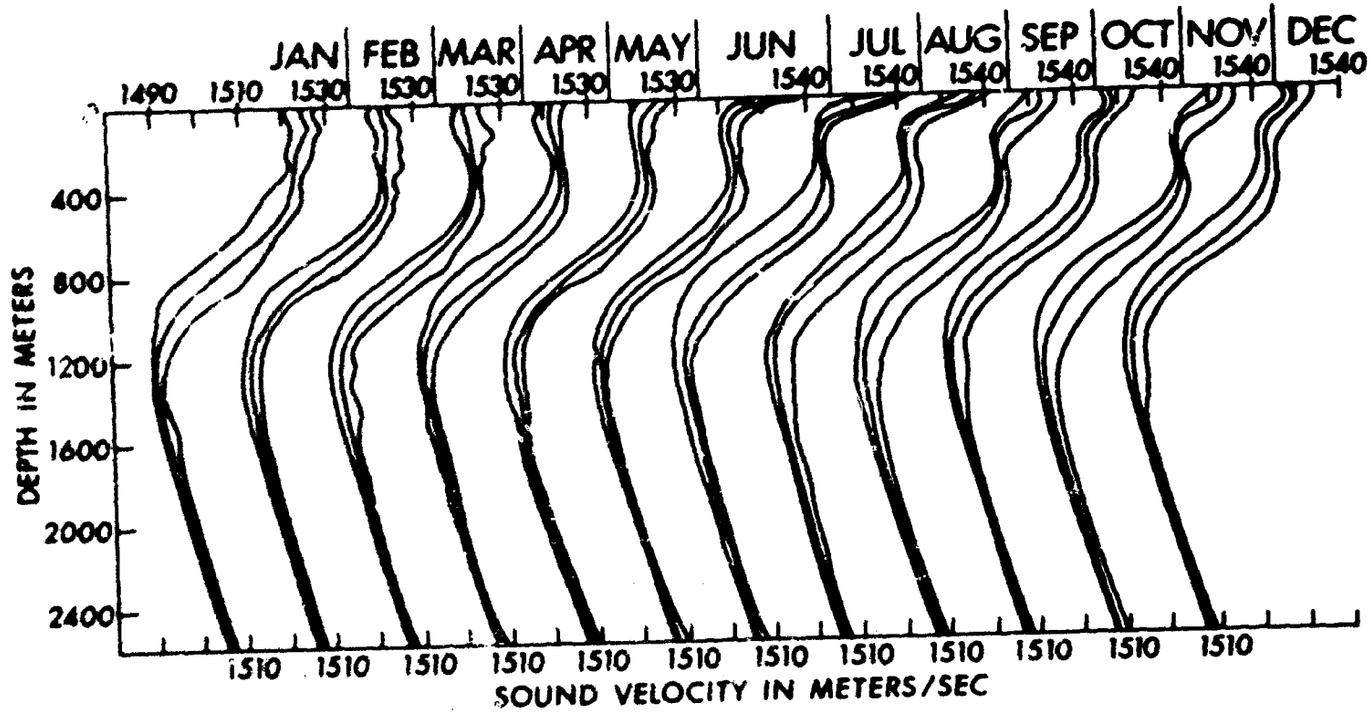

FIGURE 1 SOUND VELOCITY PROFILES SHOWING MEANS AND
AND EXTREMES FOR EACH MONTH

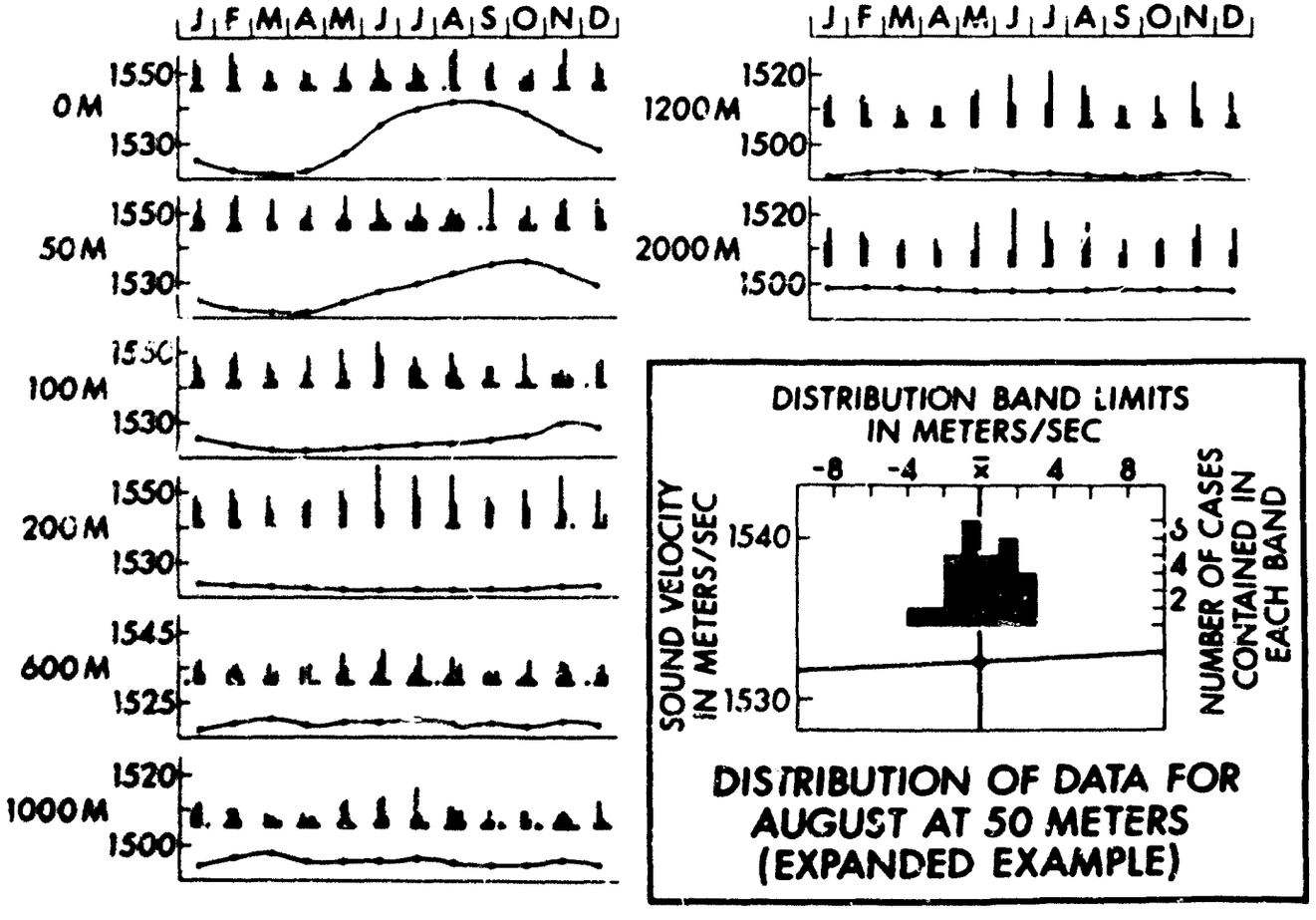

FIGURE 2 MONTHLY VARIATION OF SOUND VELOCITY SHOWING DISTRIBUTIONS ABOUT THE MEANS

Also of interest are monthly temperature profiles.[3] (See Figure 3.) Note the surface changes which occur as summer approaches and then as winter returns. A slight delay in the effects is observed as the depth increases until, at 1000 meters, little temperature change is observed. A time-lapse motion picture film, "Bathythermograms in the Bermuda Area" (Motion Picture Brief No. 16) is available on loan to anyone interested in these temperature profile changes.[4]

Monthly salinity profiles[3] are shown in Figure 4. These profiles are quite regular in their structure except for the first 50 meters. Observe the straight profiles from the surface to 500 meters in January through May and then the gradual bending as the salinity decreases through September and increases again from October through December. December is affected down to 100 meters before the profile returns to the higher values of January.

A second grouping of the data was made to obtain seasonal profiles. (See Figure 5.) Again, the means are shown for each season with the extremes which occur in the data for each season.

After a study of the temperature profiles and of the monthly velocity gradients and as a result of search through the literature for supplementary data, the division of the year into seasons for this volume of the ocean was made. Winter is January through April, spring is May and June, summer is July through October, and fall is November and December. (A note of interest is that June's profile looks rather like a summer profile, although its negative gradient is not as extreme as October's and the average June temperatures at the surface and at 25 meters are lower than those for October.) Figure 5A is a comparison of monthly profiles with a seasonal profile to show that monthly profiles have appreciably less variation.

A very general picture of the velocity structure for the area under consideration is shown in Figure 6. In this composite profile, the mean and the extremes for the entire eleven years of data are plotted. The value of this composite profile is that it indicates the limits of any profile which might exist in this volume of the ocean.

The resolution of these data is considered to be ±0.01° C temperature, ±0.01 parts per thousand salinity, and ±2 percent for depth. Since all positive errors are additive and all negative errors subtract, possible errors can be combined to observe the maximum possible error. (See Figure 7.) The maximum error shown is about 1 meter/second.

Because the minimum velocity point of a velocity profile is often of interest, especially for determinations of the deep sound channel, data from each of the individual profiles were examined and the minimum velocity of each determined.

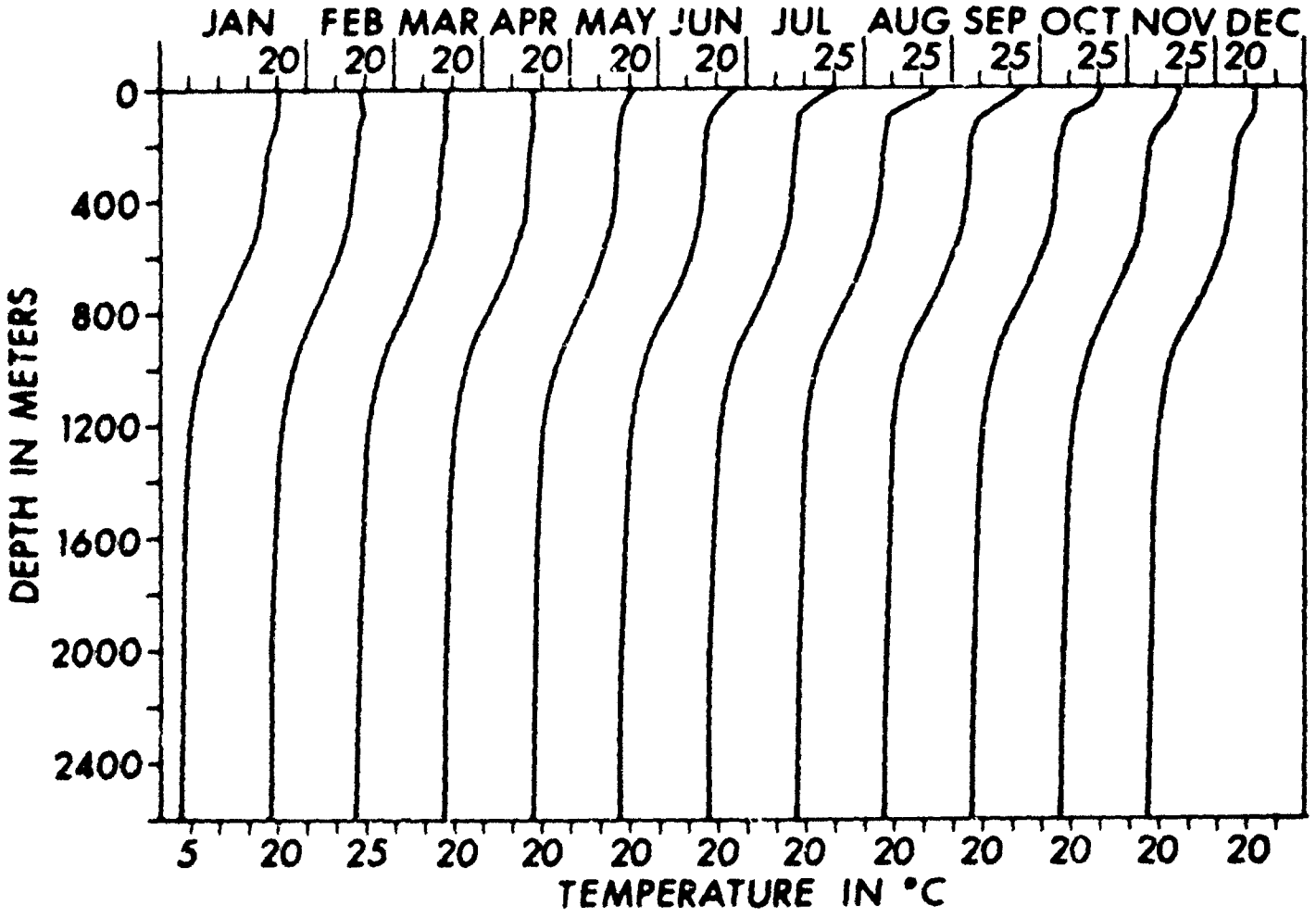

FIGURE 3 TEMPERATURE PROFILES-MONTHLY MEANS

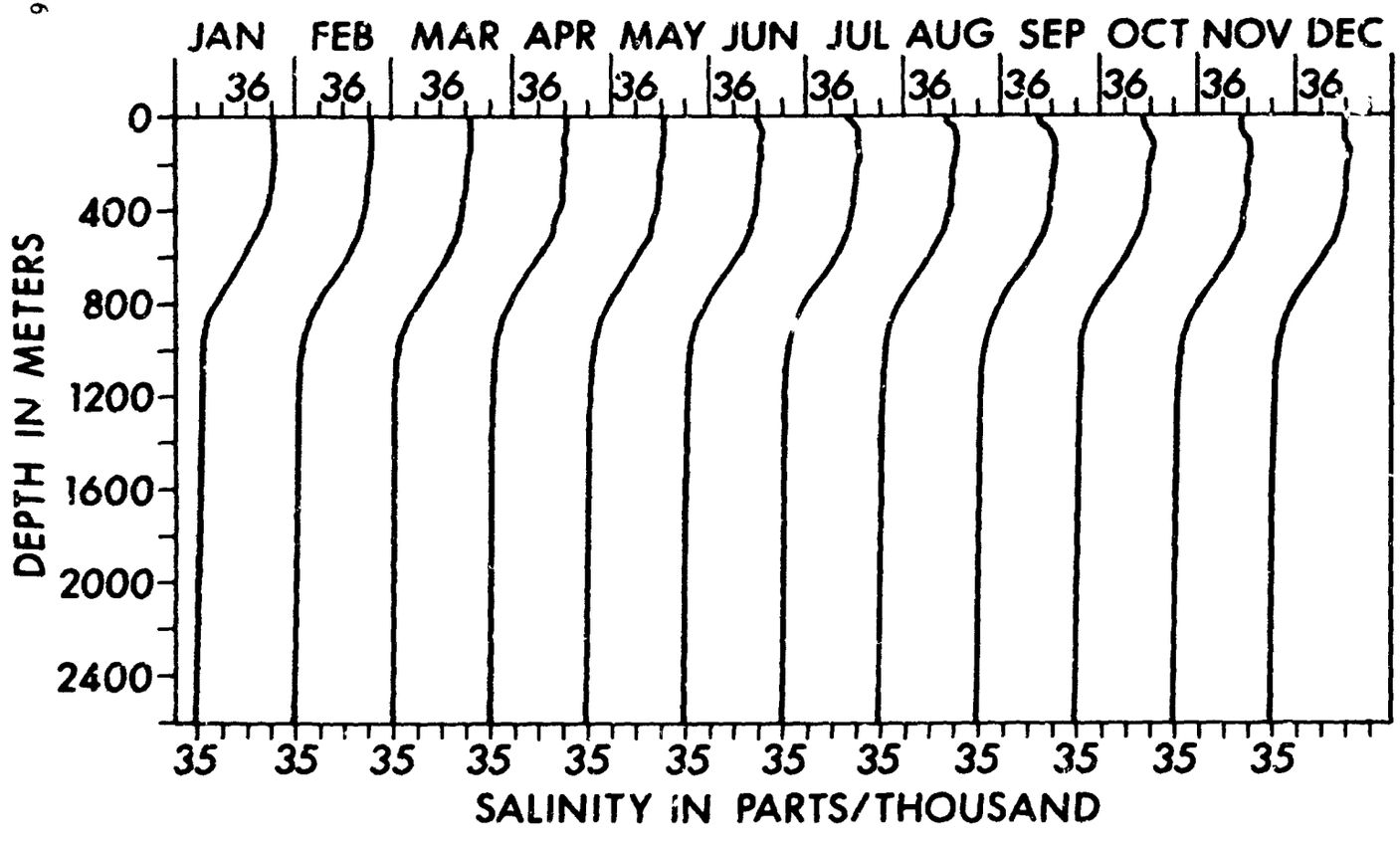

FIGURE 4 SALINITY PROFILES-MONTHLY MEANS

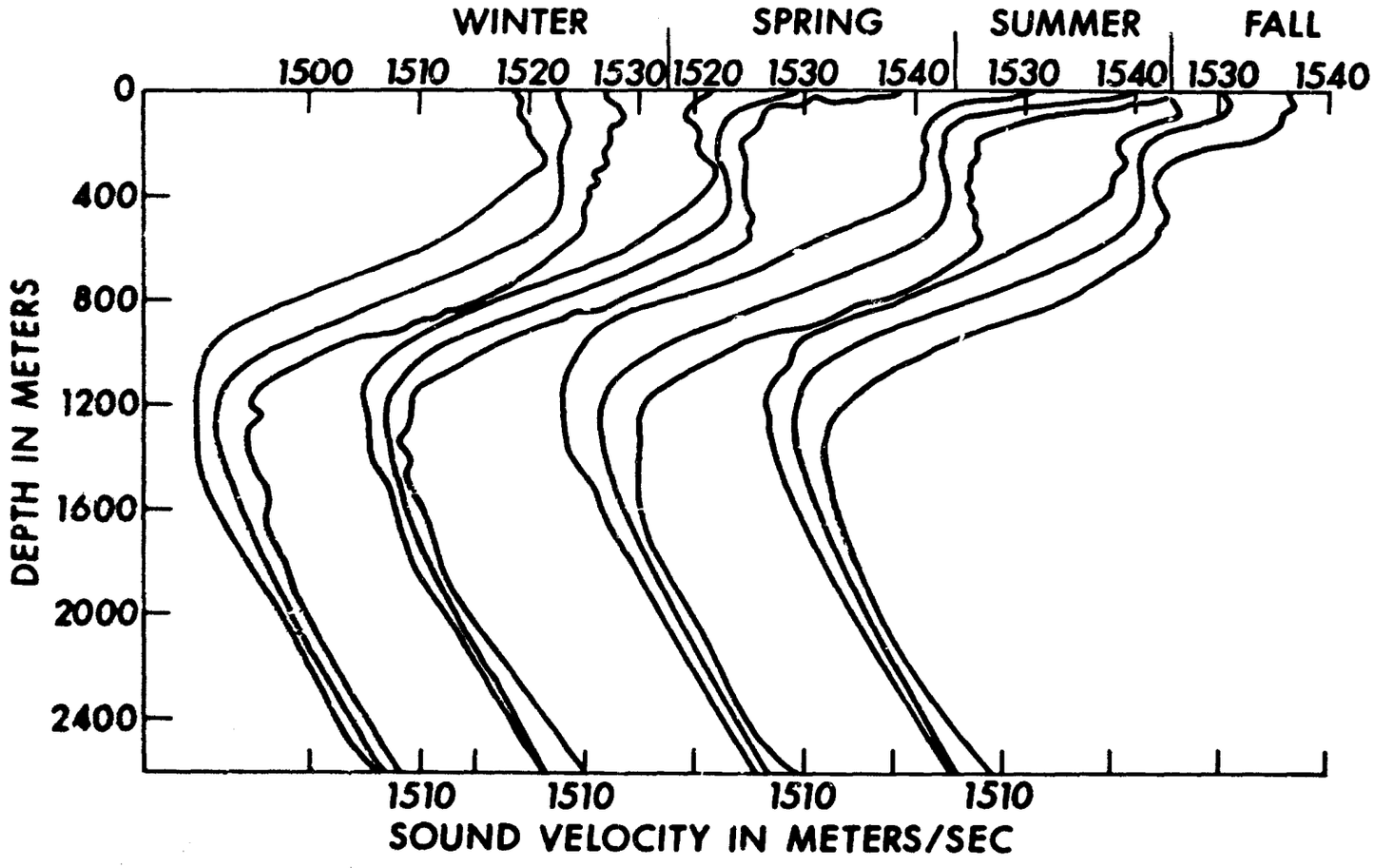

FIGURE 5 SOUND VELOCITY PROFILES SHOWING SEASONAL MEANS AND EXTREMES

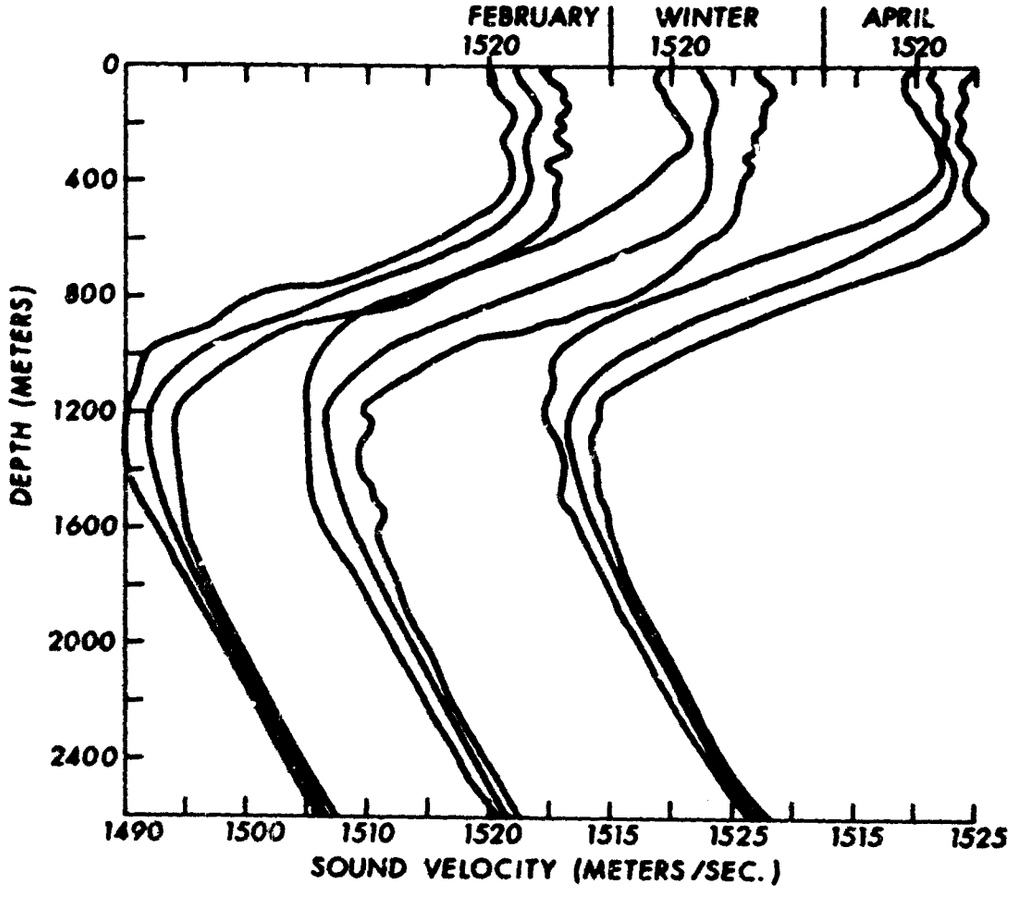

FIGURE 5A COMPARISON OF THE WINTER PROFILE WITH TWO MONTHLY PROFILES

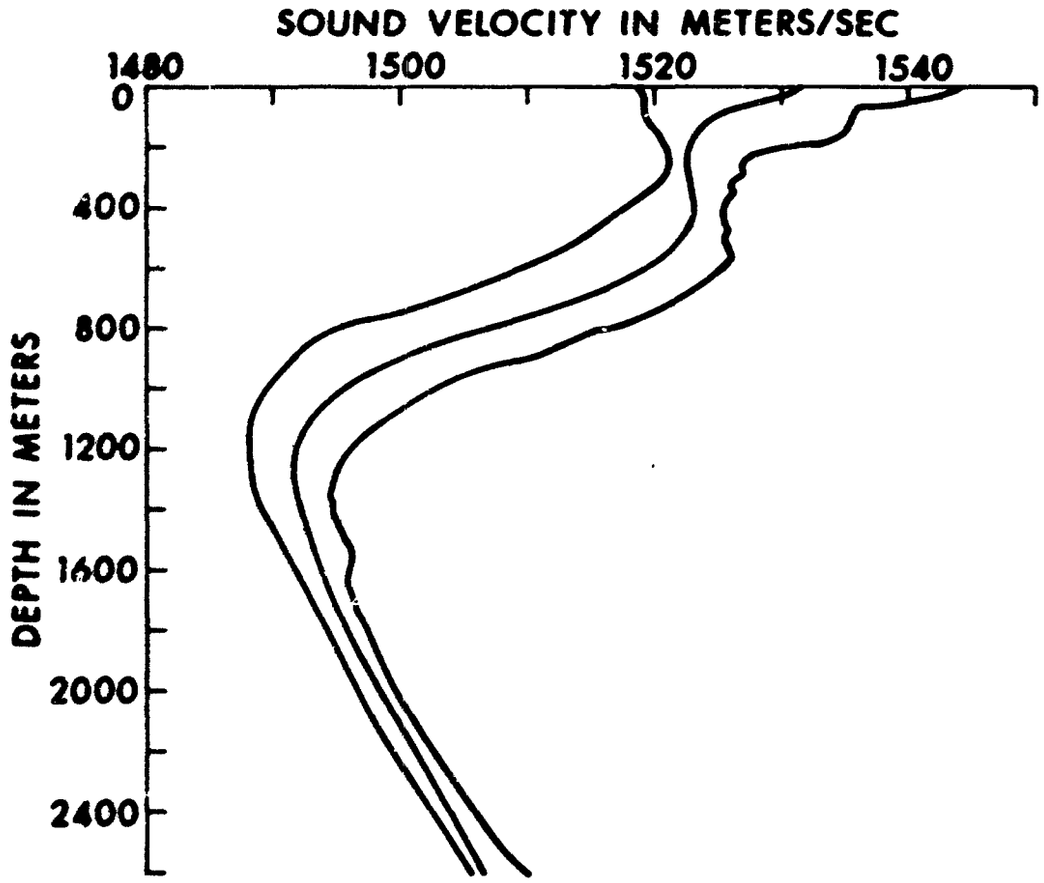

FIGURE 6 COMPOSITE SOUND VELOCITY PROFILES SHOWING MEANS AND EXTREMES JUNE 1954 TO AUGUST 1965

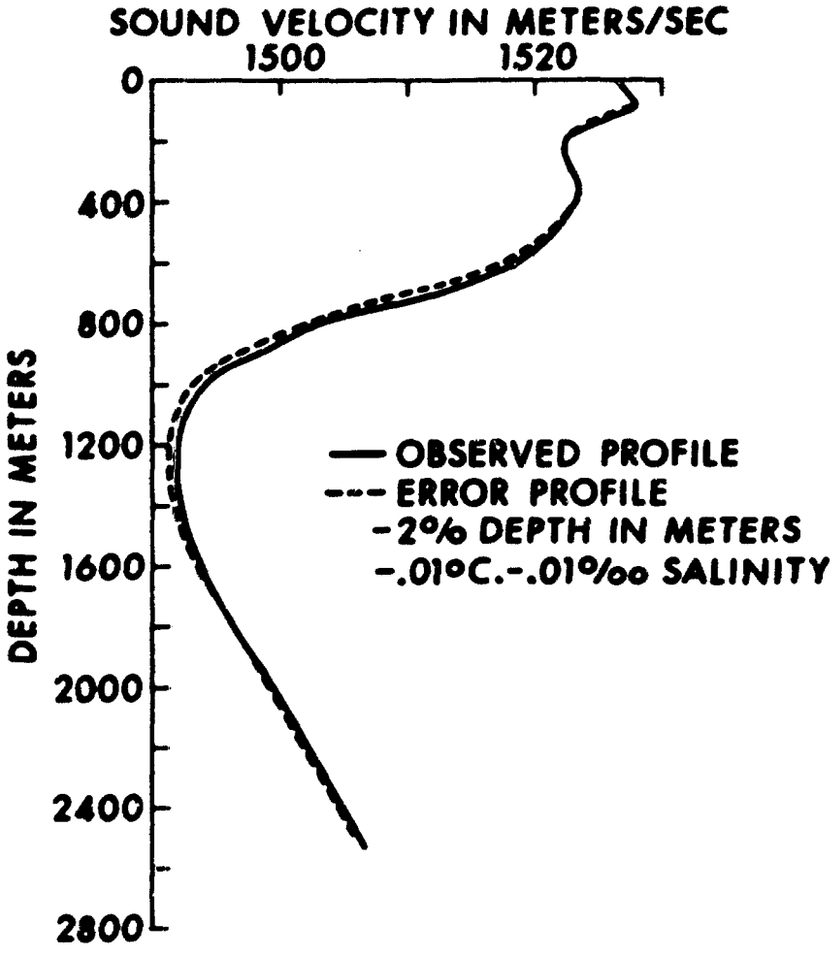

FIGURE 7 COMPARISON OF OBSERVED PROFILE WITH A PROFILE RESULTING FROM POSSIBLE ERRORS

Figure 8 is a histogram of minimum velocities and the depths at which they occurred for each station. The mean minimum velocity is 1491.9 meters/second (standard deviation is 1.1 meters /second) and the mean depth for the minimum velocity point occurred at 1249 meters (standard deviation is 95 meters). Note that the points plotted are not randomly distributed about the mean but rather occur in groups, especially for the plot of the depth of occurrence which shows one group near 1200 meters and another about 1350 meters. This grouped distribution is, of course, partially attributable to the fact that the data were taken in specific increments of depth and not through a continuous depth increase.

Monthly means and the variation of the data within each month are shown in Figure 9. The monthly means do not seem to follow any pattern but are close to the mean of all the data. One observation is that less variation appears in the spring months.

To compare these data with data from another volume of the ocean south of Bermuda, Figure 10 is shown. The profiles compare quite well. A time-lapse motion picture film will present the indivudal profiles to show the gradual change in the velocity profile of this part of the ocean as the seasons change.

USL Motion Picture Brief No. 22,[4] "Sound Velocity Profiles in an Area South of Bermuda," presents the results of eleven years of data as a guide to an understanding of the effects on sound velocity of seasonal changes within the ocean. Composite and average results are shown first. These are followed by presentation of each individual profile by the method of time-lapse photography to give insight into the gradual change of the velocity profile as the months and seasons advance through the years.

The results of this study present an interesting and rather complete set of velocity profiles for an area in the Atlantic Ocean south of Bermuda. This information should prove to be of value to those interested in the velocity structure of the ocean.

REFERENCES

1. The first nine years of data were obtained through the good offices of Dr. Menzel and Dr. Beers and have been published by the authors in "Sound Velocity Profiles in an Area South of Bermuda," USL Report No. 632.

2. Wilson, Wayne, D., Journal of the Acoustical Society of America, October 1960, p. 1327.

3. Temperature and salinity data for the first nine years were combined into monthly means by H. J. Doebler and J. P. Beam of the Underwater Sound Laboratory. Unpublished data.

4. A copy of either of these films may be obtained on loan by writing to the Commanding Officer and Director, U. S. Navy Underwater Sound Laboratory, Fort Trumbull, New London, Connecticut 06321.

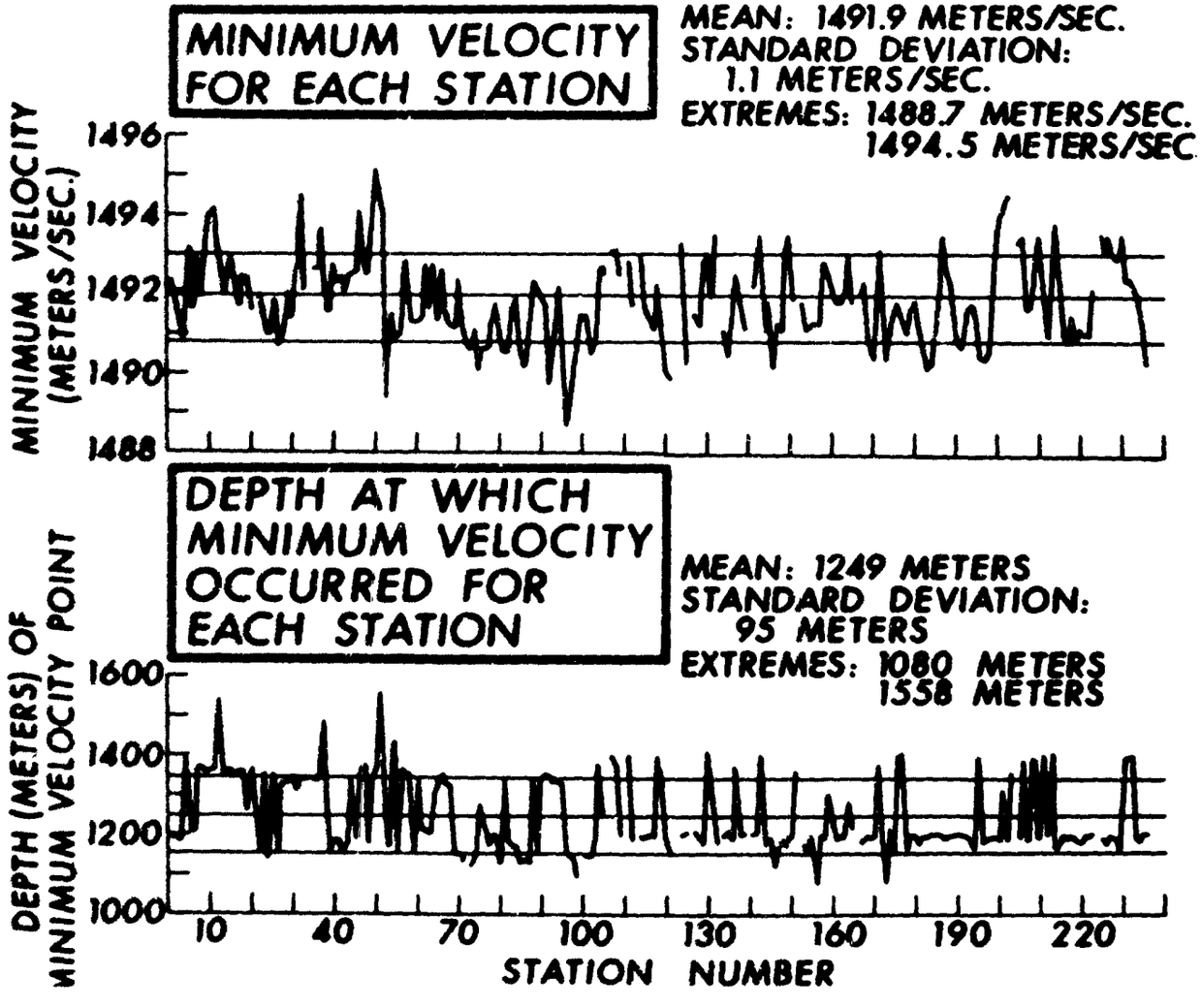

FIGURE 8 MINIMUM VELOCITY FOR EACH STATION

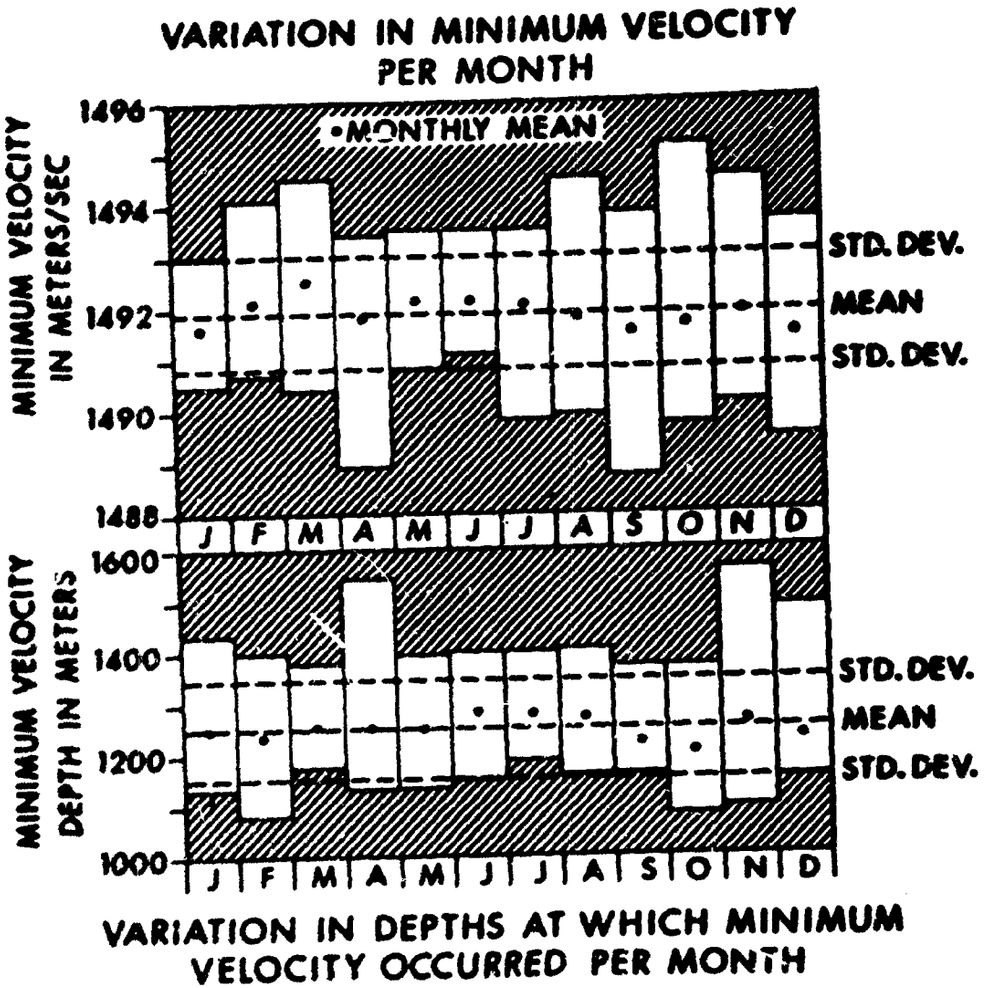

FIGURE 9 VARIATION IN MINIMUM VELOCITY PER MONTH

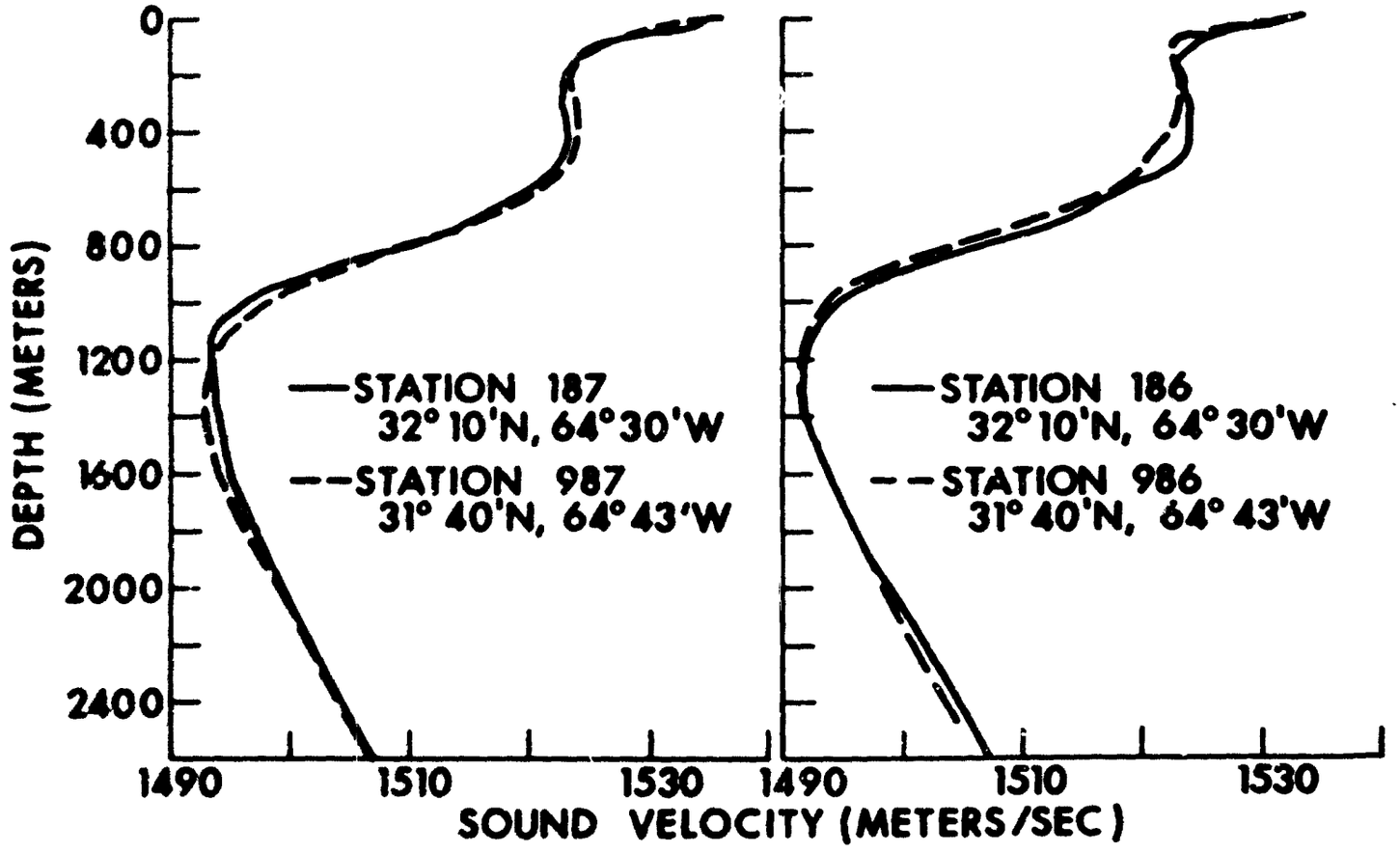

FIGURE 10 COMPARISON OF SOUND VELOCITY PROFILES AT TWO LOCATIONS

SOUND VELOCITY PROFILES IN AN AREA SOUTH OF BERMUDA

William A. Von Winkle, Linda Mary Jones
U. S. Navy Underwater Sound Laboratory
Fort Trumbull, New London, Connecticut

Sound velocity profiles of an area in the Atlantic Ocean fifteen miles south of Bermuda have been derived, using Wilson's formula, from Nansen cast data taken during an eleven-year period. The casts were made approximately every two weeks from June 1954 to August 1965 to a depth of 2600 meters. Individual profiles were computed for each set of data.

To improve the usefulness of the profiles, statistical analyses were made of the data to combine the profiles into convenient groupings. First, mean and extreme monthly profiles were obtained; these monthly profiles are the most meaningful for any general predictions. To supplement the monthly velocity profiles, temperature and salinity profile for each month have also been prepared from the data. Mean and extreme seasonal profiles were also derived. In order to make a realistic division of the year into seasons for this volume of the ocean, a study was made of these temperature profiles and velocity gradients and of other data in the literature. The velocity profiles show a seasonal grouping as follows: winter - January through April; spring - May and June; summer - July through October; and fall - November and December. A composite profile was also derived using all of the data.

The minimum velocity points of each profile were determined. The mean value of the minimum velocity was calculated to be 1492 (±3) meters per second. The depths at which this minimum velocity occurs was found to vary between 1080 and 1558 meters with a mean depth of 1250 meters.

A time-lapse motion picture film presenting the gradual change of the velocity profile with the cycle of the seasons will be shown.